

# **Rethinking Measures of Brain Connectivity via Feature Extraction**

by

Rosaleena Mohanty

A dissertation submitted in partial fulfillment of  
the requirements for the degree of

Doctor of Philosophy  
(Electrical Engineering)

at the

UNIVERSITY OF WISCONSIN–MADISON

2019

Date of final oral examination: 05/07/2019

The dissertation is approved by the following members of the Final Oral Committee:

William A. Sethares, Professor, Electrical and Computer Engineering

Vivek Prabhakaran, Associate Professor, Radiology

Robert D. Sanders, Assistant Professor, Anesthesiology

Yu Hen Hu, Professor, Electrical and Computer Engineering



*In loving memory of my inspiration, my father, Bijoy.  
Baba, I can only hope that I have made you proud.*

## Acknowledgements

It is hard to summarize my journey of pursuing this doctoral degree in a few words for there have been innumerable people and experiences, big and small, that have impacted and shaped this work. However, there are a few key people who have left an indelible mark and for whom I shall remain eternally grateful.

William Sethares, whom I cannot thank enough for his immense patience, brilliant guidance and mentoring through the years of our weekly discussions. He taught me the importance of breaking down any challenging problem to realistic, achievable goals and thinking creatively in research, that there is almost always an alternative perspective to any problem if you look hard enough.

My most sincere thanks to Vivek Prabhakaran for introducing me to the fascinating world of neuroscience and providing so many fantastic opportunities to explore the field through the many projects in his lab. Many thanks to him for always being approachable, generous and fostering creative liberty in research, paving the way to grow as an independent researcher.

I am very thankful for the wonderful collaboration with Robert Sanders, who exemplified the importance of perseverance in research. His incessant scientific curiosity and practice of ‘telling a story’ through research was a major source of inspiration and also taught me that when you are tired and frustrated of looking really hard and yet find nothing, look some more for it makes all the difference.

I would like to extend my gratitude towards Yu Hen Hu for his constructive feedback, encouragement and for serving on my committee. Much of this work would not have been possible without Veena Nair. I am incredibly thankful for and very appreciative of her kindness, discipline and excellent practical advice in all spheres of research. My thanks to all the lab members over the years from both Prabhakaran and Sanders labs who have enabled and realized this work by forging a collaborative and enjoyable work and team ethic.

Thanks to my fellow Madisonians, whom I have had a great pleasure to meet and be friends with: Ayushi, Haliee, Ken and Sally (and her beloved critters) for sharing so many of their creative, intellectual, gastronomic, artistic and social endeavors with me. Thanks to my brother, Gaurav, who was my role-model growing up and introduced me to the possibility of studying in and experiencing the exuberance of Madison. Anindita and Biswa (and the kids), my aunt and uncle, were my home away from home and my go to for advice on all aspects of life, from cooking to research to philosophy.

Last but foremost, I am indebted to my family for their unconditional love and unlimited support at all times: Priyadarshini, my sister, who is my unsung hero and the guiding light of my life; my mother, Rachita, who has been an epitome of grace, endurance and courage in times low and high and Bijoy, my father, who transformed my life in more ways than he could ever have imagined and to whom I owe my everything.

## Contents

Acknowledgements .....	ii
List of Figures .....	v
List of Tables .....	vii
List of Publications .....	ix
CHAPTER 1: Introduction .....	1
1. Motivation .....	1
2. Specific Aims at a Glance .....	2
3. Research Support .....	7
CHAPTER 2: Machine Learning Classification to Identify the Stage of Brain-Computer Interface Therapy for Stroke Rehabilitation using Functional Connectivity .....	8
1. Introduction .....	10
2. Methods .....	13
3. Results .....	23
4. Discussion .....	32
5. Conclusion .....	35
CHAPTER 3: Functional Connectivity Correlates of Behavioral Outcomes of Brain-Computer Interface Stroke Rehabilitation using Machine Learning .....	41
1. Introduction .....	43
2. Materials and methods .....	46
3. Results .....	61
4. Discussion .....	72
5. Conclusion .....	76
CHAPTER 4: Identification of Subclinical Language Deficit Based on Post-Stroke Functional Connectivity Derived from Low Frequency Oscillations .....	82
1. Introduction .....	84
2. Methods .....	86
3. Results .....	96
4. Discussion .....	106
5. Conclusion .....	110
CHAPTER 5: Neural Correlates of Perioperative Executive Function Associated With Noncardiac Surgery in the Elderly .....	115
1. Introduction .....	117

2. Methods .....	118
3. Results.....	125
4. Discussion.....	131
5. Conclusion .....	134
CHAPTER 6: Changes in Functional Connectivity Associated with the Inflammatory Response to Noncardiac Surgery in Older Adults.....	139
1. Introduction.....	141
2. Methods .....	142
3. Results.....	148
4. Discussion.....	152
5. Conclusion .....	156
CHAPTER 7: Rethinking Measures of Brain Connectivity via Feature Extraction .....	159
1. Introduction.....	161
2. Methods .....	162
3. Results.....	179
4. Discussion.....	192
5. Conclusion .....	196
APPENDIX I .....	199
CHAPTER 8: Automated Classification of Ink Strokes in van Gogh's Drawings using Dictionary Learning .....	208
1. Introduction.....	209
3. Feature-Based Dictionary Learning Paradigm.....	216
4. Experiments and comparisons .....	221
5. Conclusions.....	227
CHAPTER 9: Conclusion .....	234
1. Relevance within the Big Picture.....	235
2. Opposing Views.....	237
3. Future Directions .....	238

## List of Figures

<b>Figure 2. 1.</b> Study paradigm.....	14
<b>Figure 2. 2.</b> Seed regions included in the analysis .....	17
<b>Figure 2. 3.</b> Methodology for single-participant analysis .....	18
<b>Figure 2. 4.</b> Methodology for group-level analysis.....	22
<b>Figure 2. 5.</b> Principal component analysis (PCA) on FC data .....	24
<b>Figure 2. 6.</b> Variance explained by PCA.....	25
<b>Figure 2. 7.</b> The ROC for the learned SVM classifier.....	28
<b>Figure 2. 8.</b> Visualization of discriminatory functional connections .....	29
<b>Figure 2. 9.</b> Distribution of discriminating features .....	31
<b>Figure 2. 10.</b> Involvement of seed regions in classification.....	32
<b>Figure 3. 1.</b> Study paradigm.....	46
<b>Figure 3. 2.</b> Steps for individual subject analysis.....	53
<b>Figure 3. 3.</b> Motor network with seed regions used in analysis .....	54
<b>Figure 3. 4.</b> Overview of group-level analysis .....	60
<b>Figure 4. 1.</b> The 23 brain regions used of the language network in this study.....	91
<b>Figure 4. 2.</b> Methodology for single subject analysis .....	95
<b>Figure 4. 3.</b> Methodology for group level analysis .....	95
<b>Figure 4. 4.</b> Brain regions involved among the discriminating features .....	105
<b>Figure 5. 1.</b> Study paradigm.....	118
<b>Figure 5. 2.</b> Decreased within-network connectivity associated with poorer cognitive performance postoperatively .....	126
<b>Figure 5. 3.</b> Clusters of brain regions (axial/top view) that showed significant correlations with respect to changes in cognitive outcomes ( $\Delta$ TMT) obtained from seed-level analyses.....	128
<b>Figure 5. 4.</b> Outside-network effects associated with cognitive change .....	129
<b>Figure 6. 1.</b> Schematic diagram of the study design .....	142
<b>Figure 6. 2.</b> Overview of methodology .....	143
<b>Figure 6. 3.</b> Within-network effects for inflammatory changes.....	150
<b>Figure 6. 4.</b> Outside-network effects for inflammatory changes.....	152

<b>Figure 7. 1.</b> A contrary case .....	163
<b>Figure 7. 2.</b> Comparison of FC based on Pearson’s correlation in young healthy adults between task and resting-state conditions for <b>E1</b> in:.....	180
<b>Figure 7. 3.</b> Whole brain resting-state FC in young healthy adults defined based on Pearson’s correlation in 13 distinct brain networks given by Power functional atlas in <b>E1</b> .....	184
<b>Supplementary Figure 7. 1.</b> The pipeline designed for <b>E3</b> (shown for Pearson’s correlation) .....	199
<b>Supplementary Figure 7. 2.</b> Comparison of FC based on all measures in young healthy adults for <b>E1</b> in motor and language networks .....	200
<b>Supplementary Figure 7. 3.</b> Whole brain resting-state FC in young healthy adults defined based on various measures in 13 distinct brain networks in <b>E1</b> .....	203
<b>Supplementary Figure 7. 4.</b> The distribution of Sørensen-Dice similarity coefficients obtained for 1000 iterations of k-means clustering. ....	204
<b>Figure 8. 1.</b> A portion of <b>Sower with Setting Sun</b> by Vincent van Gogh.....	209
<b>Figure 8. 2.</b> A patch from the <b>Sower with Setting Sun</b> , 1888 by Vincent van Gogh illustrates the selection of regions in which three basic types of strokes appear: dots, vertical strokes and horizontal strokes .....	210
<b>Figure 8. 3.</b> <b>Arums</b> by Vincent van Gogh, drawing .....	212
<b>Figure 8. 4.</b> <b>Street in Saintes-Maries-de-la-Mer</b> by Vincent van Gogh.....	213
<b>Figure 8. 5.</b> Breakdown of the multi-scale approach .....	215
<b>Figure 8. 6.</b> The experimental process of individual sub-feature extraction.....	217
<b>Figure 8. 7.</b> An example of a training patch from ‘dots’ class is utilized to illustrate that feature-based dictionary learning can extend the application of K-SVD to large sized patches.....	218
<b>Figure 8. 8.</b> The <b>Sower with the setting Sun</b> of <b>Figure 8.1</b> is superimposed on the multi-level classification scheme of Subsection 3.1 .....	223
<b>Figure 8. 9.</b> The drawing <b>Arums</b> of <b>Figure 8.3</b> is superimposed on the multi-level classification of Subsection 3.1 .....	224
<b>Figure 8. 10.</b> The <b>Street in Saintes-Maries-de-la-Mer</b> of <b>Figure 8.4</b> is superimposed on the multi-level classification of Subsection 3.1.....	224
<b>Figure 8. 11.</b> The <b>Sower with the setting Sun</b> of <b>Figure 8.1</b> is superimposed on the multi-scale classification of Subsection 3.2.....	225
<b>Figure 8. 12.</b> The drawing <b>Arums</b> of <b>Figure 8.3</b> is superimposed on the multi-scale classification of Subsection 3.2.....	225
<b>Figure 8. 13.</b> The <b>Street in Saintes-Maries-de-la-Mer</b> of <b>Figure 8.4</b> is superimposed on the multi-scale classification of Subsection 3.1.....	226
<b>Figure 8. 14.</b> Depict eight independent test patches from the <b>Sower</b> .....	227
<b>Figure 8. 15.</b> The <b>Sower</b> of <b>Figure 8.1</b> is used to compare several classification schemes .....	228



## List of Tables

<b>Table 2. 1.</b> Study Sample Characteristics .....	15
<b>Table 2. 2.</b> Step-by-step feature selection procedure .....	25
<b>Table 2. 3.</b> Classification performance evaluation .....	27
<b>Table 2. 4.</b> Overall discriminating features .....	30
<b>Table 3. 1.</b> Demographic and clinical characteristics of the study cohort.....	48
<b>Table 3. 2.</b> Summary of all the behavioral assessments used as outcomes .....	51
<b>Table 3. 3.</b> Estimation of behavior at succeeding time-point using FC and clinical variables at preceding time-point.....	62
<b>Table 3. 4.</b> Correlates of behavior at a succeeding time-point .....	63
<b>Table 3. 5.</b> Estimation of $\Delta$ behavioral measures using $\Delta$ FC and clinical variables .....	66
<b>Table 3. 6.</b> <i>Correlates of <math>\Delta</math>behavioral measures</i> .....	67
<b>Table 3. 7.</b> Estimation of behavioral measures at succeeding time-point using behavioral measures at preceding time-point and clinical variables .....	70
<b>Table 3. 8.</b> Behavioral and clinical correlates of behavioral outcomes at succeeding time-points .....	71
<b>Table 4. 1.</b> Study sample characteristics .....	88
<b>Table 4. 2</b> Group means and group differences in head motion.....	97
<b>Table 4. 3.</b> The number of FC features outlier removal and feature selection for each frequency band....	98
<b>Table 4. 4.</b> Multiclass classification performance in three frequency bands.....	100
<b>Table 4. 5.</b> One-vs-rest classification .....	101
<b>Table 4. 6.</b> Discriminating features in three frequency bands.....	103
<b>Table 4. 7.</b> Brain regions involved in classification in the three frequency bands .....	104
<b>Table 5. 1.</b> Peak brain areas showing significant correlations with changes in executive function ( $\Delta$ TMT) obtained from seed-level (within-network) regression analyses.....	127
<b>Table 5. 2.</b> Peak brain areas showing significant correlations with changes in executive function ( $\Delta$ TMT) obtained from network-level analyses .....	130
<b>Table 6. 1.</b> Brain regions showing significant negative associations with changes in inflammatory response ( $\Delta$ IL-6) obtained from seed-level (within-network) analyses .....	149
<b>Table 6. 2.</b> Brain areas showing significant negative associations with changes in inflammatory response ( $\Delta$ IL-6) obtained from network-level (outside-network) analyses.....	151

<b>Table 7. 1.</b> Characteristics of young healthy participants included in <b>E1</b> .....	173
<b>Table 7. 2.</b> Characteristics of younger and older healthy participants included for <b>E2</b> . ....	175
<b>Table 7. 3.</b> Consistency of each measure of FC .....	183
<b>Table 7. 4.</b> Age-based classification between younger and older healthy adults in nine major brain networks.....	185
<b>Table 7. 5.</b> Comparison of Sørensen-Dice similarity coefficient between the original brain configuration and the best possible reconfiguration obtained via clustering into 10 clusters or networks. ....	187
<b>Table 7. 6.</b> Brain-behavior relationship in original and reconfigured brain .....	189
<b>Supplementary Table 7. 1.</b> Multiple measures used to characterize FC and their properties .....	205
<b>Supplementary Table 7. 2.</b> Age-based classification between younger and older healthy adults in nine major brain networks in <b>E2</b> .....	206
<b>Table 8. 1.</b> Feature dimensions of the pixel-based features of classical dictionary learning .....	216
<b>Table 8. 2.</b> Feature dimensions of the regional and individual stroke features in feature-based dictionary learning .....	221
<b>Table 8. 3.</b> Classification test for classical dictionary learning: confusion matrix from testing the image patches of <b>Sower</b> .....	229
<b>Table 8. 4.</b> Classification test for multi-level feature-based dictionary learning: confusion matrix from testing the image patches of <b>Sower</b> .....	230
<b>Table 8. 5.</b> Classification test for multi-scale feature-based dictionary learning: confusion matrix from testing the image patches of <b>Sower</b> .....	231
<b>Table 8. 6.</b> Time required to learn the optimal dictionary with $L = 3$ .....	231

## List of Publications

A number of journal publications were produced as a part of this dissertation and are listed as follows:

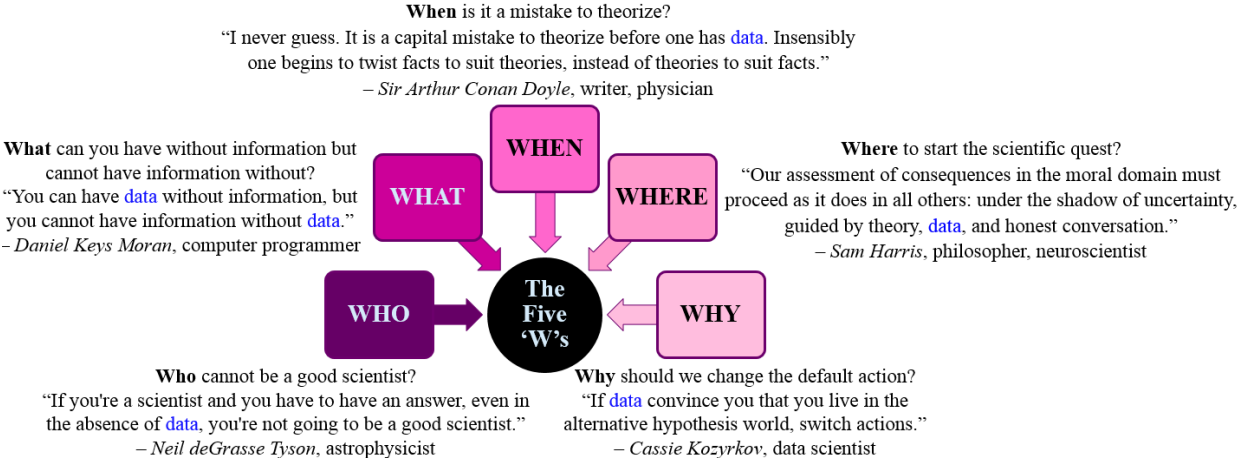
1. Mohanty, R., Sinha, A.M., Remsik, A.B., Dodd, K.C., Young, B.M., Jacobson, T., McMillan, M., Thoma, J., Advani, H., Nair, V.A., Kang, T.J., Caldera, K., Edwards, D. F., Williams, J. C., Prabhakaran, V., 2018. “Machine learning classification to identify the stage of brain-computer interface therapy for stroke rehabilitation using functional connectivity”, *Frontiers in neuroscience*, 12.
2. Mohanty, R., Sinha, A.M., Remsik, A.B., Dodd, K.C., Young, B.M., Jacobson, T., McMillan, M., Thoma, J., Advani, H., Nair, V.A., Kang, T.J., Caldera, K., Edwards, D. F., Williams, J. C., Prabhakaran, V., 2018. “Early Findings on Functional Connectivity Correlates of Behavioral Outcomes of Brain-Computer Interface Stroke Rehabilitation Using Machine Learning”, *Frontiers in neuroscience*, 12.
3. Mohanty, R., Nair, V.A., Tellapragada, N., Williams Jr, L.M., Kang, T.J. and Prabhakaran, V., 2018. “Identification of Subclinical Language Deficit Using Machine Learning Classification Based on Poststroke Functional Connectivity Derived from Low Frequency Oscillations.” *Brain Connectivity*.
4. Mohanty, R., Lindroth, H., Twadell, S., Nair, V. A., Prabhakaran, V., Sanders, R. D., “Neural Correlates of Perioperative Executive Function associated with Noncardiac Surgery in the Elderly”, *British Journal of Anaesthesia* (under review).
5. Mohanty, R., Lindroth, H., Casey, C., Nair, V. A., Prabhakaran, V., Sanders, R. D., “Changes in Functional Connectivity Associated with the Inflammatory Response to Noncardiac Surgery in Older Adults”, *Journal of Neuroinflammation* (in preparation).
6. Mohanty, R., Sethares, W. A., Nair, V. A., Prabhakaran, V., “Meaning of Functional Magnetic Resonance Imaging-based Brain Functional Connectivity: Empirical Evidence and Hypotheses”, *Nature Neuroscience* (in preparation).
7. Mohanty, R., Sethares, W. A., Meedendorp, T., van Tilborgh, Louis, “Dictionary Learning-based Classification of Ink Strokes in Vincent van Gogh’s Drawings”, 2019, *International Journal of Arts and Technology*, 11 (1), 80-98.

Other journal publications related to but not included within this thesis are listed as follows:

8. Hou, J. \*, Mohanty, R. \*, Nair, V. A., Dodd, K. C., Beniwal-Patel P., Prabhakaran, V. and Saha, S., “Alterations in resting-state functional connectivity in patients with Crohn’s disease in remission”, 2019, *Scientific Reports* (accepted; \*equal contribution).
9. Casey, C. \*, Lindroth, H. \*, Mohanty, R. \*, Farahbakhsh Z., Ballweg T., Twadell S., Krause B., Prabhakaran, V., Blennow K., Zetterberg H., Sanders, R. D., “Postoperative delirium is associated with increased plasma neurofilament light”, *Brain* (submitted; \*equal contribution)
10. Lindroth, H., Nair, V. A., Staneld, C., Casey, C., Mohanty, R., Wayer, D., Rowley, P., Brown, R., Prabhakaran, V., Sanders, R. D. “Examining the identification of age-related atrophy between T1 and T1+T2-FLAIR cortical thickness measurements”, *Scientific Reports* (under review).
11. Hwang, G., Nair, V. A., Mathis, J., Cook, C. J., Mohanty, R., Zhao, G., Tellapragada, N., Ustine, C., Nwoke, O., Rivera-Bonet, C., Rozman, M., Allen, L., Forseth, C., Almane, D. N., Kraegel, P., Nencka, A., Felton, E., Struck, A., Birn, R., Maganti, R., Conant, L., Humphries, C., Hermann, B., Raghavan, M., DeYoe, E., Binder, J., Meyerand, M. E., Prabhakaran, V., “Using low-frequency oscillations to detect temporal lobe epilepsy with machine learning”, *Brain Connectivity*, 2019 (in Press).
12. Remsik, A. B., Williams Jr., L., Gjini, K., Dodd, K. C., Thoma, J., Jacobson, T., Walczak, M., McMillian, M., Rajan, S., Young, B. M., Nigogosyan, Z., Advani, H., Mohanty, R., Tellapragada, N., Allen, J., Mazrooyisebdani, M., Walton, L. M., van Kan, P. L. E., Kang, T. J., Sattin, J. A., Nair, V. A., Edwards, D. F., Williams, J. C., Prabhakaran, V., “Ipsilesional Mu Rhythm Desynchronization and Changes in Motor Behavior following Post Stroke BCI Intervention for Motor Rehabilitation”, *Frontiers in Neuroscience*, 13, p.53, 2019 (in Press).
13. Remsik, A. B., Dodd, K. C., Williams Jr., L., Thoma, J., Jacobson, T., Allen, J., Advani, H., Mohanty, R., McMillian, M., Rajan, S., Walczak, M., Young, B. M., Nigogosyan, Z., Rivera, C. A., Mazrooyisebdani, M., Tellapragada, N., Walton, L. M., Gjini, K., van Kan, P. L. E., Kang, T. J., Sattin, J. A., Nair, V. A., Edwards, D. F., Williams, J. C., Prabhakaran, V., “Behavioral Outcomes Following BrainComputer Interface Intervention for Upper Extremity Rehabilitation in Stroke: A Randomized Controlled Trial”, *Frontiers in Neuroscience*, 12, p.752, 2018.

# CHAPTER 1: Introduction

## 1. Motivation



One common theme that connects the aforementioned questions is that of ‘**data**’. Given that data exist in abundance in the world we live in today, it is imperative that they be used to generate evidence, solve and better inform critical issues in science. Among simpler recipes to make sense of them are categorization into meaningful classes and prediction of associated outcomes, which have found utility in myriad scientific sub-fields involving data of different nature, shapes and sizes. Reasonable performance of statistical models developed to achieve these objectives is incumbent upon extracting meaningful “features” which could uniquely represent the data at hand. While features created by approaches of the likes of data transformation, combination or projection into a different space can attain the objectives of classification and estimation, realization of intuitive features is critical and can be of paramount significance in several applications.

The beauty of studying signal processing lies in that it offers a wide range of tools to mathematically formulate and investigate research questions, most pertinent to data, irrespective of the source or domain of application. The crux of this body of work was to examine the role of domain-specific features from up to four-dimensional signals, specifically image-based signals, that could improve discovery of non-trivial patterns in datasets, particularly within the disciplines of neuroscience and art history. While conventional statistical models offer data-inspired approaches to draw group-level inferences, the advent of machine

learning models allows for data-driven methods to operate and to draw inferences on individual cases. Rapid progression within artificial intelligence (e.g. artificial neural networks in deep learning) have led to potential solutions to a wide spread of applications. They, however, require the size of the dataset to scale up quickly in order to design the parameters of models which can reliably make decisions. Covered within this thesis are some investigations based on neuroimaging and art historical data using data-inspired methods, others using machine learning-based data-driven approaches (given the availability of limited data), finally, culminating in identification of a fundamental gap or problem within the area of neuroimaging along with a proposed solution using a combination of data-inspired as well as data-driven methodologies.

## **2. Specific Aims at a Glance**

Application of techniques from signal processing was realized in two specific disciplines: (a) neuroimaging and (b) art history. An outline of the structure of this thesis is provided below.

- (a) Within neuroimaging, a series of six sub-studies were conducted. Aims 1-3 were focused toward study of the population suffering brain stroke. Aims 4-5 were geared toward study of the aging population undergoing major surgery. Aim 6 investigated an issue common to all preceding aims.

***Aim 1: To understand the impact of brain-computer interface intervention on non-targeted brain networks in chronic stroke survivors***

***Problem Statement:*** Brain-Computer Interface-aided intervention has been a promising approach for facilitation of motor recovery in stroke survivors, even at later stages. However, the effect of such an intervention on brain regions outside of the targeted motor network is not well-understood.

***Proposed Solution:*** Brain connectivity was evaluated based on functional MRI, collected prior to and post completion of the intervention, in stroke survivors with motor impairments. Comparison between the two time-points was modeled as a classification problem. A standard data-driven machine learning classifier differentiated between the time-points, taking into account functional brain connectivity from targeted (motor) as well as non-targeted (non-motor) brain areas.

Significance: In addition to motor network, the fronto-parietal task control, default mode, subcortical, and visual networks emerged as important contributors toward classification. A net strengthening of connectivity post-intervention supports the potential clinical utility of this intervention that not only benefits motor recovery but also facilitates recovery in other brain networks. Specific whole-brain changes could inform more optimal designs of the intervention, thus, tailoring it to each patient.

***Aim 2: To identify neural correlates of behavioral outcomes of brain-computer interface stroke rehabilitation in chronic stroke survivors***

Problem Statement: Tracking of recovery is key in chronic stroke survivors with motor impairments undergoing brain-computer interface-based intervention. This necessitates the study of changes in behavioral outcomes and brain-behavior relationship to inform not only immediate but also carry-over effects of such a rehabilitative intervention or lack thereof.

Proposed Solution: Functional MRI and behavioral (motor) outcomes were collected at three time-points (pre-, immediately post- and one-month post-intervention). Three types of associations were investigated between: (i) past motor behavior and future motor behavior, (ii) functional brain connectivity and motor behavior, and (iii) change in functional brain connectivity and change in motor behavior using a standard data-driven machine learning regression model.

Significance: Behavioral outcomes were best predicted by past behavior, functional brain connectivity and changes in functional brain connectivity in the specified order, thus, allowing to track the motor trajectory of the stroke survivors. From a clinical perspective, such an application could serve as a supplementary prognostic tool for patients and their families in estimating the timeline or capacity of potential recovery via intervention.

***Aim 3: To automate detection of subclinical language deficit in early-stage stroke***

Problem Statement: Post-stroke neuropsychological evaluation can be a time-, task- and personnel-intensive procedure to assess impairments in survivors with subclinical deficits (with no overt clinical

deficits). Timely identification of such subtle deficits could improve efficiency of diagnosis, facilitating better treatment plans for improved patient outcomes, speedy recovery and rehabilitation.

*Proposed Solution:* Alternative or supplementary to neuropsychological assessment could be the use of task-free, time-efficient and non-invasive resting-state functional MRI. When treated as a classification problem, identification of subclinical deficits can be automated with a data-driven standard machine learning classifier using functional brain connectivity as input to generate diagnostic labels for each test case (subclinical impairment present or absent).

*Significance:* Expedited assessment and identification of subclinical impairments occurring in different domains in the brain post stroke could enable timely intervention for potential rehabilitation at an early stage in order to improve patient outcomes.

***Aim 4: To examine neural correlates of executive function associated with noncardiac surgery in the elderly***

*Problem Statement:* Most acute changes in the cognitive domain are likely to occur in the perioperative period. However, understanding of the underlying neural mechanisms remains elusive and could be key to tracking of the cognitive trajectory in older adults undergoing major surgery.

*Proposed Solution:* This question was investigated by analyzing resting-state functional MRI and corresponding cognitive performance, specifically executive control function, collected preoperatively and postoperatively. Multiple regression model, a data-inspired approach for estimation of outcomes, was used to understand the association between changes in functional brain connectivity in specific hypothesized networks and changes in executive control function.

*Significance:* Poorer postoperative executive function corresponded with decreased within-network and increased outside-network functional brain connectivity, indicative of cognitive dysfunction after a major surgery. Study of change in functional brain connectivity allowed to dynamically track neural correlates of cognitive changes perioperatively.



***Aim 5: To identify neural correlates of inflammatory response to noncardiac surgery in older adults***

*Problem Statement:* Undergoing major surgery may invoke inflammatory response in the immune system due to many factors including but not limited to anesthetic, surgical complications, predisposition factors, etc., especially in the elderly. Given that the neural substrates associated with inflammation are still unclear and may induce neuronal loss or cognitive dysfunction in patients, it is essential to better quantify this relationship.

*Proposed Solution:* The neural and inflammatory responses were characterized on the basis of resting functional MRI and blood samples, collected preoperatively and postoperatively. Data-inspired multiple regression model was implemented to study the relationship between changes in neuroimage-based functional brain connectivity and changes in blood-based interleukin-6 inflammation levels of the hypothesized brain areas and networks.

*Significance:* Decreased within-network connectivity, demonstrating neural impairment, was associated with increased inflammatory response, a marker of dysfunction, after surgery. Combination of data from two time-points enabled tracking of the connection between brain and surgical outcome.

***Aim 6: To investigate alternative characterizations of functional MRI-based brain connectivity***

*Problem Statement:* Functional connectivity derived from functional MRI is widely applied to describe how anatomically distinct regions could be connected within the brain. It is conventionally quantified by Pearson's correlation and captures the linear and time-domain relationship among neural signals. The reliability and extent to which this measure can completely and comprehensively characterize neural interactions are not thoroughly understood.

*Proposed Solution:* Several alternative measures (linear and non-linear ones, from time-, frequency and wavelet-domains) to evaluate functional connectivity were examined, compared and contrasted to Pearson's correlation based on functional MRI in healthy normal participants. Reliability of each measure was assessed by comparing task and rest scans. A data-driven machine learning classifier

differentiated between younger and older healthy brains using each measure. Reconfigurations of the brain connectivity in the light of alternative measures were computed. A data-inspired regression model was utilized to confirm plausibility of alternative measures by studying brain-behavior relationship.

Significance: Pearson's correlation alone may be insufficient to quantify functional connectivity completely. Canonical brain network configurations may differ based on the measure used to describe functional connectivity. Thus, a multi-metric characterization of functional connectivity including information from multiple domains may serve as a more comprehensive definition.

(b) In the art historical context, one main objective was assessed.

***Aim 7: To classify ink strokes in Vincent van Gogh's drawings automatically***

Problem Statement: Characterization of van Gogh's discerning style of painting and brushstrokes remains an open and challenging question in art history, answer to which could aid in dating his works to the right period, identifying possible counterfeits, educating scholars of his style, etc.

Proposed Solution: While probing the information derived from van Gogh's paintings would be a direct approach to solving this problem, an alternative method proposed here included examining his ink drawings which form the bases to many of his paintings. Using a classification paradigm, distinct types of ink strokes were analyzed within a data-driven dictionary learning framework with the goal of typifying each kind of stroke by a limited set of basic elements, learned iteratively, which then recreated test images of unseen ink drawings when transformed appropriately.

Significance: A feature-based dictionary learning scheme to decode van Gogh's ink strokes could be a first step toward quantifying the brushstrokes found in his paintings. Current understanding of ink strokes could be of interest and importance to art scholars studying his techniques, novices learning drawing, computer-generated drawing based on imagery and possibly examination of authenticity.

### **3. Research Support**

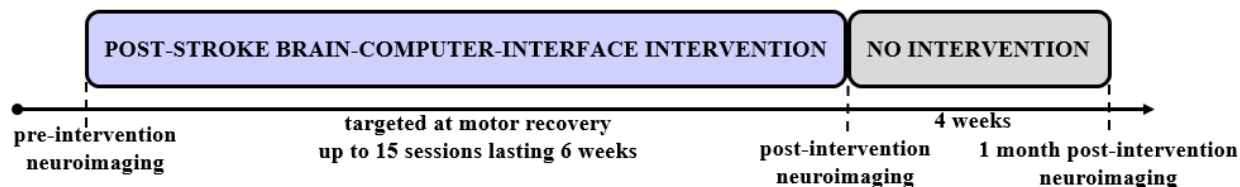
Aims 1-3 were part of an ongoing study conceptualized, designed, supported and led by Dr. Vivek Prabhakaran and his team. Aims 4-5 were part of an ongoing study conceptualized, designed, supported and led by Dr. Robert D. Sanders and his team. Aim 6 was an exploratory study carried out with support from Dr. Vivek Prabhakaran, his team and Professor William A. Sethares. Aim 7 was conceptualized, designed, supported and led by Professor William A. Sethares.

Several of the studies included in this work were made possible due to participation from members of the community, their families, the MRI technologists and study coordinators. Financial support for these projects include the following grants. NIH: RC1MH090912-01, T32GM008692, UL1TR000427, K23NS086852, T32EB011434, R01EB000856-06, R01EB009103-01, K23AG055700; DARPA: RCI Program MTO, N66001-12-C-4025, HIST Program MTO, N66001-11-1-4013; AHA: 1T32EB011434-01A1; Innovative Research Award – National Marcus Foundation, 15IRG22760009, Midwest Grant in Aid Award 15GRNT25780033, Foundation of ASNR, UW Milwaukee-Madison Intercampus Grants, Shapiro Foundation Grants and UW-Madison Graduate School.

## CHAPTER 2: Machine Learning Classification to Identify the Stage of Brain-Computer Interface Therapy for Stroke Rehabilitation using Functional Connectivity

---

### Graphical Summary



### Research Question

What is the impact of the Brain-Computer-Interface intervention on non-targeted brain regions?

### Publication

Mohanty, R., Sinha, A.M., Remsik, A.B., Dodd, K.C., Young, B.M., Jacobson, T., McMillan, M., Thoma, J., Advani, H., Nair, V.A., Kang, T.J., Caldera, K., Edwards, D. F., Williams, J. C., Prabhakaran, V., 2018. “Machine learning classification to identify the stage of brain-computer interface therapy for stroke rehabilitation using functional connectivity”, *Frontiers in neuroscience*, 12.

### Abstract

Interventional therapy using brain-computer interface (BCI) technology has shown promise in facilitating motor recovery in stroke survivors; however, the impact of this form of intervention on functional networks outside of the motor network is not well understood. Here, resting-state functional connectivity (FC) in stroke participants undergoing BCI therapy across stages, namely pre- and post-intervention, was investigated to identify discriminative neural changes using a machine learning classifier with the goal of categorizing participants into one of the two therapy stages. Twenty chronic stroke participants with persistent upper-extremity motor impairment received neuromodulatory training using a closed-loop neurofeedback BCI device and resting-state functional MRI (resting-state functional MRI) scans were collected at two time points: pre- and post-therapy. To evaluate the peak effects of this intervention, FC was analyzed at whole-brain level encompassing 236 seeds spanning both motor and non-motor regions at each stage. A univariate feature selection was applied to reduce the number of features followed by a principal component-based data transformation used by a linear binary support vector machine (SVM) classifier to classify each participant into a therapy stage. The SVM classifier achieved a cross-validation

accuracy of 92.5% using a leave-one-out method. Outside of the motor network, seeds from the fronto-parietal task control, default mode, subcortical, and visual networks emerged as important contributors to the classification. Furthermore, a higher number of neural changes were observed to be strengthening from the pre- to post-therapy stage than the ones weakening, both of which involved motor and non-motor regions of the brain. These findings may provide new evidence to support the potential clinical utility of BCI intervention as a form of stroke rehabilitation that not only benefits motor recovery but also facilitates recovery in other brain networks. Moreover, delineation of stronger and weaker changes may inform more optimal designs of BCI interventional therapy to facilitate strengthened and suppress weakened changes in the recovery process.

## 1. Introduction

Recent advancements in neurotechnology have led to the emergence of the brain-computer interface (BCI), which records neural signals and translates them into signals that can control assistive devices, such as computers or prostheses. To date, BCI-based approaches are being investigated as therapeutic strategies to facilitate recovery for several neurological diseases, including stroke, epilepsy, and Parkinson's Disease. For stroke, the long-term objective of the rehabilitation is to improve impaired brain functions to restore autonomy in daily activities for stroke survivors. While conventional approaches such as physical therapy and occupational therapy have proven to be successful in aiding stroke recovery in the acute and sub-acute stages [1], [2] modern technologies involving robotics [3], transcranial magnetic stimulation [4], and virtual reality [5] have demonstrated promise in promoting additional motor and cognitive recovery to improve autonomy and overall quality of life for stroke survivors even in the chronic stages. The use of an electroencephalogram (EEG)-based brain-computer-interface (BCI) is an unconventional rehabilitation strategy that has emerged as a potentially effective therapeutic modality for promoting motor recovery in patients with stroke [6]. An EEG-based BCI detects and uses a patient's neural signals as inputs to provide real-time feedback, effectively enabling users to modulate their brain activity [7]. Additional feedback presented by means of functional electrical stimulation (FES) [8] and tongue stimulation (TS) [9] also provide users with multi-modal feedback as a form of reward for producing certain brain activity patterns while performing tasks. While BCI intervention is often explicitly targeted at restoring motor functions, simultaneous changes in non-motor-related functions in the brain may also result after intervention; to date, neural reorganization of cortical regions outside of the motor network is not well characterized. Distinction between the overall brain state before and after the therapy could facilitate a more thorough understanding of the mechanisms underlying both the strengthening and/or weakening in motor and non-motor networks in participants. Access to this information could allow us to optimize the design and execution of this therapy for stroke rehabilitation.

While EEG allows for study of real-time brain activity during the BCI intervention with a high temporal resolution, neuroimaging methods have afforded us the ability to study both large-scale and small-scale reorganization of brain networks [10] at a relatively higher spatial resolution. Resting state functional magnetic resonance imaging (resting-state functional MRI), specifically, has been demonstrated as a powerful and attractive tool to study changes in brain functions as it is non-invasive, time-efficient, and task-free. Resting-state functional MRI allows us to measure the temporal correlation of the spontaneous, low-frequency (<0.1 Hz) blood-oxygenation-level-dependent (BOLD) signals across regions in the resting brain. Oscillations in the BOLD functional MRI signals are indicative of cortical dynamic self-organization and have been associated with the neural reorganization underlying cognitive and motor function during stroke recovery [11], [12]. Previous studies have demonstrated that there are overlapping networks between the resting-state functional MRI-derived motor network and those observed during motor imagery and motor execution functional MRI tasks [13], [14]. A growing number of studies have utilized neuroimaging methods to study the efficacy of BCI intervention in stroke recovery and found modulating changes in neuroplasticity and improvement in motor functions [14], [15], [16], [17], [18], [19]. In the present study, the aim was to use resting-state functional MRI to examine changes in neuroplasticity in whole-brain networks and to examine interactions between motor and non-motor cortical regions in chronic stroke participants following BCI intervention.

A whole-brain analysis resulting in high-dimensional data calls for the application of machine learning-based approaches which have become increasingly more integrated in neuroimaging research as they enable discovery of multivariate relationships beyond those identifiable by traditional univariate approaches. Several studies have underscored the utility of machine learning to not only differentiate among population groups [20], [21], [22], [23], [24], [25] but also make predictions about behavioral outcomes using regression models [26], [27], [28], all of which have advanced our understanding of altered brain functionalities associated with several neurological diseases. In the context of BCI systems, linear and non-linear machine learning classification algorithms [29], [30] including support vector machines [31], nearest

neighbors [32] and neural networks [33] have mainly been limited to improvement and optimization of the BCI2000 system from a system design perspective to make it more adaptive and user-friendly [34], [35], [36]. Relatively fewer studies have applied machine learning techniques to elucidate the therapeutic impact of BCI interventional therapy in stroke patients based on the dynamics of brain connectivity changes. Specifically, support vector machine-based classifiers have demonstrated the ability to not only draw a distinction between different classes but also provide insight into underlying features that lead to the separation between them [26], [27]. Given that the aim is to extensively investigate whole-brain effects of BCI intervention, a similar classification approach is befitting due to its efficiency in handling high-dimensional resting-state functional MRI data. Recent developments have brought deep learning approaches into view with involving applications in the field of medical imaging such as tissue/lesion/tumor segmentation [37], [38], image reconstruction/enhancement [39], [40] and population-based classification [41], [42]. The efficiency of deep learning algorithms, however, is highly dependent on samples available for training a reliable model. Thus, in the present study, supervised machine learning classifiers were adopted given the limited sample size.

With the above considerations in mind, the goal of this study is to identify the stage of therapy using whole brain resting-state functional MRI data in stroke participants undergoing EEG-based BCI intervention along with additional feedback provided by FES and TS. Changes in non-motor regions of the brain were analyzed in addition to well-studied motor regions following the intervention in chronic stroke participants. To this end, this was modeled as a classification problem of discriminating between pre-therapy and post-therapy stages of intervention. Specifically, it was illustrated using resting-state functional MRI that connectivity at the pre-therapy stage can be differentiated from that at post-therapy with reasonable accuracy. A support vector machine (SVM)-based machine learning classifier was employed to identify specific functional nodes and connections in the brain between the two stages. The significance of this study is four-fold: this study suggests that (i) a ten-minute task-free resting-state functional MRI scan could aid in identifying and tracking changes in functional connectivity in the brain over the course of the BCI interventional therapy;



(ii) SVM-based classification can automate the process of categorizing participants into pre-therapy or post-therapy stages and identify features discriminating between the stages of therapy; (iii) BCI therapy, targeted towards upper-extremity motor restoration, can promote recovery effects related to brain connectivity in both motor and non-motor networks; (iv) identification of specific neural changes that strengthen and weaken between stages of BCI-therapy could inform more tailored designs of BCI systems that facilitate stronger changes and suppress weaker changes to maximize the efficacy of this interventional therapy and improve outcomes for stroke survivors.

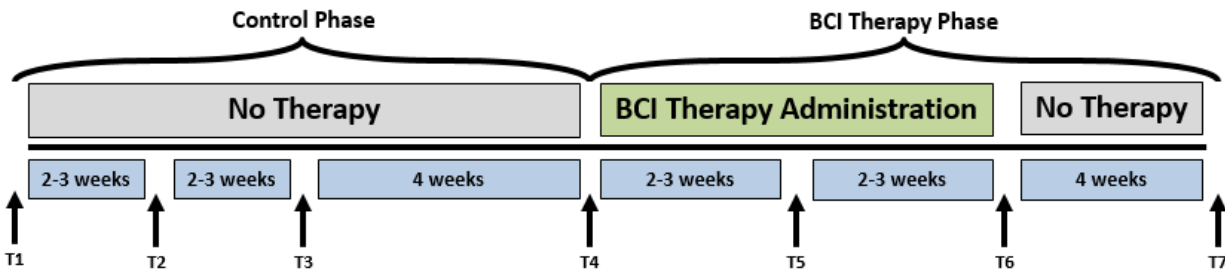
## 2. Methods

### 2.1 Study design

A permuted-block design [43] that accounted for participant characteristics such as gender, stroke chronicity, and severity of motor impairment was used to randomly assign participants to one of two groups: crossover control group and BCI Therapy group. The study paradigm is schematized in **Figure 2.1**. Ten participants in the BCI therapy group received interventional rehabilitation therapy and were scanned for MRI and resting-state functional MRI at four time points: pre-therapy (T4), mid-therapy (T5), immediately post-therapy (T6) and one month after completing the last BCI therapy (T7) as per the figure. Ten Participants in the crossover control group first received three functional assessments and MRI scans during the control phase in which no BCI therapy was administered (T1 through T3 in **Figure 2.1**), and their assessments were spaced at intervals similar to those given during the BCI therapy phase. Upon completion of the control phase of the study, the crossover control group “crossed over” into the BCI therapy phase of the study. For this study, participants from the crossover control group and the BCI therapy were combined ( $N = 20$ ), treated as a single sample group and studied at the pre-therapy (T4) and post-therapy (T6) stages to provide additional power to the analysis. Even though imaging data were collected at four distinct time-points, changes between pre-therapy and post-therapy were examined as maximal changes would be

expected to occur between these two time-points. Therefore, results from this study should be used to demonstrate proof-of-concept.

*Figure 2. 1. Study paradigm*



Note: The time-points at which neuroimaging data were collected are represented by: T1 = Control baseline 1, T2 = Control baseline 2, T3 = Control baseline 3, T4 = Therapy baseline T5 = Mid-therapy, T6 = Post-therapy, and T7 = One-month post-therapy. While the crossover control group completed visits T1 through T7, the BCI group completed visits T4 through T7 only.

## 2.2 Participants

All participants were recruited as part of an ongoing stroke rehabilitation study to investigate the effects of interventional therapy using an EEG-based BCI device targeting upper extremity motor function. The inclusion criteria for participation were: (1) at least 18 years of age; (2) persistent upper extremity motor impairment resulting from an ischemic or hemorrhagic stroke; (3) ability to provide written informed consent. Exclusion criteria consisted of: (1) concomitant neurodegenerative or other neurological disorders; (2) psychiatric disorders or cognitive deficits that would preclude a participant's ability to provide informed consent; (3) pregnant or likely to become pregnant during the study; (4) allergies to electrode gel, metal and/or surgical tape, contraindications to MRI; (5) concurrent treatment for infectious disease. The study was approved by the University of Wisconsin-Madison Health Sciences Institutional Review Board. All participants provided written informed consent prior to the start of the study. Participant age was reported corresponding to the first session of BCI therapy. This analysis was limited to chronic stroke participants only (time between stroke onset and the first session of BCI therapy > 6 months) since participants in the acute or sub-acute stages often exhibit spontaneous post-stroke recovery that may prove difficult to distinguish from the effects of BCI therapy. While stroke severity was evaluated based on NIH Stroke Scale

(NIHSS) score [44], the severity of motor impairment was assessed on the basis of standardized scores on the Action Research Arm Test [45], [46] and was dichotomized into severe and moderate. Group participant characteristics are summarized in **Table 2.1**.

**Table 2. 1. Study Sample Characteristics**

<b>Characteristic</b>	<b>Value</b>
Sample Size	20
Age (M $\pm$ SD)	62.4 $\pm$ 14.3 years
Gender (Male/Female)	12/8
Lesion Hemisphere (Left/Right)	8/12
Time Since Stroke (M $\pm$ SD)	37.6 $\pm$ 40.8 months
Stroke Severity (Severe/Moderate)	11/9

Note: M = mean; SD = standard deviation;

### **2.3 BCI interventional therapy**

The primary purpose of using BCI therapy in this work was to promote restorative function by providing neuromodulatory training with concurrent assistive stimulation that generated actual movement in the impaired upper limb. The BCI device was controlled by actual attempted movement of the user and not imagined movement. The attempted movement, in turn, generated neural activity, as recorded by EEG signals, which translated into computer-generated feedback in real time. Here a concise summary of the procedure for the BCI intervention is provided. The steps of intervention were consistent with those described in depth in prior studies [47], [48]. Neural activity was recorded using a 16-channel EEG cap (g.GAMMA cap, Cortech Solutions) and amplifier (Guger Technologies) and processed using BCI2000 software [49]. Movements of the impaired upper extremity were facilitated with two forms of external stimulation: TS (TDU 01.30, Wicab Inc.) and FES (LG-7500, LGMedSupply; Arduino 1.0.4). Three main components of the intervention included: (i) open-loop attempted movement without any feedback for determination of channels and frequencies for subsequent steps; (ii) closed-loop attempted movement with

visual feedback in the form of a cursor task that utilized EEG signals of the user in real time; and (iii) closed-loop attempted movement as in step (ii) with additional feedback in the form of TS and FES to the muscles of the impaired arm.

## **2.4 Data acquisition: neuroimaging data**

Structural MRI scans lasting about five minutes were acquired on 3T GE 750 scanners (GE Healthcare, Waukesha, WI) equipped with an eight-channel head coil. These were T1-weighted axial anatomical scans and were collected using FSPGR BRAVO sequence with the following specifications: TR = 8.132 ms, TE = 3.18 ms, TI = 450 ms over a  $256 \times 256$  matrix and 156 slices, flip angle =  $12^\circ$ , FOV = 25.6 cm, slice thickness = 1 mm. Ten-minute resting-state functional MRI were collected with participants lying in the scanner with their eyes closed. Participants were instructed to relax with their eyes closed while trying not to fall asleep during this scan. Resting-state functional MRI scans were obtained using single-shot echo-planar T2\*-weighted imaging with the following parameters: TR = 2.6 s, 231 time-points, TE = 22 ms, FOV = 22.4 cm, flip angle =  $60^\circ$ , voxel dimensions  $3.5 \times 3.5 \times 3.5 \text{ mm}^3$  and 40 slices.

## **2.5 Individual participant analysis**

### **2.5.1 Data preprocessing**

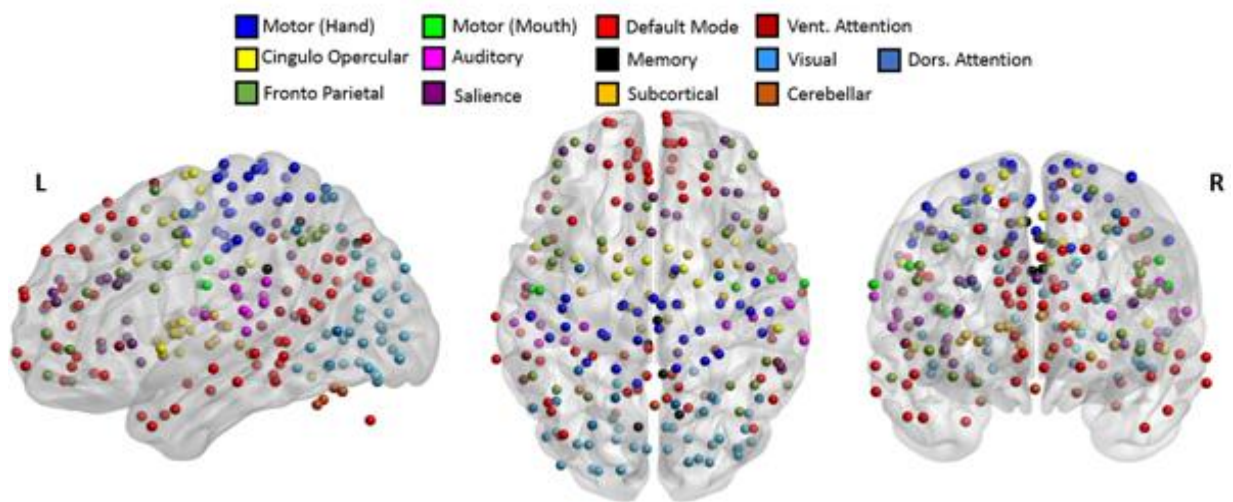
All scans were inspected visually to ensure they were free of any apparent artifacts. Resting-state functional MRI data were processed using Analysis of Functional NeuroImaging (AFNI) [50] software. Functional scans were despiked, slice time corrected, motion corrected, aligned with the anatomical scan, normalized to the standard MNI (Montreal Neurological Institute) space using the T1 scan, resampled to  $3.5 \text{ mm}^3$ , and spatially smoothed with a 4-mm full-width-half-maximum Gaussian kernel. Motion censoring (per TR motion  $>1 \text{ mm}$  or  $1^\circ$ ), regression of white matter and cerebrospinal fluid signals, and bandpass frequency filtering were performed simultaneously in one regression model. The bandpass filtering was focused to

the typical low oscillation fluctuations within 0.01-0.1 Hz. Global signal regression was omitted due to ongoing controversy in the literature associated with its use [51].

### 2.5.2 Seed-based functional connectivity

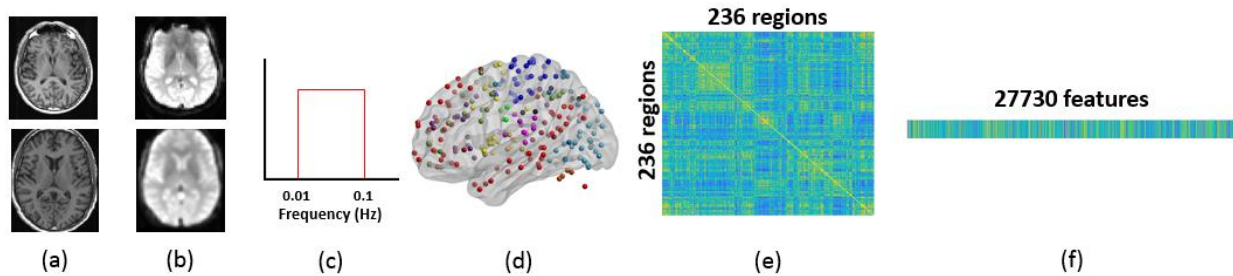
Based on a previous study [52], 236 seed regions of interest (ROI) spanning brain regions from 13 distinct networks were selected. This seed template provides full coverage of various motor and non-motor brain regions and has been utilized to study functional reorganization of the brain in healthy participants. The regions are depicted in **Figure 2.2**, as per the standard brain MNI coordinates. Spherical seeds of 5 mm radius each were created for each participant. This seed template was applied to the spatially normalized, smoothed, and filtered residuals of the resting data and BOLD time series was extracted at each of the 236 seed regions. A correlation matrix of size  $236 \times 236$  was generated by temporally correlating time series from all pairs of seeds. Of the 55696 correlation coefficients generated, 27730  $\left(= \frac{236 \times (236 - 1)}{2}\right)$  unique coefficients were retained for analysis and the duplicates were discarded. The unique correlation coefficients were computed from data at the pre- and post-therapy stages and used as input features for the discrimination between the stages. The methodology at single-participant level is outlined in **Figure 2.3**.

*Figure 2. 2. Seed regions included in the analysis*



Note: The 236 seeds regions involving motor and non-motor regions include 13 major brain networks color coded and visualized using BrainNet Viewer [53]. The seed regions falling outside the template of cerebrum were part of the cerebellum.

**Figure 2. 3. Methodology for single-participant analysis**



Note: (a) raw structural T1 scan (top) was preprocessed and spatially normalized to MNI space (bottom); (b) raw functional scan (top) was preprocessed up to smoothing (bottom); (c) smoothed functional MRI was temporally filtered to obtain the low frequency oscillations within the range of 0.01-0.1 Hz using a bandpass filter; (d) 236 seeds comprising of 13 major brain networks were used to extract BOLD time courses at each seed region; (e)  $236 \times 236$  FC matrix was computed using the BOLD time courses; (f) unique pairwise correlations contained in the lower triangle of the FC matrix were extracted and vectorized into a 27730-dimensional vector.

## 2.6 Group Level Analysis

Applications of classification using machine learning algorithms such as SVM on resting-state functional MRI have been demonstrated in multiple studies [26], [27]. For the purpose of this study, similar strategy was adopted, i.e. a binary linear-kernel SVM was applied to FC in order to classify between the two classes, namely pre-therapy and post-therapy. The FC data for all participants were aggregated and the steps described as follows were implemented.

### 2.6.1 Outlier removal

It is acknowledged that with a limited sample size, the data could be skewed due to the presence of outliers; therefore, possible outlier features were detected and removed from the data set. To this end, a median absolute deviation (MAD) [54] method detected any value that is more than three scaled median absolute deviations away from the median in a given feature which is deemed an outlier. This was repeated for each feature within the pre-therapy stage and post-therapy stage. The features containing these outliers were eliminated, saving only common features across pre- and post-therapy.

### 2.6.2 Feature selection and transformation

The FC per participant consisted of 27730 coefficients resulting in a high-dimensional dataset. Drawing useful conclusions based on a reasonable classifier is incumbent upon selecting meaningful and important features. One way to achieve this is by means of dimension reduction. Given that a large number of features with a small sample size can result in overfitting to noise, a feature selection step followed by a feature transformation step was applied. The feature selection was a preprocessing step to select a subset of 27730 features using a univariate paired t-test between the features of pre-therapy and post-therapy stages. Features were tested for normality using the Kolmogorov-Smirnov test [55] and a subset of normal features was selected on the basis of the  $p$ -value for each individual feature that indicated its effectiveness in the separation between the two aforementioned stages. However, the filtered features were still high-dimensional and could easily lead to overfitting. Therefore, the reduced data obtained from the previous step were transformed to a lower dimensional space using principal component analysis (PCA) [56], [57]. A PCA-based feature transformation was suitably chosen as it assumes that data can consist of correlated variables (features) and the redundancy can be simplified by forming an uncorrelated basis composed of the principal components which is low-dimensional and accounts for a large fraction of variance in the original data. Each principal component is simply a linear combination of the original FC features. PCA is based upon computation of covariance matrix of the raw data. Only mean centering was applied to the raw data prior to application of PCA. Variance was not standardized as it can change the covariance matrix and lead to misleading principal components. The first few principal component scores were selected based on the amount of variance accounted for in the raw data and were used in the classification step.

### 2.6.3 Classification

Once the appropriate number of principal components was extracted in the feature selection and transformation step, classification between the pre-therapy and post-therapy stages was performed using the learned principal component-based features. The inputs to the classifier were no longer the raw FC coefficients. Instead, the principal component scores, each of which corresponded to a linear combination

of multiple FC features, were fed into the classifier as features. Additionally, since SVM-based classifiers do not assume data to be normally distributed, the traditional Fisher z-transformation was not necessary. However, the principal component scores were scaled and standardized so that each component score had the same mean and variance to avoid some features from potentially dominating others due to large magnitude. This was realized by mean centering and scaling by the standard deviation of each component score. A binary classifier was trained on these features and cross-validated on an out-of-sample participant. To allow for more straightforward interpretation of results, a linear-kernel SVM was applied due to the advantage of ease of interpretation of results. Additionally, the choice of a linear-kernel classifier was supported by the linear separability in the data. As observed in three-dimensional space, the principal component features are almost linearly separable. Thus, there is a likelihood that the two classes are linearly separable in higher dimensions which are used for classification [58].

#### **2.6.4 Cross-validation**

A leave-one-out cross-validation (LOOCV) method [59] was adopted to estimate classifier performance as it provides an approximation of the test error with lower bias and is more suitable for a dataset with a small sample size such as here. Since this analysis followed a within-participant design, LOOCV by participant was performed to avoid introducing possible ‘twinning’ bias. This means that the data consisting of 40 observations (pre-therapy FC and post-therapy FC from 20 participants) were subdivided into 20 folds such that each fold comprised of pre-therapy FC and post-therapy FC data from a single participant. The classifier was trained using features from 19 folds (equivalent to 38 observations from pre- and post-stages of 19 participants) and tested on the left-out fold (2 observations from pre- and post-stages of 1 participant). This was repeated 20 times such that data from each participant was left out once while a model was generated using the rest of the data. The performance of the model was assessed by averaging the accuracies over all iterations.



### **2.6.5 Model parameter optimization**

To achieve high classification accuracy, the SVM classifier relies on both feature selection and learning optimized model parameters. Specifically, the misclassification cost and kernel scale parameters of the classifier were optimized with a Bayesian optimization [60] approach. By minimizing the cross-validation error over a range of values for 30 iterations, the optimal parameter values were obtained that further improve the classification performance.

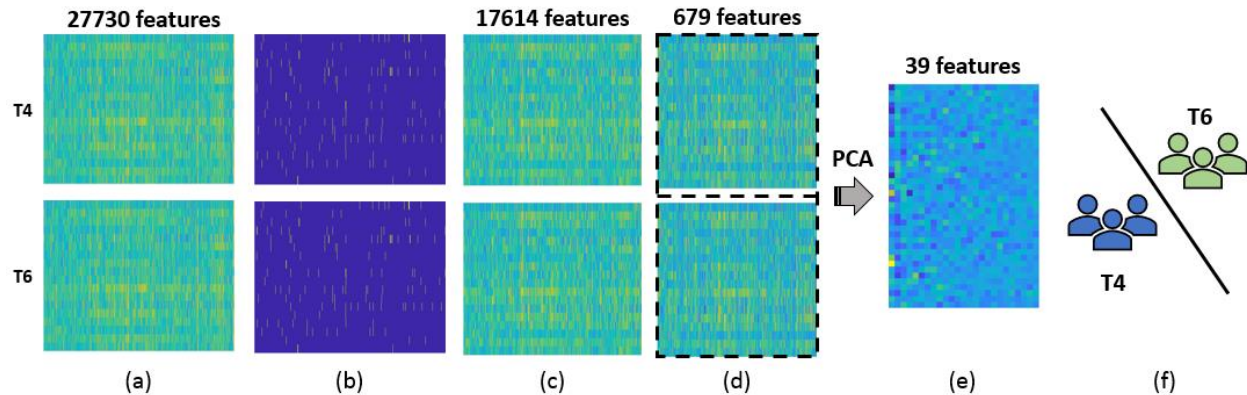
### **2.6.6 Feature contribution**

Once a model was learned with the optimal parameters, the use of a linear-kernel SVM allowed understanding of underlying discriminatory brain connections. The PCA feature transformation yielded linear coefficients that weigh features and the importance of each feature was dependent upon the magnitude of the associated coefficient.

### **2.6.7 Seed contribution**

Based upon the feature weights obtained for each of the discriminating functional connections, seed region weights were calculated for individual brain regions. This was achieved by halving the feature weight of each functional connection and assigning this value to the two seeds involved [24]. A cumulative measure of weight corresponding to each seed was computed by averaging the half-weights across all discriminating connections.

**Figure 2. 4. Methodology for group-level analysis**



Note: (a) vectorized form of FC matrix for each participant aggregated for T4, i.e. pre-therapy and T6, i.e. post-therapy time points. Each group had 20 participants with 27730-dimensional features; (b) outliers (marked in yellow) at pre- and post-therapy were identified using MAD approach; (c) reduced FC matrix after cumulative outliers were removed, i.e. each stage consisted of 20 participants and 17614 features; (d) 679 features that were significantly different between pre- and post-therapy stages as identified by a paired t-test were retained and data across the two stages were combined together for a feature transformation step; (e) feature transformation using PCA was performed that resulted in data with 40 participants and 39 low-dimensional principal components features. Of them 25 features accounted for more than 85% variance and were used as final features for classification; (f) the selected features were fed to the binary SVM classifier that labels each test participant to either pre-therapy or post-therapy stage using LOOCV.

### 2.6.8 Overview of methodology

Overall, a classification model using FC was learned and optimized, and the contributing FC features and ROIs that provided the maximum discriminative power based on cross-validation performance were identified. All computations were carried out using the Statistics and Machine Learning Toolbox in MATLAB R2017a (The MathWorks, Inc., Natick, Massachusetts, United States). The group-level analysis pipeline is illustrated in **Figure 2.4**.

### 3. Results

#### 3.1 Performance of Classifier

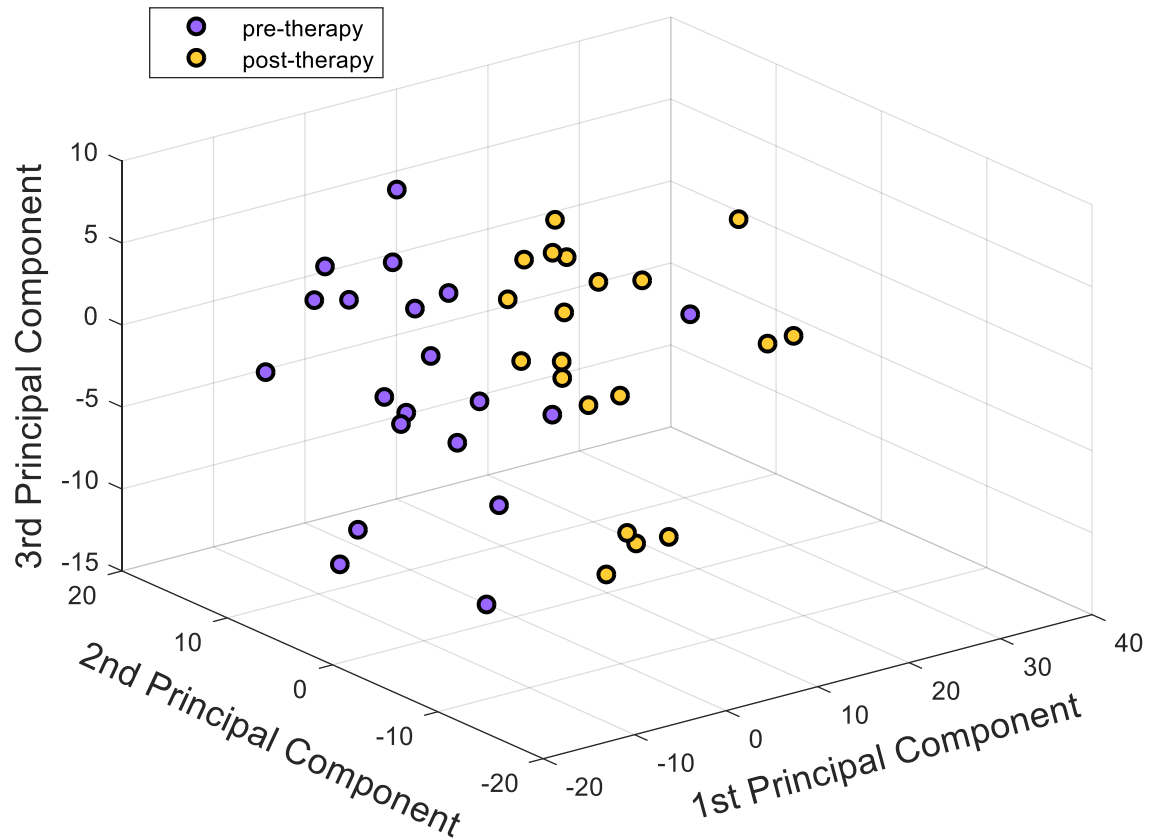
##### 3.1.1 Outlier removal

Each of the 27730 features was tested for the presence of outliers within the pre- and post-therapy stages separately. Features were removed if they contained values that were more than three scaled deviations from the median. MAD was chosen as it is more robust in comparison to the standard deviation measure. Outliers constituted 21.99% of the features in the pre-therapy stage and 19.53% of the features in the post-therapy stage. After outliers across both time-points were removed, 17,614 features were retained in each class.

##### 3.1.2 Feature selection and transformation

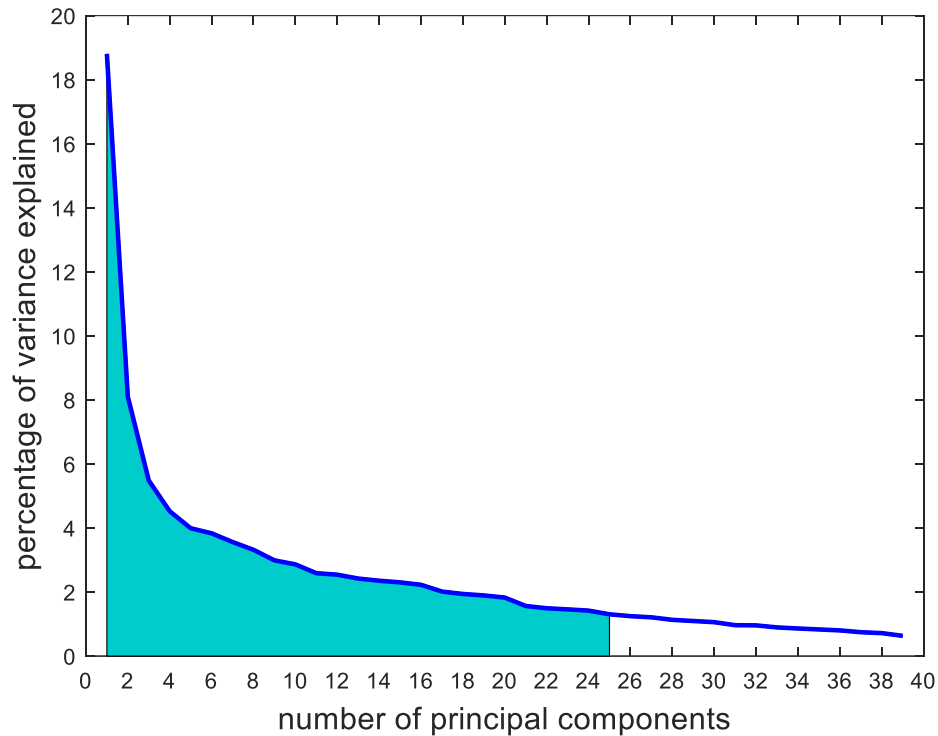
The 17614 features remaining after outlier elimination were used as input to the feature selection step. Each feature was tested for normality and the univariate paired t-test resulted in 679 features that were significantly different between the two stages. During feature transformation using PCA, the number of principal components was determined to be the smaller of these two: number of samples - 1 or number of input features. Thus, application of PCA resulted in 39 principal components in this case, each of which was uncorrelated to each other and was realized as a linear combination of the 679 input features. Of the 39 components, 25 components were able to account for over 85% of the variance in the data and were fed into the classifier. Due to lack of visualization tools in 25 dimensions, a simpler plot with the first three components was generated as displayed in **Figure 2.5**. The separation observed in the visualization suggests that PCA was able to build useful low-dimensional features that can help in differentiating between the two stages. For classification, the chosen number of components was based on the variance explained by them as shown in **Figure 2.6**. An account of number of features retained at each step of processing from original space (i.e. features are FC coefficients) to reduced space (i.e. features are principal components) is provided in **Table 2.2**.

*Figure 2. 5. Principal component analysis (PCA) on FC data*



**Note:** First three principal components corresponding to pre-therapy FC and post-therapy FC for all participants were visualized. Each point in the 3-D plot corresponds to a participant. There appeared to be an almost clear separation between the two stages just with three principal components. Adding higher number of components better explained the variance in the data. The present analysis used 25 components that explained over 85% of the variance in the dataset.

**Figure 2. 6. Variance explained by PCA**



Note: The principal components are arranged in order of importance so that the first component accounts for the largest proportion of variance in the FC data. Of the 39 principal components, 25 were chosen as marked in the graph as they cumulatively explained over 85% of the variance in the data, represented by the shaded area under the curve.

**Table 2. 2. Step-by-step feature selection procedure**

<b>Analysis Step</b>	<b>Number of Features</b>	<b>Feature Space</b>
Original features	27730	FC
After outlier removal	17614	FC
After univariate filtering	679	FC
After principal component analysis	39	reduced
Chosen principal components for classification	25	reduced

Note: The number of features derived from the FC data utilized in various steps of the analysis. The feature space indicates whether the corresponding features were measures of functional connectivity, i.e. FC space or principal components comprised of linear combination of multiple FC features, i.e. reduced space.

### 3.1.3 Cross-validation

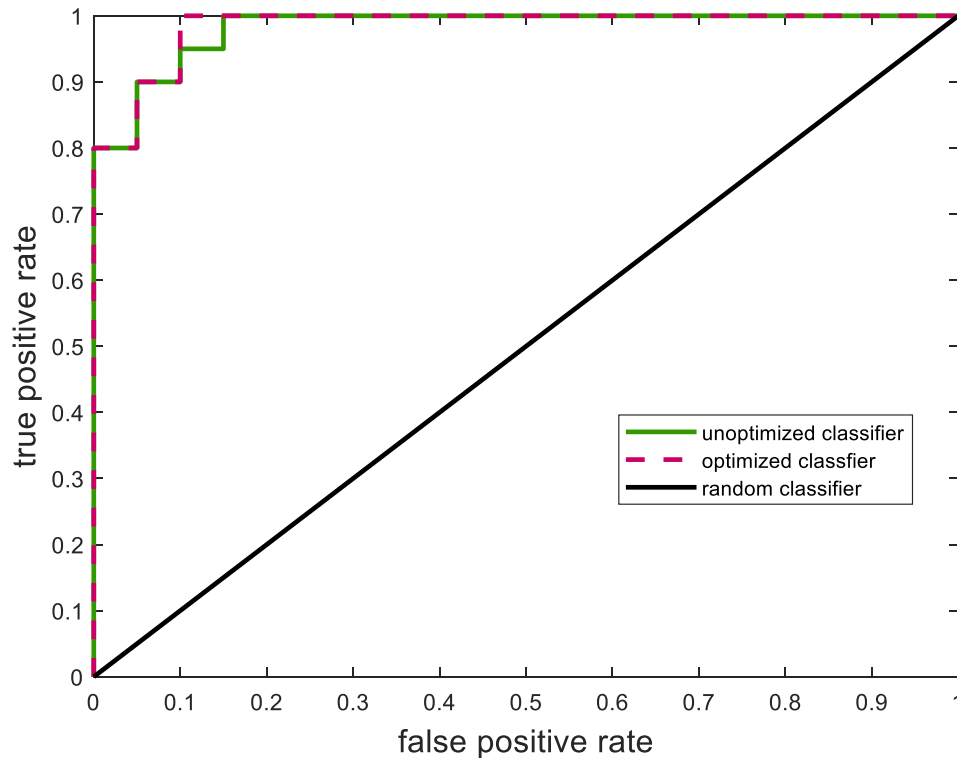
A binary SVM classifier was built using 25 principal component features. Classification performance was cross-validated using the LOOCV method and was used to assess and compare results as quantified in **Table 2.3**. The accuracy of LOOCV represents the percentage of individual samples that were correctly classified when left out. Since accuracy is a single-point statistic, the results were further broken down into a confusion matrix metric to understand the bias of the classifier towards each class, if any. In addition, multiple performance evaluation metrics were evaluated such as specificity, sensitivity, and area under the curve. The receiver operator curve (ROC) plotted in **Figure 2.7** indicated that the classifiers developed here have superior performance as compared to a random classifier.

*Table 2. 3. Classification performance evaluation*

<b>Metric</b>	<b>Performance without Optimization</b>			<b>Performance with Optimization</b>		
LOOCV Accuracy	90 %			92.5 %		
Confusion Matrix		<b>Pre</b>	<b>Post</b>		<b>Pre</b>	<b>Post</b>
	<b>Pre</b>	18	2	<b>Pre</b>	18	2
	<b>Post</b>	2	18	<b>Post</b>	1	19
Specificity	0.90			0.95		
Sensitivity	0.90			0.90		
Area under the Curve	0.9825			0.9850		
Misclassification Cost	1 (default)			0.0010		
Kernel Scale	1 (default)			0.0011		

Note: Overall comparative results obtained from LOOCV of binary SVM classifier. The rows of confusion matrix represent the actual class while the columns show the predicted class.

*Figure 2. 7. The ROC for the learned SVM classifier*



Note: The ROC for the learned SVM classifier was compared to that of a random classifier. The SVM classifier with optimized model parameters showed the best performance. The area under the curves for unoptimized and optimized SVM are specified in **Table 2.3**.

### 3.1.4 Model parameter optimization

The optimal values of classifier parameters, i.e., the misclassification cost and scaling factor for the linear kernel were generated by the Bayesian approach for each classifier and are listed in **Table 2.3**. As observed, optimization of the model parameters improves the classifier performance further. This is also reflected in the ROC plot in **Figure 2.7**.

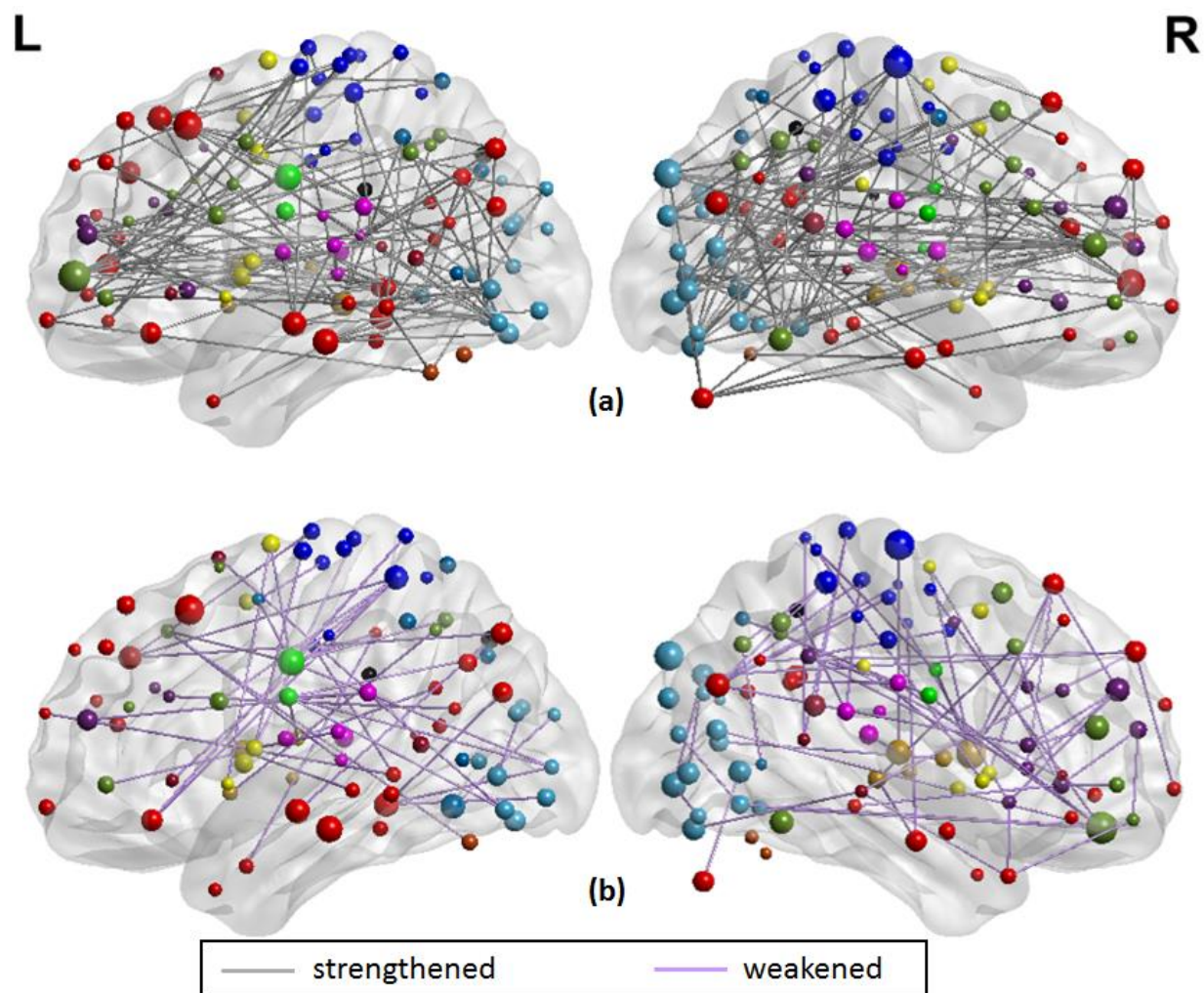
### 3.2 Strengthened and weakened functional changes as discriminating features

From the evaluation of classification performance, it is possible to extract the features that were involved in classification, as well as the importance of each feature in making the distinction between classes. Here, the objective was to identify discriminating features between groups that strengthened from pre-therapy to



post-therapy and those that weakened from pre-therapy to post-therapy. All changes in FC were assessed in terms of group means. Considering the 679 features that went into the final classification model, the distribution of features is presented in **Table 2.4**. Stronger connections outnumbered weaker connections in discriminating between the two stages of therapy both in the motor and non-motor networks. Individual functional changes that strengthened and weakened over time are visualized in **Figure 2.8**.

*Figure 2. 8. Visualization of discriminatory functional connections*



Note: (a) 441 strengthening functional connections and (b) 238 weakening functional connections. The overall number of connections involved in the motor and non-motor networks can be found in **Table 2.4**. All brain visualizations were performed using BrainNet Viewer Toolbox [53].

**Table 2. 4. Overall discriminating features**

	<b>Motor</b>	<b>Non-Motor</b>	<b>Total</b>
Strengthened	105	336	441
Weakened	71	167	238
Overall	176	503	679

Note: Breakdown of discriminating features into neural connections that strengthened and weakened from pre-therapy to post-therapy are shown for motor as well as non-motor regions. The colors correspond to the edges in **Figure 2.8**.

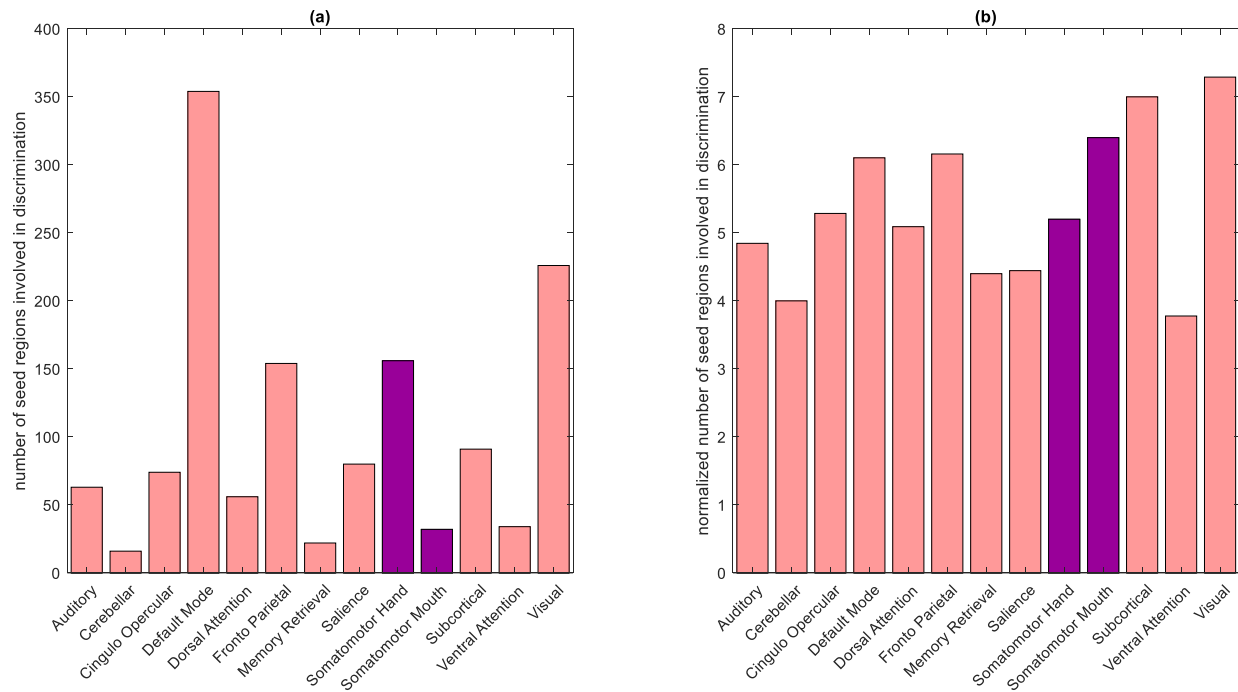
### 3.3 Discriminating seed regions

Motor as well as non-motor regions were involved in differentiating between pre- and post-therapy. Among the 679 total input features, the distribution of frequency of involved seed regions by network is presented in **Figure 2.9**. As observed, seed regions from all major motor and non-motor networks showed involvement in the discriminating features. From **Figure 2.9 (a)**, it appeared that the default mode network had the highest number of involved regions; however, the distribution of number of seeds across the networks was not equal. The number of discriminating features was normalized by the number of seeds available within each network and plotted in **Figure 2.9 (b)**. In particular, networks that exhibited greater normalized involvement included regions from visual, subcortical, fronto-parietal task control, cingulo-opercular task control, default mode, and hand-mouth motor networks.

In addition to assessing the frequency of involvement, the seeds were also assigned weights to study the importance of each seed region based on the coefficients of the principle components. The coefficient corresponding to each feature or connection was halved and assigned to the involved seed regions as per prior work by Vergun et al. [27]. This was repeated across all 25 principal components, and the average of those weights determined the final weight of the seed regions. The weighted seed regions are shown in

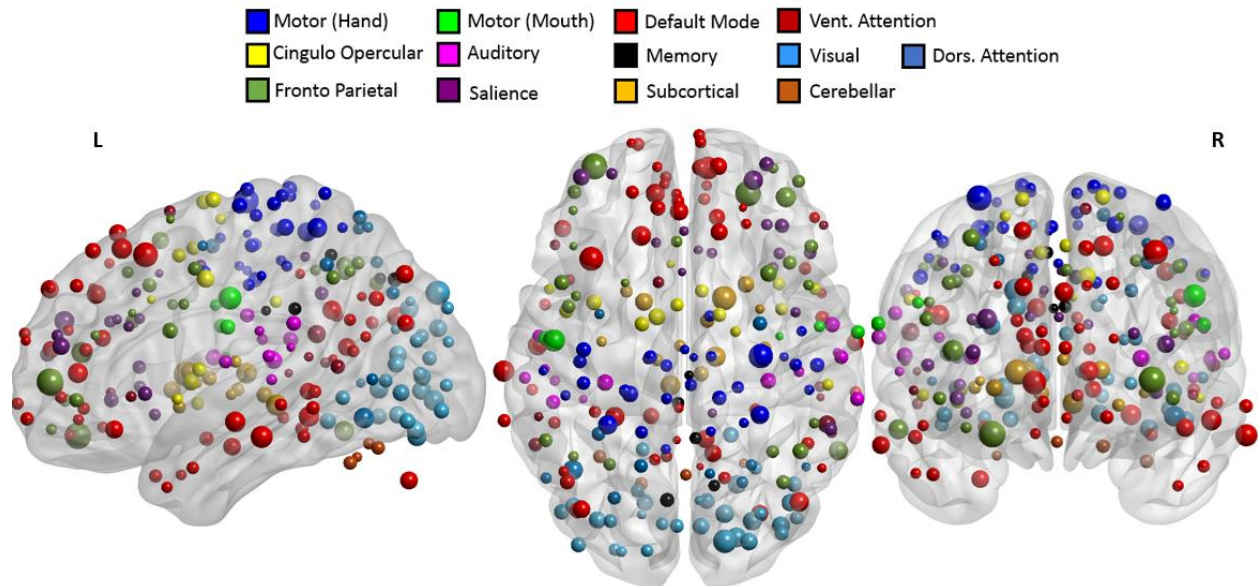
**Figure 2.10.** The highly-weighted regions identified are known to be part of the fronto-parietal task control, hand motor, subcortical, visual, and default mode networks.

**Figure 2. 9. Distribution of discriminating features**



Note: Number of discriminating connections per network is plotted below: (a) shows the distribution of involvement of various networks in discriminating features; (b) shows the involvement of various networks when normalized with respect to the number of seeds found in each network. The two networks primarily associated with motor functions are highlighted.

*Figure 2. 10. Involvement of seed regions in classification*



Note: Involved seed regions were weighted as per their contribution in classification. The size of each seed was directly proportional to assigned weight. The top weighted seeds belonged to fronto-parietal, hand motor, default mode and visual networks.

## 4. Discussion

### 4.1 Resting-state functional MRI as a tool to track stroke recovery

Results from this study highlight the utility of resting-state functional MRI as a tool to track changes in the brain during stroke recovery through rehabilitative therapy. Resting-state functional MRI is particularly attractive because it only requires about ten minutes for acquisition and is task-free. These analyses suggest that a similar analysis might be extendable to incorporate more than one time-point to gain deeper insight into the recovery process.

### 4.2 Large-scale impact of BCI stroke rehabilitation

The majority of BCI-aided interventional therapy programs are targeted at the recovery of a particular impairment, such as motor functions, as was the case for participants studied in this cohort. The findings, here, showed that such therapy can impact not only motor but also non-motor networks in the brain. A

greater number of neural connections grew stronger than ones that grew weaker over time over the course of this therapy. These results can better guide the design and implementation of BCI systems to facilitate greater changes that strengthened in patients with stroke.

#### **4.3 Machine learning as a tool to identify stage of therapy and relevant functional differences**

As evident from the confusion matrix in **Table 2.3**, it is possible to differentiate between the two stages of BCI therapy with high cross-validation accuracy. High-dimensional FC extracted from whole brain analysis was downsampled by PCA-based feature transformation that helped elucidate differences across stages of therapy regarding underlying brain connections involved. In comparison to a random classifier that is 50% accurate, the machine learning classifier developed here using low-dimensional features derived from FC performed much better with over 90% accuracy. These results indicate that with a large sample size, SVM classifier could be trained on FC data to categorize a new participant into either the pre-therapy or post-therapy stage of the recovery process by identifying the most discriminative FC features.

#### **4.4 The bigger picture**

The most common rehabilitative clinical applications of BCI systems [61] include speech [62], [63] and motor [64], [65], [66] rehabilitation. Fewer studies have adopted the BCI paradigm for cognitive rehabilitation [67]. Most of these deal with improving a specific function and study changes occurring in the associated limited brain regions. The motor regions that contributed the most to classification were found over the bilateral precentral gyrus which forms the core of the primary motor cortex. This is in alignment with findings that focus specifically on post-stroke changes in the motor network [14], [17], [68]. In addition, the current study expands the knowledge further by identifying brain changes that occurred in the non-motor areas involving fronto-parietal task control, default mode, and visual networks even though the BCI therapy was primarily targeted at the recovery of motor function. This demonstrates the importance of comprehending the gross impact of BCI therapy on a whole-brain level. Additionally, since the BCI

system is adaptive in nature [49], the knowledge about functional changes that are strengthening and/or weakening as a result of this therapy might point toward a better design of the intervention. Maladaptive changes caused by the compensatory activity of the unaffected side has been shown to prevent recovery on the affected side [69]. One direction to harness this information could involve regulating the way EEG signals are processed within BCI device. The signal processing module of the BCI system that takes into account the signal generated at each output channel could be modulated so as to maximize the changes that grew stronger and minimize the changes that grew weaker, thus tailoring the therapy for each user.

#### **4.5 Limitations**

The results presented here show that standard machine learning approach has the potential to track recovery through BCI therapy. However, the study was constrained in terms of the sample size since conventional machine learning analysis relies on training on a large dataset so as to have greater power of generalizability. Although this study attempted to include a comparable number of participants of both genders, different lesion locations and volumes, and differing levels of stroke severity, heterogeneity in any of these factors might be relevant considerations for future analysis as they could potentially influence the results. In this analysis, the number of samples available for training impacted the number of principal components (rank of covariance matrix) evaluated in the feature transformation step using PCA. Higher number of samples would provide higher degree of freedom. With continuing recruitment, using a larger and more homogeneous participant cohort would allow for more generalizable conclusions. The definition of FC was based upon Pearson's correlation, which is a classical approach and accounts for linear dynamics among the BOLD signals. Recent studies such as that conducted by Smith et al. [70] provide alternate definitions of FC such as mutual information, cosine similarity, and dynamic time warping; therefore, applying different definitions of seeds and FC could impact the underlying discriminatory features in classification. The notion of stronger and weaker changes in FC in this study might not reflect adaptive and maladaptive changes in behavioral aspects even though an overall improvement at the group-level in measures such as

the Action Research Arm Test (mean change = 0.85) and domains of the Stroke Impact Scale (mean change in hand function = 0.75; mean change in physical strength = 0.13) from pre-therapy to post-therapy was observed.

#### **4.6 Future scope**

The ongoing recruitment for this study offers a broad future scope to incorporate more participants that can form a more homogenous cohort. Comparison between stroke participants undergoing rehabilitative therapy and healthy participants undergoing the same therapy will allow comprehension of recovery specifically associated with the event of a stroke. An analysis similar to the current study could be extended to incorporate other time-points during the BCI therapy paradigm, such as the mid-therapy (T5) and one-month post-therapy (T7) time points. Aside from resting-state functional MRI, alternative neuroimaging methods such as diffusion tensor imaging, task-functional MRI, arterial spin labeling, and perfusion. imaging capture complementary information and could be used to analyze and compare classification performance.

### **5. Conclusion**

PCA-based feature transformation coupled with SVM classifier was utilized to discriminate stroke participants by stage of BCI intervention (i.e. the pre-therapy stage to the post-therapy stage) on the basis of FC in both motor and non-motor regions. The findings from this study can be summarized as follows: (i) data from a task-free resting-state functional MRI can help identify changes across stages of the BCI-aided stroke intervention and hence, has the potential to track stroke recovery; (ii) using a machine learning SVM classifier facilitates automation of discrimination between stages of therapy with a reasonably high accuracy and examination of discriminating connections; (iii) both motor and non-motor regions of the brain undergo reorganization during this intervention. Higher number of strengthening functional changes

in comparison to the ones weakening between pre- and post-therapy suggests a greater overall positive impact of BCI intervention on stroke recovery at a whole-brain level; (iv) the capability of delineating such specific changes holds promise for better design of the BCI therapy that could incorporate the information by reinforcing stronger changes while suppressing weaker changes.



## References

- [1] C. Bütetfisch, H. Hummelsheim, P. Denzler, K.-H. Mauritz, Repetitive training of isolated movements improves the outcome of motor rehabilitation of the centrally paretic hand. *Journal of the neurological sciences* 130 (1995) 59-68.
- [2] N.F. Gordon, M. Gulanick, F. Costa, G. Fletcher, B.A. Franklin, E.J. Roth, T. Shephard, Physical activity and exercise recommendations for stroke survivors. *Stroke* 35 (2004) 1230-1240.
- [3] G. Kwakkel, B.J. Kollen, H.I. Krebs, Effects of robot-assisted therapy on upper limb recovery after stroke: a systematic review. *Neurorehabilitation and neural repair* 22 (2008) 111-121.
- [4] M. Corti, C. Patten, W. Triggs, Repetitive transcranial magnetic stimulation of motor cortex after stroke: a focused review. *American journal of physical medicine & rehabilitation* 91 (2012) 254-270.
- [5] K.R. Lohse, C.G. Hilderman, K.L. Cheung, S. Tatla, H.M. Van der Loos, Virtual reality therapy for adults post-stroke: a systematic review and meta-analysis exploring virtual environments and commercial games in therapy. *PLoS one* 9 (2014) e93318.
- [6] S. Silvoni, A. Ramos-Murguialday, M. Cavinato, C. Volpato, G. Cisotto, A. Turolla, F. Piccione, N. Birbaumer, Brain-computer interface in stroke: a review of progress. *Clinical EEG and Neuroscience* 42 (2011) 245-252.
- [7] E. Felton, R. Radwin, J. Wilson, J. Williams, Evaluation of a modified Fitts law brain-computer interface target acquisition task in able and motor disabled individuals. *Journal of neural engineering* 6 (2009) 056002.
- [8] J. De Kroon, J. Van der Lee, M. IJzerman, G. Lankhorst, Therapeutic electrical stimulation to improve motor control and functional abilities of the upper extremity after stroke: a systematic review. *Clinical rehabilitation* 16 (2002) 350-360.
- [9] J.A. Wilson, L.M. Walton, M. Tyler, J. Williams, Lingual electrotactile stimulation as an alternative sensory feedback pathway for brain-computer interface applications. *Journal of neural engineering* 9 (2012) 045007.
- [10] M.P. Van Den Heuvel, H.E.H. Pol, Exploring the brain network: a review on resting-state functional MRI functional connectivity. *European neuropsychopharmacology* 20 (2010) 519-534.
- [11] S. Bajaj, A.J. Butler, D. Drake, M. Dhamala, Functional organization and restoration of the brain motor-execution network after stroke and rehabilitation. *Frontiers in human neuroscience* 9 (2015) 173.
- [12] M.H. Lee, C.D. Smyser, J.S. Shimony, Resting-state functional MRI: a review of methods and clinical applications. *American Journal of Neuroradiology* 34 (2013) 1866-1872.
- [13] C. Grefkes, S.B. Eickhoff, D.A. Nowak, M. Dafotakis, G.R. Fink, Dynamic intra-and interhemispheric interactions during unilateral and bilateral hand movements assessed with functional MRI and DCM. *Neuroimage* 41 (2008) 1382-1394.
- [14] V.A. Nair, B.M. Young, Z. Nigogosyan, A. Remsick, S. Weber, K. Diffie, L. Walton, M. Tyler, J. Sattin, D.F. Edwards, Resting-state Functional Connectivity Changes After Stroke Rehabilitation Using Closed Loop Neurofeedback, *Am Heart Assoc*, 2015.
- [15] S.R. Soekadar, N. Birbaumer, M.W. Slutzky, L.G. Cohen, Brain-machine interfaces in neurorehabilitation of stroke. *Neurobiology of disease* 83 (2015) 172-179.
- [16] B. Várkuti, C. Guan, Y. Pan, K.S. Phua, K.K. Ang, C.W.K. Kuah, K. Chua, B.T. Ang, N. Birbaumer, R. Sitaram, Resting state changes in functional connectivity correlate with movement recovery for BCI and robot-assisted upper-extremity training after stroke. *Neurorehabilitation and Neural Repair* 27 (2013) 53-62.

- [17] B.M. Young, Z. Nigogosyan, L.M. Walton, J. Song, V.A. Nair, S.W. Grogan, M.E. Tyler, D.F. Edwards, K. Caldera, J.A. Sattin, Changes in functional brain organization and behavioral correlations after rehabilitative therapy using a brain-computer interface. (2014).
- [18] M.G. Di Bono, M. Zorzi, Decoding Cognitive States from functional MRI Data Using Support Vector Regression. *PsychNology Journal* 6 (2008) 189-201.
- [19] J. Song, B.M. Young, Z. Nigogosyan, L.M. Walton, V.A. Nair, S.W. Grogan, M.E. Tyler, D. Farrar-Edwards, K.E. Caldera, J.A. Sattin, Characterizing relationships of DTI, functional MRI, and motor recovery in stroke rehabilitation utilizing brain-computer interface technology. *Frontiers in neuroengineering* 7 (2014).
- [20] X. Ding, Y. Yang, E.A. Stein, T.J. Ross, Combining Multiple Resting-State functional MRI Features during Classification: Optimized Frameworks and Their Application to Nicotine Addiction. *Frontiers in human neuroscience* 11 (2017) 362.
- [21] Z. Dai, C. Yan, Z. Wang, J. Wang, M. Xia, K. Li, Y. He, Discriminative analysis of early Alzheimer's disease using multi-modal imaging and multi-level characterization with multi-classifier (M3). *Neuroimage* 59 (2012) 2187-2195.
- [22] P. Fergus, A. Hussain, D. Hignett, D. Al-Jumeily, K. Abdel-Aziz, H. Hamdan, A machine learning system for automated whole-brain seizure detection. *Applied Computing and Informatics* 12 (2016) 70-89.
- [23] A. Khazaee, A. Ebrahimzadeh, A. Babajani-Feremi, Application of advanced machine learning methods on resting-state functional MRI network for identification of mild cognitive impairment and Alzheimer's disease. *Brain imaging and behavior* 10 (2016) 799-817.
- [24] T.B. Meier, A.S. Desphande, S. Vergun, V.A. Nair, J. Song, B.B. Biswal, M.E. Meyerand, R.M. Birn, V. Prabhakaran, Support vector machine classification and characterization of age-related reorganization of functional brain networks. *Neuroimage* 60 (2012) 601-613.
- [25] A.K. Rehme, L.J. Volz, D.-L. Feis, I. Bomilcar-Focke, T. Liebig, S.B. Eickhoff, G.R. Fink, C. Grefkes, Identifying neuroimaging markers of motor disability in acute stroke by machine learning techniques. *Cerebral cortex* 25 (2014) 3046-3056.
- [26] N.U. Dosenbach, B. Nardos, A.L. Cohen, D.A. Fair, J.D. Power, J.A. Church, S.M. Nelson, G.S. Wig, A.C. Vogel, C.N. Lessov-Schlaggar, Prediction of individual brain maturity using functional MRI. *Science* 329 (2010) 1358-1361.
- [27] S. Vergun, A.S. Deshpande, T.B. Meier, J. Song, D.L. Tudorascu, V.A. Nair, V. Singh, B.B. Biswal, M.E. Meyerand, R.M. Birn, Characterizing functional connectivity differences in aging adults using machine learning on resting state functional MRI data. *Frontiers in computational neuroscience* 7 (2013).
- [28] R. Mohanty, A. Sinha, A. Remsik, J. Allen, V. Nair, K. Caldera, J. Sattin, D. Edwards, J.C. Williams, V. Prabhakaran, Machine Learning-Based Prediction of Changes in Behavioral Outcomes Using Functional Connectivity and Clinical Measures in Brain-Computer Interface Stroke Rehabilitation, *International Conference on Augmented Cognition*, Springer, 2017, pp. 543-557.
- [29] K.-R. Muller, C.W. Anderson, G.E. Birch, Linear and nonlinear methods for brain-computer interfaces. *IEEE Transactions on Neural Systems and Rehabilitation Engineering* 11 (2003) 165-169.
- [30] F. Lotte, M. Congedo, A. Lécuyer, F. Lamarche, B. Arnaldi, A review of classification algorithms for EEG-based brain-computer interfaces. *Journal of neural engineering* 4 (2007) R1.
- [31] A. Rakotomamonjy, V. Guigue, BCI competition III: dataset II-ensemble of SVMs for BCI P300 speller. *IEEE transactions on biomedical engineering* 55 (2008) 1147-1154.
- [32] S.G. Mason, G.E. Birch, A brain-controlled switch for asynchronous control applications. *IEEE Transactions on Biomedical Engineering* 47 (2000) 1297-1307.

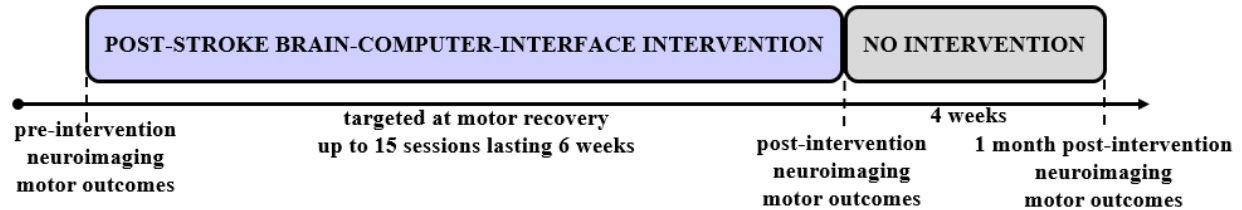
- [33] H. Cecotti, A. Graser, Convolutional neural networks for P300 detection with application to brain-computer interfaces. *IEEE transactions on pattern analysis and machine intelligence* 33 (2011) 433-445.
- [34] A. Selim, M.A. Wahed, Y. Kadah, Machine learning methodologies in brain-computer interface systems, *Biomedical Engineering Conference, 2008. CIBEC 2008. Cairo International, IEEE, 2008*, pp. 1-5.
- [35] Z. Danziger, A. Fishbach, F.A. Mussa-Ivaldi, Learning algorithms for human-machine interfaces. *IEEE Transactions on Biomedical Engineering* 56 (2009) 1502-1511.
- [36] M.H. Alomari, A. Samaha, K. AlKamha, Automated classification of L/R hand movement EEG signals using advanced feature extraction and machine learning. *arXiv preprint arXiv:1312.2877* (2013).
- [37] A. Birenbaum, H. Greenspan, Longitudinal multiple sclerosis lesion segmentation using multi-view convolutional neural networks, *Deep Learning and Data Labeling for Medical Applications*, Springer, 2016, pp. 58-67.
- [38] K. Kamnitsas, C. Ledig, V.F. Newcombe, J.P. Simpson, A.D. Kane, D.K. Menon, D. Rueckert, B. Glocker, Efficient multi-scale 3D CNN with fully connected CRF for accurate brain lesion segmentation. *Medical image analysis* 36 (2017) 61-78.
- [39] A. Benou, R. Veksler, A. Friedman, T.R. Raviv, De-noising of contrast-enhanced mri sequences by an ensemble of expert deep neural networks, *Deep Learning and Data Labeling for Medical Applications*, Springer, 2016, pp. 95-110.
- [40] N. Hoffmann, E. Koch, G. Steiner, U. Petersohn, M. Kirsch, Learning thermal process representations for intraoperative analysis of cortical perfusion during ischemic strokes, *Deep Learning and Data Labeling for Medical Applications*, Springer, 2016, pp. 152-160.
- [41] A. Payan, G. Montana, Predicting Alzheimer's disease: a neuroimaging study with 3D convolutional neural networks. *arXiv preprint arXiv:1502.02506* (2015).
- [42] T. Brosch, R. Tam, A.s.D.N. Initiative, Manifold learning of brain MRIs by deep learning, *International Conference on Medical Image Computing and Computer-Assisted Intervention*, Springer, 2013, pp. 633-640.
- [43] M. Zelen, The randomization and stratification of patients to clinical trials. *Journal of chronic diseases* 27 (1974) 365-375.
- [44] T. Brott, H.P. Adams, C.P. Olinger, J.R. Marler, W.G. Barsan, J. Biller, J. Spilker, R. Holleran, R. Eberle, V. Hertzberg, Measurements of acute cerebral infarction: a clinical examination scale. *Stroke* 20 (1989) 864-870.
- [45] D. Carroll, A quantitative test of upper extremity function. *Journal of chronic diseases* 18 (1965) 479-491.
- [46] C.E. Lang, J.M. Wagner, A.W. Dromerick, D.F. Edwards, Measurement of upper-extremity function early after stroke: properties of the action research arm test. *Archives of physical medicine and rehabilitation* 87 (2006) 1605-1610.
- [47] J.A. Wilson, G. Schalk, L.M. Walton, J.C. Williams, Using an EEG-based brain-computer interface for virtual cursor movement with BCI2000. *Journal of visualized experiments: JoVE* (2009).
- [48] B.M. Young, Z. Nigogosyan, V.A. Nair, L.M. Walton, J. Song, M.E. Tyler, D.F. Edwards, K. Caldera, J.A. Sattin, J.C. Williams, Case report: post-stroke interventional BCI rehabilitation in an individual with preexisting sensorineural disability. *Frontiers in neuroengineering* 7 (2014).
- [49] G. Schalk, D.J. McFarland, T. Hinterberger, N. Birbaumer, J.R. Wolpaw, BCI2000: a general-purpose brain-computer interface (BCI) system. *IEEE Transactions on biomedical engineering* 51 (2004) 1034-1043.
- [50] R.W. Cox, AFNI: software for analysis and visualization of functional magnetic resonance neuroimages. *Computers and Biomedical research* 29 (1996) 162-173.

- [51] K. Murphy, M.D. Fox, Towards a consensus regarding global signal regression for resting state functional connectivity MRI. *NeuroImage* (2016).
- [52] J.D. Power, A.L. Cohen, S.M. Nelson, G.S. Wig, K.A. Barnes, J.A. Church, A.C. Vogel, T.O. Laumann, F.M. Miezin, B.L. Schlaggar, Functional network organization of the human brain. *Neuron* 72 (2011) 665-678.
- [53] M. Xia, J. Wang, Y. He, BrainNet Viewer: a network visualization tool for human brain connectomics. *PloS one* 8 (2013) e68910.
- [54] C. Leys, C. Ley, O. Klein, P. Bernard, L. Licata, Detecting outliers: Do not use standard deviation around the mean, use absolute deviation around the median. *Journal of Experimental Social Psychology* 49 (2013) 764-766.
- [55] F.J. Massey Jr, The Kolmogorov-Smirnov test for goodness of fit. *Journal of the American statistical Association* 46 (1951) 68-78.
- [56] I.T. Jolliffe, *Principal Component Analysis and Factor Analysis*, Principal component analysis, Springer, 1986, pp. 115-128.
- [57] J.E. Jackson, *A user's guide to principal components*, John Wiley & Sons, 2005.
- [58] W.S. Noble, What is a support vector machine? *Nature biotechnology* 24 (2006) 1565.
- [59] T. Hastie, R. Tibshirani, J. Friedman, *The elements of statistical learning*. 2001. NY Springer (2001).
- [60] J. Snoek, H. Larochelle, R.P. Adams, Practical bayesian optimization of machine learning algorithms, *Advances in neural information processing systems*, 2012, pp. 2951-2959.
- [61] M. Bamdad, H. Zarshenas, M.A. Auais, Application of BCI systems in neurorehabilitation: a scoping review. *Disability and Rehabilitation: Assistive Technology* 10 (2015) 355-364.
- [62] J.S. Brumberg, A. Nieto-Castanon, P.R. Kennedy, F.H. Guenther, Brain-computer interfaces for speech communication. *Speech communication* 52 (2010) 367-379.
- [63] E. Mugler, R. Flint, Z. Wright, S. Schuele, J. Rosenow, J. Patton, Decoding Articulatory Properties of Overt Speech from Electrocorticography. *Proc. Fifth Int. Brain-Computer Interface Meet. 2013*, Pacific Grove, CA (2013) 4-5.
- [64] H. Sun, Y. Xiang, M. Yang, Neurological rehabilitation of stroke patients via motor imaginary-based braincomputer interface technology. *Neural Regeneration Research* 6 (2011) 2198-2202.
- [65] N. Birbaumer, Breaking the silence: brain-computer interfaces (BCI) for communication and motor control. *Psychophysiology* 43 (2006) 517-532.
- [66] R. Neshige, N. Murayama, T. Igasaki, K. Tanoue, H. Kurokawa, S. Asayama, Communication aid device utilizing event-related potentials for patients with severe motor impairment. *Brain research* 1141 (2007) 218-227.
- [67] J. Gomez-Pilar, R. Corralejo, L. Nicolas-Alonso, D. Álvarez, R. Hornero, Assessment of neurofeedback training by means of motor imagery based-bci for cognitive rehabilitation, *Engineering in Medicine and Biology Society (EMBC), 2014 36th Annual International Conference of the IEEE, IEEE, 2014*, pp. 3630-3633.
- [68] M. Lotze, P. Montoya, M. Erb, E. Hülsmann, H. Flor, U. Klose, N. Birbaumer, W. Grodd, Activation of cortical and cerebellar motor areas during executed and imagined hand movements: an functional MRI study. *Journal of cognitive neuroscience* 11 (1999) 491-501.
- [69] N. Takeuchi, S.-I. Izumi, Maladaptive plasticity for motor recovery after stroke: mechanisms and approaches. *Neural plasticity* 2012 (2012).
- [70] S.M. Smith, K.L. Miller, G. Salimi-Khorshidi, M. Webster, C.F. Beckmann, T.E. Nichols, J.D. Ramsey, M.W. Woolrich, Network modelling methods for FUNCTIONAL MRI. *Neuroimage* 54 (2011) 875-891.

## CHAPTER 3: Functional Connectivity Correlates of Behavioral Outcomes of Brain-Computer Interface Stroke Rehabilitation using Machine Learning

---

### Graphical Summary



### Research Question

What are the neural correlates of immediate and carry-over motor behavioral outcomes of the Brain-Computer-Interface intervention?

### Publication

Mohanty, R., Sinha, A.M., Remsik, A.B., Dodd, K.C., Young, B.M., Jacobson, T., McMillan, M., Thoma, J., Advani, H., Nair, V.A., Kang, T.J., Caldera, K., Edwards, D. F., Williams, J. C., Prabhakaran, V., 2018. “Early Findings on Functional Connectivity Correlates of Behavioral Outcomes of Brain-Computer Interface Stroke Rehabilitation Using Machine Learning”, *Frontiers in neuroscience*, 12.

### Abstract

The primary goal of this work was to apply data-driven machine learning regression to assess if resting-state functional connectivity (FC) could estimate measures of behavioral domains in stroke subjects who completed brain-computer interface (BCI) intervention for motor rehabilitation. The study cohort consisted of 20 chronic-stage stroke subjects exhibiting persistent upper-extremity motor deficits who received the intervention using a closed-loop neurofeedback BCI device. Over the course of this intervention, resting-state functional magnetic resonance imaging scans were collected at three time points: pre-intervention, post-intervention and one-month after completion of intervention. Behavioral assessments were administered outside the scanner at each time-point to collect objective motor function measures such as the Action Research Arm Test, Nine-Hole Peg Test, and Barthel Index as well as subjective motor function measures including the Stroke Impact Scale. The present analysis focused on neuroplasticity and behavioral outcomes measured across pre-intervention, post-intervention and one-month post-intervention to study immediate and carry-over effects. FC, changes in FC within the motor network and the behavioral measures

at preceding stages were used as input features and behavioral measures and associated changes at succeeding stages were used as outcomes for machine-learning-based linear-kernel support vector regression (SVR) model. Potential clinical confounding factors such as age, gender, lesion hemisphere, and stroke severity were included as additional features in each of the regression models. Sequential forward feature selection procedure narrowed the search for important correlates. Behavioral outcomes at preceding time-points outperformed FC-based correlates. FC and changes associated with bilateral primary motor areas were found to be important correlates of across several behavioral outcomes. NIH Stroke Scale score and motor impairment severity were the most influential clinical variables.

## 1. Introduction

Electroencephalogram (EEG)-based brain-computer interface (BCI) technology has emerged as a therapeutic modality for stroke rehabilitation that has been demonstrated to facilitate additional recovery that conventional therapies have not been able to accomplish thus far [1]. EEG-based BCI detects and uses a patient's neural signals as inputs to provide real-time feedback, effectively enabling users to modulate their brain activity. This is a promising intervention for patients with motor impairment, as they can control external devices such as computers and robots during rehabilitative tasks without relying on residual muscle control [2] which could be tailored to individuals potentially yielding greater benefits from the system [3]. Specifically, EEG-based BCI intervention using attempted movement with functional electrical stimulation (FES) [4] and tongue stimulation (TS) enables us to detect intent-to-move brain signals and provide users with both visual and tactile sensory feedback as a form of reward for producing certain brain activity patterns while performing specific tasks. Thus far, several neuroimaging studies in the realm of stroke rehabilitation have shown potential functional benefits associated with the use of BCI technology including, but not limited to, modulating changes in neuroplasticity and restoring motor function [5; 6; 7; 8].

In recent years, neuroimaging has become integral in studying the progression in neurodegenerative processes and efficacy of rehabilitation procedures [9; 5; 10; 8]. Task-free methods such as resting-state functional magnetic resonance imaging (resting-state functional MRI) allow us to measure the temporal correlation of the spontaneous, low-frequency (<0.1 Hz) blood-oxygenation-level-dependent (BOLD) signals across distinct brain regions at rest. Oscillations in these BOLD functional MRI signals are believed to reflect cortical dynamic self-organization and have been associated with the neural reorganization underlying cognitive and motor function during stroke recovery [11; 12]. Additionally, recent neuroimaging studies have demonstrated overlap among networks identified during resting-state functional MRI, motor imagery functional MRI tasks, and motor execution functional MRI tasks [13; 5]. The motor network is a complex and highly dynamic system with a unique balance of excitatory and inhibitory mechanisms which has been postulated to be significantly disturbed after stroke event [14]. This specific neuronal network

commonly includes the primary motor area (M1), premotor cortex (PMC) and supplementary motor area (SMA), as it is established that activity in these cortical regions maintains a dynamic equilibrium at resting-state and is modulated during task performance [15]. Recently, it was demonstrated that changes in task-related brain connectivity can be used as a diagnostic tool to track cortical changes and behavioral outcomes following BCI intervention in patients with stroke [8]. However, while there is evidence of overlap among resting-state and motor-related functional MRI task [13], these resting-state networks have yet to be completely characterized in the context of motor recovery facilitated by the use of a BCI device. Therefore, further investigation into changes in resting-state connectivity in relation to changes in associated motor function following BCI intervention is necessary.

The ability of data-driven machine learning techniques to model multivariate relationships can be attributed to their application in neuroimaging analysis. Several studies have shed light on the utility of machine learning to perform classification tasks [16; 17; 18; 19; 20; 21; 22]. These advance our understanding of brain function by identifying brain patterns associated with specific neurological diseases and differentiating among patient groups. However, performing simple binary classification might not suffice to answer clinically relevant questions such as prediction of recovery associated with neuropathological disease and time until onset of specific disease-related symptoms. In comparison to classification-based studies, relatively fewer studies have examined neuroimaging data from the perspective of prediction of outcomes [23; 24] using machine learning approaches. This underscores the need to use data modeling techniques that can predict outcomes on a more continuous scale while handling the high dimensionality of input data. Within machine learning, there exist a variety of algorithms to perform real-valued outcome prediction such as naïve Bayesian [25], k-nearest neighbors [26], Gaussian process [27] regression models. Rapid developments in the field are utilizing neural networks [28] in large datasets. However in this work, the focus is on using supervised support vector-based models which can model linear as well as non-linear relationships among variables with a modest sample size and extends the work previously presented [29].



Even though non-linear models may have superior performance, linear supervised methods are emphasized here as they allow to pinpoint specific correlates/predictor and offer interpretability useful for future clinical applications.

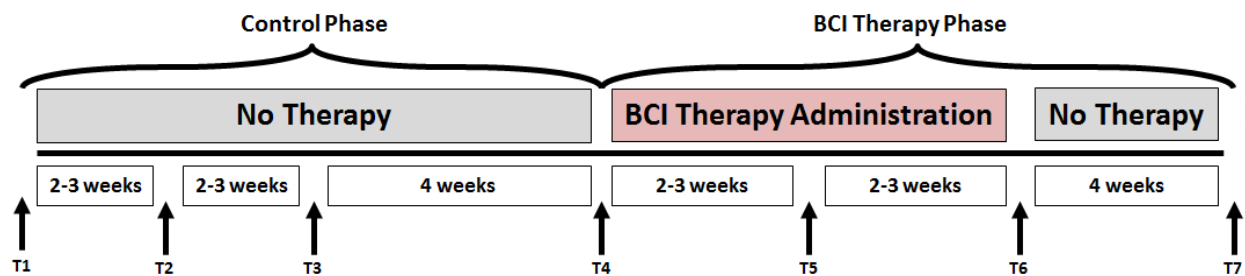
In the realm of stroke rehabilitation research, there have been concerted efforts focusing on evaluating the neurophysiological changes post-stroke [30; 31; 32; 33] and investigating novel therapeutic interventions to promote motor recovery and ultimately improve overall quality of life for patients [30; 34; 35]. While EEG-based BCI intervention has shown early promise as a form of rehabilitation post-stroke, neuroplastic changes in the form of functional connectivity and resulting therapeutic effects on behavioral outcomes following this intervention coupled with FES and TS remain to be elucidated. In this study, correlates of behavioral measures and associated changes following this EEG-based BCI intervention are investigated using brain connectivity as well as behavioral measures at preceding stages. Resting-state functional connectivity (FC) was examined in previously identified [13] motor network comprised of eight seed regions that play a dominant role in motor initiation, specification, and execution. Immediate as well as carry-over effects were investigated by examining functional MRI and behavioral measures at three stages: prior to the start of intervention, upon completion of intervention and one-month post completion of intervention. To this end, a multivariate regression scheme, based on support vector machines, was employed to handle the multi-dimensional data and examine utility in estimating individual behavioral outcomes and associated changes. The purpose of this study was four-fold: (i) to identify neural correlates based on FC within the motor network to estimate behavioral outcomes following BCI intervention; (ii) to identify neural correlates based on changes in FC within the motor network to estimate changes in behavioral measures following the BCI intervention; (iii) to identify behavioral correlates at a preceding time-point to estimate behavioral measures at a succeeding time-point; and (iv) to study the impact of potential confounds relative to FC and behavior as correlates of behavioral outcomes following the intervention.

## 2. Materials and methods

### 2. 1. Study design

This study followed a permuted-block design that accounted for gender, stroke chronicity, and severity of motor impairment in stroke subjects to randomly assign subjects to one of two groups: crossover control group or BCI therapy (intervention) group. The study paradigm is schematized in **Figure 3.1**. Subjects in the BCI therapy group received this intervention and were administered a battery of behavioral assessments and MRI scans at four time-points throughout the intervention: pre-intervention (T4), mid-intervention (T5), immediately post-intervention (T6), and one-month after completing the last BCI intervention session (T7). Subjects in the crossover control group first received three functional assessments and MRI scans during the control phase in which no BCI intervention was administered (T1 through T3), and their assessments were spaced at intervals similar to those given during the BCI intervention phase. Upon completion of the control phase of the study, the crossover control group “crossed over” into the BCI therapy phase of the study. In this study, neuroimaging and behavioral data corresponding to pre-intervention, post-intervention and one-month post-intervention time-points across the crossover control and the BCI intervention groups were combined and treated as a single sample group to provide additional power to the analysis.

*Figure 3. 1. Study paradigm*



Note: The time-points at which neuroimaging and behavioral data were collected are represented by - T1 = Control baseline 1, T2 = Control baseline 2, T3 = Control baseline 3, T4 = Intervention baseline T5 = Mid-intervention, T6 = Post-intervention, and T7 = One-month post-intervention.

## 2.2. Participants

Subjects for this analysis were recruited as part of an ongoing multi-arm stroke rehabilitation study intended to evaluate the effects of intervention using an EEG-based BCI device on the recovery of upper-extremity motor function. The inclusion criteria for participation in the study were: (1) at least 18 years of age; (2) persistent upper-extremity motor impairment resulting from an ischemic or hemorrhagic stroke; (3) ability to provide written informed consent. Exclusion criteria for the study consisted of: (1) concomitant neurodegenerative or other neurological disorders; (2) psychiatric disorders or cognitive deficits that would preclude a subject's ability to provide informed consent; (3) pregnant or likely to become pregnant during the study; (4) allergies to electrode gel, metal and/or surgical tape, contraindications to MRI; (5) concurrent treatment for infectious disease. The study was approved by the Health Sciences Institutional Review Board of University of Wisconsin-Madison. Written informed consent was obtained from all subjects prior to the start of their participation in the study. Twenty chronic stroke subjects (10 from crossover control group and 10 from BCI intervention group), who completed the BCI intervention, were included in this analysis. The cohort for this study was limited to chronic-stage (time since stroke onset > 6 months) stroke subjects only. Excluding stroke subjects in the acute (time since stroke onset < 14 days) and sub-acute (time since stroke onset < 6 months) stages was critical for this analysis to ensure that spontaneous recovery in these stages does not confound the effects of the BCI intervention. In other words, changes observed in both FC and motor behavioral performance during the acute and sub-acute phases might result from spontaneous neuroplasticity processes rather than from the BCI intervention. Time since stroke was defined to be the period between stroke onset and baseline visit. In addition, subjects were excluded from this analysis if they exhibited bilateral brain lesions for the potential reason that they could be outliers and confound the results. All neuroimaging scans were inspected by a neuroradiologist for the purposes of lesion localization. The distribution of lesion site in the cohort was as follows: middle cerebral artery territory (MCA;  $N=10$ ), frontal lobe ( $N=3$ ), cerebellum ( $N=2$ ), putamen ( $N=2$ ), occipital lobe ( $N=1$ ), basal ganglia ( $N=1$ ), and internal carotid artery occlusion ( $N=1$ ). Stroke severity was determined by NIH Stroke Scale (NIHSS) [36] scores at baseline. Severity of motor impairment was assessed based on performance on Action Research Arm

Test [37; 38] and visual inspection at the preliminary visit. Participants' handedness post-stroke was established before the start of intervention based on Edinburgh Handedness Inventory [39]. Participant characteristics are summarized in **Table 3.1**.

**Table 3. 1. Demographic and clinical characteristics of the study cohort**

<b>Characteristic</b>	<b>Value</b>
Number of Stroke Subjects	20
Chronicity	Chronic (> 6months since stroke onset)
Age (M $\pm$ SD in years)	62.4 $\pm$ 14.27
Gender	8 Females, 12 Males
Lesion Hemisphere	8 Left, 12 Right
Stroke Severity (M $\pm$ SD)	3.75 $\pm$ 3.5
Motor Impairment Severity	11 Severe, 9 Moderate
Time since Stroke (M $\pm$ SD in months)	37.65 $\pm$ 40.84
Post-stroke Handedness	16 Right, 2 Left, 2 Ambidextrous

Note: M = mean; SD = standard deviation;

### **2.3. BCI intervention**

All participants received at least 9 and up to 15 two-hour EEG-based BCI interventional sessions, with up to three sessions per week; the complete intervention lasted up to six weeks. The BCI intervention was administered using BCI2000 software [40] with modifications for administering TS (TDU 01.30, Wicab Inc.) and FES (LG-7500, LGMedSupply; Arduino 1.0.4). EEG signals, which served as the input for the BCI device, were detected and recorded from a 16-channel EEG cap and amplifier (Guger Technologies) during intervention.

A brief account of the three-step intervention is provided as follows. (i) Each intervention session began with an open-loop calibration screening task in which subjects were instructed to attempt movement of either their left or right hand with resting periods in-between by following randomly ordered visual cues on the screen, such as “Right,” “Left,” or “Rest,” in 4-second blocks. During the initial screening session, participants did not receive any form of feedback. The EEG activity, recorded in the open-loop screening task, was used by the classifier for identifying activation patterns corresponding to volitional movement of the respective left and right hands in the closed-loop task. Both in the initial screening and closed-loop feedback conditions, attempted movement was utilized to simulate the training conditions of the neurofeedback task similar to the cognitive processes involved in real-world movement. (ii) Following the initial screening, subjects performed a closed-loop task, in which they received real-time visual feedback in the context of a cursor task game. The goal of the cursor task game was to move a cursor (ball) onto a target area, with target areas positioned on either the left or right side of the computer screen. Subjects were instructed to move their left or right hand to control the corresponding movement of the cursor in the direction of the target on the screen. A 70% accuracy was set as the criteria to establish control of a BCI system in this phase [41; 42]. Real-time EEG signals were used to calculate and control lateral cursor movement, which served as the visual feedback for the remainder of the session. During each BCI intervention session, subjects completed 10 runs of this game, which included 8 – 12 trials per run, while receiving continuous visual feedback. (iii) After successful completion of 10 runs of the game with visual feedback, both TS and FES were simultaneously incorporated into the intervention session for the remaining trials (as many trials as possible within a 2-hour session). FES, with a pulse rate of stimulation 60 Hz and varied up to 5 mA in increments of 0.5 mA as per the participant’s comfort level, was administered to muscles of the subject’s impaired forearm when their neural activity signals corresponding to impaired arm movement intent were detected during a trial in which subjects attempted to move the cursor to a target on the screen corresponding to the side of the impaired arm. The stimulation thresholds for FES and TS were determined during the first intervention session and maintained at the same level in all the subsequent sessions for consistency. This EEG-based BCI system with FES and TS provides subjects

with both visual and tactile sensory feedback. To keep subjects engaged in throughout the task, the size of the target on the screen and speed of the cursor could be changed to modulate the difficulty of the task depending on their accuracy. Additional details of the procedure of the intervention can be found in prior studies such as those described by Wilson et al. [43], and Young et al. [44; 45].

#### **2.4. Neuroimaging data acquisition**

Neuroimaging data were acquired at the four aforementioned time points (T4 through T7). For the purposes of this work, data from three of these points were chosen, i.e., prior to starting the intervention or pre-intervention assessment (T4), immediately upon completion of intervention or post-intervention assessment (T6) and a month after completion of full intervention (T7) to study the potential peak and carry-over effects of the EEG-based BCI intervention. Resting-state functional MRI scans were acquired on GE 750 3T MRI scanners (GE Healthcare, Waukesha, WI) using an 8-channel head coil. Ten-minute resting state scans were acquired while participants' eyes were closed using single-shot echo-planar T2\*-weighted imaging: TR = 2600 ms, 231 time-points, TE = 22 ms, FOV = 224 mm,  $64 \times 64$  matrix size, flip angle =  $60^\circ$ , and 40 slices with voxel dimensions of  $3.5 \times 3.5 \times 3.5 \text{ mm}^3$ . Five-minute T1-weighted anatomical images were obtained at the start of each scan using a BRAVO FSPGR sequence with the following parameters: TR = 8.16 ms, TE = 3.18 ms and TI = 450, matrix size =  $256 \times 256$ , 156 slices, flip angle =  $12^\circ$ , FOV = 256 mm with slice thickness = 1 mm.

#### **2.5. Behavioral assessments**

To assess the behavioral impact of the BCI intervention, a battery of objective and subjective measures was administered to participants at each time-point. Corresponding to the neuroimaging, behavioral measures were considered at pre-intervention (T4), post-intervention (T6) and one-month post-intervention (T7) in this study. To systematically quantify motor functional outcomes, the following standard behavioral measures were evaluated as summarized in **Table 3.2**: the Action Research Arm Test (ARAT) [37; 38], 9-Hole Peg Test (9HPT) [46], Barthel Index (BI) [47], and Stroke Impact Scale (SIS) [48; 49]. The ARAT

serves as a standardized and reliable functional measure for stroke rehabilitation that measures changes in specific upper limb function among individuals who sustained cortical damage resulting in hemiplegia. The 9HPT measure is used for quantifying hand dexterity. ARAT and 9HPT were observed for the affected (ARAT(A), 9HPT(A)) as well as unaffected (ARAT(U), 9HPT(U)) upper extremity. In this study, BI was administered in questionnaire form and not observed from functional performance as it was originally designed and validated. The BI score quantifies the ability of an individual to care for her/himself in their daily life. The SIS scores are self-reported outcomes that measure the health status of stroke subjects. SIS includes the following standard domains: Activities of Daily Living (ADL) for difficulty carrying out activities in a typical day, Hand Function (HF) for difficulty in using the hand most affected by stroke, Mobility (Mob) for difficulty in ability to be mobile at home and in community, and Physical Strength (PS) for overall strength in the upper and lower limbs of the affected side.

*Table 3. 2. Summary of all the behavioral assessments used as outcomes*

<b>Motor Function/Behavioral Assessment</b>	<b>Category</b>
<b>ARAT(U)</b> : Action Research Arm Test for the upper extremity unaffected by stroke	Objective
<b>ARAT(A)</b> : Action Research Arm Test for the upper extremity affected by stroke	Objective
<b>9HPT(U)</b> : 9-Hole Peg Test for the upper extremity unaffected by stroke	Objective
<b>9HPT(A)</b> : 9-Hole Peg Test for the upper extremity affected by stroke	Objective
<b>BI</b> : Barthel Index	Objective
<b>SIS(ADL)</b> : Activities of daily life domain of Stroke Impact Scale	Subjective
<b>SIS (HF)</b> : Hand function domain of Stroke Impact Scale	Subjective
<b>SIS(Mob)</b> : Mobility domain of Stroke Impact Scale	Subjective
<b>SIS(PS)</b> : Physical strength domain of Stroke Impact Scale	Subjective

## 2.6. Individual level analysis

The main steps involved in the processing of data on a single-subject level are outlined in **Figure 3.2** and described in detail in the following subsections.

### 2.6.1. Neuroimaging preprocessing

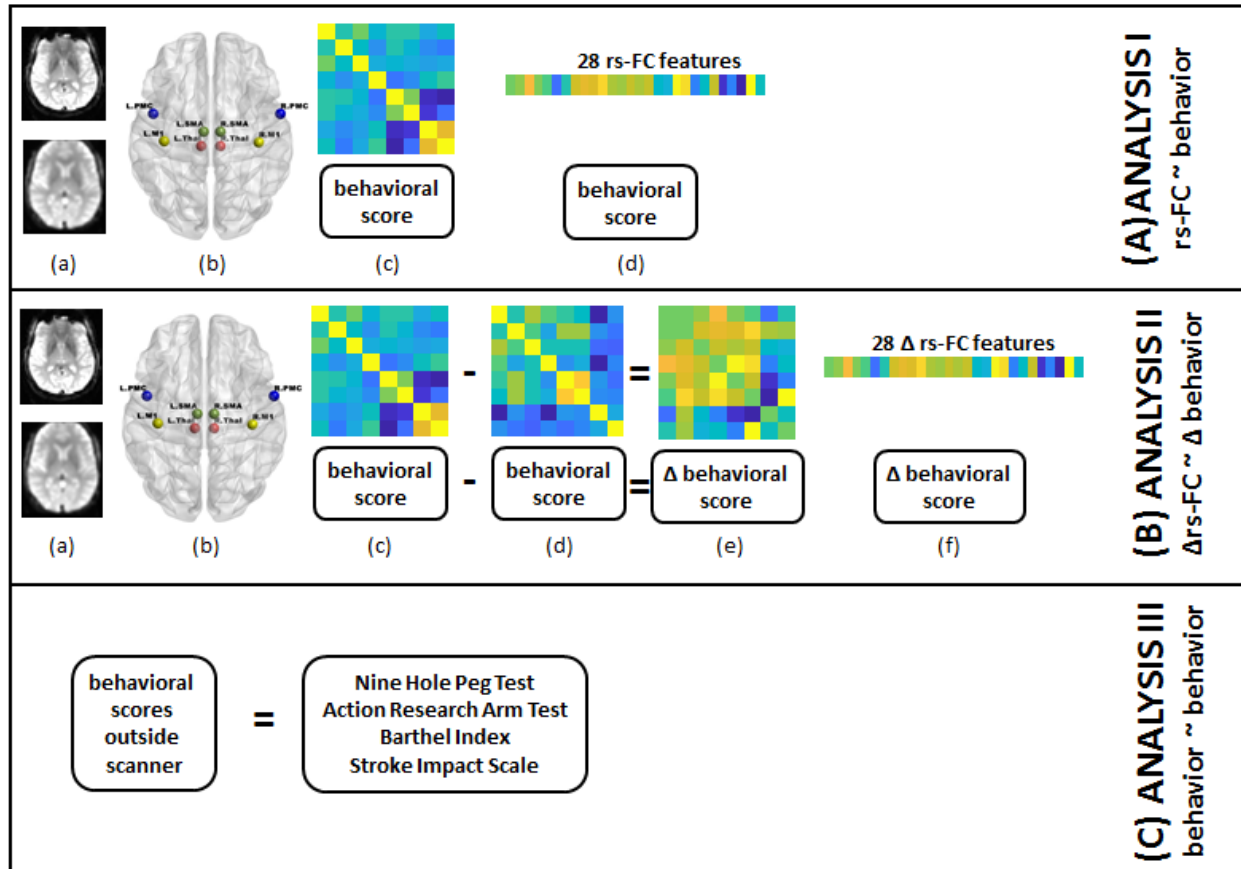
Resting-state functional MRI scans of 20 subjects were visually inspected for artifacts and preprocessed in the following sequential manner: the first three volumes of each scan were removed, images were despiked, slice time corrected, aligned with the corresponding anatomical T1 scan, spatially smoothed with a 4-mm FWHM (full width at half maximum) Gaussian kernel, transformed into the standard MNI space (3.5 mm isotropic), motion censored (per TR motion > 1 mm or 1°), regressed for nuisance variables (regressed out the signal from locally averaged white matter and cerebrospinal fluid) and bandpass filtered (0.009 - 0.08 Hz). Given the controversial nature of global signal regression [50], this processing step was not included in the analysis pipeline. All resting-state functional MRI data were preprocessed using Analysis of Functional NeuroImages (AFNI) (<http://afni.nimh.nih.gov/afni>) [51].

### 2.6.2. Functional connectivity

A seed-based analysis was adopted based on prior work that investigated FC within the motor network in stroke population [13; 5]. The seed regions were identified based on a network of cortical and subcortical areas that exhibited activation during visually paced hand movements. The seed regions for this study included the primary motor cortex (M1), supplementary motor area (SMA), thalamus, and lateral premotor cortex (PMC) in the right and left hemispheres, as illustrated in **Figure 3.3** using BrainNet Viewer [52]. The standard brain MNI coordinates for the 8 regions were used to create 8-mm spherical seeds. For each subject, BOLD time series signal from each region was extracted from the spatially standardized residuals obtained in the preprocessing stage. The extracted time series for each region was used to compute an  $8 \times 8$  ROI correlation matrix for each subject. From this symmetric matrix,  $28 \left( = \frac{8 \times (8-1)}{2} \right)$  unique correlation coefficients were extracted to represent pairwise FC within the motor network at each of the three stages of interest.

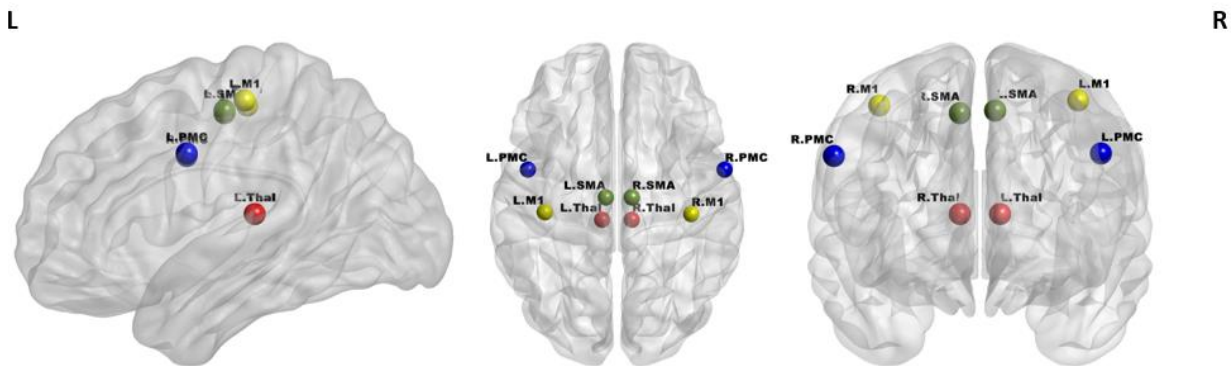


Figure 3. 2. Steps for individual subject analysis



Note: rs-FC = FC = functional connectivity; **(A) FC correlates of behavior**: (a) resting-state functional MRI from pre-, post- and one-month post-interventions were preprocessed; (b) 8 seed regions were chosen from the motor network to compute FC; (c)  $8 \times 8$  FC matrix was computed and corresponding behavioral scores were transformed as needed for each time-point; (d) FC reflected in the lower triangle of  $8 \times 8$  matrix was vectorized into 28 unique correlation coefficients per subject and 8 distinct behavioral measures were aggregated for group-level analysis. **(B)  $\Delta$ FC correlates of  $\Delta$ behavior**: (a) resting-state functional MRI from pre-, post- and one-month post-interventions preprocessed; (b) 8 seed regions were chosen from the motor network to compute FC at each time-point; (c)  $8 \times 8$  FC matrix was computed and corresponding behavioral scores were transformed as needed for a preceding time-point; (d)  $8 \times 8$  FC matrix was computed and corresponding behavioral scores were transformed as needed for a succeeding time-point; (e) change in FC and behavioral scores were calculated between the two time-points; (f) change in FC reflected in the lower triangle of  $8 \times 8$  matrix was vectorized into 28 unique correlation coefficients per subject and change in 8 distinct behavioral measures were aggregated for group-level analysis. **(C) behavioral correlates at preceding time-point of behavior at succeeding time-point**: transformed scores for 8 behavioral measures at pre-, post- and one-month post-interventions were aggregated for group-level analysis.

**Figure 3. 3. Motor network with seed regions used in analysis**



Note: Four bilateral seed regions of interest are visualized: Primary Motor Cortex (M1 in yellow), Premotor Cortex (PMC in blue), Supplementary Motor Area (SMA in green) and Thalamus (red).

### 2.6.3. Potential clinical confounds

The study cohort was heterogeneous with respect to multiple clinical factors which could confound the contribution of FC alone. Based on prior studies, the following factors were identified as potential confounds: age and stroke severity [53], severity of motor impairment, and time since stroke [54], lesion hemisphere [55], and gender [56]. These clinical variables were included as features in addition to neural and behavioral features to build the regression model for each outcome.

### 2.7. Group-level analysis

Applications of machine learning regression models such as SVR on resting-state functional MRI have been demonstrated in neuroimaging-based studies [23; 24] as SVR-based methods can efficiently handle multi-dimensional data. For the purposes of this study, a strategy similar to these studies was adopted. To understand the correlates of behavioral outcomes and changes, the following analyses were undertaken by applying SVR to correlate:

**ANALYSIS I:** FC at preceding time-points and clinical variables with behavioral outcomes at succeeding time-points (T4 with T6; T4 with T7; T6 with T7).

**ANALYSIS II:** change ( $\Delta$ ) in FC between pairs of time-points and clinical variables with corresponding change ( $\Delta$ ) in behavioral outcomes (T4 and T6; T4 and T7; T6 and T7).

**ANALYSIS III:** behavioral measures at preceding time-points and clinical variables with behavioral measures at succeeding time-points (T4 with T6; T4 with T7; T6 with T7).

In case of behavioral measures, total scores across comprising domains for BI and ARAT, average scores across two trials for 9HPT, and transformed scores to yield a percentage of possible points for the SIS domains of PS, Mob, HF, and ADL were considered.

To characterize changes among the three stages of interest (T4, T6 and T7), the following definitions were employed:

$$\Delta FC = \frac{FC_{succeeding\ stage} - FC_{preceding\ stage}}{FC_{preceding\ stage}} \quad (1)$$

where  $FC_{succeeding\ stage}$  and  $FC_{preceding\ stage}$  denote the values of FC correlation at succeeding (T6, T7) and preceding (T4, T6) stages respectively.

Unlike in case of FC, the definition for changes in behavioral measures differed by case. For 9HPT(A), 9HPT(U), ARAT(U), BI, SIS (PS, Mob, and ADL) scales, the normalized change was gauged by:

$$\Delta behavior = \frac{behavior_{succeeding\ stage} - behavior_{preceding\ stage}}{behavior_{preceding\ stage}} \quad (2)$$

However, in case of ARAT(A) and SIS(HF), the possibility of  $behavior_{preceding\ stage}$  being 0 invalidates the above normalization. Thus, a simple deviation was computed as follows:

$$\Delta behavior = behavior_{succeeding\ stage} - behavior_{preceding\ stage} \quad (3)$$

where  $behavior_{succeeding\ stage}$  and  $behavior_{preceding\ stage}$  correspond to the scores achieved by a participant in each behavioral task at succeeding (T6, T7) and preceding (T4, T6) stages. Due to lack of variability across most time-points, the ARAT(U) was discarded as a behavioral outcome for all analyses.

For each motor behavioral outcome, the input features for all subjects were aggregated and the steps described as follows were implemented.

### **2.7.1. Feature selection**

Each regression model was built using a subset of input features (28 FC features, 28  $\Delta$  FC features, 8 behavioral measures as described by ANALYSES I, II and III) through a feature selection procedure. The six identified clinical variables were also included in the feature selection in each analysis. A forward sequential feature selection (SFS) was helpful in reducing the dimensions of the original data for better interpretation of features involved [57; 58]. This method searches for a subset of features that optimally models a given outcome. The algorithm adds each candidate feature and checks the specified criteria by building a regression model based on selected features. The criteria specified for selection of a feature involved minimization of the mean squared error (MSE) arising from estimation error for SVR model. The SVR regression is described in the following section. A nested leave-one out cross-validation approach allowed for testing of estimation error on the left-out sample, where the inner loop was used to choose the features during a training-validation phase. The addition of features continues until the MSE does not decrease anymore. One advantage of methods such as SFS is that since it works in the raw feature space, it can be applied to both continuous (neural and behavioral) and categorical (clinical) features. During cross-validation, the features that were common across all the folds were reported as the contributing features for each model. The weights assigned to these features were averaged across all folds and sorted to determine the rank or importance of individual features in the regression model.

### 2.7.2. Support Vector Regression (SVR)

Once a subset of features was selected by SFS, the SVR model was trained using the selected features for each behavioral outcome. SVR was chosen due to its ability to predict real-valued behavioral outcomes based on multi-dimensional input features. In particular, regression modeling based on supervised learning support vector machines (SVM) [59] was employed. Typically used as a classifier, SVM can also be used for regression analysis [60]. SVR forms a non-parametric method via the kernel trick. This method not only provides resilience to overfitting and good generalization performance, but also helps in interpreting the contribution of individual features in high-dimensional data with a linear kernel. In the case of linear regression, the mapping function lies in the input space, so it is possible to derive the weights corresponding to each input feature.

### 2.7.3. Cross-validation

A leave-one-out cross-validation (LOOCV) approach [61] was adopted to estimate the performance of the regression model in the outer loop of the nested cross-validation as it provides an approximation of the test error with a lower bias and is more suitable for a dataset with a limited number of samples such as that used in this analysis. A LOOCV by subject was performed in this validation-testing phase. This means that the data consisting of 20 observations were subdivided into 20 folds such that each fold comprised of data from a single subject. The regression model was trained using selected features from 19 folds and tested upon the left-out fold. This was repeated 20 times such that data from each subject was left out once while a model was trained using the rest of the data. The performance of the model was quantified in terms of the average root-mean-squared error (RMSE) for SVR over all iterations of LOOCV given by:

$$RMSE = \sqrt{\frac{1}{l} \sum_{i=1}^l (y_{est_i} - y_i)^2} \quad (4)$$

where the  $y_{est_i} - y_i$  term is the measure of error between the estimated outcome and the true outcome. Reasonable performance of SVR is characterized by values of RMSE closer to 0. In addition to RMSE, the linear-kernel SVR can also be assessed in terms of goodness of fit in terms of the coefficient of determination ( $R^2$ ).

#### **2.7.4. Model parameter optimization**

The generalization performance is dependent upon both the selected features and model parameters  $C, \varepsilon$  [62; 63], and the kernel parameters. The parameter  $C$  is used to trade-off between the complexity of the model and the extent to which estimated deviations larger than  $\varepsilon$  are tolerated in formulation of the optimization. Parameter  $\varepsilon$  controls the width of the  $\varepsilon$ -insensitive zone, used to fit the training data. Both  $C, \varepsilon$  values have an impact on complexity of the model. The data points are scaled by the parameter depending upon the kernel used for regression. A randomized search method based on Bayesian optimization process attempts to minimize the MSE loss in the separate LOOCV by varying the parameters for 30 evaluations [64; 65; 66] which corresponded to the inner loop of the training-validation phase, training on all samples but one with the best chosen parameters and testing on the left out sample were performed.

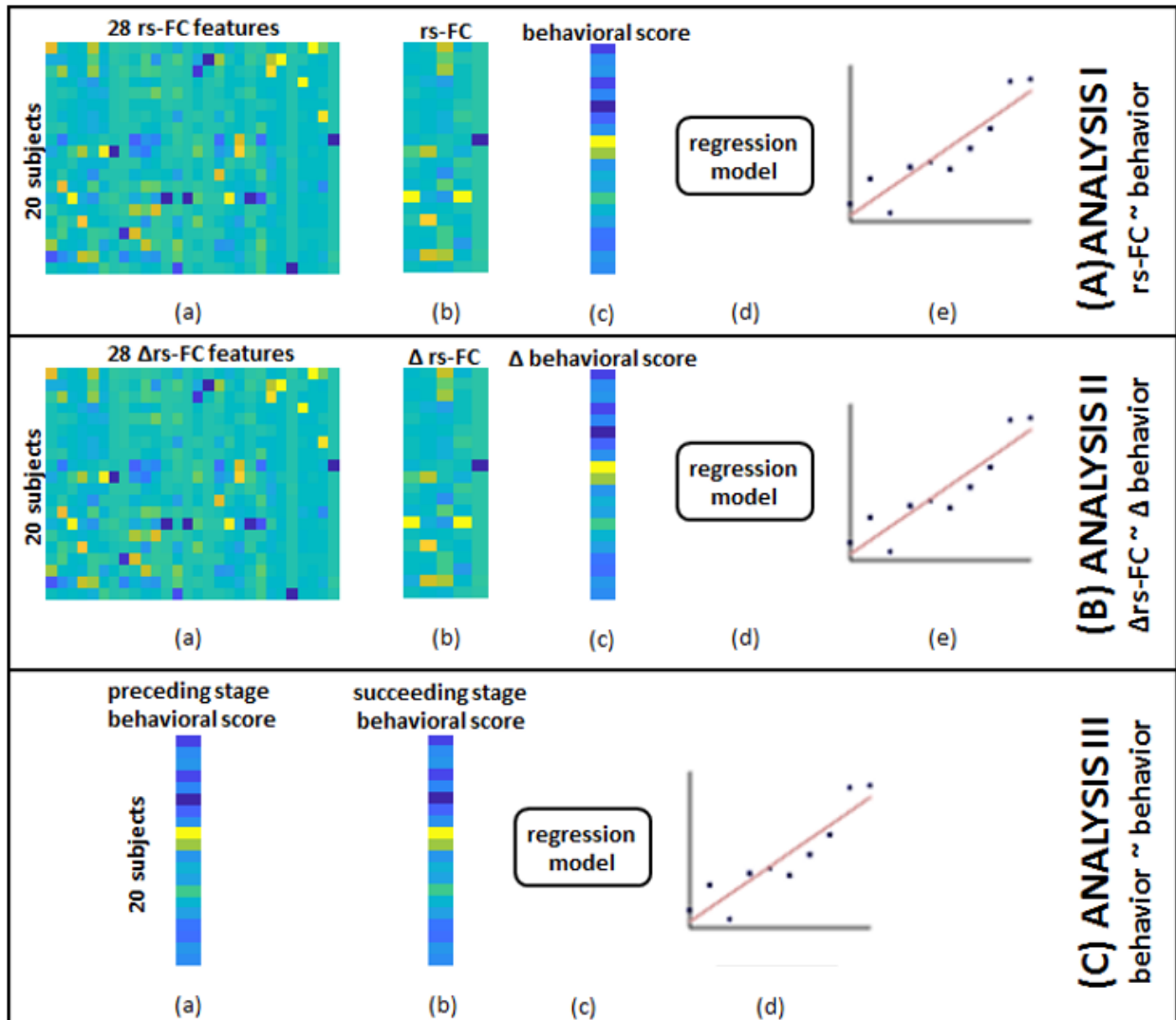
#### **2.7.4. Evaluation of regression model**

In order to validate the results against chance levels, non-parametric permutation tests were performed. For each regression model, the outcome labels were randomly permuted 1000 times and feature selection and LOOCV were repeated for each permuted dataset to create a null distribution. The performance of the regression model corresponding to the non-permuted data was considered significantly better than chance if the RMSE of the model was lower than at least 95% of those obtained from the null-hypothesis.

### **2.7.5. Overview of methodology**

Overall, SVR models were trained using selected FC,  $\Delta$ FC, and behavioral measures, optimized the model and identified the contributing input features that provided the minimum RMSE upon LOOCV. All computations were carried out using the Statistics and Machine Learning Toolbox in MATLAB R2017a (The MathWorks, Inc., Natick, Massachusetts, United States). The group-level pipeline of analysis is visualized in **Figure 3.4**.

Figure 3. 4. Overview of group-level analysis



Note: rs-FC = FC = functional connectivity; **(A) FC correlates of behavior:** (a) aggregated data from single-subject analysis gave 28 FC features for each of the 20 subjects; (b) SFS was used to select specific correlates corresponding to each behavioral outcome; (c) aggregated behavioral scores for 20 subjects served as outcomes in separate models; (d) data from (b) and (c) were fed into the SVR model; (e) linear-kernel was specified to perform regression. Steps (a) through (e) were repeated by adding identified clinical variables to FC data as input features. **(B)  $\Delta$ FC correlates of  $\Delta$ behavior:** (a) aggregated data from single-subject analysis gave 28 change in FC features for each of the 20 subjects between pairs of time-points; (b) SFS was used to select specific correlates corresponding to each behavioral outcome; (c) aggregated change in behavioral scores between corresponding pair of time-points for 20 subjects served as outcomes in separate models; (d) data from (b) and (c) were fed into the SVR model; (e) linear-kernel was specified to perform regression. Steps (a) through (e) were repeated by adding identified clinical variables to change in FC data as input features. **(C) behavioral correlates at preceding time-point of behavior at succeeding time-point:** (a) aggregated behavioral scores from a preceding time point gave 8 distinct measures; (b) aggregated behavioral scores from a succeeding time-point gave the corresponding 8 measures; (c) data from steps (a) and (b) were fed to the SVR model; (d) linear-kernel SVR were specified to perform regression.



### 3. Results

#### 3.1. Choice of time-points of interest

The analyses, undertaken here, revolved around three time-points, namely T4, T6 and T7, i.e. pre-intervention, post-intervention and one-month post-intervention. The objective was to study the immediate as well as potential residual impact of the intervention after a month. A comparison of group medians of behavioral outcomes at these three time-points showed increased values at T7 relative to T4 or T6 for the following outcomes: SIS(Mob), SIS(HF), ARAT(A) although not significant (based on a Mann Whitney U-test). The time-points from the control period, i.e., T1 through T3 were not included in the regression analyses due to limited samples (N=10). However, there were no significant differences (using Mann Whitney U-test on each pair of time-points) when the group medians of the behavioral outcomes during the control period were compared with those of T4. Thus, presumably, measures at T4 could be considered to serve as representative scores for the control period.

#### 3.2. Performance of correlates

Behavioral outcomes were estimated using FC,  $\Delta$ FC as well as behavioral measures at preceding time-points. In terms of  $R^2$ , better estimation of outcomes was observed using behavioral correlates, followed by FC and  $\Delta$ FC in this order.

##### *FC as correlates of behavioral outcomes*

The performances of SVR using FC as correlates of behavioral outcomes are presented in **Table 3.3**. All the SVR models, developed here, performed better than chance-level based on permutation test ( $p < 0.05$ ). Individual predictors involved in estimating the different outcomes are listed in **Table 3.4**. Overall, FC associated with L.M1, R.M1 and R.PMC were the main contributors towards estimation. Among the three time-points, better performances were found in cases of correlating FC at T6 and behavioral measures at T7

**Table 3. 3.** Estimation of behavior at succeeding time-point using FC and clinical variables at preceding time-point

Outcome	T4 FC ~ T6 behavior			T4 FC ~ T7 behavior			T6 FC ~ T7 behavior		
	Features	RMSE	R <sup>2</sup>	Features	RMSE	R <sup>2</sup>	Features	RMSE	R <sup>2</sup>
<b>9HPT(A)</b>	10	69.627*	0.69	14	71.349*	0.68	7	61.391*	0.76
<b>9HPT(U)</b>	4	4.187*	0.28	4	3.822*	0.34	9	1.508*	0.9
<b>ARAT(A)</b>	2	5.143*	0.96	4	5.723*	0.95	2	7.009*	0.92
<b>BI</b>	7	9.452*	0.43	7	13.378*	0.22	12	14.099*	0.13
<b>SIS(ADL)</b>	7	16.146*	0.78	2	23.484*	0.51	11	15.1018	0.8
<b>SIS(HF)</b>	5	9.766*	0.03	8	9.4*	0.54	5	10.514*	0.43
<b>SIS(Mob)</b>	1	16.361*	0.37	4	13.523*	0.32	6	12.528*	0.41
<b>SIS(PS)</b>	4	6.796*	0.41	7	4.591*	0.64	10	3.817*	0.75

Note: Linear-kernel SVR performances based on leave-one out cross-validation to correlate FC and clinical variables at preceding time-point with behavioral measures at succeeding time-point are presented. Specific correlates are listed in **Table 3.4.**; \*significant against chance-level based on permutation-test ( $p < 0.05$ ); T4 = pre-therapy; T6 = post-therapy; T7 = 1-month post-therapy.

**Table 3. 4. Correlates of behavior at a succeeding time-point**

Rank	9HPT(A)	9HPT(U)	ARAT(A)	SIS(ADL)	SIS(HF)	SIS(Mob)	SIS(PS)	BI	Input FC and Clinical Features at T4	Outcomes at T6
1	Motor Imp.	L.PMC-R.M1	Motor Imp.	TSS	Motor Imp.	L.Thal-R.PMC	NIHSS	Motor Imp.		
2	NIHSS	Age	NIHSS	R.SMA- R.PMC	L.SMA- R.PMC		Lesion Hemi	R.Thal-L.SMA		
3	Lesion Hemi	L.SMA-L.M1		R.Thal-R.PMC	R.M1-L.M1		R.SMA-R.M1	NIHSS		
4	R.M1-L.M1	NIHSS		Motor Imp.	R.PMC-R.M1		L.Thal-R.PMC	Age		
5	R.SMA- R.PMC			Lesion Hemi	R.Thal-R.M1			L.SMA-R.M1		
6	L.SMA-R.M1			R.Thal-L.M1				R.Thal-L.PMC		
7	TSS			R.PMC-R.M1				L.PMC-L.M1		
8	R.Thal-L.Thal									
9	R.SMA-R.M1									
10	R.PMC-R.M1									
Rank	9HPT(A)	9HPT(U)	ARAT(A)	SIS(ADL)	SIS(HF)	SIS(Mob)	SIS(PS)	BI	Input FC and Clinical Features at T4	Outcomes at T7
1	Motor Imp.	R.SMA- L.SMA	Motor Imp.	R.SMA-L.M1	R.PMC-L.M1	R.PMC-R.M1	Motor Imp.	TSS		
2	NIHSS	R.SMA-L.M1	NIHSS	R.Thal-L.M1	Motor Imp.	L.SMA-L.M1	R.Thal-L.Thal	Motor Imp.		
3	Lesion Hemi	R.PMC-R.M1	L.Thal-R.PMC		R.SMA-R.M1	R.SMA-L.M1	L.Thal-R.SMA	Age		
4	TSS	NIHSS	R.Thal-R.PMC		R.PMC- L.PMC	L.SMA- L.PMC	L.Thal-R.PMC	R.PMC-R.M1		

5	R.SMA-R.M1				R.SMA-L.M1		L.Thal-R.M1	R.PMC- L.PMC		
6	R.M1-L.M1				L.PMC-L.M1		R.Thal-L.PMC	R.M1-L.M1		
7	L.PMC-L.M1				TSS		NIHSS	R.SMA-R.M1		
8	L.SMA-R.M1				NIHSS					
9	L.Thal-L.M1									
10	R.Thal-L.SMA									
11	R.Thal-L.PMC									
12	R.Thal- R.SMA									
13	R.SMA-L.M1									
14	R.PMC-R.M1									
<b>Rank</b>	<b>9HPT(A)</b>	<b>9HPT(U)</b>	<b>ARAT(A)</b>	<b>SIS(ADL)</b>	<b>SIS(HF)</b>	<b>SIS(Mob)</b>	<b>SIS(PS)</b>	<b>BI</b>		<b>Input FC and Clinical Features at T6</b> <b>Outcomes at T7</b>
1	Motor Imp.	L.Thal-L.M1	Motor Imp.	R.PMC-L.M1	Motor Imp.	R.Thal-L.PMC	L.SMA- L.PMC	Motor Imp.		
2	NIHSS	L.Thal-R.SMA	NIHSS	R.SMA- R.PMC	L.SMA- L.PMC	R.Thal-L.SMA	R.SMA- L.SMA	R.Thal-L.PMC		
3	Lesion Hemi	L.Thal-R.PMC		TSS	TSS	R.Thal-L.M1	Motor Imp.	R.PMC- L.PMC		
4	R.SMA- L.PMC	R.Thal-L.M1		L.SMA-R.M1	R.Thal-L.PMC	R.PMC- L.PMC	L.Thal-R.M1	R.Thal-R.M1		

5	R.PMC- L.PMC	R.SMA-L.M1		NIHSS	NIHSS	L.Thal-L.M1	R.SMA-R.M1	R.Thal-R.PMC	
6	L.SMA- R.PMC	NIHSS		L.SMA- L.PMC		R.PMC-L.M1	R.PMC-L.M1	R.Thal- R.SMA	
7	R.PMC-R.M1	Gender		R.Thal-R.M1			R.PMC- L.PMC	Age	
8		L.Thal-L.SMA		L.PMC-L.M1			NIHSS	TSS	
9		R.SMA- R.PMC		R.PMC-R.M1			L.Thal-R.SMA	R.PMC-R.M1	
10				R.SMA-L.M1			R.Thal-R.PMC	R.M1-L.M1	
11				R.Thal-L.PMC				NIHSS	
12								R.SMA-R.M1	

Note: FC and clinical correlates of behavior between all pairs of time-points identified by using linear-kernel SVR are presented below; T4 = pre-therapy; T6 = post-therapy; T7 = 1-month post-therapy

### ***$\Delta FC$ as correlates of $\Delta$ behavioral outcomes***

The performance of SVR using  $\Delta FC$  as correlates of  $\Delta$ behavioral outcomes are presented in **Table 3.5**. SVR models corresponding to ARAT(A) and SIS(HF) performed better than chance-level based on permutation test ( $p < 0.05$ ). Individual predictors involved in estimating the different outcomes are listed in **Table 3.6**. Overall, FC associated with L.M1, R.M1, L.Thal and L.M1, R.M1, R.Thal were the main contributors towards estimation without and with clinical variables respectively. Among the three time-points, better performances were found in cases of correlating  $\Delta FC$  between T6 and T7 and  $\Delta$ behavioral measures between the same time-period.

**Table 3. 5.** Estimation of  $\Delta$ behavioral measures using  $\Delta FC$  and clinical variables

Outcome	$\Delta FC_{T6-T4} \sim \Delta \text{behavior}_{T6-T4}$			$\Delta FC_{T7-T4} \sim \Delta \text{behavior}_{T7-T4}$			$\Delta FC_{T7-T6} \sim \Delta \text{behavior}_{T7-T6}$		
	Features	RMSE	R <sup>2</sup>	Features	RMSE	R <sup>2</sup>	Features	RMSE	R <sup>2</sup>
$\Delta 9HPT(A)$	5	69.63	0.69	3	71.35	0.68	3	61.39	0.76
$\Delta 9HPT(U)$	3	4.19	0.28	3	0.1	0.22	3	1.51	0.9
$\Delta ARAT(A)$	16	5.14*	0.96	8	5.72*	0.95	16	7.01*	0.92
$\Delta BI$	3	0.05	0.1	7	4.59	0.64	8	3.82	0.75
$\Delta SIS(ADL)$	4	9.45	0.43	5	13.38	0.22	4	14.1	0.13
$\Delta SIS(HF)$	5	16.15*	0.78	5	23.48*	0.51	4	15.1*	0.8
$\Delta SIS(Mob)$	4	9.77	0.03	7	9.4	0.54	5	10.51	0.43
$\Delta SIS(PS)$	4	16.36	0.37	4	13.52	0.32	8	12.53*	0.41

Note: Linear-kernel SVR performances based on leave-one out cross-validation to correlate  $\Delta FC$  and clinical variables between two time-points with  $\Delta$  behavioral measures between corresponding time-points are presented. Specific correlates are listed in **Table 3.6.**; \*significant against chance-level based on permutation-test ( $p < 0.05$ ); T4 = pre-therapy; T6 = post-therapy; T7 = 1-month post-therapy.

**Table 3. 6. Correlates of  $\Delta$ behavioral measures**

(A) With Clinical Variables								
Rank	$\Delta$ 9HPT(A)	$\Delta$ 9HPT(U)	$\Delta$ SIS(ADL)	$\Delta$ SIS(Mob)	$\Delta$ SIS(PS)	$\Delta$ BI	$\Delta$ ARAT(A)	$\Delta$ SIS(HF)
1	R.Thal-R.SMA	NIHSS	L.SMA-R.PMC	R.Thal-L.M1	L.SMA-R.M1	R.PMC-L.M1	NIHSS	R.PMC-L.M1
2	Gender	R.Thal-L.PMC	L.Thal-R.PMC	L.Thal-R.M1	L.SMA-L.M1	R.Thal-L.PMC	Motor Imp.	R.Thal-L.SMA
3	R.SMA-L.M1	L.SMA-R.PMC	TSS	R.PMC-R.M1	R.SMA-L.SMA	R.SMA-L.M1	L.SMA-R.PMC	R.Thal-R.SMA
4	R.Thal-R.M1		R.M1-L.M1	L.SMA-R.M1	L.Thal-R.M1		R.Thal-L.PMC	L.Thal-R.M1
5	R.Thal-L.PMC						Lesion Hemi.	R.SMA-L.PMC
6							R.Thal-L.SMA	
7							L.SMA-L.PMC	
8							L.SMA-L.M1	
9							R.Thal-R.SMA	
10							R.PMC-R.M1	
11							L.SMA-R.M1	
12							R.M1-L.M1	
13							R.SMA-R.M1	
14							L.Thal-L.M1	
15							R.PMC-L.M1	
16							TSS	
Rank	$\Delta$ 9HPT(A)	$\Delta$ 9HPT(U)	$\Delta$ SIS(ADL)	$\Delta$ SIS(Mob)	$\Delta$ SIS(PS)	$\Delta$ BI	$\Delta$ ARAT(A)	$\Delta$ SIS(HF)
1	R.Thal-L.SMA	R.SMA-R.PMC	Motor Imp.	R.Thal-R.M1	R.SMA-L.M1	L.PMC-L.M1	L.Thal-L.PMC	R.Thal-L.M1

Input  $\Delta$ FC at T4 + Clinical Features

Outcome at T6

Outcome at T6

Outcome at T6

2	NIHSS	R.Thal-R.M1	R.Thal-R.M1	Age	R.Thal-L.PMC	L.Thal-R.PMC	NIHSS	L.PMC-L.M1	
3	R.Thal-R.PMC	Lesion Hemi	L.SMA-R.PMC	L.Thal-L.M1	R.PMC-L.M1	R.SMA-R.M1	R.SMA-L.M1	R.Thal-R.PMC	
4			R.SMA-L.M1	R.Thal-L.SMA	Lesion Hemi	L.Thal-L.M1	R.Thal-R.SMA	L.Thal-R.PMC	
5			R.SMA-R.PMC	L.Thal-L.PMC		R.M1-L.M1	R.Thal-L.M1	R.SMA-L.M1	
6				Motor Imp.		R.Thal-L.PMC	L.Thal-R.PMC		
7				L.Thal-R.SMA		NIHSS	L.PMC-R.M1		
8							L.SMA-L.PMC		
<b>Rank</b>	<b>Δ9HPT(A)</b>	<b>Δ9HPT(U)</b>	<b>ΔSIS(ADL)</b>	<b>ΔSIS(Mob)</b>	<b>ΔSIS(PS)</b>	<b>ΔBI</b>	<b>ΔARAT(A)</b>	<b>ΔSIS(HF)</b>	
1	R.Thal-R.SMA	R.PMC-R.M1	L.SMA-L.PMC	R.SMA-R.M1	L.SMA-R.M1	R.SMA-L.SMA	L.Thal-L.SMA	L.SMA-L.M1	
2	L.PMC-L.M1	L.SMA-R.PMC	R.SMA-R.M1	R.Thal-R.M1	Lesion Hemi	L.PMC-R.M1	L.Thal-L.PMC	L.Thal-L.M1	
3	R.PMC-L.PMC	R.SMA-L.PMC	L.SMA-R.M1	Motor Imp.	R.SMA-L.PMC	L.Thal-L.PMC	L.Thal-L.M1	R.SMA-R.PMC	
4			L.Thal-L.PMC	R.Thal-L.Thal	R.Thal-L.Thal	R.Thal-L.PMC	R.SMA-R.PMC	R.Thal-L.Thal	
5				R.PMC-L.M1	L.Thal-R.PMC	R.SMA-L.M1	Age		
6					L.SMA-L.M1	R.Thal-L.SMA	TSS		
7					L.PMC-L.M1	R.Thal-R.PMC	L.PMC-R.M1		
8					NIHSS	L.Thal-R.M1	L.SMA-L.M1		
9							R.Thal-L.Thal		
10							R.M1-L.M1		
11							L.PMC-L.M1		
12							Gender		
13							L.Thal-R.SMA		
14							NIHSS		

Input ΔFC at T6 + Clinical Features

Outcome at T7



15							L.Thal-R.PMC		
16							L.Thal-R.M1		

Note:  $\Delta FC$  correlates of  $\Delta$ behavior between all pairs of time-points identified by using linear-kernel SVR are presented; T4 = pre-therapy; T6 = post-therapy; T7 = 1-month post-therapy

***Behavioral correlates at preceding stages of behavioral outcomes at succeeding stages***

The performance of SVR using behavioral measures at preceding time-points as correlates of behavioral outcomes at succeeding time-points are presented in **Table 3.7**. All the SVR models performed better than chance-level based on permutation test ( $p < 0.05$ ). Individual predictors involved in estimating the different outcomes are listed in **Table 3.8**. Overall, the behavioral measures from the preceding time-point were almost always the highest-ranked correlates, relative to the clinical variables. Among the three time-points, better overall performances were found in cases of correlating behavior at T4 with those at T6.

**Table 3. 7.** Estimation of behavioral measures at succeeding time-point using behavioral measures at preceding time-point and clinical variables

Outcome	T4 behavior ~ T6 behavior			T4 behavior ~ T7 behavior			T6 behavior ~ T7 behavior		
	Features	RMSE	R <sup>2</sup>	Features	RMSE	R <sup>2</sup>	Features	RMSE	R <sup>2</sup>
<b>9HPT(A)</b>	2	2.52*	0.74	1	3.28*	0.52	3	3.25*	0.53
<b>9HPT(U)</b>	4	37.36*	0.91	5	23.4*	0.97	5	9.05*	0.99
<b>ARAT(A)</b>	3	2.73*	0.99	3	3.31*	0.98	3	3.13*	0.98
<b>BI</b>	1	5.48*	0.62	2	5.19*	0.54	3	4.83*	0.6
<b>SIS(ADL)</b>	3	8.56*	0.54	3	10.24*	0.54	3	11.42*	0.43
<b>SIS(HF)</b>	4	12.74*	0.86	4	13.03*	0.85	4	7.9*	0.94
<b>SIS(Mob)</b>	4	5.36*	0.71	2	11.8*	0.28	3	10.09*	0.47
<b>SIS(PS)</b>	2	14.7*	0.49	2	12.03*	0.46	3	8.85*	0.71

**Note:** Linear-kernel SVR performances based on leave-one out cross-validation to correlate behavioral measures at preceding time-point and clinical variables with behavioral measures at succeeding time-point are presented. Specific correlates are listed in **Table 3.8.**; \*significant against chance-level based on permutation-test ( $p < 0.05$ ); T4 = pre-therapy; T6 = post-therapy; T7 = 1-month post-therapy

**Table 3. 8.** Behavioral and clinical correlates of behavioral outcomes at succeeding time-points

Rank	9HPT(A)	9HPT(U)	ARAT(A)	SIS(ADL)	SIS(HF)	SIS(Mob)	SIS(PS)	BI	Outcome at T6 Input Behavior at T4 + Clinical Variables
1	9HPT(A)	9HPT(U)	Motor Imp.	SIS(ADL)	SIS(HF)	SIS(Mob)	SIS(PS)	BI	
2	NIHSS	Motor Imp.	ARAT(A)	Lesion Hemi	NIHSS	NIHSS	NIHSS		
3		NIHSS	NIHSS	NIHSS	TSS	TSS			
4		Lesion Hemi			Motor Imp.	Lesion Hemi			
Rank	9HPT(A)	9HPT(U)	ARAT(A)	SIS(ADL)	SIS(HF)	SIS(Mob)	SIS(PS)	BI	Outcome at T7 Input Behavior at T4 + Clinical Variables
1	9HPT(A)	9HPT(U)	ARAT(A)	SIS(ADL)	SIS(HF)	SIS(Mob)	SIS(PS)	BI	
2		NIHSS	Motor Imp.	Motor Imp.	NIHSS	Motor Imp.	Motor Imp.	TSS	
3		Motor Imp.	NIHSS	TSS	TSS				
4		Lesion Hemi			Motor Imp.				
5		TSS							
Rank	9HPT(A)	9HPT(U)	ARAT(A)	SIS(ADL)	SIS(HF)	SIS(Mob)	SIS(PS)	BI	Outcomes at T7 Input Behavior at T6 + Clinical Variables
1	9HPT(A)	9HPT(U)	ARAT(A)	SIS(ADL)	SIS(HF)	SIS(Mob)	SIS(PS)	BI	
2	TSS	Lesion Hemi	Motor Imp.	Motor Imp.	Motor Imp.	Motor Imp.	Age	TSS	
3	Motor Imp	Motor Imp.	NIHSS	TSS	NIHSS	NIHSS	Motor Imp.	Motor Imp.	
4		TSS			TSS				
5		NIHSS							

Note: Behavioral and clinical correlates at preceding time-points using linear-kernel SVR for estimation of measures at succeeding time-points are presented below; T4 = pre-therapy; T6 = post-therapy; T7 = 1-month post-therapy

### **3.3. Impact of clinical variables**

Each SVR model was tested for the impact of the identified clinical variables to account for potential confounding effects they might have. The most involved clinical features were: NIHSS, motor impairment severity for ANALYSIS I and III and NIHSS, motor impairment severity and lesion hemisphere for ANALYSIS II. In terms of ROI contribution, FC associated with L.M1, R.M1 and R.PMC were the important contributors for ANALYSIS I after adjusting for clinical confounds. For ANALYSIS II, the important contributors included L.M1, R.M1 and R.Thal with clinical variables.

## **4. Discussion**

### **4.1. Impact of BCI intervention based on identified correlates**

The objective of this study was to assess behavioral outcomes following the described BCI intervention. To do so, FC,  $\Delta$ FC and behavioral measures were utilized. Evaluation of outcomes at the third time-point, namely the one-month post-intervention, would be particularly important to understand the potential long-term impact of the intervention. As would be expected, behavioral measures at preceding time-points estimated the behavioral measures at succeeding time-points better than FC or  $\Delta$ FC. However, using behavioral measures alone does not provide the knowledge of possible neural reorganization in the brain. Neuroimaging-based FC features can offer this complementary information and serve as an alternative means to assess outcomes. In comparison to pre-intervention measures, the post-intervention input (FC,  $\Delta$ FC, behavioral) measures were more indicative of outcomes at one-month post-intervention. That could suggest neural reorganization occurring between pre- and post-intervention that is at least partially retained at one-month post-therapy.

#### **4.2. FC as a tool for predicting behavioral changes**

Functional MRI has been shown as a useful biomarker in predicting the impact of several forms of rehabilitation on the recovery of function in the stroke population [67; 68; 7; 69; 70]. Resting-state functional MRI, in particular, is a useful non-invasive method used to study impaired subjects such as stroke survivors, as it is time-efficient and task-free, reducing the burden on study participants. In the present study, the impact of BCI intervention was examined using FC and associated changes corresponding to several objective and subjective behavioral outcomes. Using FC as correlates formed reliable SVR models across all outcomes. However, with  $\Delta FC$ , models corresponding to ARAT(A) and SIS(HF) were only significant above chance-level. ARAT(A) and SIS(HF) are objective and subjective measures of impairment due to stroke and ability to use the impaired hand respectively. Improvement in these outcomes following the intervention demonstrates the impact of BCI-aided therapy. The models that were not significant against chance level could potentially be due to low variability in the normalized outcomes as well as limited sample size. Additionally, the main contributing regions remained focused on bilateral M1 areas with and without the influence of the clinical features. These findings illustrate that FC serves as a stable imaging biomarker in understanding the functional correlates of the recovery process and could, thus, guide future rehabilitative studies in tracking changes over time.

#### **4.3. Machine learning as a tool for predictive modeling**

In the context of functional MRI studies, fewer studies have used prediction of outcomes on a continuous scale [23; 71; 72; 24], where SVR-based models have been adopted to address different parts of data analysis, the majority of which, are based on a simple linear-kernel SVR. Findings, here, suggest promise in that, given functional MRI data from a large cohort, machine learning-based regression models may be trained to predict behavioral change resulting from BCI intervention on a single-subject level. From the clinical perspective, such an application could serve as a supplementary prognostic tool for patients and their families in estimating the timeline and/or capacity of potential recovery through this intervention.

#### 4.4. The bigger picture

This work adds to the ongoing investigation of understanding the trajectory of motor recovery in the chronic stage of stroke as a result of BCI-aided rehabilitative intervention using a data-driven approach. These findings are in line with works that suggest that using rehabilitative therapies have enabled recovery even at the chronic stage of stroke [9; 73]. This means that even though motor recovery associated with the paretic side might have plateaued, there could still be potential for further recovery. This was evident from the predominant involvement of FC and  $\Delta$ FC associated with the bilateral M1, which is primarily known to be a center for voluntary motor behavior including but not limited to movement planning, movement initiation and motor learning. While the roles of neuroimaging methods such as task-functional MRI [70] and diffusion images [10] in relation to motor recovery facilitated by BCI in the current cohort have been explored, the current study fills a gap by examining resting-state functional MRI as a potential biomarker for recovery. Since it is established that activations identified by task-functional MRI have overlapping functional areas with resting-state functional MRI within the motor network [74], it allows us to draw parallels between our study and those based on task-functional MRI. Additionally, thalamic  $\Delta$ FC also emerged as a region with strong involvement in estimating changes in ARAT(A) and SIS(HF), which was demonstrated using task-functional MRI activation associated with the same outcomes in our precedent study [70]. Another task-functional MRI-based study by Ward et al. [75] also reported thalamic correlations with motor recovery especially in stroke subjects (time since stroke onset > 3 months) with MCA lesions. It could be possible that the findings of this study are similar as half of the subjects included exhibited MCA lesions as well. From data modeling perspective, while traditional methods such as general linear models assume a certain distribution of data, SVR offers a non-parametric method that can model both linear and non-linear relationships in the data and adds to the growing body of studies using machine learning prediction models to analyze functional MRI [76; 23; 24].

#### **4.5. Limitations**

This study highlights how machine learning holds potential to provide useful information by correlating neuroimaging changes to behavioral changes. However, the results can be limited by the sample size that can, in turn, affect the capability of drawing generalizable conclusions as machine learning models such as SVR are typically based on training on data from a much larger cohort. Involvement of NIHSS stroke severity as a feature across multiple outcomes could suggest that lesion size and/or volume might be an important consideration [77; 78] and should be included in future analysis. Feature selection, realized by SFS, was important in deciding the role of relevant correlates of each behavioral scale. However, SFS suffers from the drawback that it cannot remove features from the model that become obsolete upon addition of new features. Recent work suggested that FC can be quantified in several ways using metrics such as cosine similarity and dynamic time warping [79]. Thus, the choice of metric used for FC might affect the features selected for each outcome.

#### **4.6. Future scope**

With ongoing recruitment, a larger and more generalizable prediction model could be developed by considering the following. The complete BCI-aided intervention involved both imaging as well as behavioral data at multiple distinct time points, of which only pre-, post- and one-month post-intervention data have been used in the current analysis. With a larger sample size, the analysis, therefore, could be expanded further by considering the changes in FC over other time-points and correlating them with corresponding behavioral outcomes and changes. Since recovery is a multi-faceted process, other imaging methods, such as diffusion tensor images, structural images, and perfusion images can provide complementary information about brain changes and could be incorporated as features to SVR. Potentially, multiple of these neuroimaging methods could be combined so as to assess the relative importance of each as a biomarker of stroke recovery through the BCI-intervention. Correlation and interaction among the different behavioral measures could be simultaneously accounted for by implementing a multiple-output SVR that uses a single model to predict multiple outcomes. Additionally, differences and similarities among

predictors between stroke subjects and matched healthy subjects undergoing the BCI-intervention will help to further understand the impact of this intervention.

## **5. Conclusion**

This investigation demonstrated that FC, changes in FC and early-stage behavior can estimate behavioral outcomes and changes in chronic-stage stroke subjects following this BCI-aided intervention for rehabilitation. Machine learning-based SVR models helped to identify specific correlates of for objective as well as subjective behavioral scales. Among the neural substrates identified, important regions contributing to the estimation involved the left and right primary motor areas. Given the promise of this kind of BCI intervention in stroke rehabilitation, the coupling of machine learning with neuroimaging and behavioral measures can aid further identification of neuroplastic changes corresponding to behavioral outcomes to estimate and track stroke recovery, both in terms of neural reorganization and improvements to motor function.



## References

- [1] S. Silvoni, A. Ramos-Murguialday, M. Cavinato, C. Volpato, G. Cisotto, A. Turolla, F. Piccione, N. Birbaumer, Brain-computer interface in stroke: a review of progress. *Clinical EEG and Neuroscience* 42 (2011) 245-252.
- [2] E. Felton, R. Radwin, J. Wilson, J. Williams, Evaluation of a modified Fitts law brain–computer interface target acquisition task in able and motor disabled individuals. *Journal of neural engineering* 6 (2009) 056002.
- [3] N.A. Bhagat, A. Venkatakrishnan, B. Abibullaev, E.J. Artz, N. Yozbatiran, A.A. Blank, J. French, C. Karmonik, R.G. Grossman, M.K. O'Malley, Design and optimization of an EEG-based brain machine interface (BMI) to an upper-limb exoskeleton for stroke survivors. *Frontiers in neuroscience* 10 (2016) 122.
- [4] A. Biasucci, R. Leeb, I. Iturrate, S. Perdakis, A. Al-Khodairy, T. Corbet, A. Schnider, T. Schmidlin, H. Zhang, M. Bassolino, Brain-actuated functional electrical stimulation elicits lasting arm motor recovery after stroke. *Nature communications* 9 (2018) 2421.
- [5] V.A. Nair, B.M. Young, Z. Nigogosyan, A. Remsick, S. Weber, K. Diffie, L. Walton, M. Tyler, J. Sattin, D.F. Edwards, Resting-state Functional Connectivity Changes After Stroke Rehabilitation Using Closed Loop Neurofeedback, *Am Heart Assoc*, 2015.
- [6] S.R. Soekadar, N. Birbaumer, M.W. Slutzky, L.G. Cohen, Brain–machine interfaces in neurorehabilitation of stroke. *Neurobiology of disease* 83 (2015) 172-179.
- [7] B. Várkuti, C. Guan, Y. Pan, K.S. Phua, K.K. Ang, C.W.K. Kuah, K. Chua, B.T. Ang, N. Birbaumer, R. Sitaram, Resting state changes in functional connectivity correlate with movement recovery for BCI and robot-assisted upper-extremity training after stroke. *Neurorehabilitation and Neural Repair* 27 (2013) 53-62.
- [8] B.M. Young, Z. Nigogosyan, L.M. Walton, J. Song, V.A. Nair, S.W. Grogan, M.E. Tyler, D.F. Edwards, K. Caldera, J.A. Sattin, Changes in functional brain organization and behavioral correlations after rehabilitative therapy using a brain-computer interface. (2014).
- [9] A. Caria, C. Weber, D. Brötz, A. Ramos, L.F. Ticini, A. Gharabaghi, C. Braun, N. Birbaumer, Chronic stroke recovery after combined BCI training and physiotherapy: a case report. *Psychophysiology* 48 (2011) 578-582.
- [10] J. Song, B.M. Young, Z. Nigogosyan, L.M. Walton, V.A. Nair, S.W. Grogan, M.E. Tyler, D. Farrar-Edwards, K.E. Caldera, J.A. Sattin, Characterizing relationships of DTI, functional MRI, and motor recovery in stroke rehabilitation utilizing brain-computer interface technology. *Frontiers in neuroengineering* 7 (2014).
- [11] S. Bajaj, A.J. Butler, D. Drake, M. Dhamala, Functional organization and restoration of the brain motor-execution network after stroke and rehabilitation. *Frontiers in human neuroscience* 9 (2015) 173.
- [12] M.H. Lee, C.D. Smyser, J.S. Shimony, Resting-state functional MRI: a review of methods and clinical applications. *American Journal of Neuroradiology* 34 (2013) 1866-1872.
- [13] C. Grefkes, S.B. Eickhoff, D.A. Nowak, M. Dafotakis, G.R. Fink, Dynamic intra-and interhemispheric interactions during unilateral and bilateral hand movements assessed with functional MRI and DCM. *Neuroimage* 41 (2008) 1382-1394.
- [14] C. Grefkes, G.R. Fink, Reorganization of cerebral networks after stroke: new insights from neuroimaging with connectivity approaches. *Brain* 134 (2011) 1264-1276.
- [15] F. Debaere, S.P. Swinnen, E. Béatse, S. Sunaert, P. Van Hecke, J. Duysens, Brain areas involved in interlimb coordination: a distributed network. *Neuroimage* 14 (2001) 947-958.

- [16] Z. Dai, C. Yan, Z. Wang, J. Wang, M. Xia, K. Li, Y. He, Discriminative analysis of early Alzheimer's disease using multi-modal imaging and multi-level characterization with multi-classifier (M3). *Neuroimage* 59 (2012) 2187-2195.
- [17] X. Ding, Y. Yang, E.A. Stein, T.J. Ross, Combining Multiple Resting-State functional MRI Features during Classification: Optimized Frameworks and Their Application to Nicotine Addiction. *Frontiers in human neuroscience* 11 (2017) 362.
- [18] P. Fergus, A. Hussain, D. Hignett, D. Al-Jumeily, K. Abdel-Aziz, H. Hamdan, A machine learning system for automated whole-brain seizure detection. *Applied Computing and Informatics* 12 (2016) 70-89.
- [19] A. Khazaee, A. Ebrahimzadeh, A. Babajani-Feremi, Application of advanced machine learning methods on resting-state functional MRI network for identification of mild cognitive impairment and Alzheimer's disease. *Brain imaging and behavior* 10 (2016) 799-817.
- [20] T.B. Meier, A.S. Desphande, S. Vergun, V.A. Nair, J. Song, B.B. Biswal, M.E. Meyerand, R.M. Birn, V. Prabhakaran, Support vector machine classification and characterization of age-related reorganization of functional brain networks. *Neuroimage* 60 (2012) 601-613.
- [21] R. Mohanty, A.M. Sinha, A.B. Remsik, K.C. Dodd, B.M. Young, T. Jacobson, M. Mcmillan, J. Thoma, H. Advani, V.A. Nair, Machine Learning Classification to Identify the Stage of Brain-Computer Interface Therapy for Stroke Rehabilitation Using Functional Connectivity. *Frontiers in neuroscience* 12 (2018).
- [22] A.K. Rehme, L.J. Volz, D.-L. Feis, I. Bomilcar-Focke, T. Liebig, S.B. Eickhoff, G.R. Fink, C. Grefkes, Identifying neuroimaging markers of motor disability in acute stroke by machine learning techniques. *Cerebral cortex* 25 (2014) 3046-3056.
- [23] N.U. Dosenbach, B. Nardos, A.L. Cohen, D.A. Fair, J.D. Power, J.A. Church, S.M. Nelson, G.S. Wig, A.C. Vogel, C.N. Lessov-Schlaggar, Prediction of individual brain maturity using functional MRI. *Science* 329 (2010) 1358-1361.
- [24] S. Vergun, A.S. Deshpande, T.B. Meier, J. Song, D.L. Tudorascu, V.A. Nair, V. Singh, B.B. Biswal, M.E. Meyerand, R.M. Birn, Characterizing functional connectivity differences in aging adults using machine learning on resting state functional MRI data. *Frontiers in computational neuroscience* 7 (2013).
- [25] E. Frank, L. Trigg, G. Holmes, I.H. Witten, Naive Bayes for regression. *Machine Learning* 41 (2000) 5-25.
- [26] T. Hastie, R. Tibshirani, Discriminant adaptive nearest neighbor classification and regression, *Advances in Neural Information Processing Systems*, 1996, pp. 409-415.
- [27] A. Marquand, M. Howard, M. Brammer, C. Chu, S. Coen, J. Mourão-Miranda, Quantitative prediction of subjective pain intensity from whole-brain functional MRI data using Gaussian processes. *Neuroimage* 49 (2010) 2178-2189.
- [28] S. Pereira, A. Pinto, V. Alves, C.A. Silva, Brain tumor segmentation using convolutional neural networks in MRI images. *IEEE transactions on medical imaging* 35 (2016) 1240-1251.
- [29] R. Mohanty, A. Sinha, A. Remsik, J. Allen, V. Nair, K. Caldera, J. Sattin, D. Edwards, J.C. Williams, V. Prabhakaran, Machine Learning-Based Prediction of Changes in Behavioral Outcomes Using Functional Connectivity and Clinical Measures in Brain-Computer Interface Stroke Rehabilitation, *International Conference on Augmented Cognition*, Springer, 2017, pp. 543-557.
- [30] G. Kwakkel, B.J. Kollen, H.I. Krebs, Effects of robot-assisted therapy on upper limb recovery after stroke: a systematic review. *Neurorehabilitation and neural repair* 22 (2008) 111-121.
- [31] P.M. Rossini, C. Calautti, F. Pauri, J.-C. Baron, Post-stroke plastic reorganisation in the adult brain. *The Lancet Neurology* 2 (2003) 493-502.
- [32] R. Teasell, N.A. Bayona, J. Bitensky, Plasticity and reorganization of the brain post stroke. *Topics in stroke rehabilitation* 12 (2005) 11-26.

- [33] L. Wang, C. Yu, H. Chen, W. Qin, Y. He, F. Fan, Y. Zhang, M. Wang, K. Li, Y. Zang, Dynamic functional reorganization of the motor execution network after stroke. *Brain* 133 (2010) 1224-1238.
- [34] C.E. Levy, D.S. Nichols, P.M. Schmalbrock, P. Keller, D.W. Chakeres, Functional MRI evidence of cortical reorganization in upper-limb stroke hemiplegia treated with constraint-induced movement therapy. *American Journal of physical medicine & rehabilitation* 80 (2001) 4-12.
- [35] B.M. Young, J. Williams, V. Prabhakaran, BCI-FES: could a new rehabilitation device hold fresh promise for stroke patients?, Taylor & Francis, 2014.
- [36] T. Brott, H.P. Adams, C.P. Olinger, J.R. Marler, W.G. Barsan, J. Biller, J. Spilker, R. Holleran, R. Eberle, V. Hertzberg, Measurements of acute cerebral infarction: a clinical examination scale. *Stroke* 20 (1989) 864-870.
- [37] D. Carroll, A quantitative test of upper extremity function. *Journal of chronic diseases* 18 (1965) 479-491.
- [38] C.E. Lang, J.M. Wagner, A.W. Dromerick, D.F. Edwards, Measurement of upper-extremity function early after stroke: properties of the action research arm test. *Archives of physical medicine and rehabilitation* 87 (2006) 1605-1610.
- [39] R.C. Oldfield, The assessment and analysis of handedness: the Edinburgh inventory. *Neuropsychologia* 9 (1971) 97-113.
- [40] G. Schalk, D.J. McFarland, T. Hinterberger, N. Birbaumer, J.R. Wolpaw, BCI2000: a general-purpose brain-computer interface (BCI) system. *IEEE Transactions on biomedical engineering* 51 (2004) 1034-1043.
- [41] A. Kübler, N. Neumann, J. Kaiser, B. Kotchoubey, T. Hinterberger, N.P. Birbaumer, Brain-computer communication: self-regulation of slow cortical potentials for verbal communication. *Archives of physical medicine and rehabilitation* 82 (2001) 1533-1539.
- [42] A. Kübler, F. Nijboer, J. Mellinger, T.M. Vaughan, H. Pawelzik, G. Schalk, D.J. McFarland, N. Birbaumer, J.R. Wolpaw, Patients with ALS can use sensorimotor rhythms to operate a brain-computer interface. *Neurology* 64 (2005) 1775-1777.
- [43] J.A. Wilson, G. Schalk, L.M. Walton, J.C. Williams, Using an EEG-based brain-computer interface for virtual cursor movement with BCI2000. *Journal of visualized experiments: JoVE* (2009).
- [44] B.M. Young, Z. Nigogosyan, V.A. Nair, L.M. Walton, J. Song, M.E. Tyler, D.F. Edwards, K. Caldera, J.A. Sattin, J.C. Williams, Case report: post-stroke interventional BCI rehabilitation in an individual with preexisting sensorineural disability. *Frontiers in neuroengineering* 7 (2014).
- [45] B.M. Young, Z. Nigogosyan, L.M. Walton, J. Song, V.A. Nair, S.W. Grogan, M.E. Tyler, D.F. Edwards, K. Caldera, J.A. Sattin, Changes in functional brain organization and behavioral correlations after rehabilitative therapy using a brain-computer interface. *Frontiers in neuroengineering* 7 (2014).
- [46] H.-M. Chen, C.C. Chen, I.-P. Hsueh, S.-L. Huang, C.-L. Hsieh, Test-retest reproducibility and smallest real difference of 5 hand function tests in patients with stroke. *Neurorehabilitation and neural repair* (2009).
- [47] R. Mahoney, Barthel Index (BI). Surya Shah, PhD, OTD, MEd, OTR, FAOTA, Professor Occupational Therapy and Neurology, Visiting Professor Neurorehabilitation, University of Tennessee Health Sciences Center 930 (1965) 1.
- [48] F.J. Carod-Artal, L.F. Coral, D.S. Trizotto, C.M. Moreira, The Stroke Impact Scale 3.0. *Stroke* 39 (2008) 2477-2484.
- [49] P.W. Duncan, D. Wallace, S.M. Lai, D. Johnson, S. Embretson, L.J. Laster, The stroke impact scale version 2.0. *Stroke* 30 (1999) 2131-2140.
- [50] K. Murphy, M.D. Fox, Towards a consensus regarding global signal regression for resting state functional connectivity MRI. *NeuroImage* (2016).
- [51] R.W. Cox, AFNI: software for analysis and visualization of functional magnetic resonance neuroimages. *Computers and Biomedical research* 29 (1996) 162-173.

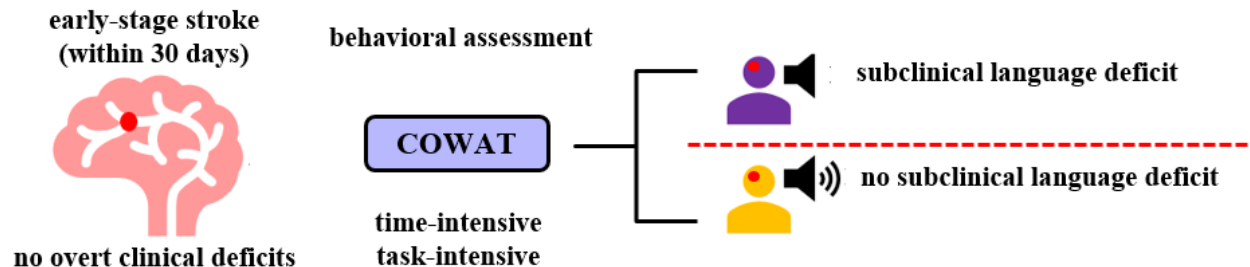
- [52] M. Xia, J. Wang, Y. He, BrainNet Viewer: a network visualization tool for human brain connectomics. *PloS one* 8 (2013) e68910.
- [53] M. Ferraro, J. Palazzolo, J. Krol, H. Krebs, N. Hogan, B. Volpe, Robot-aided sensorimotor arm training improves outcome in patients with chronic stroke. *Neurology* 61 (2003) 1604-1607.
- [54] A.K. Rehme, S.B. Eickhoff, C. Rottschy, G.R. Fink, C. Grefkes, Activation likelihood estimation meta-analysis of motor-related neural activity after stroke. *Neuroimage* 59 (2012) 2771-2782.
- [55] J. Crinion, J. Ashburner, A. Leff, M. Brett, C. Price, K. Friston, Spatial normalization of lesioned brains: performance evaluation and impact on functional MRI analyses. *Neuroimage* 37 (2007) 866-875.
- [56] M. Kelly-Hayes, A. Beiser, C.S. Kase, A. Scaramucci, R.B. D'Agostino, P.A. Wolf, The influence of gender and age on disability following ischemic stroke: the Framingham study. *Journal of Stroke and Cerebrovascular Diseases* 12 (2003) 119-126.
- [57] L. He, Y. Hu, Y. Li, D. Li, Channel selection by Rayleigh coefficient maximization based genetic algorithm for classifying single-trial motor imagery EEG. *Neurocomputing* 121 (2013) 423-433.
- [58] J. Lu, K.A. Mamun, T. Chau, Pattern classification to optimize the performance of Transcranial Doppler Ultrasonography-based brain machine interface. *Pattern Recognition Letters* 66 (2015) 135-143.
- [59] B. Scholkopf, A.J. Smola, *Learning with kernels: support vector machines, regularization, optimization, and beyond*, MIT press, 2001.
- [60] V. Vapnik, *The nature of statistical learning theory*, Springer science & business media, 2013.
- [61] T. Hastie, R. Tibshirani, J. Friedman, *The elements of statistical learning*. 2001. NY Springer (2001).
- [62] C.J. Burges, A tutorial on support vector machines for pattern recognition. *Data mining and knowledge discovery* 2 (1998) 121-167.
- [63] A.J. Smola, B. Schölkopf, A tutorial on support vector regression. *Statistics and computing* 14 (2004) 199-222.
- [64] A.D. Bull, Convergence rates of efficient global optimization algorithms. *Journal of Machine Learning Research* 12 (2011) 2879-2904.
- [65] M.A. Gelbart, J. Snoek, R.P. Adams, Bayesian optimization with unknown constraints. *arXiv preprint arXiv:1403.5607* (2014).
- [66] J. Snoek, H. Larochelle, R.P. Adams, Practical bayesian optimization of machine learning algorithms, *Advances in neural information processing systems*, 2012, pp. 2951-2959.
- [67] H. Johansen-Berg, H. Dawes, C. Guy, S.M. Smith, D.T. Wade, P.M. Matthews, Correlation between motor improvements and altered functional MRI activity after rehabilitative therapy. *Brain* 125 (2002) 2731-2742.
- [68] N. Sharma, J.C. Baron, J.B. Rowe, Motor imagery after stroke: relating outcome to motor network connectivity. *Annals of neurology* 66 (2009) 604-616.
- [69] N. Ward, M. Brown, A. Thompson, R. Frackowiak, Neural correlates of motor recovery after stroke: a longitudinal functional MRI study. *Brain* 126 (2003) 2476-2496.
- [70] B.M. Young, Z. Nigogosyan, A. Remsik, L.M. Walton, J. Song, V.A. Nair, S.W. Grogan, M.E. Tyler, D.F. Edwards, K. Caldera, Changes in functional connectivity correlate with behavioral gains in stroke patients after therapy using a brain-computer interface device. *Frontiers in neuroengineering* 7 (2014).
- [71] G. Ganesh, E. Burdet, M. Haruno, M. Kawato, Sparse linear regression for reconstructing muscle activity from human cortical functional MRI. *Neuroimage* 42 (2008) 1463-1472.
- [72] V. Michel, A. Gramfort, G. Varoquaux, E. Eger, B. Thirion, Total variation regularization for functional MRI-based prediction of behavior. *IEEE transactions on medical imaging* 30 (2011) 1328-1340.

- [73] S.E. Fasoli, H.I. Krebs, J. Stein, W.R. Frontera, N. Hogan, Effects of robotic therapy on motor impairment and recovery in chronic stroke. *Archives of physical medicine and rehabilitation* 84 (2003) 477-482.
- [74] B. Biswal, F. Zerrin Yetkin, V.M. Haughton, J.S. Hyde, Functional connectivity in the motor cortex of resting human brain using echo-planar mri. *Magnetic resonance in medicine* 34 (1995) 537-541.
- [75] N. Ward, M. Brown, A. Thompson, R. Frackowiak, Neural correlates of outcome after stroke: a cross-sectional functional MRI study. *Brain* 126 (2003) 1430-1448.
- [76] M.G. Di Bono, M. Zorzi, Decoding Cognitive States from functional MRI Data Using Support Vector Regression. *PsychNology Journal* 6 (2008) 189-201.
- [77] C.-L. Chen, F.-T. Tang, H.-C. Chen, C.-Y. Chung, M.-K. Wong, Brain lesion size and location: effects on motor recovery and functional outcome in stroke patients. *Archives of physical medicine and rehabilitation* 81 (2000) 447-452.
- [78] F. de Nap Shelton, M.J. Reding, Effect of lesion location on upper limb motor recovery after stroke. *Stroke* 32 (2001) 107-112.
- [79] S.M. Smith, K.L. Miller, G. Salimi-Khorshidi, M. Webster, C.F. Beckmann, T.E. Nichols, J.D. Ramsey, M.W. Woolrich, Network modelling methods for FUNCTIONAL MRI. *Neuroimage* 54 (2011) 875-891.

## CHAPTER 4: Identification of Subclinical Language Deficit Based on Post-Stroke Functional Connectivity Derived from Low Frequency Oscillations

---

### Graphical Summary



### Research Question

Can we identify post-stroke subclinical language deficit in a time-efficient and task-free manner?

### Publication

Mohanty, R., Nair, V.A., Tellapragada, N., Williams Jr, L.M., Kang, T.J. and Prabhakaran, V., 2018. "Identification of Subclinical Language Deficit Using Machine Learning Classification Based on Poststroke Functional Connectivity Derived from Low Frequency Oscillations." *Brain connectivity*.

### Abstract

Post-stroke neuropsychological evaluation can take a long time to assess impairments in subjects without overt clinical deficits. The current study utilized functional connectivity (FC) from ten-minute non-invasive resting-state functional MRI (resting-state functional MRI) to identify stroke survivors at risk for subclinical language deficit (SLD) using a machine learning classifier. Discriminative ability of FC derived from slow-4 (0.027-0.073 Hz), slow-5 (0.01-0.027 Hz) and low frequency oscillations (LFO; 0.01-0.1 Hz) were compared. Sixty clinically non-aphasic right-handed subjects were categorized into three subgroups based on stroke status and normalized verbal fluency score (VFS) based on Controlled Oral Word Association Test (COWAT): 20 ischemic stroke subjects at a higher risk of SLD (LD+; mean VFS=-1.77), 20 ischemic stroke subjects with lower risk of SLD (LD-; mean VFS=-0.05), 20 healthy controls (HC; mean VFS=0.29). T1-weighted and resting-state functional MRI scans were acquired within 30 days of stroke onset. Blood-oxygen-level-dependent signal was extracted from brain regions in the language network and FC based on Pearson's correlation was evaluated. Selected features were used by a multiclass support vector machine to classify test subject into one of the subgroups. Classifier performance was assessed using a nested leave-

one-out cross-validation. FC derived from slow-4 (70%) band provided the best accuracy in comparison to LFO (65%) and slow-5 (50%), reasonably higher than random chance (33.33%). Based on subgroup-specific accuracy, classification was best realized within the slow-4 band for LD+ (81.6%) and LD- (78.3%) and slow-4 and LFO bands for HC (80%), i.e., early stage stroke subjects showed a slow-4 FC dominance whereas HC also indicated the normalized involvement of FC in LFO. While frontal FC differentiated between stroke and healthy, occipital FC differentiated between the two stroke groups. We demonstrated that stroke survivors at risk for SLD can be differentiated from control subjects using task-free resting-state functional MRI with a classifier with reasonable accuracy in an expedited manner.

## 1. Introduction

Stroke is typically associated with high rates of morbidity, mortality and high levels of disability (e.g. loss in motor, speech, cognitive, visual functions) in survivors. The degree of impairment is largely determined by severity of stroke. On one hand, clinical deficits are severe impairments, easier to diagnose and well understood. On the other hand, subclinical deficits are milder forms of impairments, harder to identify and have been paid limited attention to in the literature. While subclinical deficits resulting from neurological diseases might not significantly deter normal brain functions, they may still impact the quality of life of the survivor in the long run. This has been shown for cognitive domains [1] and might be extended to the non-cognitive domains of the brain as well. Behavioral and neuropsychological assessments [2] serve as a medium to identify the extent of impairments caused due to the occurrence of stroke [3; 4]. Such assessments are especially important to identify subclinical impairments. This typically requires administration of a battery of tests, tasks, and questionnaires by a trained professional to evaluate post-stroke brain functions. The scores achieved by the subject on these tests reflect the areas and degrees of impairments. While the neuropsychological exams are very detailed and helpful in determination and extent of deficits, the administration is time-intensive, and assessments can be task-intensive for the participants. Here, the goal was to assess if neuroimaging methods can provide information, equivalent or supplementary, to neuropsychological testing in terms of diagnosing post-stroke subclinical deficits. Specifically, this was tested for the language domains in stroke survivors relative to control subjects within stroke as well as healthy populations. To this end, it is important to choose a suitable modality of imaging to use and the specific information to be extracted from it. A convenient method is resting-state functional MRI (resting-state functional MRI) which is non-invasive, time-efficient and task-free for the subjects. Examination of network-based functional connectivity could additionally narrow down the search for specific subclinical deficits among stroke survivors.

From the perspective of neuroimaging, overt clinical post-stroke impairments and recovery in various domains such as cognition, motor, language, emotional, etc. are largely well explored [5; 6; 7]. However,



limited studies have examined the subclinical impairments following stroke. While many studies have delved deep into discerning the nature of mild impairments in cognitive brain functions [8; 9; 10] due to association with dementia and Alzheimer's disease, such subclinical impairments may or may not be the consequence of stroke. Several studies have examined mild deficits occurring after stroke and are limited to mainly cognitive, motor domains [11; 12; 13; 14]. Relatively fewer studies have analyzed mild impairments in language network following stroke [15; 16]. The present study adds to this by presenting a resting-state functional MRI based approach to analyze subclinical deficits in the language domain in sample stroke subjects. Low frequency blood-oxygen-level dependent (BOLD) fluctuations are typically extracted from resting-state functional MRI in the frequency range of 0.01-0.1 Hz to filter out the effect of physiological noise [17]. Based on electrophysiological studies, this frequency band is further subdivided into multiple bands, i.e. slow-5 (0.01-0.027 Hz), slow-4 (0.027-0.073 Hz) and partially slow-3 (0.073–0.198 Hz) [18; 19]. Specifically, grey matter corresponds to the slow-4 and slow-5 bands while slow-3 and slow-2 (0.198-0.25 Hz) have been typically associated with signals arising due to respiratory, cardiac processes and linked to white matter [20]. Recently Gohel and colleagues [21] suggested that resting-state functional MRI exhibits functional connectivity (FC) distributed over multiple frequency bands in healthy adults. While this multi-band FC approach has also been demonstrated in epileptic population and in population with vascular dementia [22] using machine learning classification, similar effects have not been documented in case of stroke population. These factors serve as the primary motivation for the current study.

This study was focused on identification of subclinical deficits at an early-stage (within 30 days of stroke onset) after stroke by examining neuroimaging data in place of commonly used neuropsychological test scores. Specifically, we demonstrated, using resting-state functional MRI, that cases of subclinical language deficit (SLD) can be differentiated from the cases without SLD. This was achieved by evaluating the resting-state FC in the language network. While FC is most commonly evaluated in the low frequency oscillation band (LFO; 0.01-0.1 Hz), motivated by the evidence on the multi-band phenomenon of FC

described in the previous section, we examined two subset bands namely the slow-4 and slow-5 bands to test their discriminative powers in identification of SLD. A multi-class support vector machine (SVM) based machine learning classifier was employed to identify specific brain regions and connections between stroke subjects with and without SLD. Additionally, a third group of healthy subjects was included as a control group to account for changes in FC due to normal aging. The significance of this work is three-fold: (i) findings suggest that task-free neuroimaging such as resting-state functional MRI, acquired in a span of about ten-minutes, could provide useful information to identify SLD which otherwise takes longer to assess via neuropsychological assessments; (ii) results demonstrate that FC derived from slow-4 band that corresponds to the grey matter in the brain is more relevant and informative than the conventionally used FC in LFO or slow-5 bands to study stroke population, and (iii) the distinction between the presence or absence of SLD can be automated with a high performance machine learning classifier.

## **2. Methods**

### **2.1 Subjects**

Sixty subjects were recruited as a part of an ongoing longitudinal study investigating neuroplasticity and recovery in stroke survivors. The cohort consisted of three subgroups formed on the basis of stroke status and normalized score on the verbal fluency (NVF) behavioral task:

- (i) 20 ischemic early-stage stroke subjects at a higher risk of SLD (LD+)
- (ii) 20 ischemic early-stage stroke subjects at a lower risk of SLD (LD-)
- (iii) 20 healthy control subjects (HC)

The inclusion criteria for enrollment of stroke subjects in this study were: 18 years or older with ischemic stroke and ability to provide written consent. The lower age limit of 18 years was the only inclusion criterion for enrollment of healthy subjects in the study. The exclusion criteria for the study were: subjects with contraindications for MRI such as having pacemakers, defibrillator, aneurysm clips, metallic components etc., subjects under certain types of medication for psychiatric illness or confounding neurological disorders

and subjects with history of drug abuse. The group membership of the stroke subjects to LD+ or LD- was determined based on a median-split of collective NVF scores of the 40 stroke subjects. The sample characteristics of the subjects are listed in **Table 4.1**. Subjects were age, gender and education matched across the three subgroups. Time since stroke was calculated as the time between stroke onset and the date of scan. Lesion hemisphere was determined based on the scan by a neuroradiologist to be either left (L), right (R) or bilateral (B). Stroke severity was based on NIHSS score and was trichotomized into: (a) minor (min; NIHSS = 0-4); (b) moderate (mod; NIHSS = 5-16); (c) missing (miss; NIHSS not available). The study was conducted in accordance with protocol approved by the local Health Sciences Institutional Review Board. All subjects provided written informed consent. All subjects were clinically non-aphasic. Additionally, for the purposes of this analysis, only right-handed subjects were chosen since language network in the brain could be lateralized depending upon handedness [23].

**Table 4. 1. Study sample characteristics**

	<b>LD+</b>			<b>LD-</b>			<b>HC</b>
Sample Size	20			20			20
Handedness	R			R			R
Age (mean age $\pm$ SD)	58.35 $\pm$ 15.23			63.10 $\pm$ 12.59			57.85 $\pm$ 7.75
Gender (Male/Female)	12/8			15/5			11/9
Education (mean years $\pm$ SD)	14.84 $\pm$ 2.71			14.84 $\pm$ 2.26			16.5 $\pm$ 3.13
Lesion Hemisphere	<b>L</b>	<b>R</b>	<b>B</b>	<b>L</b>	<b>R</b>	<b>B</b>	N/A
	14	6	0	10	7	3	
Stroke Severity	<b>Min</b>	<b>Mod</b>	<b>Miss</b>	<b>Min</b>	<b>Mod</b>	<b>Miss</b>	N/A
	15	3	2	18	1	1	
Time Since Stroke (mean days $\pm$ SD)	7.15 $\pm$ 3.67			8.45 $\pm$ 9.62			N/A
NVF score (mean NVF $\pm$ SD)	-1.776 $\pm$ 0.62			-0.05 $\pm$ 0.53			0.29 $\pm$ 0.97

Note: The three subgroups are: LD+ (stroke subgroup at higher risk of SLD), LD- (stroke subgroup at lower risk of SLD), HC (healthy control subgroup). NVF refers to the normalized verbal fluency score as measured by COWAT during behavioral testing outside the scanner.; Lesion Hemisphere: L = left, R = right, B = bilateral; Stroke Severity: Min = minor, Mod = moderate, Miss = missing; SD = standard deviation; NVF = normalized verbal fluency score;

## 2.2 Data Acquisition: Neuroimaging and Behavioral Data

Five-minute structural MRI scans were acquired on 3T GE 750 scanners (GE Healthcare, Waukesha, WI) equipped with an eight-channel head coil. These were T1-weighted axial anatomical scans and were collected using FSPGR BRAVO sequence with the following specifications: TR = 8.132 ms, TE = 3.18 ms, TI = 450 ms over a 256  $\times$  256 matrix and 156 slices, flip angle = 12°, FOV = 25.6 cm, slice thickness = 1 mm. Resting-state functional MRI were collected with subjects lying in the scanner eyes closed lasting about 10 minutes. Resting-state functional MRI were obtained using single-shot echo-planar T2\*-weighted imaging with the following parameters: TR = 2.6 s, 231 time-points, TE = 22 ms,

FOV = 22.4 cm, flip angle =  $60^\circ$ , voxel dimensions  $3.5 \times 3.5 \times 3.5 \text{ mm}^3$  and 40 slices. Assessment of SLD was based on verbal fluency task administered outside the scanner during behavioral testing by conducting the Controlled Oral Word Association Test (COWAT)[24]. The scores obtained on this test facilitate detection of disorders in and characterization of the language network in the brain.

### **2.3 Data Preprocessing: Neuroimaging Data**

Subjects were chosen so that their scans were free of any obvious artifacts upon visual inspection. Resting-state functional MRI data were processed using AFNI [25]. For functional MRI, the first 3 volumes were discarded, rest of the volumes were despiked to truncate spikes in time course of each voxel arising due to motion, slice time corrected with the initial volume as the reference, aligned with the structural scan, normalized to the standard MNI (Montreal Neurological Institute) space, censored for motion (based on the Euclidean norm computed from motion parameters and derivatives ; threshold = 0.25 mm) and bandpass filtered simultaneously, spatially smoothed with a 4-mm full-width-half-maximum Gaussian kernel based on a prior similar study [16]. Motion-based volume removal was performed when more than 10% of the automasked brain were deemed outliers. Regression of motion parameters, derivatives of motion parameters, rate of change of BOLD signal (DVARs), white matter and cerebrospinal fluid signals were performed simultaneously in a single general linear regression model. The bandpass filtering was focused to the three frequency bands of interest: the conventional LFO (0.01-0.1 Hz), slow-4 (0.027-0.073 Hz) and slow-5 (0.01-0.027 Hz) frequency bands. This resulted in three sets of data that were separately analyzed and compared. Global signal regression was omitted due to the controversial position associated with it in the literature [26].

## 2.4 Data Preprocessing: Behavioral Data

Raw values of scores achieved on the verbal fluency task were corrected for age and education as proposed by Tombaugh and colleagues [27]. The raw score was transformed as follows:

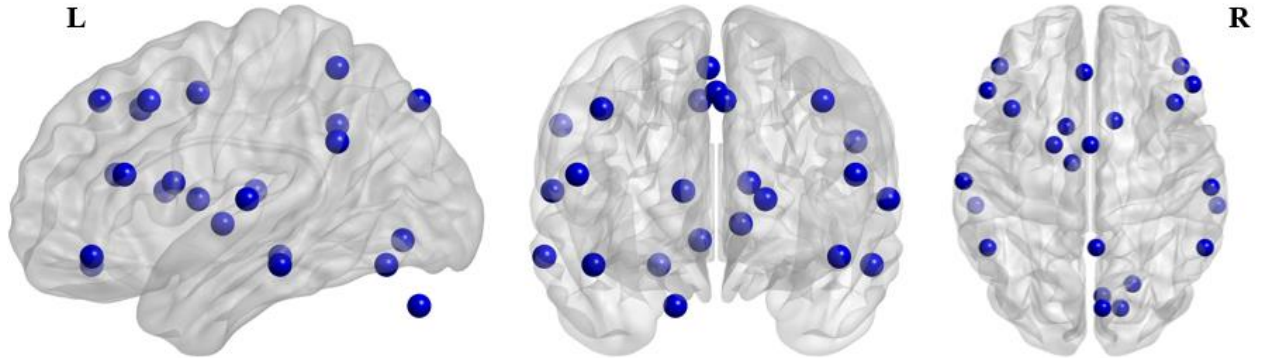
$$NVF = \frac{RVF - M}{SD} \quad (1)$$

where,  $NVF$  is the normed verbal fluency score,  $RVF$  is the raw verbal fluency score,  $M$  is the mean percentile score specific to the age group and level of education, and  $SD$  is the standard deviation percentile score specific to the age group and level of education.

## 2.5 Seed-based Functional Connectivity

Since this work was focused on the language network, a seed-based FC approach was adopted. Based on a prior study [28], 23 seed regions of interest (ROI) were chosen. This ROI template provides coverage of brain regions responsible for multiple aspects of language processing such as phonological and lexical-semantic functions, speech comprehension and production. The MNI coordinates of the seeds are visualized in **Figure 4.1** using BrainNet Viewer [29]. Spherical seeds at the specified MNI coordinates were created, each of radius 6 mm for each subject. This template was applied to the spatially normalized residuals of the resting data and BOLD time series was extracted at each ROI. A correlation matrix of size  $23 \times 23$  was generated by temporally correlating time series from pairs of seeds. Of the 529 total correlation coefficients,  $253 = \left(\frac{23 \times (23-1)}{2}\right)$  unique coefficients were retained for analysis and duplicates were discarded. This process was replicated for each subject and for each frequency band.

**Figure 4. 1.** *The 23 brain regions used of the language network in this study*



## 2.6 Data Analysis: Sample Characteristics

The subjects were chosen so as to have similar distributions in terms of age, gender and education levels across the three subgroups. A two-sample t-test was carried out to identify any group differences in terms of age, education levels, time since stroke and NVF. Since gender is a categorical variable, Fisher exact test was performed to study group differences. All tests were performed between pairs of subgroups. A number of metrics were evaluated for the purposes of quality control and to measure the impact of head motion on subsequent FC measures. We compared the six directional motion parameters obtained during motion correction from preprocessing [30; 31], frame-wise displacement (FD) to measure change in position of the head based on the derivatives of the motion parameters [32], DVARS index to capture the rate of change of BOLD signal intensity [33] and the temporal signal-to-noise ratio (tSNR) [34].

## 2.7 Data Analysis: Group Classification

Machine learning classification algorithms such as support vector machines (SVM) have been shown to be have reasonably reliable performance with FC data [35; 36; 37]. A similar paradigm was adopted here and expanded it further by implementing multiclass linear-kernel SVM to perform classifications among the classes: LD+, LD-, and HC based on a one-vs-one coding scheme. Since classification can be influenced by the number of features with respect to the sample size, we compared the performance with and without

feature selection procedures. Appropriate feature selection can enhance classification accuracy by limiting the data to useful information [38].

### **2.7.1 Outlier Removal**

Prior to training a classifier, to ensure that the FC features were not impacted by outliers, an outlier removal step was deployed over all the features. Any value that was more than three scaled median absolute deviations (MAD) [39] away from the median was deemed an outlier and was removed. This was repeated for features of each subgroup and all possible outlier features were eliminated retaining common features across all subgroups.

### **2.7.2 Feature Selection**

FC features were ranked by importance depending upon their contribution towards the classification with a feature selection procedure. The aim of this step was to narrow down the search to a smaller subset of important features which can achieve a good classification performance. A neighborhood component analysis (NCA) algorithm [40] facilitated selection of features as it does not assume any parametric distribution of the features and is also suitable for multiclass classification using high dimensional features [41]. This method learns weights corresponding to each feature while minimizing the cross-validation error. The features assigned with non-zero weights were then retained and fed into a multiclass SVM for classification among subgroups.

### **2.7.3 Model Parameter Optimization**

The hyperparameters namely the misclassification cost and kernel scale corresponding to the classifier were optimized with a Bayesian optimization [42] approach to prevent overfitting. By minimizing the cross-validation error over a range of values for 30 iterations, the optimal parameter values were obtained.



#### **2.7.4 Classification**

The goal of the current study was to be able to classify a given subject into one of the groups based on the selected FC data as representative features. A three-class linear-kernel SVM [43] was applied due to the advantage of ease of interpretation of results. Data were standardized so that each feature had the same mean and variance to avoid one feature from dominating others due to a large magnitude. Since the dataset consists of three classes (LD+, LD-, HC), the identification of SLD was modeled as a multi-(three)class problem [44]. A one-vs-one scheme was adopted which follows a pairwise decomposition [45], within which, all possible pairwise classifiers were trained and evaluated. This means individual binary classifiers to differentiate between LD+ vs LD-, LD- vs HC and HC vs LD+ were considered. This was adopted over one-vs-all approach, which would lead to an imbalance in class representation for the FC data in this cohort. Each learned binary classifier is applied to the test sample and the winning class gets one vote. Finally, the test sample was labeled to the class that received the greatest number of votes.

#### **2.7.5 Cross-validation**

A nested leave-one-out cross-validation (LOOCV) [46; 47] was adopted to estimate classifier performance as it provides an unbiased approximation of the test error and is more suitable for a dataset with limited number samples such as here. In the inner loop of this LOOCV, feature selection was performed by training and validation based on the NCA method described above. The winning model from the inner loop corresponded to the one that used the minimum number of features to avoid over-fitting and predicted maximum posterior probability. The outer loop of LOOCV optimized the validated winning model from the inner loop by tuning the hyperparameters, tested the new or unseen data and was used to evaluate the quality of classifier performance. Since the training and testing data subsets are completely independent, nested cross validation avoided learning an over optimistic model and provided generalizable classifier performance [46].

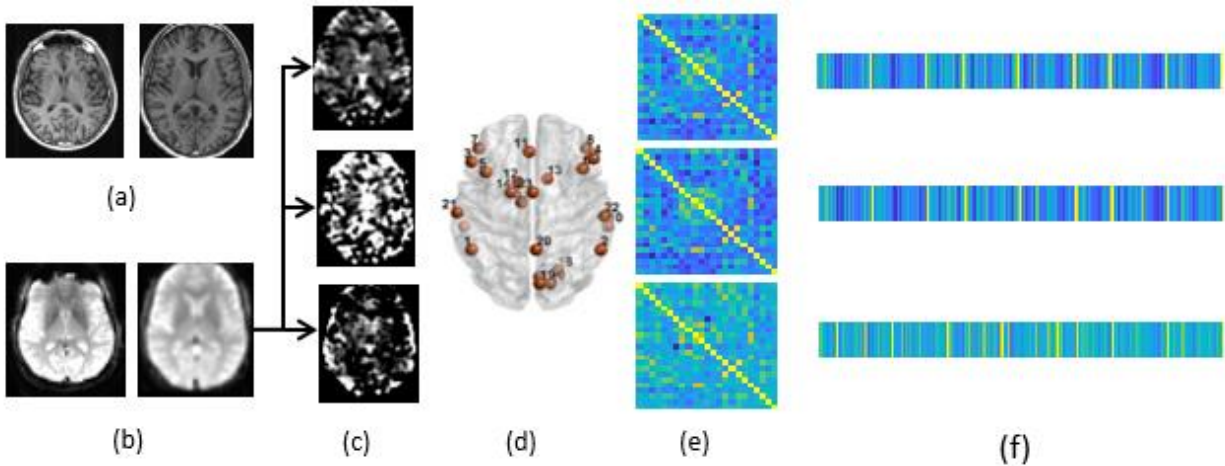
### **2.7.6 Feature Contribution**

Once a model was learned with optimal parameters, the use of a linear-kernel SVM enabled analysis of individual feature importance. The most discriminatory features were the FC connections which were involved in classification of each left out sample during independent testing in the outer loop of nested cross-validation. The learned classifier model yielded a weighting coefficient corresponding to each of the selected features from the NCA model, whose magnitude was proportional to the importance of the features in discriminating between subgroups. These weights for the FC features were used to determine the weights of the involved ROIs [35; 48].

### **2.7.7 Overview of Methodology**

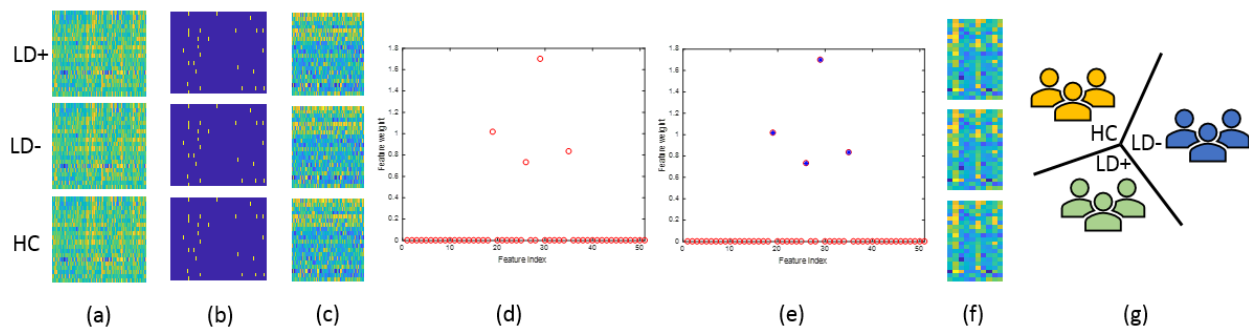
Overall, optimized classification models were learned using FC in each frequency band, the subset of contributing features and ROIs were identified that provided the maximum discriminative power for each based on cross-validation performance and comparisons were drawn. All computations were carried out with the Statistics and Machine Learning Toolbox in MATLAB R2017a (The MathWorks, Inc., Natick, Massachusetts, United States). The individual subject-level and group-level pipelines are visualized in **Figure 4.2** and **Figure 4.3** respectively.

**Figure 4. 2. Methodology for single subject analysis**



Note: (a) raw structural T1 scan (left) and T1 scan spatially normalized to MNI space (right); (b) raw functional scan (left) and preprocessed up to smoothing (right); (c) smoothed functional MRI is temporally filtered in the LFO (top), slow-4 (center), slow-5 (bottom) bands; (d) 23 ROIs of the language network used to extract BOLD time courses for each of the three frequency bands; (e)  $23 \times 23$  FC matrix computed for LFO (top), slow-4 (center) and slow-5 (bottom) bands; (f) FC matrix reduced to 235-dimensional vector constituting of unique correlation coefficients between pairs of ROIs.

**Figure 4. 3. Methodology for group level analysis**



Note: (a) vectorized form of FC matrix for each subject aggregated by subgroup, i.e. LD+, LD- and HC each have 20 subjects with 253-dimensional features; (b) outliers (marked in yellow) in each subgroup identified using MAD approach; (c) reduced FC matrix after cumulative removal of outliers, i.e. each subgroup consists of 20 subjects but fewer than 253 features; (d) plot of the remaining features marked in red circles weighted as per the NCA feature selection method in the inner loop of nested cross-validation; (e) plot of selected features with significant weights marked in blue to be used for classification of the left out sample in the inner loop of nested cross-validation; (f) model selection based on reduced FC matrix limited to features selected in the previous step; (g) the selected features are then fed to the multiclass SVM classifier that labels the left out test subject to LD+, LD- or HC in the outer loop of nested cross-validation. Steps (a) through (g) are repeated for LFO, slow-4 and slow-5 bands.

### 3. Results

#### 3.1 Effect of Sample Characteristics

The three subgroups were selected to be right handed and tested for differences with respect to age, gender and education. Two-sample t-test confirmed that there were no significant differences in either age ( $p$ -value  $> 0.12$  for each pair) or education ( $p$ -value  $> 0.06$  for each pair) among the subgroups. A Fisher exact test suggested no significant difference in gender distribution across the subgroups ( $p$ -value  $> 0.19$  for each pair). The two stroke subgroups, i.e. LD+ and LD-, did not significantly differ with respect to the time since stroke ( $p$ -value  $> 0.49$ ). Two-sample t-test on NVF scores showed significant differences between LD+ and LD- ( $p$ -value  $< 0.05$ ) as well as LD+ and HC ( $p$ -value  $< 0.05$ ) but not between LD- and HC ( $p$ -value  $> 0.16$ ).

#### 3.2 Head Motion Analysis

With the data for measuring motion being normally distributed, two sample t-test identified a significant group difference in terms of DVARS between LD- and HC subgroups as seen in **Table 4.2**. We added DVARS as a regressor in addition to motion parameters and derivatives to the general linear model during preprocessing to remove any impact it might have on computation of FC.

**Table 4. 2** Group means and group differences in head motion

Metric	LD+	LD-	HC	<i>p</i> -values for group differences		
				LD+ vs LD-	LD- vs HC	HC vs LD+
Translation along x	0.06	0.14	0.06	0.42	0.41	0.97
Translation along y	0.11	-0.10	-0.12	0.22	0.91	0.16
Translation along z	0.05	0.14	0.06	0.35	0.38	0.95
Rotation along x	0.24	0.16	0.21	0.55	0.72	0.75
Rotation along y	0.03	0.13	0.01	0.12	0.13	0.86
Rotation along z	-0.06	-0.05	-0.02	0.93	0.41	0.38
FD	0.10	0.10	0.09	0.93	0.53	0.62
DVARS	34.99	38.41	29.84	0.37	<b>0.01*</b>	0.15
tSNR	443.12	448.93	450.46	0.86	0.94	0.80

Note: \*significant group difference with  $p < 0.05$ ; FD = frame-wise displacement; DVARS = rate of change of BOLD signal; tSNR = temporal signal-to-noise-ratio;

### 3.3 Performance Evaluation

The performance of the learned classifiers was evaluated with as well as without the steps of outlier detection and feature selection. The classifier accuracies were enhanced when outlier features were excluded, and specific features were selected. In both cases, the slow-4 band demonstrated the best classification performance. The results from individual steps are described below.

#### 3.3.1 Outlier Removal

The 253 FC coefficients were each tested for presence of outliers. Features were removed if they contained values that were more than three scaled MAD from the median. MAD was chosen as it is more robust in comparison to the standard deviation measure. The number of features remaining are listed in **Table 4.3** and were comparable across the three frequency bands.

**Table 4. 3.** *The number of FC features outlier removal and feature selection for each frequency band*

<b>Data Processing Step</b>	<b>LFO</b>	<b>Slow-4</b>	<b>Slow-5</b>
Initial number of features	253	253	253
Number of features retained after outlier removal using median absolute deviation (MAD)	148	157	145
Number of features selected by neighborhood component analysis (NCA) during LOOCV	5	9	5

### 3.3.2 Feature Selection

The features remaining after outlier elimination were used as input to the NCA method which was carried out as the part of the inner loop of nested cross-validation. A subset of the input features from the training set that were assigned with significant weights were chosen as the final features for classification of each left out sample. The number of features retained after NCA, computed as the number of FC features used by each winning model in the inner loop that were common across all folds, is summarized in **Table 4.3**.

### 3.3.3 Cross-validation and Model Parameter Optimization

A three-class classifier, based on the features chosen in the previous step, was selected and tested on the completely independent left-out sample in the outer cross-validation for each frequency band. Each selected model was also optimized for the hyperparameters. Classification performance was tested using the outer loop of LOOCV method and the average performance was used to assess and compare results as quantified in **Table 4.4**. Accuracy of LOOCV represents the percentage of individual samples that were correctly

classified when left out completely independent of training or validation. Slow-4 band showed the highest accuracy with outlier detection and feature selection, followed by LFO and slow-5 bands with all of them performing better than random classifier. Since accuracy is a single point statistic, a  $3 \times 3$  confusion matrix metric was realized demonstrating that the slow-4 band showed a more balanced confusion matrix relative to the other two bands. Additionally, samples from the LD+ subgroup were classified better than the other subgroups in the slow-4 band. The overall results were broken down further by reducing the multiclass  $3 \times 3$  confusion matrix into a  $2 \times 2$  confusion matrix as in **Table 4.5 (I)**. This allowed us to study, in detail, the proportion of samples that were correctly classified for each subgroup as enumerated in **Table 4.5 (II)**. Multiple performance evaluation metrics, in addition to accuracy, were evaluated for each class such as sensitivity (=recall), specificity, precision, F-score. Across all measures, the LD+ subgroup was best classified. In terms of the overall specificity and precision, the HC subgroup was better classified than LD- subgroup. Based on the overall sensitivity, accuracy and F-score, LD- subgroup was better classified than the HC subgroup. Slow-4 band appeared to be dominant in identifying samples from the two stroke subgroups (LD+ and LD-) while both slow-4 and LFO performed similarly in identifying samples from HC subgroup.

**Table 4. 4. Multiclass classification performance in three frequency bands**

	<b>LFO</b>			<b>Slow-4</b>			<b>Slow-5</b>			
Random classifier accuracy	33.33 %									
<b>Without outlier detection or feature selection</b>										
Input features	253			253			253			
LOOCV accuracy	48.33 %			56.67 %			46.67 %			
<b>With outlier detection and feature selection</b>										
Input features	5			9			5			
LOOCV accuracy	65 %			70 %			50 %			
Confusion matrix		<b>LD+</b>	<b>LD-</b>	<b>HC</b>	<b>LD+</b>	<b>LD-</b>	<b>HC</b>	<b>LD+</b>	<b>LD-</b>	<b>HC</b>
	<b>LD+</b>	11	7	2	16	3	1	12	2	6
	<b>LD-</b>	2	15	3	3	13	4	2	10	8
	<b>HC</b>	2	5	13	4	3	13	5	7	8

Note: Overall comparative results obtained from nested cross-validation of multiclass SVM classifiers for the three frequency bands. In comparison to the 33.3% accuracy of random classification, the multiclass classifiers perform better. SVM based on feature selection outperform the ones not using feature selection.



**Table 4. 5. One-vs-rest classification**

**(I)** Confusion matrix reduced to one-vs-rest confusion table for each class with outlier detection and feature selection based on the nested cross-validation

		LFO			Slow-4			Slow-5		
		Predicted Labels								
LD+ versus Rest	Actual Labels		LD+	Rest		LD+	Rest		LD+	Rest
		LD+	11	4	LD+	16	7	LD+	12	7
		Rest	9	36	Rest	4	33	Rest	8	33
LD- versus Rest			LD-	Rest		LD-	Rest		LD-	Rest
		LD-	15	12	LD-	13	6	LD-	10	9
		Rest	5	28	Rest	7	34	Rest	10	31
HC versus Rest			HC	Rest		HC	Rest		HC	Rest
		HC	13	5	HC	13	5	HC	8	14
		Rest	7	35	Rest	7	35	Rest	12	26

**(II)** Class-specific performance metrics derived from the one-vs-rest confusion table

	LD+			LD-			HC		
	LFO	Slow-4	Slow-5	LFO	Slow-4	Slow-5	LFO	Slow-4	Slow-5
Sensitivity	55 %	80 %	60 %	75 %	65 %	50 %	65 %	65 %	40 %
Specificity	90 %	82.5 %	82.5 %	70 %	85 %	77.5 %	87.5 %	87.5 %	65 %
Precision	73.3 %	69.5 %	63.1 %	55.5 %	68.4 %	52.6 %	72.2 %	72.2 %	36.3 %
Accuracy	78.3 %	81.6 %	75 %	71.6 %	78.3 %	68.3 %	80 %	80 %	56.6 %
F-score	0.628	0.744	0.615	0.638	0.667	0.513	0.684	0.684	0.384

### 3.4 Discriminating Features and Seed Regions for Classification

#### 3.4.1 Discriminating FC Features

A comparison of selected features across subgroups was performed. The mean FC for each subgroup corresponding to the discriminating features (features common across all folds of cross-validation used by the winning model) were further analyzed. An independent two-sample t-test revealed the features that showed significant differences. In the LFO band, the features that were significantly different showed increasing trend in the group mean FC values from LD+ to LD- to HC. In the slow-4 band, the features that were significantly different showed similar gradual increase across some features as well as comparable mean FC levels between LD- and HC but significantly different from LD+ across other features. No consistent pattern among the mean FC values across subgroups were observed in the slow-5 band. The individual features are listed in **Table 4.6**. The common features across frequency bands are highlighted in **Table 4.6**. In particular, connectivity between the right pars opercularis and the left middle frontal seeds was observed to be the only common discriminating feature across all three frequency bands.

**Table 4. 6. Discriminating features in three frequency bands**

Feature Index	LFO		Slow-4		Slow-5	
	ROI 1	ROI 2	ROI 1	ROI 2	ROI 1	ROI 2
1	*†L Superior Temporal	L Inferior Temporal	†L Superior Frontal	Cingulate	L Wernicke	L Inferior Temporal
2	R Pars Orbitalis	L Inferior Temporal	***†R Pars Opercularis	L Middle Frontal	***R Pars Opercularis	L Middle Frontal
3	***†R Pars Opercularis	L Middle Frontal	*R Striate	L Middle Frontal	L Ventral Thalamus	L Putamen
4	†L Ventral Thalamus	L Putamen	*†R Inferior Temporal	L Wernicke	*†R Superior Temporal	R Inferior Temporal
5	R Pars Triangularis	R Inferior Temporal	*†R Striate	L Wernicke	R Superior Temporal	R Pars Orbitalis
6			R Inferior Temporal	R Inferior Parietal		
7			***R Superior Temporal	R Pars Orbitalis		
8			*†R Striate	R Pars Triangularis		
9			***R Superior Temporal	R Striate		
<b>Color Legend</b>						
	Discriminating features common to all frequency bands					
	Discriminating features common to slow-4 and slow-5 frequency bands					
	Discriminating features common to LFO and slow-5 frequency bands					

Note: Specific FC features that discriminate between pairs of subgroups during classification for the LFO, slow-4 and slow-5 bands arranged in order of their contribution determined by SVM weights. Common features across subgroups are highlighted as per the color legend below; \*significant difference between group means of LD+ and LD-; †significant difference between group means of LD+ and HC; \*\*\*significant difference between group means of LD- and HC

### 3.4.2 Discriminating ROIs

Based on the weights assigned to individual connectivity features, weights corresponding to individual ROIs were computed by halving weights on FC and assigning to each involved ROI. The weighted ROIs for each classification per frequency band are arranged in order of importance in **Table 4.7** and visualized

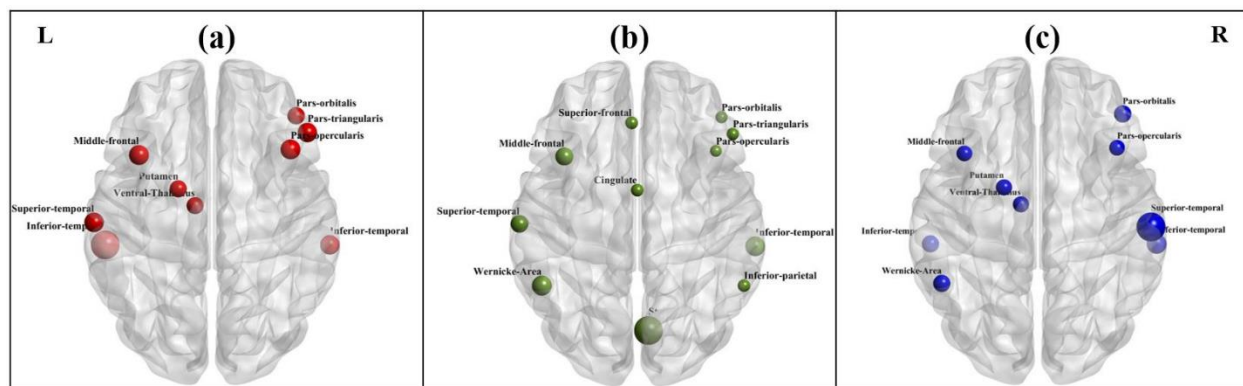
in **Figure 4.4** using BrainNet Viewer [29]. From **Figure 4.4**, discriminating brain areas common to all three frequency bands involve structures in the frontal brain, namely, the left middle frontal gyrus and the right inferior frontal gyrus (pars opercularis and pars orbitalis). While the frontal and temporal sources appear showed involvement in classification across all three bands, the slow-4 band elicited major contribution from the occipital brain (striate) which could be the reason for a higher classification performance in this band.

**Table 4. 7.** Brain regions involved in classification in the three frequency bands

<b>ROI ID</b>	<b>LFO</b>	<b>Slow-4</b>	<b>Slow-5</b>
1	L Inferior Temporal	R Striate	R Superior Temporal
2	L Middle Frontal	L Wernicke	R Inferior Temporal
3	R Pars Opercularis	R Inferior Temporal	R Pars Orbitalis
4	L Superior Temporal	L Middle Frontal	L Inferior Temporal
5	R Inferior Temporal	R Superior Temporal	L Wernicke
6	R Pars Triangularis	Cingulate	L Putamen
7	R Pars Orbitalis	L Superior Frontal	L Ventral Thalamus
8	L Putamen	R Inferior Parietal	L Middle Frontal
9	L Ventral Thalamus	R Pars Triangularis	R Pars Opercularis
10		R Pars Orbitalis	
11		R Pars Opercularis	

Note: Weighted ROIs for each binary classifier per frequency band are listed below. The ROIs are arranged in descending order of the weights, i.e. ROIs at the top are most important. These ROIs are also visualized by importance in Figure 4.4.

**Figure 4. 4.** Brain regions involved among the discriminating features



Note: (a) LFO, (b) slow-4 and (c) slow-5 bands are visualized in the axial brain view. The size of the sphere used to represent the ROI is directly proportional to cumulative importance of the ROI.

### 3.5 Main Takeaways

#### 3.5.1 Resting-state functional MRI as a Tool for Identification of SLD

Results from this study show promise that neuroimaging modality such as resting-state functional MRI can guide and facilitate the identification of SLD. Unlike neuropsychological assessments that can be time-consuming and require active participation from subjects, resting-state functional MRI requires about ten minutes to acquire, is task-free for the subjects and can expedite the detection SLD in the early-stage post stroke subjects such as in our cohort that might facilitate a speedy recovery and rehabilitation. Whether the same holds true for subclinical deficits arising in non-language domains would require further investigation.

#### 3.5.2 Impact of Frequency Bands on Classification

Comparing the classifier performances across the different frequency bands, it is clear from **Table 4.4** that the FC in the slow-4 band provided the most discriminative power. It was followed by the performances in LFO and slow-5 bands respectively. This illustrates that FC exhibits multi-band property with information distributed over a range of frequencies and limiting the BOLD signal to the LFO could attenuate the effect of individual slow frequency bands. Slow-4 band elicited contributions from occipital brain regions which the other two frequency bands did not. Superior classification based on FC in the slow-4 band might point towards greater amount of disruptions occurring in slow-4 band in comparison to slow-5 band which could reveal more important biomarkers specific to a sample of stroke population such as used in this study.

### 3.5.3 Machine Learning as a Tool for Automating Identification of SLD

In comparison to a random three-class classifier that is 33.3% accurate, all the three classifiers developed here performed reasonably better as per the accuracy levels in **Table 4.4**. This demonstrates that machine learning classification can automate the distinction among the LD+, LD- and HC. Moreover, such a classification also divulges information about the underlying discriminating features among subgroups. These features are as enumerated in **Table 4.6** and their significance is discussed in further detail in the following section.

## 4. Discussion

### 4.1 Overview

Overall, a data-driven approach to differentiate sample stroke subjects with SLD from normal adults was presented here. Two types of stroke subgroups were studied, namely, stroke subjects at a higher risk of SLD, i.e. LD+ versus those at lower risk of SLD, i.e. LD-. The results suggested that FC data of the language network can provide relevant information to identify a given subject as belonging to one of the three subgroups and this might potentially serve as an expedited alternative or supplement to administering the complete detailed battery of neuropsychological assessment. To this end, we automated the classification using multiclass SVM classifier of high performance and identified relevant features and their distribution across the subgroups. Moreover, we analyzed the contribution of FC across slow-4 and slow-5 frequency bands, compared it to LFO band and found that slow-4 offered a better discrimination power in categorizing subjects.

## 4.2 Involved Brain Regions

We found connectivity associated with structures of the right inferior frontal gyrus (pars opercularis, pars orbitalis, pars triangularis in LFO, slow-4; pars orbitalis and pars opercularis in slow-5) to be discriminatory which are homologous to the left inferior frontal language areas in right handed subjects. This could be the result of recruitment of the homotopic right cortex due to damage to left language regions in LD+ [49; 50]. The other common node found across all bands included the left middle frontal gyrus (BA 46) and demonstrated decreased FC in the stroke (LD+ and LD-) subgroups relative to the HC subgroup which could be suggestive of the differences in executive control resulting from stroke [51]. Unique to the slow-4 band was the connectivity associated with the striate (BA 17). Majority of the associated connections exhibited a significant difference between the LD+ and LD- subgroups but no significant difference between the LD- and HC subgroups. Under-engagement in this posterior cortical system could be indicative of deficit in phonological processing in LD+ [52; 53]. Congruence of results of this study with prior research suggests biological plausibility of the features selected by NCA for classification.

## 4.3 Slow-4 Dependence of FC

On one hand, numerous studies have reported relevance of resting-state functional MRI connectivity measures derived from the slow-4 band. Amplitude fluctuations in slow-4 have proven to offer greater test-retest reliability in a cohort of healthy adults [20]. Specifically, Zuo and colleagues also pointed at robustness in slow-4 band in brain regions including basal ganglia which has been shown to be an important center in the language network of the brain [54]. Slow-4 has also been demonstrated to be important in finding abnormalities in Schizophrenia in regions and linked with reduced FC in lingual gyrus [55]. Furthermore, slow-4 has been capable of offering superior diagnostic information in case of autism, which is primarily associated with language abnormalities, in children [56] and adolescents [57]. The boosted classification using FC in the slow-4 band with a focus on the language network puts findings from the present study in alignment with the aforementioned studies.

#### **4.4 Slow-5 Dependence of FC**

On the other hand, there is strong evidence of connectivity in slow-5 band being important as well. Previous studies have demonstrated FC in the slow-5 band to be a marker of stroke recovery [58a; 59b]. Regional and network level FC metrics were found to be more relevant in the healthy brain specific to sensorimotor structures [60]. The potential of FC in the slow-5 band as a biomarker in other neurological and psychiatric disorders have also been reported. For example, in subjects with mild cognitive impairment, amplitude based FC was greater in the slow-5 band concentrated in the occipital regions of the brain [61]. Topographical changes in functional MRI revealed significant information in the sensorimotor and default mode networks in subjects with bipolar disorder and mania [62]. Greater performance in differentiation using SVM between a vascular dementia group relative to a healthy control group were illustrated in the slow-5 band [22].

#### **4.5 Frequency Dependence of FC**

In agreement with the studies described above and others [21], the findings here reveal that contribution of neuronal information, as measured by BOLD signals, is different across frequency bands in our sample study cohort. While this effect has been observed in sample groups from different populations as described above, our study adds to the literature for the stroke population based on FC from a representative cohort. Our results could imply that disruptions in brain due to stroke are more pronounced in slow-4 than in slow-5 and combining them into the whole band might be diminishing the effects of individual slow bands. Amplitude-based (non-FC) metric has been known to exhibit reduced connectivity in posterior parts of default mode network in stroke subjects [59b]. A possible ramification of varying information across frequency bands could be that BOLD signal might be sensitive to different frequency bands based on the population, i.e. connectivity in the slow-4 band played a dominant role for the stroke subgroups (LD+ and LD-). However, the LFO band also was equally indicative in differentiating the HC subgroup. This could imply that slow-4 oscillations could be better indicative of the early stages of stroke in comparison to LFO found in healthy subjects. From the findings of the current study, language regions in the occipital brain



appeared to be relatively more involved and sensitive in the slow-4 band while language areas of the frontal and temporal brain seemed sensitive in the slow-5 and LFO bands. A comprehensive and comparative analysis of FC from major brain networks would be required to confirm this in other brain networks.

#### **4.6 Limitations**

This study was constrained in terms of the sample size since conventional machine learning analysis is built upon training on a large dataset so as to have greater power of generalizability. While the accuracy levels obtained from the nested cross-validation were reasonably better than random chance levels, the performance could be further boosted with a larger sample size. Thus, results from this study should not be used to draw conclusions about the stroke population in general. However, this study showed that machine learning has the potential to automate the system of identification of SLD, given a wide variety of brain profiles. Resting-state FC within the language network was assessed using the seed regions provided in a prior study [28]. While this template covers crucial regions of the language network, multiple studies have located varying coordinates for the same [63; 64]. Additionally, to evaluate FC, interregional Pearson's correlation coefficient was used which is a classical measure. However, statistical dependence between BOLD signals could be alternatively defined based on measures such as mutual information, cosine similarity, dynamic time warping, etc. Using different definitions of seeds and FC could influence the selected features in the FC pattern classification. There could be several confounding factors while studying brain differences in population groups. The potential confounding effects were eliminated by limiting the analysis to right-handed subjects who were matched by age, gender and education. Effects of subclinical deficits may have long term impact on subject's life as time since stroke increases. It is potentially easier to detect deficits at the earliest after the stroke to pursue adequate management to have better patient outcomes. To avoid variability of time since stroke onset, stroke subjects in the early-stage (within 30 days of stroke onset) only were included in this analysis. Although stroke severity could be considered a surrogate for lesion volume in stroke subjects, the impact could not be studied due to missing data for a few subjects. The ongoing recruitment of this study offers future scope to incorporate more subjects that can

form a more homogenous cohort and even expand the analysis to subclinical deficits in the non-language networks of the brain. Findings from this study are in alignment with several works in literature and draw attention to investigation of population with subclinical deficits which could often be overlooked.

## **5. Conclusion**

SVM classifier was used to discriminate sample stroke subjects at high risk of SLD from stroke subjects at lower risk of SLD from healthy normal subjects using FC in the language network derived from three frequency bands. These analyses point to the following conclusions: (i) FC derived from a ten-minute resting-state functional MRI has the potential to identify whether a given subject is at risk of having SLD post-stroke; (ii) resting-state FC corresponding to the slow-4 frequency band offers better classification performance in comparison to that from slow-5 or LFO bands, thus, suggesting that slow-4 reflects more relevant FC; (iii) using a multiclass machine learning SVM classifier facilitates automated identification of SLD as validated by the LOOCV accuracy from nested cross-validation; These outcomes imply the possibility of using such an automated methodology in conjunction with or as a surrogate to neuropsychological assessment for easier and accelerated identification of SLD.

## References

- [1] A.J. Mitchell, S. Kemp, J. Benito-León, M. Reuber, The influence of cognitive impairment on health-related quality of life in neurological disease. *Acta Neuropsychiatrica* 22 (2010) 2-13.
- [2] R.J. Ivnik, J.F. Malec, G.E. Smith, E.G. Tangalos, R.C. Petersen, Neuropsychological tests' norms above age 55: COWAT, BNT, MAE token, WRAT-R reading, AMNART, STROOP, TMT, and JLO. *The Clinical Neuropsychologist* 10 (1996) 262-278.
- [3] J. Patterson, Controlled oral word association test, *Encyclopedia of Clinical Neuropsychology*, Springer, 2011, pp. 703-706.
- [4] J.P. Szaflarski, J. Vannest, S.W. Wu, M.W. DiFrancesco, C. Banks, D.L. Gilbert, Excitatory repetitive transcranial magnetic stimulation induces improvements in chronic post-stroke aphasia. *Medical science monitor: international medical journal of experimental and clinical research* 17 (2011) CR132.
- [5] G. Nys, M. Van Zandvoort, P. De Kort, B. Jansen, H. Van der Worp, L. Kappelle, E. De Haan, Domain-specific cognitive recovery after first-ever stroke: a follow-up study of 111 cases. *Journal of the International Neuropsychological Society* 11 (2005) 795-806.
- [6] K.N. Ochsner, S.A. Bunge, J.J. Gross, J.D. Gabrieli, Rethinking feelings: an FUNCTIONAL MRI study of the cognitive regulation of emotion. *Journal of cognitive neuroscience* 14 (2002) 1215-1229.
- [7] N. Ward, M. Brown, A. Thompson, R. Frackowiak, Neural correlates of motor recovery after stroke: a longitudinal functional MRI study. *Brain* 126 (2003) 2476-2496.
- [8] B. Dickerson, D. Salat, D. Greve, E. Chua, E. Rand-Giovannetti, D. Rentz, L. Bertram, K. Mullin, R. Tanzi, D. Blacker, Increased hippocampal activation in mild cognitive impairment compared to normal aging and AD. *Neurology* 65 (2005) 404-411.
- [9] A. Hämäläinen, M. Pihlajamäki, H. Tanila, T. Hänninen, E. Niskanen, S. Tervo, P.A. Karjalainen, R.L. Vanninen, H. Soininen, Increased functional MRI responses during encoding in mild cognitive impairment. *Neurobiology of aging* 28 (2007) 1889-1903.
- [10] S.A. Rombouts, F. Barkhof, R. Goekoop, C.J. Stam, P. Scheltens, Altered resting state networks in mild cognitive impairment and mild Alzheimer's disease: an functional MRI study. *Human brain mapping* 26 (2005) 231-239.
- [11] M. Hommel, S.T. Miguel, B. Naegele, N. Gonnet, A. Jaillard, Cognitive determinants of social functioning after a first ever mild to moderate stroke at vocational age. *Journal of Neurology, Neurosurgery & Psychiatry* 80 (2009) 876-880.
- [12] C. Rosso, R. Valabregue, Y. Attal, P. Vargas, M. Gaudron, F. Baronnet, E. Bertasi, F. Humbert, A. Peskine, V. Perlberg, Contribution of corticospinal tract and functional connectivity in hand motor impairment after stroke. *PLoS One* 8 (2013) e73164.
- [13] J.D. Schaechter, Motor rehabilitation and brain plasticity after hemiparetic stroke. *Progress in neurobiology* 73 (2004) 61-72.
- [14] S. Stephens, R.A. Kenny, E. Rowan, R.N. Kalaria, M. Bradbury, R. Pearce, K. Wesnes, C.G. Ballard, Association between mild vascular cognitive impairment and impaired activities of daily living in older stroke survivors without dementia. *Journal of the American Geriatrics Society* 53 (2005) 103-107.
- [15] R. Mohanty, V.A. Nair, N. Tellapragada, H. Advani, L.M. Williams Jr, V. Prabhakaran, Abstract WP141: Prediction of Subclinical Language Deficit Using Machine Learning Based on Post-stroke Functional Connectivity Derived From Low Frequency Oscillations. *Stroke* 49 (2018) AWP141-AWP141.
- [16] V.A. Nair, B.M. Young, C. La, P. Reiter, T.N. Nadkarni, J. Song, S. Vergun, N.S. Addepally, K. Mylavarapu, J.L. Swartz, Functional connectivity changes in the language network during stroke recovery. *Annals of clinical and translational neurology* 2 (2015) 185-195.

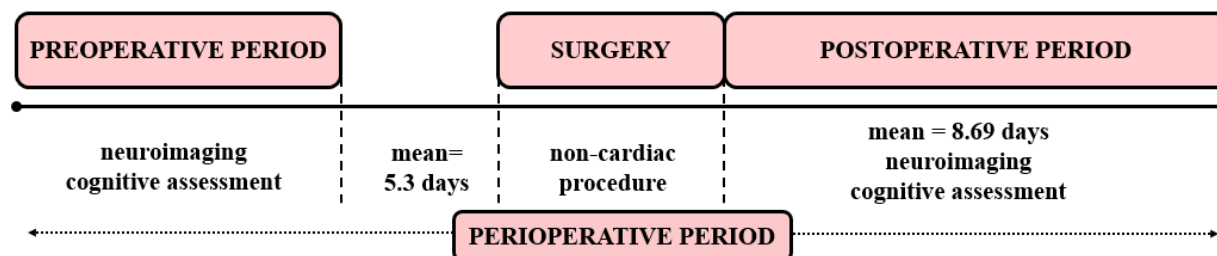
- [17] B. Biswal, F. Zerrin Yetkin, V.M. Haughton, J.S. Hyde, Functional connectivity in the motor cortex of resting human brain using echo-planar mri. *Magnetic resonance in medicine* 34 (1995) 537-541.
- [18] G. Buzsáki, A. Draguhn, Neuronal oscillations in cortical networks. *science* 304 (2004) 1926-1929.
- [19] M. Penttonen, G. Buzsáki, Natural logarithmic relationship between brain oscillators. *Thalamus & Related Systems* 2 (2003) 145-152.
- [20] X.-N. Zuo, A. Di Martino, C. Kelly, Z.E. Shehzad, D.G. Gee, D.F. Klein, F.X. Castellanos, B.B. Biswal, M.P. Milham, The oscillating brain: complex and reliable. *Neuroimage* 49 (2010) 1432-1445.
- [21] S.R. Gohel, B.B. Biswal, Functional integration between brain regions at rest occurs in multiple-frequency bands. *Brain connectivity* 5 (2015) 23-34.
- [22] D. Zhang, B. Liu, J. Chen, X. Peng, X. Liu, Y. Fan, M. Liu, R. Huang, Determination of vascular dementia brain in distinct frequency bands with whole brain functional connectivity patterns. *PloS one* 8 (2013) e54512.
- [23] S. Knecht, M. Deppe, B. Dräger, L. Bobe, H. Lohmann, E.-B. Ringelstein, H. Henningsen, Language lateralization in healthy right-handers. *Brain* 123 (2000) 74-81.
- [24] R. Ruff, R. Light, S. Parker, H. Levin, Benton controlled oral word association test: Reliability and updated norms. *Archives of Clinical Neuropsychology* 11 (1996) 329-338.
- [25] R.W. Cox, AFNI: software for analysis and visualization of functional magnetic resonance neuroimages. *Computers and Biomedical research* 29 (1996) 162-173.
- [26] K. Murphy, M.D. Fox, Towards a consensus regarding global signal regression for resting state functional connectivity MRI. *NeuroImage* (2016).
- [27] T.N. Tombaugh, J. Kozak, L. Rees, Normative data stratified by age and education for two measures of verbal fluency: FAS and animal naming. *Archives of clinical neuropsychology* 14 (1999) 167-177.
- [28] D. Tomasi, N.D. Volkow, Resting functional connectivity of language networks: characterization and reproducibility. *Molecular psychiatry* 17 (2012) 841-854.
- [29] M. Xia, J. Wang, Y. He, BrainNet Viewer: a network visualization tool for human brain connectomics. *PloS one* 8 (2013) e68910.
- [30] R.W. Cox, A. Jesmanowicz, Real-time 3D image registration for functional MRI. *Magnetic Resonance in Medicine: An Official Journal of the International Society for Magnetic Resonance in Medicine* 42 (1999) 1014-1018.
- [31] K.J. Friston, J. Ashburner, C.D. Frith, J.B. Poline, J.D. Heather, R.S. Frackowiak, Spatial registration and normalization of images. *Human brain mapping* 3 (1995) 165-189.
- [32] J.D. Power, K.A. Barnes, A.Z. Snyder, B.L. Schlaggar, S.E. Petersen, Spurious but systematic correlations in functional connectivity MRI networks arise from subject motion. *Neuroimage* 59 (2012) 2142-2154.
- [33] C.D. Smyser, T.E. Inder, J.S. Shimony, J.E. Hill, A.J. Degnan, A.Z. Snyder, J.J. Neil, Longitudinal analysis of neural network development in preterm infants. *Cerebral cortex* 20 (2010) 2852-2862.
- [34] K.R. Van Dijk, M.R. Sabuncu, R.L. Buckner, The influence of head motion on intrinsic functional connectivity MRI. *Neuroimage* 59 (2012) 431-438.
- [35] N.U. Dosenbach, B. Nardos, A.L. Cohen, D.A. Fair, J.D. Power, J.A. Church, S.M. Nelson, G.S. Wig, A.C. Vogel, C.N. Lessov-Schlaggar, Prediction of individual brain maturity using functional MRI. *Science* 329 (2010) 1358-1361.
- [36] R. Mohanty, A.M. Sinha, A.B. Remsik, K.C. Dodd, B.M. Young, T. Jacobson, M. Mcmillan, J. Thoma, H. Advani, V.A. Nair, Machine Learning Classification to Identify the Stage of Brain-Computer Interface Therapy for Stroke Rehabilitation Using Functional Connectivity. *Frontiers in neuroscience* 12 (2018).
- [37] S. Vergun, A.S. Deshpande, T.B. Meier, J. Song, D.L. Tudorascu, V.A. Nair, V. Singh, B.B. Biswal, M.E. Meyerand, R.M. Birn, Characterizing functional connectivity differences in aging adults using

- machine learning on resting state functional MRI data. *Frontiers in computational neuroscience* 7 (2013).
- [38] A. Demirhan, T.M. Nir, A. Zavaliangos-Petropulu, C.R. Jack, M.W. Weiner, M.A. Bernstein, P.M. Thompson, N. Jahanshad, Feature selection improves the accuracy of classifying alzheimer disease using diffusion tensor images, *Biomedical Imaging (ISBI), 2015 IEEE 12th International Symposium on, IEEE, 2015*, pp. 126-130.
- [39] C. Leys, C. Ley, O. Klein, P. Bernard, L. Licata, Detecting outliers: Do not use standard deviation around the mean, use absolute deviation around the median. *Journal of Experimental Social Psychology* 49 (2013) 764-766.
- [40] J. Goldberger, G.E. Hinton, S.T. Roweis, R.R. Salakhutdinov, Neighbourhood components analysis, *Advances in neural information processing systems, 2005*, pp. 513-520.
- [41] W. Yang, K. Wang, W. Zuo, Neighborhood Component Feature Selection for High-Dimensional Data. *JCP* 7 (2012) 161-168.
- [42] J. Snoek, H. Larochelle, R.P. Adams, Practical bayesian optimization of machine learning algorithms, *Advances in neural information processing systems, 2012*, pp. 2951-2959.
- [43] C. Cortes, V. Vapnik, Support-vector networks. *Machine learning* 20 (1995) 273-297.
- [44] E.L. Allwein, R.E. Schapire, Y. Singer, Reducing multiclass to binary: A unifying approach for margin classifiers. *Journal of machine learning research* 1 (2000) 113-141.
- [45] S. Knerr, L. Personnaz, G. Dreyfus, Single-layer learning revisited: a stepwise procedure for building and training a neural network. *Neurocomputing: algorithms, architectures and applications* 68 (1990) 71.
- [46] G.C. Cawley, N.L. Talbot, On over-fitting in model selection and subsequent selection bias in performance evaluation. *Journal of Machine Learning Research* 11 (2010) 2079-2107.
- [47] T. Hastie, R. Tibshirani, J. Friedman, *The elements of statistical learning*. 2001. NY Springer (2001).
- [48] T.B. Meier, A.S. Desphande, S. Vergun, V.A. Nair, J. Song, B.B. Biswal, M.E. Meyerand, R.M. Birn, V. Prabhakaran, Support vector machine classification and characterization of age-related reorganization of functional brain networks. *Neuroimage* 60 (2012) 601-613.
- [49] S.C. Blank, H. Bird, F. Turkheimer, R.J. Wise, Speech production after stroke: The role of the right pars opercularis. *Annals of neurology* 54 (2003) 310-320.
- [50] H. Rosen, S. Petersen, M. Linenweber, A. Snyder, D. White, L. Chapman, A. Dromerick, J. Fiez, M. Corbetta, Neural correlates of recovery from aphasia after damage to left inferior frontal cortex. *Neurology* 55 (2000) 1883-1894.
- [51] R. Elliott, Executive functions and their disorders: Imaging in clinical neuroscience. *British medical bulletin* 65 (2003) 49-59.
- [52] K.R. Pugh, W.E. Mencl, B.A. Shaywitz, S.E. Shaywitz, R.K. Fulbright, R.T. Constable, P. Skudlarski, K.E. Marchione, A.R. Jenner, J.M. Fletcher, The angular gyrus in developmental dyslexia: task-specific differences in functional connectivity within posterior cortex. *Psychological science* 11 (2000) 51-56.
- [53] B.A. Shaywitz, S.E. Shaywitz, K.R. Pugh, R.K. Fulbright, W.E. Mencl, R.T. Constable, P. Skudlarski, J.M. Fletcher, G.R. Lyon, J.C. Gore, The neurobiology of dyslexia. *Clinical Neuroscience Research* 1 (2001) 291-299.
- [54] J.R. Booth, L. Wood, D. Lu, J.C. Houk, T. Bitan, The role of the basal ganglia and cerebellum in language processing. *Brain research* 1133 (2007) 136-144.
- [55] M.J. Hoptman, X.-N. Zuo, P.D. Butler, D.C. Javitt, D. D'Angelo, C.J. Mauro, M.P. Milham, Amplitude of low-frequency oscillations in schizophrenia: a resting state functional MRI study. *Schizophrenia research* 117 (2010) 13-20.

- [56] A. Di Martino, M. Ghaffari, J. Curchack, P. Reiss, C. Hyde, M. Vannucci, E. Petkova, D.F. Klein, F.X. Castellanos, Decomposing intra-subject variability in children with attention-deficit/hyperactivity disorder. *Biological psychiatry* 64 (2008) 607-614.
- [57] H. Chen, X. Duan, F. Liu, F. Lu, X. Ma, Y. Zhang, L.Q. Uddin, H. Chen, Multivariate classification of autism spectrum disorder using frequency-specific resting-state functional connectivity—a multi-center study. *Progress in Neuro-Psychopharmacology and Biological Psychiatry* 64 (2016) 1-9.
- [58] C. La, P. Mossahebi, V.A. Nair, B.M. Young, J. Stamm, R. Birn, M.E. Meyerand, V. Prabhakaran, Differing Patterns of Altered Slow-5 Oscillations in Healthy Aging and Ischemic Stroke. *Frontiers in human neuroscience* 10 (2016).
- [59] C. La, V.A. Nair, P. Mossahebi, B.M. Young, M. Chacon, M. Jensen, R.M. Birn, M.E. Meyerand, V. Prabhakaran, Implication of the Slow-5 oscillations in the disruption of the default-mode network in healthy aging and stroke. *Brain connectivity* 6 (2016) 482-495.
- [60] S.-W. Xue, D. Li, X.-C. Weng, G. Northoff, D.-W. Li, Different neural manifestations of two slow frequency bands in resting functional magnetic resonance imaging: a systemic survey at regional, interregional, and network levels. *Brain connectivity* 4 (2014) 242-255.
- [61] Y. Han, J. Wang, Z. Zhao, B. Min, J. Lu, K. Li, Y. He, J. Jia, Frequency-dependent changes in the amplitude of low-frequency fluctuations in amnesic mild cognitive impairment: a resting-state functional MRI study. *Neuroimage* 55 (2011) 287-295.
- [62] M. Martino, P. Magioncalda, Z. Huang, B. Conio, N. Piaggio, N.W. Duncan, G. Rocchi, A. Escelsior, V. Marozzi, A. Wolff, Contrasting variability patterns in the default mode and sensorimotor networks balance in bipolar depression and mania. *Proceedings of the National Academy of Sciences* 113 (2016) 4824-4829.
- [63] E.C. Ferstl, J. Neumann, C. Bogler, D.Y. Von Cramon, The extended language network: a meta-analysis of neuroimaging studies on text comprehension. *Human brain mapping* 29 (2008) 581-593.
- [64] D. Saur, B.W. Kreher, S. Schnell, D. Kümmerer, P. Kellmeyer, M.-S. Vry, R. Umarova, M. Musso, V. Glauche, S. Abel, Ventral and dorsal pathways for language. *Proceedings of the national academy of Sciences* 105 (2008) 18035-18040.

## CHAPTER 5: Neural Correlates of Perioperative Executive Function Associated With Noncardiac Surgery in the Elderly

### Graphical Summary



### Research Question

What are the neural bases indicative of perioperative cognitive processes in older adults?

### Publication

Mohanty, R., Lindroth, H., Twadell, S., Nair, V. A., Prabhakaran, V., Sanders, R. D., “Neural Correlates of Perioperative Executive Function associated with Noncardiac Surgery in the Elderly”, currently under peer review for publication in the British Journal of Anaesthesia.

### Abstract

Acute changes in cognition occur in the perioperative period, however, the underlying neural mechanisms are yet to be elucidated. This study investigated the role of functional connectivity based on resting-state functional magnetic resonance imaging (functional MRI) to characterize changes in executive function in older adults undergoing non-cardiac surgery in the perioperative period. Twenty-seven subjects undergoing non-cardiac surgery were recruited, executive function assessed by Trail making test (TMT; A and B), and functional MRI data were collected at preoperative and postoperative time-points. Functional connectivity associated with the default mode (DMN) and executive control (ECN) brain networks were computed at each time-point and difference maps reflected the changes in functional connectivity (FC) from pre- to postoperative time-points. Seed- and network-level analyses were conducted to examine within-network and outside-network effects respectively for DMN and ECN separately. Group analyses were conducted using multiple regression models to investigate the relationship between the difference maps for FC and corresponding changes in executive function. Tests were corrected for multiple comparisons using Family

Wise Error correction. Seed-level effects mostly showed a significant negative association between connectivity changes and TMT changes. Particularly, decreased within-network neural functional connectivity was observed in relation to poorer executive function postoperatively. In contrast, increased outside-network neural functional connectivity corresponded with poorer executive function postoperatively. Study of change in functional connectivity allowed to dynamically track neural correlates of cognitive changes perioperatively. Future studies should investigate the factors that contribute to a breakdown in network connectivity.



## 1. Introduction

Short term changes in cognition occur following surgery [1; 2; 3; 4; 5]; however, the underlying mechanism remains unclear. In particular, the perioperative dynamics in neural networks have not been robustly characterized. Perioperative network mechanisms may be of importance in understanding the cognitive trajectory linked with surgery [6]. Understanding the mechanisms of acute changes in cognition, is important for both understanding the pathogenesis of postoperative cognitive decline (POCD) and cognition more broadly with potential ramifications for the study of important clinical disorders including delirium and dementia.

Correlates of cognitive dysfunction have been characterized using genotype markers [7], cellular attributes [8] and clinical variables [9]. Recent studies have brought neuroimaging into the picture to delineate the neural correlates of cognition in terms of structural and functional variations [10; 11; 12]. Magnetic resonance imaging (MRI) offers a non-invasive modality to track perioperative neuroplasticity. Resting-state functional MRI (functional MRI), specifically, quantifies the spontaneous low frequency variations in the blood oxygen-level dependent (BOLD) signal which is an indirect measure of neuronal activity. Resting-state functional connectivity (FC; meaning there is no associated cognitive task during the scan) of higher-order brain networks such as the default mode (DMN) and executive control networks (ECN) can be assessed by studying the correlations in changes of amplitude of the oscillations in the BOLD signal. FC changes occur with altered cognition in aging, even in absence of neurodegeneration. Within the DMN, which elicits undirected attention, these could manifest as the loss of frontal and posterior connectivity [13; 14]. Within the ECN, which requires goal-directed attention, these may arise in the form of frontal recruitment/over-activation reflecting age-induced compensatory connectivity [15; 16] or be the source of dysfunction [17; 18]. Notably, resting-state ECN connectivity has been associated with cognitive performance on an executive function (EF) task, the Trail Making Test [19]. Understanding regional brain changes in terms of FC, associated with cognitive impairment, would provide critical mechanistic information for the study of POCD. Here we characterized perioperative EF in older adults undergoing

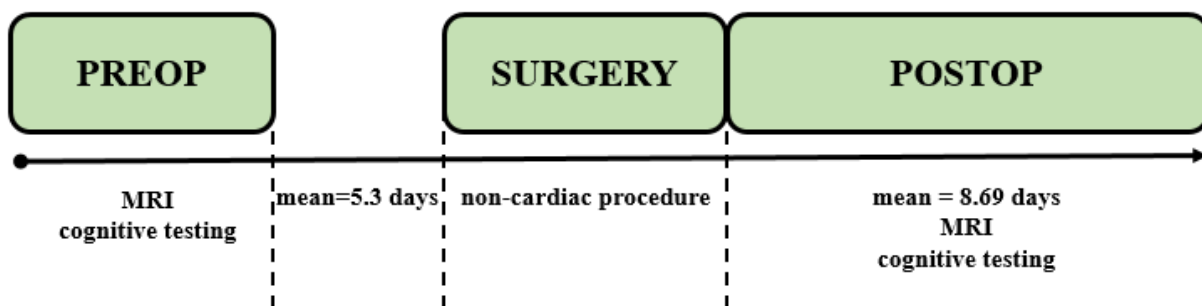
noncardiac surgery. Specifically, we investigated which perioperative FC changes are associated with those in EF. Based on the hypothesis in this study, seed (within-network) and network-level (outside-network) changes were examined for the DMN and ECN.

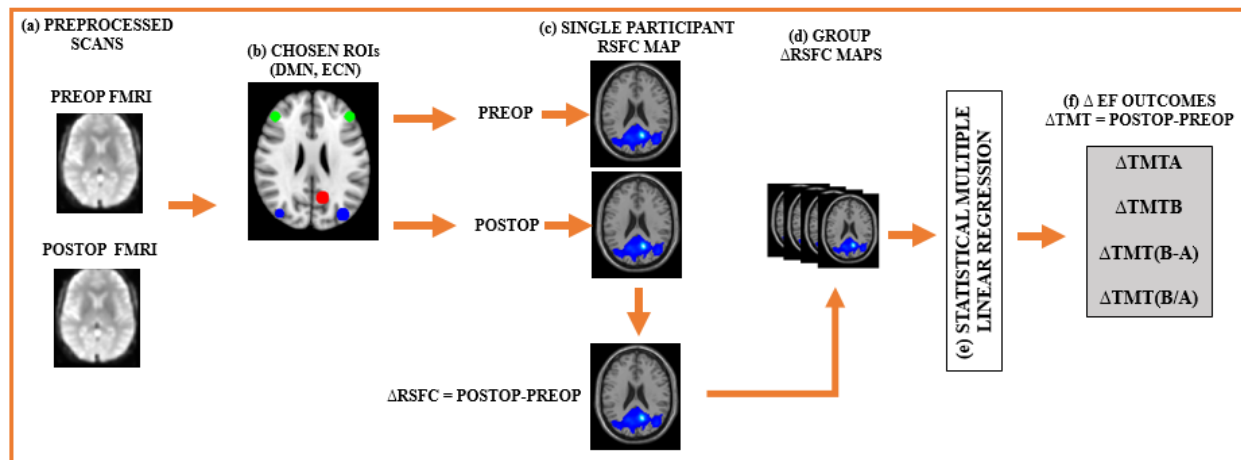
## 2. Methods

The present study comprised of three main stages as schematized in **Figure 5.1 (a)**: (a) *preoperative stage*: defined as the time period leading up to the scheduled surgery during which the MRI and cognitive assessments were conducted; (b) *intra-operative stage*: during which participants underwent elective non-cardiac surgery including general, vascular, spinal, urologic or otolaryngologic procedures under general or neuraxial anesthesia; (c) *postoperative stage*: defined as the time period following the surgery through the entire stay at the hospital during which participants underwent the MRI and behavioral assessments, screening for delirium and tracking for any complications and discharge disposition. The protocol followed for this study was approved by the Health Sciences Institutional Review Board, University of Wisconsin-Madison and registered with ClinicalTrials.gov (NCT03124303, NCT01980511). Patients were co-enrolled with the NeuroVISION study [20] conducted at the University of Wisconsin-Madison.

*Figure 5. 1. Study paradigm*

*(a) Schematic diagram of the study design*



*(b) Overview of methodology*

Note: RSFC = FC = functional connectivity; Identification of change in functional connectivity as correlates of changes in executive function: (a) Individual scans were preprocessed; (b) BOLD time-courses corresponding to hypothesized seeds in the DMN (PCC/precuneus, MPFC) and ECN (DLPFC, SPL) were extracted preoperatively and postoperatively; (c) individual FC map associated with each ROI was computed at each stage and  $\Delta FC$  was computed; (d)  $\Delta FC$  maps were aggregated for group-level analyses; (e) separate linear regression analyses were conducted for each ROI to identify  $\Delta FC$  associated with (f) corresponding  $\Delta EF$  outcomes as measured by Trail Making Test (TMT).

## 2.1. Participants

As this was a pilot study associated with an ongoing perioperative cohort study sample size was not determined a priori, however based on the work by Seeley et al. [19], we estimated that a minimum of 14 subjects would be required to identify changes in connectivity with changes in cognitive function. Twenty-seven older participants (mean age =  $71.74 \pm 4.66$  years; 14 females) were recruited who underwent non-cardiac surgery and completed MRI exams and behavioral assessments prior to as well as post-surgery. The inclusion criteria for recruitment were: (i) at least 65 years of age or older; (ii) ability to provide written informed consent and (iii) undergoing a major surgical procedure requiring a minimum of two-day stay. Exclusion criteria consisted of: (i) contraindication to MRI (e.g. implanted devices not safe for MRI studies, claustrophobia); (ii) unable or unwilling to attend the follow-up appointments; (iii) documented history of dementia; (iv) residing in a nursing home; (v) undergoing carotid artery surgery or intracranial surgery; (vi) unable to complete neurocognitive/behavioral testing due to language, vision or hearing impairment; (vii)

unable to communicate with the research staff due to language barriers. All participants provided written and informed consent. Most participants were right handed ( $N=19$ ) with education level of 12 years or more ( $N=21$ ). The most common surgical procedures performed on these participants included spine, general and vascular surgery. The average duration of hospitalization was  $3.2 \pm 1.93$  days. None of the participants were delirious at the time of postoperative MRI exam confirmed by the 3D Confusion Assessment Method [21]. A total of eight participants were excluded during data processing due to missing cognitive data ( $N=4$ ) and quality check of MRI data ( $N=4$ ) retaining an effective sample size of 19 for further analyses. The reasons that the four participants that were discarded after quality check were: one subject exhibited high levels of motion in postoperative MRI due to delirium, one subject scan showed imaging artefacts, two subjects had to be scanned on a 1.5 T scanner (for clinical reasons) leading to low resolution scans.

## **2.2. Behavioral Data**

### **2.2.1. Cognitive Outcomes**

The written version of the two-part trail making test (TMT) [22] was administered as a part of the behavioral assessment preoperatively and postoperatively. Scores achieved on TMT served as the outcome measure for EF as TMT is known to be an assessment of cognitive domains including processing speed, task-switching, mental flexibility and visual-motor skills. Specifically, for part A (TMTA), participants were presented with a paper-form test with randomly arranged encircled numbers from 1 through 25 and instructed to connect them in numerical order as quickly as possible. This was followed by part-B (TMTB) in which participants were presented with a paper-form test comprised of randomly arranged numbers from 1 through 13 and alphabets from A through L and instructed connect sequentially while alternating between numbers and letters as quickly as possible. The time required for completion of each task was recorded as the score hence a longer time (or TMT score) equates to worse cognition.

### 2.2.2. Cognitive Outcome Processing

Four participants were excluded as a result of missing cognitive data at the time of postoperative MRI leading to a sample size of nineteen. The primary cognitive outcome was TMTB as it is the most routinely employed of the tests however, as this was a relatively exploratory analysis several different metrics from the test are reported. Based on the TMT, four scales were derived from scores of the participants preoperatively and postoperatively which are useful in evaluation of distinct domains of cognition: (i) TMTA: represented by the raw score (time of completion) achieved on the part-A; (ii) TMTB: represented by the raw score (time of completion) achieved on part-B; (iii) TMT(B-A): represented by the difference between TMTB and TMTA [23]; (iv) TMT(B/A): represented by the ratio of TMTB to TMTA [23]. TMTA primarily measures visual search, attention, motor speed, working memory [24]. TMTB, being slightly more complex, accounts for attention switching, executive function, mental flexibility [24] and since it is used frequently in POCD research, this was designated the primary endpoint here. Higher TMTA and TMTB scores correspond to slower performance on assessments and hence impaired cognition. The difference, TMT(B-A), assesses cognitive efficiency [25]. A positive value of TMT(B-A) represents slower performance on TMTB that requires higher cognitive functions relative to the simpler functions associated with TMTA. The ratio, TMT(B/A), gauges executive function controlled for age, education [26; 27]. A ratio closer to 1 implies equivalent performance on parts A and B. Increased values of TMT(B/A) (>3) could be indicator of potential EF impairment. Since our sample was relatively homogenous in terms of age and education levels, TMT scores were not further adjusted. We quantified perioperative cognition by evaluating the change from the preoperative to the postoperative stage, i.e. for each scale, we computed:

$$\Delta TMT = TMT_{postop} - TMT_{preop} \quad (1)$$

where  $TMT_{postop}$  and  $TMT_{preop}$  represent the scores achieved on the TMT (A and B) at the postoperative and preoperative time-points respectively and  $\Delta TMT$  signifies the change.

## 2.3. Neuroimaging Data

### 2.3.1. Acquisition Protocol

Neuroimaging data were acquired on 3.0 T GE 750 scanners (GE Healthcare, Waukesha, WI) equipped with an eight-channel head coil. Ten minutes long resting-state functional MRI were obtained using single-shot echo-planar T2\*-weighted imaging and the following parameters: TR = 2.6 s, 231 time-points, TE = 22 ms, FOV = 22.4 cm, flip angle = 60°, voxel dimensions 3.5×3.5×3.5 mm<sup>3</sup>, 40 slices. All participants were instructed to lay with their eyes closed. Five minutes long T1-weighted axial anatomical scans were collected at the beginning of each scan using FSPGR BRAVO sequence using the following parameters: TR = 8.132 ms, TE = 3.18 ms, TI = 450 ms, over a 256×256 matrix and 156 slices, flip angle = 12°, FOV = 25.6 cm, slice thickness = 1 mm.

### 2.3.2. Neuroimaging Data Processing

An overview of the hypothesis-driven methodology followed to investigate changes in FC as correlates of changes in EF is summarized in **Figure 5.1 (b)**. During preprocessing, the functional MRI and T1 scans were realigned, slice-time corrected, normalized to the standard Montreal Neurological Institute (MNI) space, spatially smoothed with a 8-mm full width at half-maximum Gaussian kernel using SPM12 (Statistical Parametric Mapping, Wellcome Trust Centre for Neuroimaging; [www.fil.ion.ucl.ac.uk](http://www.fil.ion.ucl.ac.uk)) [28]. Low-frequency BOLD fluctuations were investigated with the help of temporal filtering within the range of 0.07-0.1 Hz in order to remove physiological noise [29] using FSL 3.2 (Oxford Centre for Functional MRI of the Brain Laboratory Software Library; <http://www.functionalMRIb.ox.ac.uk/fsl>) [30]. The first eigenvariate of the time courses of voxels in each region of interest (ROI) was extracted. Nuisance covariates included signals arising due to white matter, lateral ventricles and global brain changes. Signals from white matter and ventricles were represented by the first eigenvariate of the time courses extracted from voxels in the respective regions. Additionally, movement parameters and corresponding squared

parameters were added for simultaneous regression in a single generalized linear model (GLM). During the parameter estimation phase, a restricted maximum likelihood algorithm based on an intrinsic autoregressive model was applied for estimation of serial correlations. A separate GLM was run corresponding to each ROI and effects of interest were evaluated with the help of a parametric T-maps for each participant. Connectivity analyses were conducted similar to previous studies [31; 32; 19] by computing a contrast map which identified regions in the brain that significantly correlated with activity in the specified ROI.

## **2.4. Regions of Interest**

We focused on brain regions from two main large-scale networks associated with cognitive processes in the elderly: (i) the DMN encompassing the posterior cingulate/precuneus and medial prefrontal cortices. This task-negative network was chosen as it is one of the most robust networks in the resting brain and is frequently studied. (ii) the ECN covering the frontal and parietal cortices such as dorsolateral prefrontal cortex and superior parietal lobules [19]. This task-positive network was chosen as we intended to investigate the correlations with EF.

### **2.4.1. Seed-level (or Within-network) Analysis**

Within the DMN, the posterior cingulate (PCC)/precuneus (MNI 12,-60,24) and medial prefrontal cortex (MPFC) (0,40,-4) were considered based on previous studies [31; 33; 34; 19]. Within the ECN, the dorsolateral prefrontal cortex (DLPFC) [19; 35] (MNI  $\pm$ 44,36,20) and lateral intraparietal sulcus/superior parietal lobule (SPL) [36; 37; 19] (MNI 36,-80,26 and -38,-78,36) were examined. A sphere of radius 6-mm centered at the MNI location of each seed was created and the first eigenvariate of the BOLD time course was extracted for connectivity analyses.

### 2.4.2. Network-level (or Outside-network) Analysis

To complement the seed-based analysis, we also analyzed correlations with seeds outside of the networks, looking for exaggeration of the increased outside-network connectivity changes that accumulate with aging [38] and sudden cognitive changes such as delirium [39]. To this end, we investigated FC associated with the DMN, left ECN and right ECN. Each network comprised of multiple individual ROIs, defined as per the Willard atlas [40]. BOLD activity was extracted by averaging time course over all voxels of the ROIs within each network and utilized for connectivity analyses. This mean signal was then correlated voxel-wise with the rest of the brain looking for voxels that correlate with change in performance on the cognitive tests.

### 2.5. Perioperative FC

For each seed region and network of interest, the contrast maps generated from preoperative and postoperative functional MRI were used to quantify the change in perioperative FC corresponding to each participant. Hence, each subject acted as their own control, muting the impact of preoperative differences in connectivity and allowing us to assess the changes induced by perioperative care. This amounted to evaluating a simple difference between the two contrast maps reflecting change in functional connectivity:

$$\Delta FC = FC_{postop} - FC_{preop} \quad (2)$$

where FC at postoperative and preoperative stages are symbolized by  $FC_{postop}$  and  $FC_{preop}$  respectively and  $\Delta FC$  is the change between them.

The individual difference maps were aggregated to perform regression analyses to draw group-level inferences.



## 2.6. Statistical Analysis

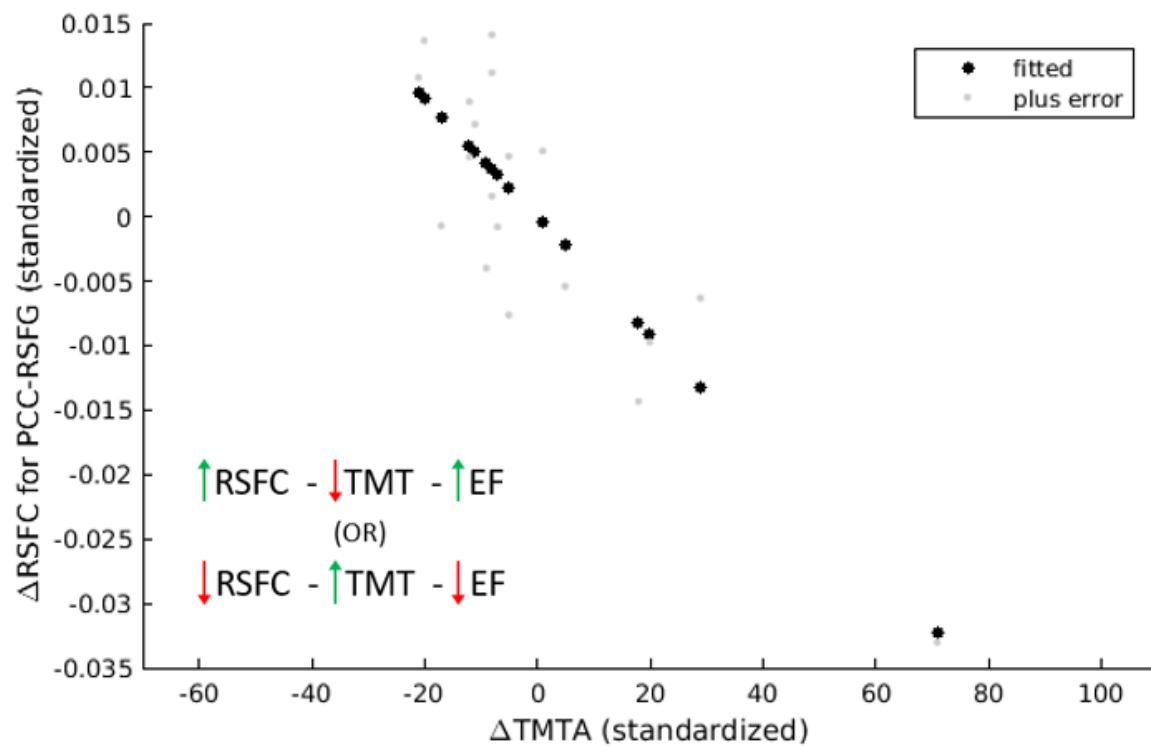
Multiple linear regression analyses were implemented at seed- as well as network-levels to test for correlations between  $\Delta FC$  and each of the four  $\Delta TMT$  outcomes. In this analysis, the change in one metric was correlated with a change in another, thus, accounting for baseline differences within subjects. Voxels exhibiting significant correlations were identified and results were corrected for multiple comparisons at the whole-brain level with the family-wise error (FWE) approach ( $p < 0.05$ ). While this is a stringent approach to multiple comparisons within a given test (for example, far more stringent than  $p < 0.001$  uncorrected that is often reported in imaging research), we did not account for the multiple comparisons across the different TMT metrics and seeds as we considered each of these analyses independent. We also did not attempt further analyses to probe the mechanism of these effects, such as accounting for medication use, as we would likely be underpowered for these analyses. Nonetheless, we test a clear hypothesis that a decline in perioperative cognition would be associated with reduced FC within a given network.

## 3. Results

### 3.1. Sample Characteristics

For identification of neural correlates of  $\Delta TMT$ , 19 cases were considered after accounting for missing cognitive data and quality control of neuroimaging data. Overall, the cognitive data were normally distributed and the mean change (SD) of the cognitive measures were: 16.05 (21.78) for  $\Delta TMTA$  ( $p = 0.004$ ), 30.84 (66.17) for  $\Delta TMTB$  ( $p = 0.057$ ), 14.78 (54.41) for  $\Delta TMT(B-A)$  ( $p = 0.251$ ) and 0.35 (1.12) for  $\Delta TMT(B/A)$  ( $p = 0.187$ ).

**Figure 5. 2.** *Decreased within-network connectivity associated with poorer cognitive performance postoperatively*



Note: Figure exemplifies the association between changes in PCC connectivity and changes in TMTA performance. Similar effects were found for the default mode (MPFC) and executive control networks (bilateral DLPFC, RSPL); RSFC = FC = functional connectivity; TMT = trail making test score; EF = executive function;

### 3.2. Correlates of $\Delta$ TMT

#### 3.2.1. Seed-level (or Within-network) Effects

Predominant negative correlations were observed between  $\Delta$ FC and multiple  $\Delta$ TMT measures. A negative correlation represents the correspondence between poorer postoperative FC and longer time of completion (or poorer cognition) postoperatively as exemplified by **Figure 5.2**. Regions in the brain where significant correlations were observed between change in connectivity and change in cognition are listed in **Table 5.1** and are visualized in **Figure 5.3**. Overall, the significant effects were found to encompass frontal-to-frontal or frontal-to-parietal brain connectivity, particularly involving the ECN, consistent with its known association with EF [19]. Bilateral DLPFC showed significant frontal connectivity. Left DLPFC

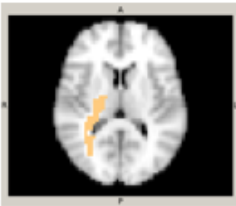
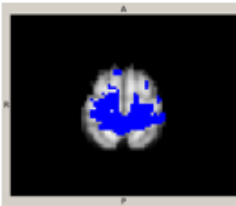
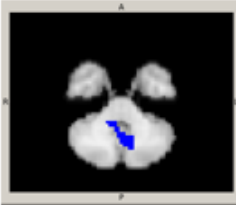
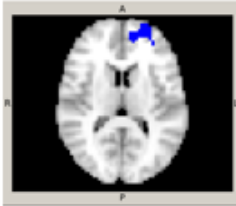
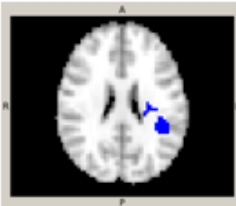
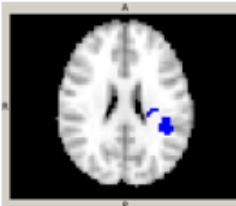
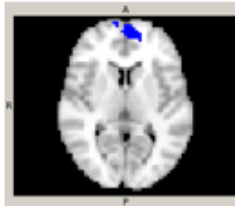
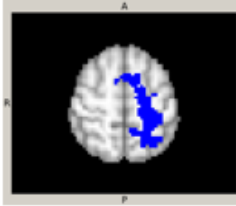
additionally showed parietal connectivity ( $R^2 = 0.58$ ; peak  $p = 0.02$ ;  $\beta = -0.003$ ). Connectivity of right SPL was observed with the precentral gyrus ( $R^2 = 0.57$ ; peak  $p = 0.036$ ;  $\beta = -0.002$ ). The only positive correlation to cognitive change was found in the DMN with a change in posterior cingulate-thalamic connectivity ( $R^2 = 0.6$ ; peak  $p = 0.011$ ;  $\beta = -0.004$ ).

**Table 5. 1.** Peak brain areas showing significant correlations with changes in executive function ( $\Delta$ TMT) obtained from seed-level (within-network) regression analyses

Seed Region	Activated Region	Outcome	MNI x,y,z	Peak-level $p$ -value	$R^2$	Z-score	$\beta$
PCC/ Precuneus	Right thalamus proper	$\Delta$ TMTA	24,-25,8	0.011	0.6	5.05	0.0044
	Right superior frontal gyrus		9,-4,68	0.031	0.57	4.79	-0.001
MPFC	Cerebellar vermal lobules VIII-X	$\Delta$ TMTA	-6,-58,-37	0.032	0.57	4.81	-0.0051
R DLPFC	L medial superior frontal gyrus	$\Delta$ TMT(B/A)	-12,56,8	0.006	0.60	5.15	-0.0051
L DLPFC	L parietal operculum	$\Delta$ TMTB	-39,-40,20	0.030	0.57	4.81	-0.0033
	L parietal operculum	$\Delta$ TMT(B-A)	-39,-40,20	0.02	0.58	4.91	-0.0033
	L medial superior frontal gyrus	$\Delta$ TMT(B/A)	-6,59,5	0.030	0.57	4.81	-0.0080
R SPL	L precentral gyrus	$\Delta$ TMTA	-21,-19,53	0.036	0.57	4.75	-0.0022

Note: All  $p$ -values are FWE corrected; Positive and negative correlations are highlighted in beige and blue colors respectively; TMT = trail making test; L = left; R = right; PCC = posterior cingulate cortex; MPFC = medial prefrontal cortex; DLPFC = dorsolateral prefrontal cortex; SPL = superior parietal lobule;

**Figure 5. 3.** Clusters of brain regions (axial/top view) that showed significant correlations with respect to changes in cognitive outcomes ( $\Delta$ TMT) obtained from seed-level analyses

WITHIN-NETWORK EFFECTS			
PCC/Precuneus	$\Delta$ TMTA (positive) right thalamus proper	$\Delta$ TMTA (negative) right superior frontal gyrus	
			
MPFC	$\Delta$ TMTA (negative) cerebellar vermal lobules VIII-X		
			
R-DLPFC	$\Delta$ TMT(B/A) (negative) left medial superior frontal gyrus		
			
L-DLPFC	$\Delta$ TMTB (negative) left parietal operculum	$\Delta$ TMT(B-A) (negative) left parietal operculum	$\Delta$ TMT(B/A) (negative) left medial superior frontal gyrus
			
R-SPL	$\Delta$ TMTA (negative) left precentral gyrus		
			

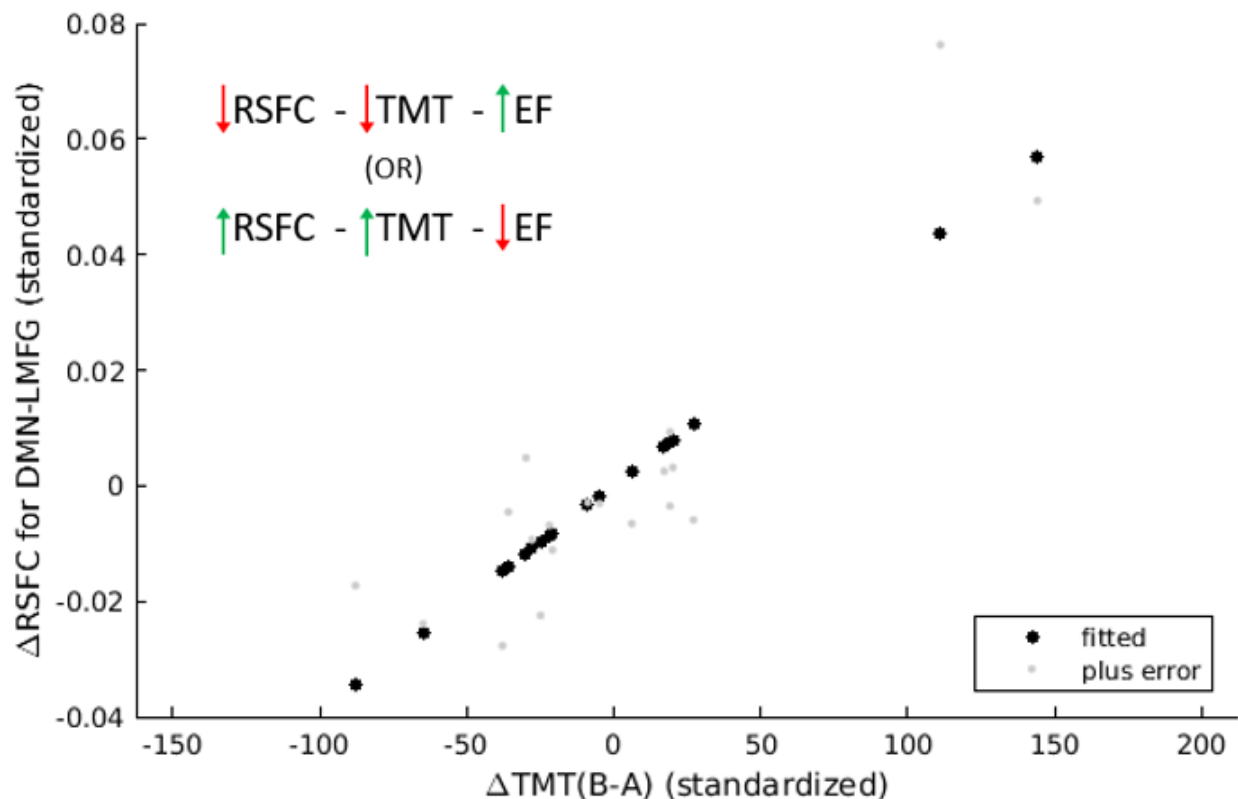
Note: Positive and negative correlations are visualized in beige and blue colors respectively;

### 3.2.2. Network-level (or Outside-network) Effects

All correlations observed between changes in network-based connectivity and cognitive measures were observed to be positive (DMN:  $R^2 = 0.58$ ; peak  $p = 0.024$ ;  $\beta = 0.0042$ ; Right ECN:  $R^2 = 0.6$ ; peak  $p = 0.021$ ;  $\beta = 0.0026$ ). This would imply correspondence between higher postoperative outside-network FC and increased time taken for postoperative TMT (poor cognition) as illustrated by **Figure 5.4 (a)**. The areas of the brain where these correlations were found to be significant involved frontal connectivity and are listed under **Table 5.2** and visualized in **Figure 5.4 (b)**.

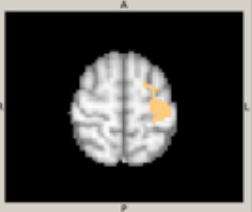
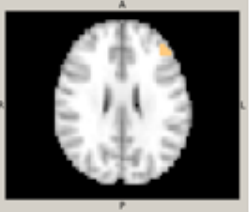

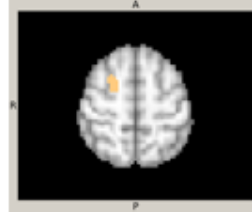
*Figure 5. 4. Outside-network effects associated with cognitive change*

*(a). Increased outside-network connectivity associated with poorer cognitive performance postoperatively*



Note: Figure exemplifies the association between changes outside DMN connectivity and changes in TMT(B-A). Similar effects were found for the executive control network; RSFC=FC=functional connectivity; TMT = trail making test score; EF = executive function; RSFC = FC = functional connectivity;

(b). Clusters of brain regions (axial/top view) that showed significant correlations with respective to changes in cognitive outcomes ( $\Delta$ TMT) obtained from network-level analyses.

OUTSIDE-NETWORK EFFECTS			
DMN	$\Delta$ TMT(B-A) (positive) left middle frontal gyrus		
			
RECN	$\Delta$ TMTB (positive) left middle frontal gyrus	$\Delta$ TMT(B-A) (positive) left middle frontal gyrus	$\Delta$ TMT(B/A) (positive) right superior frontal gyrus
			

Note: Positive correlations are visualized in beige.

**Table 5. 2.** Peak brain areas showing significant correlations with changes in executive function ( $\Delta$ TMT) obtained from network-level analyses

Network	Activated Region	Outcome	MNI x,y,z	Peak- level p- value	R <sup>2</sup>	Z- score	$\beta$
DMN	L middle frontal gyrus	$\Delta$ TMT(B-A)	-30,5,65	0.024	0.58	4.85	0.0042
RECN	L middle frontal gyrus	$\Delta$ TMTB	-45,35,23	0.006	0.60	5.13	0.0026
	L middle frontal gyrus	$\Delta$ TMT(B-A)	-45,35,23	0.025	0.57	4.79	0.0026
	R superior frontal gyrus		24,5,59	0.042	0.55	4.65	0.0028

Note: All  $p$ -values are FWE corrected; Positive correlations are highlighted in beige; L = left; R = right; TMT = trail making test; DMN = default mode network; RECN = right executive control network;

## 4. Discussion

### 4.1. Within-network Connectivity Changes associated with Cognitive Changes

In this work, we reported interactions between FC changes in the DMN and the ECN and acute changes in cognition associated with major surgery. The two chosen networks are commonly studied and plausibly associated with cognition in the ageing brain [41; 42]. Using seed-based analyses, it was observed that within-network connectivity was directly proportional to executive function (**Figure 5.2**). This was apparent for both the DMN and ECN. These findings provide preliminary support for the hypothesis that cognitive changes in the perioperative period are associated with a breakdown of connectivity in cognitive networks [43].

Within the DMN, connectivity changes predictive of cognitive decline were found between PCC and superior frontal gyrus which is in agreement with the known roles of the connectivity of these brain and cognition [14; 44; 45]. Additionally, connectivity changes were noted between MPFC and cerebellar vermis VIII-IX which have been reported in previous studies [46] [47]. Importantly, a positive correlation was found between increased posterior cingulate-thalamic connectivity and TMT times implying cognitive impairment. It is unclear whether this increase in connectivity: (i) reflects a compensatory mechanism to limit further decline in cognitive performance, (ii) reflects a redistribution of connectivity from frontal to thalamic regions, (iii) itself is a pathological process or (iv) could be a combination of these factors. Future study should explore the role of the thalamus in mediating perioperative changes in cognition.

Within the ECN, connectivity associated with the frontal and parietal cortices (DLPFC and SPL) have consistently been linked with cognitive flexibility, working memory and cognitive set shifting. Specifically, the DLPFC has emerged to be an important node based on the prior studies involving the TMT. With a verbal adaption of TMT, Moll et al. demonstrated activation of the left DLPFC in particular [48]. Anterior regions of the left hemisphere, which are known to be critical in performing tasks requiring rapid action

and cognitive shift, were activated and included the DLPFC as well as the medial frontal gyrus when right handed healthy participants performed the TMT within a task-functional MRI paradigm [49]. It has been shown in the patient population that those with damage to the DLPFC regions are most impaired on specifically the TMTB [50]. Many studies have also shown recruitment of parietal regions during cognitively demanding tasks. For instance, increased activity between DLPFC and parietal operculum has been noted by Seeley and colleagues, although not significant when correlated with TMT [19]. Rather, this study showed that connectivity of parietal seeds of the ECN correlated with cognitive performance on the TMT. In addition to involvement of the frontal areas, increased activation in supplementary motor areas, precentral gyrus and intraparietal sulcus (closely connected to SPL) have been reported during TMT [51; 48; 49]. Structurally, deterioration in terms of reduced levels of gray matter reduction in the left hemisphere including parietal operculum has been observed in Corticobasal Degeneration Syndrome [52] which has been shown to manifest with symptoms similar to frontotemporal dementia [53]. Herein these prior findings were extended by demonstrating that acute change in cognitive function (in the perioperative period) is associated with changes in network connectivity in the ECN involving these brain regions.

#### **4.2. Outside-network Connectivity Changes associated with Cognitive Changes**

Based on the outside-network analyses, positive associations were discovered between connectivity changes and cognitive changes in both the DMN and ECN. In general, this means that outside-network connectivity was inversely proportional to executive function (**Figure 5.4 (a)**). This implies that increased postoperative FC between networks was linked to poorer cognitive performance. These effects were primarily observed in the frontal regions of the brain which are thought to be increasingly recruited to compensate for lack of activation in typical brain regions due to healthy ageing based on the compensation hypothesis [54; 55; 56; 57]. In addition, within a surgical cohort such as in the current study, loss of anti-correlations between networks may represent a postoperative dysfunction comprised of a compensatory mechanism that fails to overcome the cognitive changes occurring postoperatively. However, it also cannot



be excluded that recruitment of these alternate brain regions somehow interferes with cognitive function, precipitating a decline. Tracking the resolution of the changes in cognition with serial functional MRI scanning may help resolve these ambiguities. Furthermore, given that impaired EF is noted in delirium, and preliminary evidence for increased outside-network connectivity in that state [36], it appears likely that there is a continuum of network changes that traverse short-term postoperative cognitive decline (POCD) and delirium. It remains to be tested if this is specific to the cognitive domain or if there truly is biological gradient such that the changes are more profound in delirium. Testing the latter will be complex given that subject with delirium had to be excluded from the present study due to motion artefacts.

#### **4.3. $\Delta$ FC rather than FC as a measure to track EF**

Findings from this study highlight the utility of resting-state functional MRI as a tool to track the dynamics of the brain during the perioperative period. This modality is especially advantageous as it is non-invasive, task-free for the participants and time-efficient in terms of acquisition. If extended to multiple time-points following surgery, functional MRI could allow the study of trajectory of EF and delirium in the elderly, thus, providing insight to their recovery process. Rather than treating functional MRI data at each time-point distinctly, the approach adopted in this work allowed us to study effects of interest perioperatively by examining the changes in FC as well as cognitive outcomes across these time-points. Adding the knowledge from both stages could provide a more complete picture of the course of cognitive changes occurring perioperatively [58; 6; 59].

#### **4.4. Methodological Considerations**

While the present study was strengthened by combining preoperative and postoperative data as well as inclusion of seed-based and network-based analyses, it suffers from the following limitations. Even though the sample size is not very large, it meets the requirement of approximately 20 samples as recommended by Thirion and colleagues for reliability of results based on functional MRI [60]. It must be emphasized that the current analyses are paired-change measurements, reducing the intra-individual variation over

cross-sectional designs (covered by Thirion and colleagues [60]). TMT measure is known to be affected by factors such as age, education [23]. Since the cohort in this study was limited to older adults and demonstrated low variability in the distribution of age, education, raw scores were used in the analysis. Additionally, TMT(B/A) was included as an outcome which partially removes the effect of age and education [27]. However, the impact of factors such as intelligence [61] and smoking habits [62] are also known to affect TMT which were not studied here. Given that the *change* in TMT and *change* in FC were studied here (by normalizing to the baseline data), these confounds are not relevant to this study. The change in FC could be potentially driven by anesthesia, surgical complications, such as delirium, and medication use. However, as this is a pilot study, it was decided a priori that the sample size would be too small to conduct further mechanistic analyses. Present data, herein, can be used to power those analyses to understand the mechanisms of postoperative cognitive decline more clearly.

## **5. Conclusion**

This study aimed at characterizing perioperative EF on the basis of change in FC perioperatively in older adults undergoing non-cardiac surgery. The seed-based (within-network) analysis showed that the DMN and ECN networks demonstrated impaired connectivity correlated with poorer cognition postoperatively. In contrast, the network-based analyses showed attenuated anti-correlations for out-of-network connectivity. Understanding the shift in the dynamics of these neural networks during the perioperative period will inform the mechanisms of POCD and acute changes in cognition in the elderly more generally.

## References

- [1] H. Abildstrom, L. Rasmussen, P. Rentowl, C. Hanning, H. Rasmussen, P. Kristensen, J. Moller, I. group, Cognitive dysfunction 1–2 years after non-cardiac surgery in the elderly. *Acta Anaesthesiologica Scandinavica* 44 (2000) 1246-1251.
- [2] J. Moller, P. Cluitmans, L. Rasmussen, P. Houx, H. Rasmussen, J. Canet, P. Rabbitt, J. Jolles, K. Larsen, C. Hanning, Long-term postoperative cognitive dysfunction in the elderly: ISPOCD1 study. *The Lancet* 351 (1998) 857-861.
- [3] C.C. Price, C.W. Garvan, T.G. Monk, Type and severity of cognitive decline in older adults after noncardiac surgery. *Anesthesiology: The Journal of the American Society of Anesthesiologists* 108 (2008) 8-17.
- [4] L. Rasmussen, T. Johnson, H.M. Kuipers, D. Kristensen, V.D. Siersma, P. Vila, J. Jolles, A. Papaioannou, H. Abildstrom, J. Silverstein, Does anaesthesia cause postoperative cognitive dysfunction? A randomised study of regional versus general anaesthesia in 438 elderly patients. *Acta Anaesthesiologica Scandinavica* 47 (2003) 260-266.
- [5] R.D. Sanders, P.P. Pandharipande, A.J. Davidson, D. Ma, M. Maze, Anticipating and managing postoperative delirium and cognitive decline in adults. *Bmj* 343 (2011) d4331.
- [6] M. Nadelson, R. Sanders, M. Avidan, Perioperative cognitive trajectory in adults. *British journal of anaesthesia* 112 (2014) 440-451.
- [7] D.L. McDonagh, J.P. Mathew, W.D. White, B. Phillips-Bute, D.T. Laskowitz, M.V. Podgoreanu, M.F. Newman, Cognitive function after major noncardiac surgery, apolipoprotein E4 genotype, and biomarkers of brain injury. *Anesthesiology: The Journal of the American Society of Anesthesiologists* 112 (2010) 852-859.
- [8] T. Rappold, A. Laflam, D. Hori, C. Brown, J. Brandt, C. Mintz, F. Sieber, A. Gottschalk, G. Yenokyan, A. Everett, Evidence of an association between brain cellular injury and cognitive decline after non-cardiac surgery. *British journal of anaesthesia* 116 (2016) 83-89.
- [9] T.G. Monk, B.C. Weldon, C.W. Garvan, D.E. Dede, M.T. Van Der Aa, K.M. Heilman, J.S. Gravenstein, Predictors of cognitive dysfunction after major noncardiac surgery. *Anesthesiology: The Journal of the American Society of Anesthesiologists* 108 (2008) 18-30.
- [10] M. Cavallari, W. Dai, C.R. Guttman, D.S. Meier, L.H. Ngo, T.T. Hshieh, A.E. Callahan, T.G. Fong, E. Schmitt, B.C. Dickerson, Neural substrates of vulnerability to postsurgical delirium as revealed by presurgical diffusion MRI. *Brain* 139 (2016) 1282-1294.
- [11] M.-h. Chen, Y. Liao, P.-f. Rong, R. Hu, G.-x. Lin, W. Ouyang, Hippocampal volume reduction in elderly patients at risk for postoperative cognitive dysfunction. *Journal of anesthesia* 27 (2013) 487-492.
- [12] C.C. Price, J.J. Tanner, I. Schmalfluss, C.W. Garvan, P. Gearen, D. Dickey, K. Heilman, D.L. McDonagh, D.J. Libon, C. Leonard, A pilot study evaluating presurgery neuroanatomical biomarkers for postoperative cognitive decline after total knee arthroplasty in older adults. *Anesthesiology: The Journal of the American Society of Anesthesiologists* 120 (2014) 601-613.
- [13] J.R. Andrews-Hanna, A.Z. Snyder, J.L. Vincent, C. Lustig, D. Head, M.E. Raichle, R.L. Buckner, Disruption of large-scale brain systems in advanced aging. *Neuron* 56 (2007) 924-935.
- [14] J.S. Damoiseaux, C. Beckmann, E.S. Arigita, F. Barkhof, P. Scheltens, C. Stam, S. Smith, S. Rombouts, Reduced resting-state brain activity in the “default network” in normal aging. *Cerebral cortex* 18 (2007) 1856-1864.
- [15] R. Cabeza, S.M. Daselaar, F. Dolcos, S.E. Prince, M. Budde, L. Nyberg, Task-independent and task-specific age effects on brain activity during working memory, visual attention and episodic retrieval. *Cerebral cortex* 14 (2004) 364-375.
- [16] P.A. Reuter-Lorenz, C. Lustig, Brain aging: reorganizing discoveries about the aging mind. *Current opinion in neurobiology* 15 (2005) 245-251.

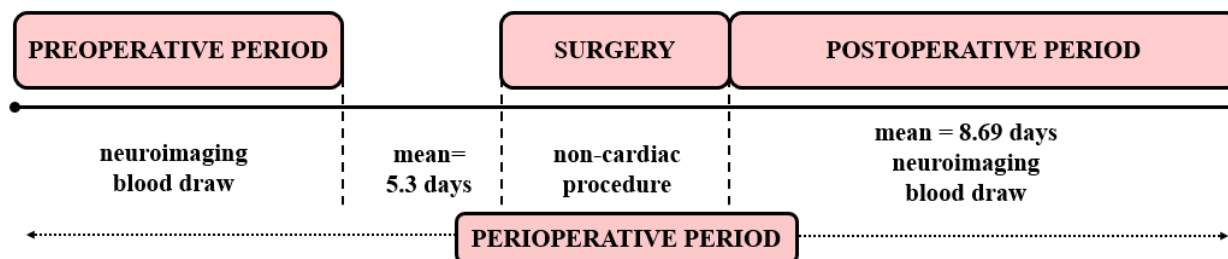
- [17] I.M. McDonough, J.T. Wong, D.A. Gallo, Age-related differences in prefrontal cortex activity during retrieval monitoring: Testing the compensation and dysfunction accounts. *Cerebral Cortex* 23 (2012) 1049-1060.
- [18] R.A. Sperling, J. Bates, E. Chua, A. Cocchiarella, D. Rentz, B. Rosen, D. Schacter, M. Albert, functional MRI studies of associative encoding in young and elderly controls and mild Alzheimer's disease. *Journal of Neurology, Neurosurgery & Psychiatry* 74 (2003) 44-50.
- [19] W.W. Seeley, V. Menon, A.F. Schatzberg, J. Keller, G.H. Glover, H. Kenna, A.L. Reiss, M.D. Greicius, Dissociable intrinsic connectivity networks for salience processing and executive control. *Journal of Neuroscience* 27 (2007) 2349-2356.
- [20] M. Mrkobrada, M.T. Chan, D. Cowan, J. Spence, D. Campbell, C.Y. Wang, D. Torres, G. Malaga, R.D. Sanders, C. Brown, Rationale and design for the detection and neurological impact of cerebrovascular events in non-cardiac surgery patients cohort evaluation (NeuroVISION) study: a prospective international cohort study. *BMJ open* 8 (2018) e021521.
- [21] E.W. Ely, S.K. Inouye, G.R. Bernard, S. Gordon, J. Francis, L. May, B. Truman, T. Speroff, S. Gautam, R. Margolin, Delirium in mechanically ventilated patients: validity and reliability of the confusion assessment method for the intensive care unit (CAM-ICU). *Jama* 286 (2001) 2703-2710.
- [22] R.M. Reitan, Validity of the Trail Making Test as an indicator of organic brain damage. *Perceptual and motor skills* 8 (1958) 271-276.
- [23] J.D. Corrigan, N.S. Hinkeldey, Relationships between parts A and B of the Trail Making Test. *Journal of clinical psychology* 43 (1987) 402-409.
- [24] S.F. Crowe, The differential contribution of mental tracking, cognitive flexibility, visual search, and motor speed to performance on parts A and B of the Trail Making Test. *Journal of clinical psychology* 54 (1998) 585-591.
- [25] R.K. Heaton, L.M. Nelson, D.S. Thompson, J.S. Burks, G.M. Franklin, Neuropsychological findings in relapsing-remitting and chronic-progressive multiple sclerosis. *Journal of consulting and clinical psychology* 53 (1985) 103.
- [26] K. Arbuthnott, J. Frank, Trail making test, part B as a measure of executive control: validation using a set-switching paradigm. *Journal of clinical and experimental neuropsychology* 22 (2000) 518-528.
- [27] G.J. Lamberty, S.H. Putnam, D.M. Chatel, L.A. Bieliauskas, Derived Trail Making Test indices: A preliminary report. *Neuropsychiatry, Neuropsychology, & Behavioral Neurology* (1994).
- [28] W. Penny, J. Ashburner, S. Kiebel, R. Henson, D. Glaser, C. Phillips, K. Friston, Statistical parametric mapping: An annotated bibliography, 2001.
- [29] D. Cordes, V.M. Haughton, K. Arfanakis, J.D. Carew, P.A. Turski, C.H. Moritz, M.A. Quigley, M.E. Meyerand, Frequencies contributing to functional connectivity in the cerebral cortex in "resting-state" data. *American Journal of Neuroradiology* 22 (2001) 1326-1333.
- [30] S.M. Smith, M. Jenkinson, M.W. Woolrich, C.F. Beckmann, T.E. Behrens, H. Johansen-Berg, P.R. Bannister, M. De Luca, I. Drobnjak, D.E. Flitney, Advances in functional and structural MR image analysis and implementation as FSL. *Neuroimage* 23 (2004) S208-S219.
- [31] P. Boveroux, A. Vanhaudenhuyse, M.-A. Bruno, Q. Noirhomme, S. Lauwick, A. Luxen, C. Degueldre, A. Plenevaux, C. Schnakers, C. Phillips, Breakdown of within-and between-network resting state functional magnetic resonance imaging connectivity during propofol-induced loss of consciousness. *Anesthesiology: The Journal of the American Society of Anesthesiologists* 113 (2010) 1038-1053.
- [32] P. Fransson, Spontaneous low-frequency BOLD signal fluctuations: An functional MRI investigation of the resting-state default mode of brain function hypothesis. *Human brain mapping* 26 (2005) 15-29.

- [33] P. Fransson, G. Marrelec, The precuneus/posterior cingulate cortex plays a pivotal role in the default mode network: Evidence from a partial correlation network analysis. *Neuroimage* 42 (2008) 1178-1184.
- [34] M.D. Greicius, B. Krasnow, A.L. Reiss, V. Menon, Functional connectivity in the resting brain: a network analysis of the default mode hypothesis. *Proceedings of the National Academy of Sciences* 100 (2003) 253-258.
- [35] A.D. Wagner, A. Maril, R.A. Bjork, D.L. Schacter, Prefrontal contributions to executive control: functional MRI evidence for functional distinctions within lateral prefrontal cortex. *Neuroimage* 14 (2001) 1337-1347.
- [36] C.E. Curtis, M. D'Esposito, Persistent activity in the prefrontal cortex during working memory. *Trends in cognitive sciences* 7 (2003) 415-423.
- [37] V. Menon, N.E. Adelman, C.D. White, G.H. Glover, A.L. Reiss, Error-related brain activation during a Go/NoGo response inhibition task. *Human brain mapping* 12 (2001) 131-143.
- [38] C. La, P. Mossahebi, V.A. Nair, B.B. Bendlin, R. Birn, M.E. Meyerand, V. Prabhakaran, Age-related changes in inter-network connectivity by component analysis. *Frontiers in aging neuroscience* 7 (2015) 237.
- [39] S.-H. Choi, H. Lee, T.-S. Chung, K.-M. Park, Y.-C. Jung, S.I. Kim, J.-J. Kim, Neural network functional connectivity during and after an episode of delirium. *American Journal of Psychiatry* 169 (2012) 498-507.
- [40] W. Shirer, S. Ryali, E. Rykhlevskaia, V. Menon, M. Greicius, Decoding subject-driven cognitive states with whole-brain connectivity patterns. *Cerebral cortex* 22 (2012) 158-165.
- [41] M.D. Greicius, D.L. Kimmel, Neuroimaging insights into network-based neurodegeneration. *Current opinion in neurology* 25 (2012) 727-734.
- [42] K.K. Ng, J.C. Lo, J.K. Lim, M.W. Chee, J. Zhou, Reduced functional segregation between the default mode network and the executive control network in healthy older adults: a longitudinal study. *Neuroimage* 133 (2016) 321-330.
- [43] R.D. Sanders, Hypothesis for the pathophysiology of delirium: Role of baseline brain network connectivity and changes in inhibitory tone. *Medical hypotheses* 77 (2011) 140-143.
- [44] M.D. Fox, A.Z. Snyder, J.L. Vincent, M. Corbetta, D.C. Van Essen, M.E. Raichle, The human brain is intrinsically organized into dynamic, anticorrelated functional networks. *Proceedings of the National Academy of Sciences* 102 (2005) 9673-9678.
- [45] M.D. Greicius, G. Srivastava, A.L. Reiss, V. Menon, Default-mode network activity distinguishes Alzheimer's disease from healthy aging: evidence from functional MRI. *Proceedings of the National Academy of Sciences* 101 (2004) 4637-4642.
- [46] C. Habas, N. Kamdar, D. Nguyen, K. Prater, C.F. Beckmann, V. Menon, M.D. Greicius, Distinct cerebellar contributions to intrinsic connectivity networks. *Journal of neuroscience* 29 (2009) 8586-8594.
- [47] L. Sang, W. Qin, Y. Liu, W. Han, Y. Zhang, T. Jiang, C. Yu, Resting-state functional connectivity of the vermal and hemispheric subregions of the cerebellum with both the cerebral cortical networks and subcortical structures. *Neuroimage* 61 (2012) 1213-1225.
- [48] J. Moll, R.d. Oliveira-Souza, F.T. Moll, I.E. Bramati, P.A. Andreiuolo, The cerebral correlates of set-shifting: an functional MRI study of the trail making test. *Arquivos de neuro-psiquiatria* 60 (2002) 900-905.
- [49] K.K. Zakzanis, R. Mraz, S.J. Graham, An functional MRI study of the trail making test. *Neuropsychologia* 43 (2005) 1878-1886.
- [50] D.T. Stuss, S.M. Bisschop, M.P. Alexander, B. Levine, D. Katz, D. Izukawa, The Trail Making Test: a study in focal lesion patients. *Psychological assessment* 13 (2001) 230.

- [51] S.C. Jacobson, M. Blanchard, C.C. Connolly, M. Cannon, H. Garavan, An functional MRI investigation of a novel analogue to the Trail-Making Test. *Brain and Cognition* 77 (2011) 60-70.
- [52] B. Borroni, V. Garibotto, C. Agosti, S.M. Brambati, G. Bellelli, R. Gasparotti, A. Padovani, D. Perani, White matter changes in corticobasal degeneration syndrome and correlation with limb apraxia. *Archives of neurology* 65 (2008) 796-801.
- [53] B.F. Boeve, A.E. Lang, I. Litvan, Corticobasal degeneration and its relationship to progressive supranuclear palsy and frontotemporal dementia. *Annals of Neurology: Official Journal of the American Neurological Association and the Child Neurology Society* 54 (2003) S15-S19.
- [54] R.L. Buckner, Memory and executive function in aging and AD: multiple factors that cause decline and reserve factors that compensate. *Neuron* 44 (2004) 195-208.
- [55] R. Cabeza, Hemispheric asymmetry reduction in older adults: the HAROLD model. *Psychology and aging* 17 (2002) 85.
- [56] C.L. Grady, F.I. Craik, Changes in memory processing with age. *Current opinion in neurobiology* 10 (2000) 224-231.
- [57] P.A. Reuter-Lorenz, C. Marshuetz, J. Jonides, E.E. Smith, A. Hartley, R. Koeppel, Neurocognitive ageing of storage and executive processes. *European Journal of Cognitive Psychology* 13 (2001) 257-278.
- [58] G. Crosby, D.J. Culley, B.T. Hyman, Preoperative Cognitive Assessment of the Elderly Surgical Patient A Call for Action. *Anesthesiology: The Journal of the American Society of Anesthesiologists* 114 (2011) 1265-1268.
- [59] A.J. Saleh, G.-X. Tang, S.M. Hadi, L. Yan, M.-H. Chen, K.-M. Duan, J. Tong, W. Ouyang, Preoperative cognitive intervention reduces cognitive dysfunction in elderly patients after gastrointestinal surgery: a randomized controlled trial. *Medical science monitor: international medical journal of experimental and clinical research* 21 (2015) 798.
- [60] B. Thirion, P. Pinel, S. Mériaux, A. Roche, S. Dehaene, J.-B. Poline, Analysis of a large functional MRI cohort: Statistical and methodological issues for group analyses. *Neuroimage* 35 (2007) 105-120.
- [61] O. Spreen, E. Strauss, A compendium of neuropsychological tests: Administration, norms, and commentary, Oxford University Press, 1998.
- [62] M. Wagner, S. Schulze-Rauschenbach, N. Petrovsky, J. Brinkmeyer, C. von der Goltz, G. Gründer, K.N. Spreckelmeyer, T. Wienker, A. Diaz-Lacava, A. Mobascher, Neurocognitive impairments in non-deprived smokers—results from a population-based multi-center study on smoking-related behavior. *Addiction biology* 18 (2013) 752-761.

## CHAPTER 6: Changes in Functional Connectivity Associated with the Inflammatory Response to Noncardiac Surgery in Older Adults

### Graphical Summary



### Research Question

What are the neural indicators of inflammatory response to major surgery in older adults?

### Publication

Mohanty, R., Lindroth, H., Casey, C., Nair, V. A., Prabhakaran, V., Sanders, R. D., “Changes in Functional Connectivity Associated with the Inflammatory Response to Noncardiac Surgery in Older Adults”, currently in preparation for publication in the Journal of Neuroinflammation.

### Abstract

Major non-cardiac surgery and related variables such as the anesthetic, surgical complications, predisposition factors, etc. can invoke inflammatory response in the immune system, especially in the elderly. Systemic inflammation, upon exaggeration, may induce neuronal loss and dysfunction in cognition postoperatively. It is thus, essential to probe the relationship between perioperative neural changes and corresponding inflammatory response. In this study, twenty-seven older adults undergoing non-cardiac surgery were recruited and monitored perioperatively. Blood samples and resting-state functional magnetic resonance imaging data were collected at preoperative and postoperative time-points. Corresponding to each time-point, interleukin (IL)-6 was evaluated based on the blood sample and functional connectivity (FC) was evaluated for the default mode (DMN), executive control (ECN), salience (ASN) and thalamic (BGN) brain networks. Perioperative measures were assessed by difference maps of FC and differences in IL-6 levels from pre- to postoperative time-points. Within and outside-network effects were examined. Multiple regression along with family wise error correction for multiple comparisons were conducted to

investigate the relationship between the difference maps for FC and corresponding changes in IL-6. Within-network effects demonstrated significant negative association between connectivity (FC) changes and inflammatory (IL-6) changes in all the hypothesized networks. Specifically, declined connectivity was observed in relation to elevated IL-6 levels postoperatively. Connectivity with temporal cortices emerged to be most impacted across the various networks. The neural substrates of inflammatory response to non-cardiac surgery were dynamically tracked perioperatively here. Decreased within-network connectivity, indicating neural impairment, corresponded with increased postoperative inflammation, a potential indicator of dysfunction. Future studies should investigate the factors that contribute to a breakdown in network connectivity.



## 1. Introduction

Chronic inflammation contributes to many neurodegenerative pathologies ranging from multiple sclerosis to dementia. More acutely, inflammation can induce sudden changes in cognitive function ranging from cognitive impairment from systemic illness (even if mild such as the common cold) up to the severe disorientation observed in the state of delirium. These changes are of even greater importance in the elderly where inflammation can induce states associated with increased morbidity and mortality, again exemplified by delirium.

The underlying mechanisms through which inflammation can alter cognitive function are poorly understood. Recent data in healthy, younger subjects suggest that functional connectivity in the brain, assessed by resting-state functional magnetic resonance imaging, is altered by inflammation including disrupted anterior cingulate, anterior insula and thalamic connectivity. Whether similar changes occur in elderly subjects, when an acute inflammatory effect is superimposed on chronic effects of aging and comorbidities is unclear. Studying the effects of acute inflammation in the elderly is challenging for both ethical and logistical reasons, not least as volunteer studies could put elderly subjects at increased risk. To circumvent some of these issues and provide increased knowledge to inform whether such volunteer studies are needed, elderly patients undergoing major non-cardiac surgery were recruited into a longitudinal imaging cohort where paired imaging assessments occurred with paired blood draw for cytokine levels. Then changes from the baseline scan were investigated with changes in the cytokine interleukin (IL-) 6, thus, normalizing for the baseline state of the brain. While there are confounds to this approach, for example postoperative medications or pain that are introduced between the scans, this approach has value for identifying network vulnerability in the aging brain to inflammation. Understanding the correlates of inflammation could inform potential preventive/therapeutic methods to facilitate postoperative recovery and prevent cognitive impairment. Notably inflammation can drive the profound cognitive decline of delirium. Understanding of the networks involved may provide new insights into a condition that is bereft of therapies. It is hypothesized here that similar to analyses of younger volunteers, there would be a

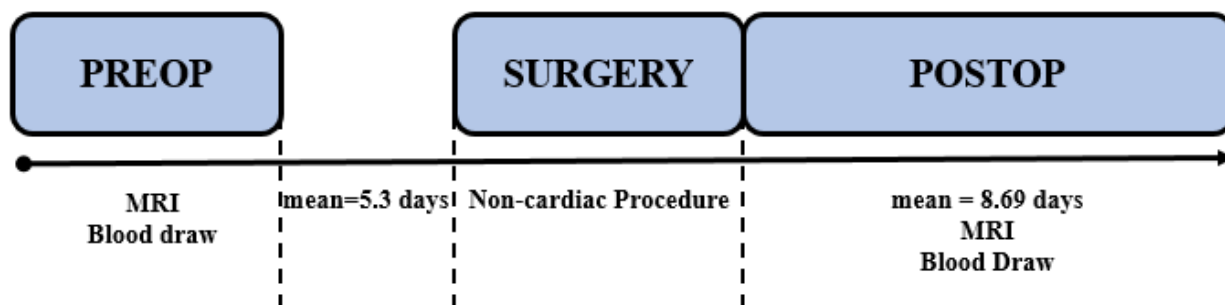
breakdown of key networks centered on posterior and anterior cingulate in the aging brain. These analyses were extended to look at a thalamic seed, suggested through studies of delirium, as well as those discovered in a recent younger subject volunteer study [1].

## 2. Methods

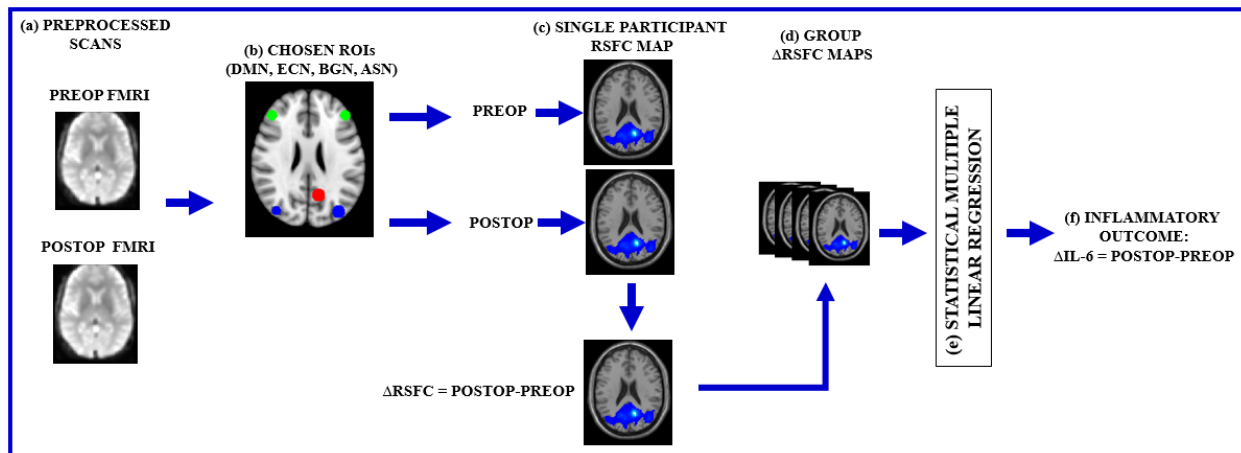
### 2.1. Study Design

As schematized in **Figure 6.1**, this study consisted of three main stages: (a) *the preoperative stage*: the time period leading up to the elective surgery during which blood draw and MRI exams were conducted; (b) *the intra-operative stage*: participants underwent elective non-cardiac surgery under general or neuraxial anesthesia and included general, vascular, spinal, urologic or otolaryngologic procedures; (c) *the postoperative stage*: the time period post-surgery through the entire stay at the hospital during which blood draw, MRI, delirium screening and tracking for complications and discharge disposition were recorded. The study protocol was approved by the Health Sciences Institutional Review Board, University of Wisconsin-Madison and registered with ClinicalTrials.gov (NCT03124303, NCT01980511). Patients were recruited from the NeuroVISION study [2] conducted at the University of Wisconsin-Madison. The methodology followed in this study to examine the association between functional connectivity changes and inflammatory response changes in the perioperative period is outlined in **Figure 6.2** and detailed in the following subsections.

*Figure 6. 1. Schematic diagram of the study design*



**Figure 6. 2. Overview of methodology**



Note: RSFC = FC = functional connectivity; Identification of perioperative change in functional connectivity (FC) as correlates of corresponding changes in inflammatory response (IL-6): **(a)** Preoperative and postoperative individual scans were preprocessed; **(b)** BOLD time-courses corresponding to hypothesized seeds in the DMN (PCC/precuneus, MPFC), ASN (dACC, bilateral insulae), ECN (bilateral DLPFC, SPL), BGN (bilateral ITN, proper thalamus), were extracted preoperatively and postoperatively; **(c)** individual FC map associated with each seed/network was computed at each stage and  $\Delta$ FC was computed; **(d)**  $\Delta$ FC maps were aggregated for group-level analyses; **(e)** linear regression analyses were conducted for each ROI/network to identify  $\Delta$ FC associated with **(f)** corresponding inflammatory changes as measured by IL-6.

## 2.2. Participants

The present study was part of an ongoing perioperative cohort study and hence the sample size was not determined a priori. Twenty-seven older participants (mean age =  $71.74 \pm 4.66$  years; 14 females) undergoing elective non-cardiac surgery were recruited who completed MRI exams prior to as well as post-surgery. Blood samples were drawn on the day of the MRI exam on eighteen of these participants. Criteria for inclusion comprised of: (i) at least 65 years of age or older; (ii) ability to provide written informed consent and (iii) undergoing a major surgical procedure requiring a minimum of two-day stay. The exclusion criteria were: (i) contraindication to MRI (e.g. implanted devices not safe for MRI studies, claustrophobia); (ii) unable or unwilling to attend the follow-up appointments; (iii) documented history of dementia; (iv) residing in a nursing home; (v) undergoing carotid artery surgery or intracranial surgery; (vi) unable to complete neurocognitive/behavioral testing due to language, vision or hearing impairment; (vii) unable to communicate with the research staff due to language barriers. All included participants provided

informed and written consent. Most participants were right handed ( $N=19$ ) with education level of 12 years or more ( $N=21$ ). The most common surgical procedures performed on these participants included spine, general and vascular surgery. The average duration of hospitalization was  $3.2 \pm 1.93$  days. As confirmed by the 3D Confusion Assessment Method [3], none of the participants were delirious at the time of postoperative MRI exam. Of the initial 27, a total of 9 participants were excluded during data processing due to missing inflammatory data ( $N=5$ ) and imaging artifacts ( $N=4$ ) retaining an effective sample size of 18 for further analyses.

### 2.3. Inflammatory Biomarker: Interleukin-6 (IL-6)

Inflammatory cytokine response was evaluated based on blood draws performed preoperatively as well as within the first four days after surgery. Each draw was performed using standard venipuncture procedures or from sterile aspiration of an indwelling line to collect 10 mL of blood. The samples were processed and stored at  $-80^{\circ}\text{C}$  before further analysis. Mass spectrometric proteomic and metabolomics analyses to assess the Interleukin-6 (IL-6 in pg/mL) inflammatory markers in the plasma with the Human Cytokine 10-Plex bead-based Discovery Assay (Eve Technologies, Calgary, Canada). Each sample was measured in duplicate and the mean intra-assay variability was  $<20\%$  (19.8% preoperatively; 13.2% postoperatively) and the mean inter-assay variability was  $<15\%$  (14.26% preoperatively; 14.45% postoperatively). Following standard practice [4], the IL-6 values were log (base 10) transformed to improve normality for statistical modeling. Perioperatively change was computed based on the following:

$$\Delta \log_{10} IL6 = \log_{10} IL6_{postop} - \log_{10} IL6_{preop} \quad (1)$$

where IL-6 levels at postoperative and preoperative stages are denoted by  $\log_{10} IL6_{postop}$  and  $\log_{10} IL6_{preop}$  respectively and the change is represented by  $\Delta \log_{10} IL6$ .

## 2.4. Neuroimaging Acquisition Protocol

MRI data were collected on 3.0 T GE 750 scanners (GE Healthcare, Waukesha, WI) equipped with an eight-channel head coil. Ten minutes long resting-state functional MRI, where participants were instructed to lay with eyes closed, were obtained using single-shot echo-planar T2\*-weighted imaging and the following parameters: TR = 2.6 s, 231 time-points, TE = 22 ms, FOV = 22.4 cm, flip angle = 60°, voxel dimensions 3.5×3.5×3.5 mm<sup>3</sup>, 40 slices. Five minutes long T1-weighted axial anatomical scans, which were used for registration, were collected using FSPGR BRAVO sequence using the following parameters: TR = 8.132 ms, TE = 3.18 ms, TI = 450 ms, over a 256×256 matrix and 156 slices, flip angle = 12°, FOV = 25.6 cm, slice thickness = 1 mm.

## 2.5. Neuroimaging Data Processing

Scans from four participants were excluded after quality check (one subject exhibited high levels of motion in postoperative MRI due to delirium, one subject showed imaging artefacts, scans from two subjects were acquired on 1.5 T scanner leading to low resolution scans). Preprocessing steps included realignment of functional MRI and T1 scans, slice-time correction, normalization to the standard Montreal Neurological Institute (MNI) space, spatial smoothing with a 8-mm full width at half-maximum Gaussian kernel using SPM12 (Statistical Parametric Mapping, Wellcome Trust Centre for Neuroimaging; [www.fil.ion.ucl.ac.uk](http://www.fil.ion.ucl.ac.uk)) [5]. Temporal filtering within 0.07-0.1 Hz was performed to isolate low-frequency blood-oxygen-level-dependent (BOLD) oscillations and remove physiologic noise [6] using FSL 3.2 (Oxford Centre for Functional MRI of the Brain Laboratory Software Library; <http://www.functionalMRIb.ox.ac.uk/fsl>) [7]. The first eigenvariate of the time courses of voxels in each region of interest (ROI) was extracted. Additionally, signals due to white matter, lateral ventricles (represented by the first eigenvariate of time course) and global brain changes were modeled as nuisance covariates. Movement parameters and square of movement parameters (12 parameter model) were also added for simultaneous regression to the general

linear model (GLM). A restricted maximum likelihood approach utilizing an autoregressive model was applied for estimation of serial correlations for parameter estimation. Then a second GLM corresponding to each ROI was fit and effects of interest were evaluated with the help of a parametric T-map on individual-subject level. Consistent with previous studies [8; 9; 10], connectivity analyses were performed by computing a contrast map identifying brain regions that significantly correlated with activity in each specified ROI.

## **2.6. Seed-level (or Within-network) Analysis**

Seed regions were chosen from four main brain networks based on the current hypothesis here including the DMN, ASN, ECN and BGN. Within the DMN, the posterior cingulate (PCC)/precuneus (MNI 12, -60, 24) and medial prefrontal cortex (MPFC; MNI 0, 40, -4) were considered based on previous studies as it is expected to be the most robust task-negative network capturing the resting brain [8; 11; 12; 10]. Functional seed masks of the dorsal anterior cingulate cortex (dACC) was investigated which form the core nodes of the ASN [13], a network that is involved in recruiting, coordinating and interconnecting other brain networks in response to salient stimuli. The task-positive ECN was examined based on the bilateral dorsolateral prefrontal cortex (DLPFC; MNI  $\pm 44$ , 36, 20) [10; 14] and lateral intraparietal sulcus/superior parietal lobule (SPL; MNI 36, -80, 26 and -38, -78, 36) [15; 16; 10] to evaluate potential neurocognitive correlates of inflammation. Thalamic involvement [17] within the BGN was assessed using the bilateral intralaminar thalamic nuclei (ITN; MNI  $\pm 13$ , -20, 10). Furthermore, proper thalamic (MNI  $\pm 3$ , -19, -2) [18] and insular (MNI  $\pm 34$ , 6, 10) [19] nodes were tested due to the critical role they play in maintaining homeostasis during inflammation [1]. For coordinate-based seed regions, a sphere of radius 6-mm centered at the MNI location was created and the first eigenvariate of the BOLD time course was extracted for connectivity analyses.

## 2.7. Network-level (or Outside-network) Analysis

Connectivity was also analyzed outside of the four neural networks to supplement the seed-based within-network analyses. To this end, FC associated with the DMN, ASN, ECN, and BGN was examined. Each network comprised of multiple individual ROIs, defined as per the Willard atlas [20; 13]. BOLD activity was extracted by averaging time course over all voxels of the ROIs within each network and utilized for connectivity analyses. This mean signal was then correlated voxel-wise with the rest of the brain looking for voxels that correlate with change in the inflammatory response.

## 2.8. Perioperative FC

The contrast maps obtained from functional MRI at preoperative and postoperative stages were used to evaluate perioperative change in FC for each ROI at seed and network-levels for each individual subject. Change was evaluated by simple subtraction allowing each subject to be their own control, muting the impact of preoperative differences in connectivity and hence assessing the changes induced by perioperative care. The perioperative FC change maps reflected the following and were used further for group-level analyses.

$$\Delta FC = FC_{postop} - FC_{preop} \quad (2)$$

where  $\Delta FC$  is the observed change in FC between preoperative value, i.e.  $FC_{preop}$  and postoperative value, i.e.  $FC_{postop}$ .

## 2.9. Statistical Analysis

The association between  $\Delta FC$  and  $\Delta IL-6$  were tested using multiple linear regression analyses at seed- as well as network-levels. Cluster-level and peak-level inferences were conducted to identify regions and specific voxels exhibiting significant associations after controlling for multiple comparisons via the family-wise error (FWE) approach ( $p < 0.05$ ). The main goal, here, was to assess the hypothesis that an inverse

association exists between functional connectivity and inflammation. The role of potential confounds such as use of medication, delirium status, surgical factors, however, could not be studied due to lack of sufficient statistical power.

### 3. Results

#### 3.1. Sample Characteristics

For identification of neural correlates of  $\Delta$ IL-6, 18 cases were considered after accounting for missing IL-6 data and quality control of neuroimaging data. Overall,  $\Delta$ IL-6 data were normally distributed and the mean change (SD) being 0.68 (0.52) ( $p = 0.187$ ). Postoperatively, all subjects demonstrated a higher value of IL-6 (greater inflammation) relative to the baseline.

#### 3.2. Correlates of $\Delta$ IL-6

##### 3.2.1. Seed-level (or Within-network) effects

Across the different seed regions, overall, a negative relationship between FC changes and IL-6 changes was observed. All significant effects are listed in **Table 6.1** and the corresponding regions are illustrated in **Figure 6.3 (A)**. Specifically, a decreased FC was associated with an increased IL-6 postoperatively as illustrated in **Figure 6.3 (B)**.

Decreased postoperative FC of PCC with the left middle cingulate gyrus ( $R^2 = 0.59$ ; peak-level FWE  $p=0.023$ ;  $\beta = -0.021$ ) and central operculum ( $R^2 = 0.56$ ; cluster-level FWE  $p=0.001$ ;  $\beta = -0.029$ ) was associated with increased postoperative IL-6. FC between dACC and right putamen was inversely related to IL-6 ( $R^2 = 0.58$ ; cluster FWE  $p=0.038$ ; peak FWE  $p=0.03$ ;  $\beta = -0.026$ ). FC of LDLPFC with right inferior temporal gyrus showed a significant negative association with IL-6 ( $R^2 = 0.58$ ; cluster FWE  $p=0.001$ ; peak FWE  $p=0.041$ ;  $\beta = -0.047$ ). A similar inverse relationship emerged associating FC between right ITN and right transverse temporal gyrus with IL-6 ( $R^2 = 0.57$ ; peak FWE  $p=0.041$ ;  $\beta = -0.026$ ). Change in left insular connectivity with the right superior temporal gyrus exhibited a negative relationship with change in IL-6



( $R^2 = 0.58$ ; peak FWE  $p=0.042$ ;  $\beta = -0.059$ ). Finally, bilateral thalamic connectivity changes at left postcentral gyrus also demonstrated a consistent inverse relationship with IL-6 changes ( $R^2 = 0.54$ ; cluster FWE  $p<0.004$ ;  $\beta = -0.021$  for left thalamus and  $-0.017$  for right thalamus).

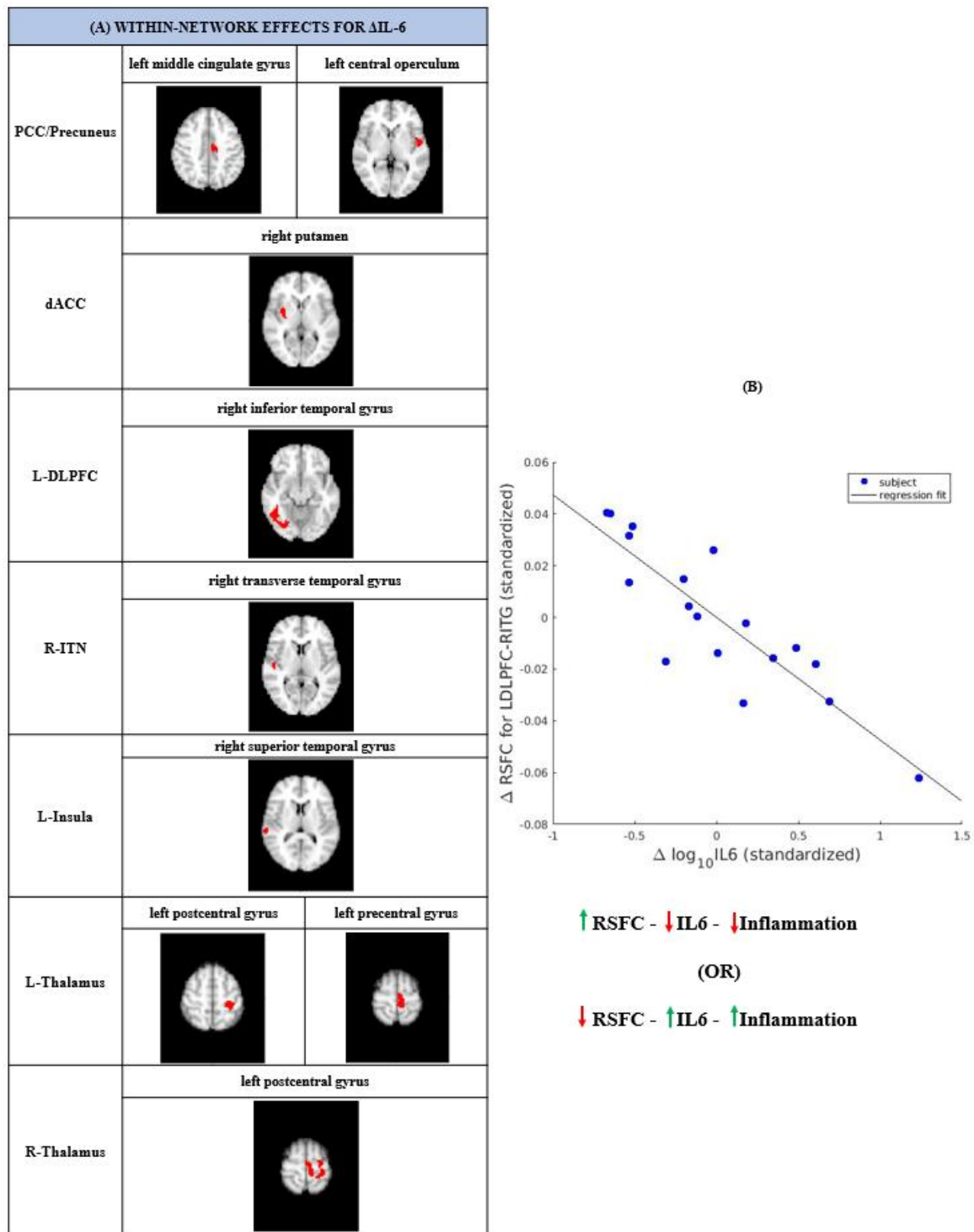
**Table 6. 1.** Brain regions showing significant negative associations with changes in inflammatory response ( $\Delta IL-6$ ) obtained from seed-level (within-network) analyses

Seed Region	Activated Region	MNI x,y,z	Peak-level <i>p</i> -value	$R^2$	Z- score	$\beta$
PCC/Precuneus	L middle cingulate gyrus	-12, -19, 41	<b>0.023*</b>	0.59	4.84	-0.021
	L central operculum	-54, -7, 2	0.076	0.56	4.52	-0.029
dACC	R Putamen	33, -1, 2	<b>0.03*</b>	0.58	4.75	-0.026
L DLPFC	R inferior temporal gyrus	54, -58, -13	<b>0.041*</b>	0.58	4.73	-0.047
R ITN	R transverse temporal gyrus	51, -16, 5	<b>0.041*</b>	0.57	4.7	-0.026
L-Insula	R superior temporal gyrus	63, -28, 8	<b>0.042*</b>	0.58	4.71	-0.059
L-Thalamus	L postcentral gyrus	-27, -31, 50	0.133	0.54	4.34	-0.026
	L precentral gyrus	-9, -31, 59	<b>0.009*</b>	0.54	4.26	-0.021
R-Thalamus	L postcentral gyrus	-30, -31, 47	0.123	0.54	4.40	-0.017

Note: All *p*-values are FWE corrected and in **bold\*** if significant ( $<0.05$ ) at peak and/or cluster levels; L = left; R = right; PCC = posterior cingulate cortex; dACC = dorsal anterior cingulate cortex; DLPFC = dorsolateral prefrontal cortex; ITN = intralaminar thalamic nuclei;

**Figure 6. 3. Within-network effects for inflammatory changes**

(A) Clusters of brain regions (in red) that showed significant associations with respect to changes in inflammation ( $\Delta IL-6$ ) obtained from seed-level (within-network) analyses; (B) an example demonstrating the inverse relationship between  $\Delta FC$  of LDLPFC and  $\Delta IL-6$ .



Note: RSFC = FC = functional connectivity;

### 3.2.2. Network-level (or Outside-network) effects

Similar to the seed-level effects, a negative association between FC changes and IL-6 changes at network-level was found. The significant effects are listed in **Table 6.2** and the involved areas are depicted in **Figure 6.4 (A)**. These networks demonstrated that attenuated FC levels corresponded with elevated IL-6 at the postoperative stage as exemplified by **Figure 6.4 (B)**.

**Table 6. 2.** Brain areas showing significant negative associations with changes in inflammatory response ( $\Delta$ IL-6) obtained from network-level (outside-network) analyses

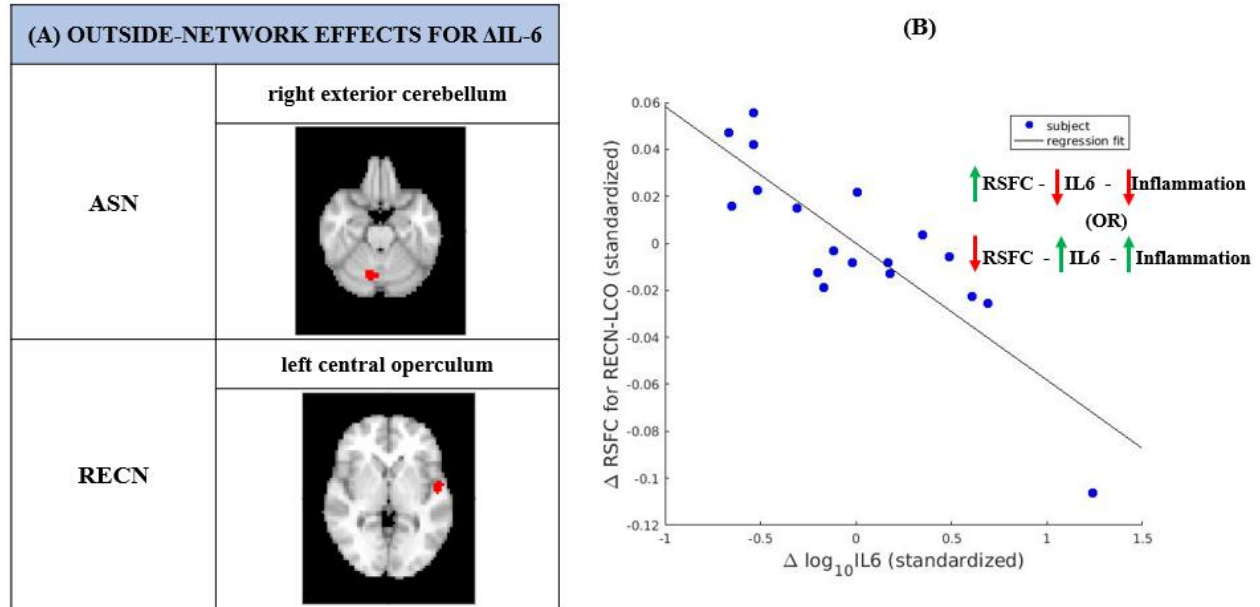
Network	Activated Region	MNI x,y,z	Cluster-level <i>p</i> -value	Peak-level <i>p</i> -value	R <sup>2</sup>	Z-score	$\beta$
ASN	R cerebellum exterior	12, -70, -25	<b>0.039*</b>	0.434	0.53	4.29	-0.045
RECN	L central operculum	-54, -7, 2	<b>0.024*</b>	0.074	0.55	4.47	-0.058

Note: All *p*-values are FWE corrected and in **bold\*** if significant (<0.05) at peak and/or cluster levels; L = left; R = right; ASN = anterior salience network; RECN = right executive control network;

These can be considered to represent outside-network effects. Specifically, significant effects were observed for the ASN and ECN while there were none with respect to the DMN and BGN. In particular, for ASN, FC with right cerebellum illustrated an inverse variation with IL-6 ( $R^2 = 0.53$ ; cluster FWE  $p=0.039$ ;  $\beta = -0.045$ ). Likewise, for ECN, FC with central operculum showed a negative relationship to IL-6 ( $R^2 = 0.55$ ; cluster FWE  $p=0.024$ ;  $\beta = -0.058$ ).

**Figure 6. 4. Outside-network effects for inflammatory changes**

(A) Clusters of brain regions (in red) that showed significant associations with respective changes in inflammation ( $\Delta IL-6$ ) obtained from network-level (outside-network) analyses; (B) an instance illustrating the negative relationship between  $\Delta FC$  of RECN and  $\Delta IL-6$ .



Note: RSFC = FC = functional connectivity;

#### 4. Discussion

Changes in systemic inflammation, as assayed by changes in IL-6, led to consistent decreases in functional connectivity across networks tested. These results are plausible as changes in connectivity have been associated with cognitive decline associated with dementia, minimal cognitive impairment and delirium, which are known to be associated with inflammation. The data and analyses here provide preliminary evidence for acute changes in network connectivity associated with perioperative rises in IL-6. The widespread nature of the decreases in connectivity observed here suggest that inflammation induces a generalized decrease in connectivity, whether this is an underlying mechanism of perioperative cognitive disorders such as delirium, needs to be tested.

#### 4.1. Neural Correlates of IL-6

Analyses included here suggest that cingulate, temporal and thalamic connectivity correlate with IL-6. However, it is critical to stress the potential differences with the prior literature that were collected in young healthy volunteers, in which inflammation was induced by lipopolysaccharide. For example, Labrenz et al., observed increased, not decreased, thalamic connectivity with inflammation [1]. However, they also observed decreased cingulate and insula connectivity, similar to us. Lekander et al. described increased connectivity between the cingulate and insula with lipopolysaccharide injection [21]. The reasons for the discordance between the Lekander and Labrenz papers is unclear as both were collected in young healthy volunteers. Harrison et al., showed that increased inflammation, induced by typhoid vaccination, in young volunteers was associated decreased anterior cingulate, limbic and temporal connectivity with overlapping sources with analyses in this study [22]. Findings of the current study seem most consistent with those of Harrison et al, with widespread decreased connectivity across seeds. However, it is unclear whether the discordance in inflammation-induced changes in connectivity, across all these studies, are due to differences between the elderly and young or mechanism of inflammation (surgery vs. lipopolysaccharide).

Changes in connectivity with chronic inflammation have been noticed previously. For example, Marsland et al. showed chronic inflammatory changes in depression correlated with increased ACC connectivity but decreased ventromedial prefrontal cortex connectivity [23]. A correlation between increased inflammation and decreased frontotemporal connectivity was also noticed in another recent study of community patients (where no immune stimulus like lipopolysaccharide was administered) [24]. Results shown here also suggest altered frontotemporal connectivity changes with inflammation, notably while the seeds for the connectivity analyses were frontal, parietal and thalamic, many of the changes of correlation were with sources in the temporal lobe. Temporal cortex is affected by inflammation in multiple neurological disorders such as dementia and herpes encephalitis. How temporal cortex may be particularly affected by systemic inflammation remains unclear but is worthy of further exploration.

#### 4.2. Within-network Effects

The seed-level analyses enabled delineation of the association between FC within networks of interest and inflammatory response. Notably, impaired connectivity within the ECN between the left DLPFC and right inferior temporal gyrus (ITG) was linked with elevated levels of IL-6 perioperatively ( $R^2 = 0.58$ ; peak-level  $p = 0.041$ ;  $\beta = -0.047$ ). This inter-hemispheric connection has been substantiated by cortical stimulation findings where a transcranial direct stimulation of DLPFC in healthy participants showed an increase in connectivity with ITG [25]. This can have a direct bearing on cognitive processes [26], especially in an elderly surgical cohort such as the one included here. Within the ASN, diminishing insular connectivity with right superior temporal gyrus (STG) was observed to be inversely related to increased IL-6 perioperatively ( $R^2 = 0.58$ ; peak-level  $p = 0.042$ ;  $\beta = -0.059$ ). Neural activity of insula, in general, has been validated to be associated with increased IL-6 in healthy volunteers who received endotoxin which may influence social pain processing [27]. Insular connectivity with STG has been corroborated by Labrenz and colleagues to induce systemic inflammation in healthy male participants during experimental endotoxemia [1] and by Cauda and colleagues [28] who showed that this connection underlies skeletomotor body orientation, environmental monitoring and response selection as a part of the visuo-motor network. Aside from peak effects, it was discovered that STG connectivity may be critical as it appeared to be involved with multiple seed regions (within DMN, ASN, BGN) in association with IL-6 changes which is backed up by a recent study revealing that greater neural activity of STG was linked with rise in IL-6 in the healthy under endotoxin-induced inflammation [27] and positively correlated with self-reported depressed mood.

#### 4.3. Research in context

As far as it is known, study of the neural correlates of inflammation following surgery have not been studied before. Present data have important ramifications for the study of inflammation-associated changes in cognition that may affect surgery and other acute events. The most notable of these is delirium. A theoretical proposal is that delirium results from a breakdown in connectivity in the brain [29]. Given that inflammation is thought to be the primary cause of postoperative delirium and effects predominantly elderly patients, this

work has distinct ramifications for the study of postoperative cognitive disorders. Preliminary data from a small case-control analysis suggests that delirium is associated with reduced posterior cingulate [30] and thalamic connectivity, consistent with observations in the current investigation that inflammation is also associated with impaired connectivity of these regions. However, it must be emphasized that none of the patients included herein were delirious as motion artefacts in such a confusional state prevented from obtaining usable imaging data. A prior study has suggested that surgery induces a breakdown in DMN connectivity, but they did not probe associations with inflammation [31]. Current results suggest that inflammation is associated with a change in PCC and thalamic connectivity, key hubs of the DMN, providing plausible mechanism for that prior work as well as the link to delirium.

#### **4.4. Limitations**

The significance of the present study is strengthened as it combines preoperative and postoperative FC and inflammatory response. The analysis of change between these stages by means of paired functional MRI data accounts for potential confounds by normalizing with respect to the baseline. However, it would also be important to acknowledge the limitations. First, the sample size of the cohort studied was constrained. However, as recommended by a recent study [32], this functional MRI cohort meets the requirement of having approximately 20 samples in order to draw reliable conclusions of results. While the inter-assay variability of IL-6 data was within the acceptable range, the intra-assay variability exceeded the expected threshold. This could be owing to the greater variability within a limited sample size and should be mitigated by studying larger samples in the future. Neuroinflammation in a surgical cohort could potentially be induced due to multiple factors including intraoperative anesthetic, type of surgery, postoperative medication use, surgical complications such as delirium [33]. Since the cohort in this study was not sufficiently powered to study the interaction among FC and the potential confounds as correlates of IL-6 changes, future investigations based on larger cohort should account for these for a better understanding of relative contribution of these factors.

#### **4.5. Future Directions**

In the future a larger cohort study should be conducted to investigate whether these changes are reproducible, and whether they are robust to clinical confounders. Understanding the underlying mechanism for the inflammation induced changes in connectivity is key. Alterations in inhibitory interneuron signaling, involving GABA<sub>A</sub> signaling, may underlie the changes in network connectivity observed herein. It may be possible to test this using Magnetic Resonance Spectroscopy for GABA levels. Alternatively, animal models may be necessary to test the synaptic events underlying these changes in connectivity. Recent observations also indicate that peripheral lipopolysaccharide leads to decreased connectivity in mice. Then mechanism for this inflammation induced change can be tested with manipulation of interneuron signaling with pharmacological and optogenetic techniques.

#### **5. Conclusion**

These data suggest an inverse relationship between functional connectivity and acute inflammation (IL-6), that affects the brain in a widespread manner. A breakdown in network connectivity may explain the cognitive changes associated with inflammatory events, such as surgery. Thus, it is proposed that understanding of underlying neural mechanisms could contribute toward decoding dynamics of acute conditions such as delirium in which inflammation drives major cognitive changes.



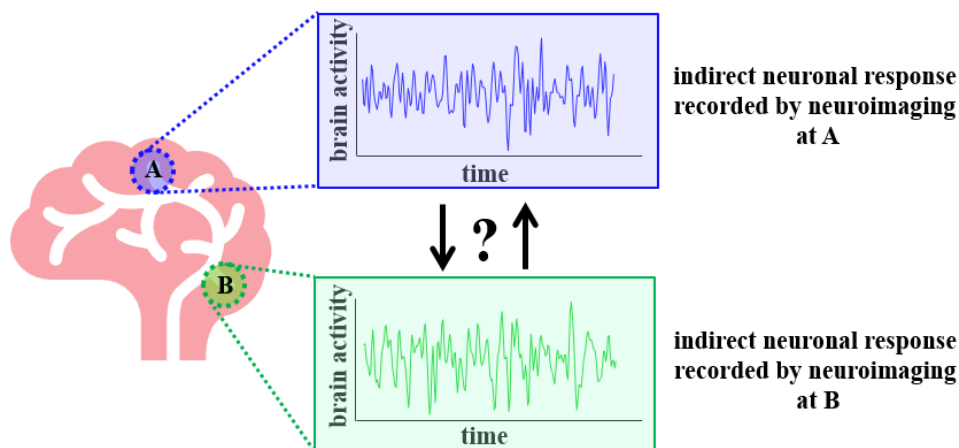
## References

- [1] F. Labrenz, K. Wrede, M. Forsting, H. Engler, M. Schedlowski, S. Elsenbruch, S. Benson, Alterations in functional connectivity of resting state networks during experimental endotoxemia—an exploratory study in healthy men. *Brain, behavior, and immunity* 54 (2016) 17-26.
- [2] M. Mrkobrada, M.T. Chan, D. Cowan, J. Spence, D. Campbell, C.Y. Wang, D. Torres, G. Malaga, R.D. Sanders, C. Brown, Rationale and design for the detection and neurological impact of cerebrovascular events in non-cardiac surgery patients cohort evaluation (NeuroVISION) study: a prospective international cohort study. *BMJ open* 8 (2018) e021521.
- [3] E.W. Ely, S.K. Inouye, G.R. Bernard, S. Gordon, J. Francis, L. May, B. Truman, T. Speroff, S. Gautam, R. Margolin, Delirium in mechanically ventilated patients: validity and reliability of the confusion assessment method for the intensive care unit (CAM-ICU). *Jama* 286 (2001) 2703-2710.
- [4] C.L. Raison, A.S. Borisov, M. Majer, D.F. Drake, G. Pagnoni, B.J. Woolwine, G.J. Vogt, B. Massung, A.H. Miller, Activation of central nervous system inflammatory pathways by interferon-alpha: relationship to monoamines and depression. *Biological psychiatry* 65 (2009) 296-303.
- [5] W. Penny, J. Ashburner, S. Kiebel, R. Henson, D. Glaser, C. Phillips, K. Friston, *Statistical parametric mapping: An annotated bibliography*, 2001.
- [6] D. Cordes, V.M. Haughton, K. Arfanakis, J.D. Carew, P.A. Turski, C.H. Moritz, M.A. Quigley, M.E. Meyerand, Frequencies contributing to functional connectivity in the cerebral cortex in “resting-state” data. *American Journal of Neuroradiology* 22 (2001) 1326-1333.
- [7] S.M. Smith, M. Jenkinson, M.W. Woolrich, C.F. Beckmann, T.E. Behrens, H. Johansen-Berg, P.R. Bannister, M. De Luca, I. Drobnjak, D.E. Flitney, *Advances in functional and structural MR image analysis and implementation as FSL*. *Neuroimage* 23 (2004) S208-S219.
- [8] P. Boveroux, A. Vanhaudenhuyse, M.-A. Bruno, Q. Noirhomme, S. Lauwick, A. Luxen, C. Degueldre, A. Plenevaux, C. Schnakers, C. Phillips, Breakdown of within-and between-network resting state functional magnetic resonance imaging connectivity during propofol-induced loss of consciousness. *Anesthesiology: The Journal of the American Society of Anesthesiologists* 113 (2010) 1038-1053.
- [9] P. Fransson, Spontaneous low-frequency BOLD signal fluctuations: An functional MRI investigation of the resting-state default mode of brain function hypothesis. *Human brain mapping* 26 (2005) 15-29.
- [10] W.W. Seeley, V. Menon, A.F. Schatzberg, J. Keller, G.H. Glover, H. Kenna, A.L. Reiss, M.D. Greicius, Dissociable intrinsic connectivity networks for salience processing and executive control. *Journal of Neuroscience* 27 (2007) 2349-2356.
- [11] P. Fransson, G. Marrelec, The precuneus/posterior cingulate cortex plays a pivotal role in the default mode network: Evidence from a partial correlation network analysis. *Neuroimage* 42 (2008) 1178-1184.
- [12] M.D. Greicius, B. Krasnow, A.L. Reiss, V. Menon, Functional connectivity in the resting brain: a network analysis of the default mode hypothesis. *Proceedings of the National Academy of Sciences* 100 (2003) 253-258.
- [13] W. Shirer, S. Ryali, E. Rykhlevskaia, V. Menon, M. Greicius, Decoding subject-driven cognitive states with whole-brain connectivity patterns. *Cerebral cortex* 22 (2012) 158-165.
- [14] A.D. Wagner, A. Maril, R.A. Bjork, D.L. Schacter, Prefrontal contributions to executive control: functional MRI evidence for functional distinctions within lateral prefrontal cortex. *Neuroimage* 14 (2001) 1337-1347.
- [15] C.E. Curtis, M. D'Esposito, Persistent activity in the prefrontal cortex during working memory. *Trends in cognitive sciences* 7 (2003) 415-423.
- [16] V. Menon, N.E. Adleman, C.D. White, G.H. Glover, A.L. Reiss, Error-related brain activation during a Go/NoGo response inhibition task. *Human brain mapping* 12 (2001) 131-143.

- [17] S.-H. Choi, H. Lee, T.-S. Chung, K.-M. Park, Y.-C. Jung, S.I. Kim, J.-J. Kim, Neural network functional connectivity during and after an episode of delirium. *American Journal of Psychiatry* 169 (2012) 498-507.
- [18] K. Tillisch, E.A. Mayer, J.S. Labus, Quantitative meta-analysis identifies brain regions activated during rectal distension in irritable bowel syndrome. *Gastroenterology* 140 (2011) 91-100.
- [19] V. Napadow, L. LaCount, K. Park, S. As-Sanie, D.J. Clauw, R.E. Harris, Intrinsic brain connectivity in fibromyalgia is associated with chronic pain intensity. *Arthritis & Rheumatism* 62 (2010) 2545-2555.
- [20] J. Richiardi, A. Altmann, A.-C. Milazzo, C. Chang, M.M. Chakravarty, T. Banaschewski, G.J. Barker, A.L. Bokde, U. Bromberg, C. Büchel, Correlated gene expression supports synchronous activity in brain networks. *Science* 348 (2015) 1241-1244.
- [21] M. Lekander, B. Karshikoff, E. Johansson, A. Soop, P. Fransson, J.N. Lundström, A. Andreasson, M. Ingvar, P. Petrovic, J. Axelsson, Intrinsic functional connectivity of insular cortex and symptoms of sickness during acute experimental inflammation. *Brain, behavior, and immunity* 56 (2016) 34-41.
- [22] N.A. Harrison, L. Brydon, C. Walker, M.A. Gray, A. Steptoe, H.D. Critchley, Inflammation causes mood changes through alterations in subgenual cingulate activity and mesolimbic connectivity. *Biological psychiatry* 66 (2009) 407-414.
- [23] A.L. Marsland, D.C.-H. Kuan, L.K. Sheu, K. Krajina, T.E. Kraynak, S.B. Manuck, P.J. Gianaros, Systemic inflammation and resting state connectivity of the default mode network. *Brain, behavior, and immunity* 62 (2017) 162-170.
- [24] M. Bang, J. Kim, S.K. An, Y. Youm, J. Chey, H.C. Kim, K. Park, K. Namkoong, E. Lee, Associations of systemic inflammation with frontotemporal functional network connectivity and out-degree social-network size in community-dwelling older adults. *Brain, behavior, and immunity* (2019).
- [25] C.-h. Park, W.H. Chang, J.-Y. Park, Y.-I. Shin, S.T. Kim, Y.-H. Kim, Transcranial direct current stimulation increases resting state interhemispheric connectivity. *Neuroscience letters* 539 (2013) 7-10.
- [26] C. Babiloni, R. Ferri, G. Binetti, A. Cassarino, G. Dal Forno, M. Ercolani, F. Ferreri, G.B. Frisoni, B. Lanuzza, C. Miniussi, Fronto-parietal coupling of brain rhythms in mild cognitive impairment: a multicentric EEG study. *Brain research bulletin* 69 (2006) 63-73.
- [27] N.I. Eisenberger, T.K. Inagaki, L.T. Rameson, N.M. Mashal, M.R. Irwin, An functional MRI study of cytokine-induced depressed mood and social pain: the role of sex differences. *Neuroimage* 47 (2009) 881-890.
- [28] F. Cauda, F. D'agata, K. Sacco, S. Duca, G. Geminiani, A. Vercelli, Functional connectivity of the insula in the resting brain. *Neuroimage* 55 (2011) 8-23.
- [29] R.D. Sanders, Hypothesis for the pathophysiology of delirium: Role of baseline brain network connectivity and changes in inhibitory tone. *Medical hypotheses* 77 (2011) 140-143.
- [30] S.J. van Montfort, E. van Dellen, A.M. van den Bosch, W.M. Otte, M.J. Schutte, S.-H. Choi, T.-S. Chung, S. Kyeong, A.J. Slooter, J.-J. Kim, Resting-state functional MRI reveals network disintegration during delirium. *NeuroImage: Clinical* (2018).
- [31] J.N. Browndyke, M. Berger, T.B. Harshbarger, P.J. Smith, W. White, T.L. Bisanar, J.H. Alexander, J.G. Gaca, K. Welsh-Bohmer, M.F. Newman, Resting-State Functional Connectivity and Cognition After Major Cardiac Surgery in Older Adults without Preoperative Cognitive Impairment: Preliminary Findings. *Journal of the American Geriatrics Society* 65 (2017) e6-e12.
- [32] B. Thirion, P. Pinel, S. Mériaux, A. Roche, S. Dehaene, J.-B. Poline, Analysis of a large functional MRI cohort: Statistical and methodological issues for group analyses. *Neuroimage* 35 (2007) 105-120.
- [33] J.X. Tang, M.F. Eckenhoff, R.G. Eckenhoff, Anesthetic modulation of neuroinflammation in Alzheimer's disease. *Current opinion in anaesthesiology* 24 (2011) 389.

## CHAPTER 7: Rethinking Measures of Brain Connectivity via Feature Extraction

### Graphical Summary



### Research Question

How to comprehensively quantify the relationship between activity of anatomically distinct brain regions?

### Publication

Mohanty, R., Sethares, W. A., Nair, V. A., Prabhakaran, V., “Meaning of Functional Magnetic Resonance Imaging-based Brain Functional Connectivity: Empirical Evidence and Hypotheses”, currently in preparation for submission to Nature Neuroscience.

### Abstract

Functional connectivity (FC), as measured via functional magnetic resonance imaging (MRI), has emerged as the basis for study of functional integration in the brain irrespective of spatial connectivity in healthy as well as pathological populations. Conventionally, FC is quantified by Pearson’s correlation which primarily captures the linear and time-domain relationship among the blood-oxygen-level-dependent (BOLD) signals of distinct brain regions. This motivated the current exploratory pilot study which investigates the following questions: (i) Is Pearson’s correlation sufficient to characterize FC? (ii) Are there alternative measures that could better quantify FC? (iii) What implications and hypotheses about FC could be uncovered in light of these alternative measures? These questions were dissected by retrospectively analyzing functional MRI in healthy adult population using data-inspired statistical models as well as data-driven machine learning methods. Preliminary findings from current data suggested the following answers to these questions: (i)

Pearson's correlation may not comprehensively capture interactions among BOLD signals. (ii) Eight distinct alternative and complementary measures were identified to quantify FC. These measures were similarly consistent when compared between task and resting-state functional MRI, improved the performance of age-based classification and in some cases provided better association with behavioral outcomes in the healthy population. (iii) Based on these findings, two hypotheses were formulated. First, in lieu of Pearson's correlation alone, an augmented and multi-metric definition of FC might be more appropriate. Second, the canonical large-scale brain networks or configurations may be dependent upon the measure used to quantify FC. A more thorough notion of FC holds promise for a better understanding of pathological conditions and variations within a given population via neuroimaging.

## 1. Introduction

The notion of connectivity in the brain can be characterized at three main levels: structural (using imaging techniques such as T1 and diffusion MRI), functional (using functional imaging such as positron emission tomography and functional MRI) and neuronal (using scalp recordings such as in electroencephalogram). Measures of connectivity are crucial to the understanding of the brain connectome. A common principle underlying the concept of connectivity (or lack thereof) represents the neural bases as evident from several animal models and human studies [1; 2; 3] and can provide useful and meaningful information to explain a wide range of pathological conditions and behavioral traits in various population groups.

In the context of functional connectivity (FC), the ideas of segregation and integration in the brain are well established [4]. It is, however, important to acknowledge that there are individual variations of a specific integrated component which may be lost during group-level analyses. Additionally, connectivity typically associated with a particular entity is not necessarily always unique. For instance, the sites of the brain included within the default mode network are not always connected with the same strength across individuals or even within individuals [5].

This problem is further complicated by the definition of connectivity used. Most conventionally, FC is defined by measuring similarity between brain signals arising from two regions. Under a traditional notion of similarity such as Pearson's correlation, signals from two brain regions may appear correlated and hence indicate that the regions are connected in the brain. Although the concept of similarity and dissimilarity appear simple, mathematical formulations reveal otherwise. Two distinct similarity measures may not measure similarity in the same way. Likewise, a similarity measure may not bear a direct and simple inverse relationship with a dissimilarity measure.

The implication that connectivity is dependent upon the measure used to quantify it remains relatively unexplored. Brain regions may appear connected under one definition but disconnected under another [6]. Thus, it would be key to understand the various measures of connectivity relative to each other in order to sensibly choose the measure to be used. A particular definition of connectivity may also convey distinct

types of information about the neural bases. This provides main motivation behind the present study, specifically in the context of FC based on functional MRI.

In brief, the goal was to identify multiple alternative measures that could be used to quantify FC. These measures may be complementary to one another and the goal is to assess them by formulating research questions specific and relevant to the study of connectivity in neuroscience. In particular, the following three research questions were formulated: (i) Does Pearson's correlation, which is the conventional way of defining FC, provide a sufficient characterization of it? (ii) Are there alternative measures that could be used to better quantify FC? (iii) How do the measures of FC compare relatively for population-based classification and prediction of behavioral data? (iv) What are the implications of using varying measures of FC? (v) What could be done to choose the best notion(s) of FC?

In this exploratory study, functional MRI data-based experimentation was adopted in healthy human population to answer these questions. The preliminary results indicated that: (i) Pearson's correlation alone may be an incomplete characterization of FC; (ii) there exist several alternative measures that can capture interactions between brain signals in different ways; (iii) no single measure of FC stands out in the context of classification or prediction; (iv) the idea of large-scale brain connectivity or functional configuration of the brain, largely identified on the basis of Pearson's correlation, may look different under the chosen definition of FC; and (v) rather than relying on one single measure of FC, a wiser option may be to combine multiple complementary measures of FC, choose a subset of them on the basis of feature selection to avoid overfitting and use the more comprehensive multi-metric definition.

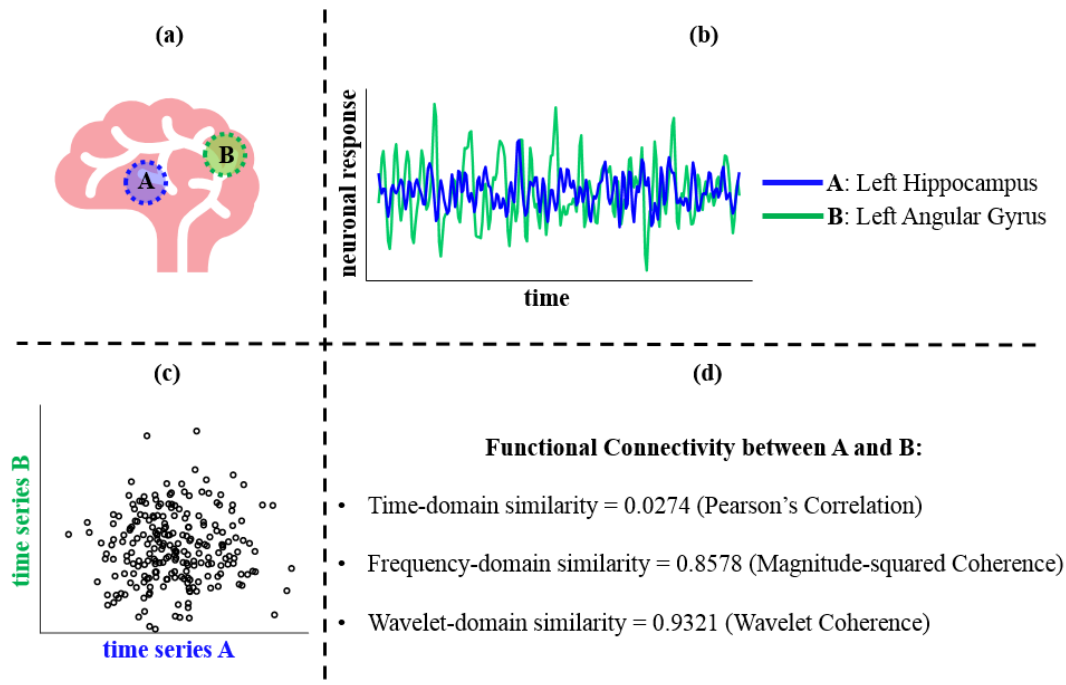
## **2. Methods**

### **2.1. Conventional characterization of functional connectivity**

One approach to characterize integration is in terms of FC, which is usually inferred on the basis of correlations among measurements of neuronal activity of anatomically separated regions. FC, originally defined as the statistical dependencies among remote neurophysiological events in positron emission

imaging [7], was subsequently applied to functional MRI data [8]. In most applications, the convention has been to use Pearson's correlation as it is simple to quantify and has an intuitive interpretation. However, statistical dependence between signals can arise in a variety of ways.

**Figure 7. 1. A contrary case**



Note: An example of FC within the standard DMN in a young healthy adult: **(a)** left hippocampus (denoted by A) and left angular gyrus (denoted by B) within the DMN are considered based on Willard functional atlas; **(b)** the BOLD time series signals from preprocessed resting-state functional MRI were extracted from each region; **(c)** a scatter plot comparing the two BOLD time series shows the temporal linear correlation between them; **(d)** three distinct similarity measures of FC between the signals are compared; FC = functional connectivity; DMN = default mode network; BOLD = blood-oxygen-level-dependent;

This has been depicted in **Figure 7.1** within the context of FC. Essentially, a fail/contrary case is presented by considering two functionally connected brain regions, assumed to be part of the standard default mode network (DMN) in the healthy brain. At a single-subject level, examination of the neurophysiological events (BOLD signals) associated with these regions appear to have a low level of correlation as captured by the time-domain similarity of Pearson's correlation, on a scale of 0 to 1. However, similarity between signals arising from the same regions in the frequency-domain (quantified by magnitude-squared coherence) and wavelet-domain (quantified by wavelet coherence) are comparatively higher (these are also

presented on the scale of 0 to 1). This case illustrates that a low correlation in time-domain must not be mistaken for no correlation and can also be supported mathematically. Rather, it should be treated as lack of linear time-dependence only. This could imply that there may still be dependencies between these BOLD signals, that are not captured well by Pearson's correlation. Capturing the true underlying dependencies is an essential task in the full understanding of brain connectivity.

## 2.2. Are there alternative measures to quantify functional connectivity?

Based on a literature review within neuroimaging and signal processing disciplines, a number of measures were identified that capture statistical dependence between two signals. For all subsequent experiments, suppose the following. Based on the preprocessed functional MRI data for any subject, BOLD time-series signal can be extracted from any region in the brain which lasts for  $t$  – timepoints. Assuming that a network of interest in the brain is comprised of  $n$  – regions, we would have a  $t \times n$  matrix, where each column vector would represent the BOLD time-series for a given region, each with  $t$  – timepoints. Variables  $x$  and  $y$  would represent time series from any pairs of distinct regions with each  $x, y \in \mathbb{R}^t$ . Pairwise FC, measuring the statistical dependence between all possible pairs in a given network would yield a  $n \times n$  matrix. This would generate a symmetric matrix and can be reduced to  $\frac{n(n-1)}{2}$  unique coefficients (from either the upper or lower triangle of the matrix). The following defines and characterizes each identified measure quantifying FC, a summary of which is presented in **Supplementary Table 7.1**.

### ***Pearson's Correlation:***

Pearson's Correlation is a similarity measure and provides a relative measure of association between two signals [9] and is given by:

$$\rho_{corr}(x, y) = \frac{cov(x, y)}{\sqrt{var(x)var(y)}} = \frac{(x - \bar{x})(y - \bar{y})^T}{\left(\sqrt{(x - \bar{x})(x - \bar{x})^T} \right) \left(\sqrt{\{(y - \bar{y})(y - \bar{y})^T\}} \right)} \quad (1)$$



where  $cov(x, y)$  is the covariance between signals,  $\bar{x}$  and  $\bar{y}$  are the mean values of the respective signals,  $var(x)$  and  $var(y)$  represent the variance of each signal respectively.

The quantity  $\rho_{corr}$  captures the linear relationship between the signals, is bounded above by 1 in absolute value and is scale-invariant in magnitude. A positive value indicates the time series signals tend to be simultaneously greater than their respective means. And a negative value implies that the signals tend to fall on opposite sides of their respective means. The absolute value reflects the strength of the tendency to be above or below their means. A value closer to 0 suggests that the signals are uncorrelated in terms of a linear correlation. This implies that a linear relationship is not enough to capture the true relationship between them; it should not be treated as evidence for an absence of a relationship.

***Cross-correlation:***

Cross-correlation [10], a similarity measure, could simply be considered as the extended version of Pearson's correlation as it calculates the linear correlation between all possible shifted versions of a signal relative to the other signal as follows:

$$\rho_{cross-corr}(x, y) = \rho_{xy}(m) = \begin{cases} \sum_{i=0}^{t-m-1} x_{i+m} y_i^* & \text{if } m \geq 0 \\ \rho_{yx}(-m) & \text{if } m < 0 \end{cases} \quad (2)$$

where  $y_i^*$  represents the complex conjugate of  $y_i$ . Index  $m$  is the displacement between the two signals and is called a lag or lead depending on whether it assumes a positive or negative value.

Since it computes the correlation between displaced versions of two signals,  $\rho_{cross-corr}$  ranges from -1 to 1 and must be interpreted just like linear correlation. While correlation between two signals generates a single similarity measure, cross-correlation generates a vector of similarity measures corresponding to each value of  $m$ . The maximum value of this vector for a particular  $m$  can be used as a feature for further analysis. This could be useful in identifying regions of the brain that might not be functionally connected at the same time but be functionally connected after a lag period.

***Coherence:***

The spectral coherence [11] allows assessment of the correlation or similarity between two signals in the frequency-domain. Also known as the magnitude-squared coherence, its value indicates how similar  $x$  and  $y$  are at each frequency. Coherence can be expressed as:

$$\rho_{coherence}(x, y) = \frac{|P_{xy}(f)|^2}{P_{xx}(f)P_{yy}(f)} \quad (3)$$

where  $P_{xx}(f)$  and  $P_{yy}(f)$  are the power spectral densities of  $x$  and  $y$  respectively and  $P_{xy}(f)$  is the cross-power spectral density of  $x$  and  $y$ .

The value of coherence lies between 0 and 1, with 0 indicating no coherence between the signals and 1 indicating strong coherence between the signals. It can be considered to reflect the phase consistency between two signals at a given frequency. On one hand, a weaker coherence is the case when the signals share a random phase relationship and on the other hand, stronger coherence results when the phase relationship is almost constant between the signals. Since a coherence value is obtained for each frequency component in the signals, the peak similarity achieved could be utilized for further analysis.

***Wavelet coherence:***

Wavelet coherence [12] captures similarity and quantifies how time signals from two sources are related in the time-frequency-domain. It is based on computing the cross-wavelet power which reveals the parts of the signals that share high common power. Wavelet coherence measures the coherence of the cross wavelet transform in time-frequency-domain and is given by:

$$\rho_{wcoherence}(x, y) = \frac{|S(C_x(a, b)C_y(a, b))|^2}{S(|C_x(a, b)|^2)S(|C_y(a, b)|^2)} \quad (4)$$

where  $S$  is the smoothing operator in time and scale,  $C_x(a, b)$  and  $C_y(a, b)$  represent the continuous wavelet transform of  $x$  and  $y$  at scales  $a$  and positions  $b$  respectively. For real-valued signals,

$\rho_{wcoherence}(x, y)$  would be real-valued by choosing real-valued wavelets. Comparing the forms presented in equation (4) and equation (1) suggests that  $\rho_{wcoherence}$  could be considered as the equivalent of  $\rho_{corr}$  in the time-frequency domain. The magnitude of  $\rho_{wcoherence}$  can vary between 0 (no similarity) and 1 (identically similar). Unlike in  $\rho_{cross-corr}$  or  $\rho_{coherence}$ ,  $\rho_{wcoherence}$  requires computation of a similarity measure at each point on the two-dimensional time-frequency plane. Subsequent analysis could be carried out by choosing the greatest similarity value corresponding to a particular time and frequency.

### ***Mutual Information:***

Inspired by information theory, if  $x$  and  $y$  were to be treated as discrete random variables over the space  $\mathcal{X} \times \mathcal{Y}$ , then the similarity in the form of mutual information [13] between them can be defined as:

$$\rho_{mutual\_info}(x, y) = I(x; y) = \sum_{y \in \mathcal{Y}} \sum_{x \in \mathcal{X}} p(x, y) \log \left( \frac{p(x, y)}{p(x)p(y)} \right) \quad (5)$$

where  $p(x, y)$  is the joint probability mass function of  $x$  and  $y$ ,  $p(x)$  and  $p(y)$  are the marginal probability mass functions of  $x$  and  $y$  respectively.

Essentially,  $\rho_{mutual\_info}$  captures the information that is shared between  $x$  and  $y$ , i.e., it measures how much knowing one of them reduces uncertainty about the other.  $\rho_{mutual\_info}$  can assume non-negative values only. On one hand, if  $\rho_{mutual\_info} = 0$ , then knowledge of  $x$  does not offer any knowledge of  $y$  and vice-versa. On the other hand, if there exists a deterministic relationship between  $x$  and  $y$ , then knowledge of  $x$  is also shared with  $y$  and vice-versa. In this case,  $\rho_{mutual\_info}$  is equivalent to the entropy of each  $x$  as well as  $y$  which represent the expected information stored by each random variable.

### ***Euclidean Distance:***

Euclidean distance is a dissimilarity measure and one of the more commonly used metrics used due to the well-studied background of Euclidean spaces. It is easy to conceptualize and intuitive as it measures the geometric distance between two points. In case of vectors, this can be computed by the following:

$$\rho_{euclidean}(x, y) = \|x - y\|_2 = \sqrt{(x - y)(x - y)^T} \quad (6)$$

The difference terms serve as the measure of similarity.  $\rho_{euclidean}$  is dependent on the magnitude of individual points of the vectors. While it is bounded below by 0 indicating low dissimilarity, there is no upper bound. However, it can be rescaled to range between 0 and 1 for interpretability. Euclidean distance is not invariant to the scale of the data. It must be applied once the data has been appropriately scaled.

### ***Cityblock Distance:***

Cityblock distance is derived by looking at the difference in absolute values in each dimension of the signals and represents dissimilarity between them. It is given by:

$$\rho_{cityblock}(x, y) = \|x - y\|_1 = \sum_{i=1}^t |x_i - y_i| \quad (7)$$

$\rho_{cityblock}$  can decompose the contributions made by each variable of the signal in terms of the difference in their absolute values. As with  $\rho_{euclidean}$ , the measure  $\rho_{cityblock}$  is bounded below by 0, is not bounded above and scale-variant. Values closer to 0 are more desirable to claim lower dissimilarity between vectors. Unlike  $\rho_{euclidean}$ , which squares the difference in amplitudes and amplifies the deviation, the larger differences in  $\rho_{cityblock}$  are not amplified.

### ***Dynamic Time Warping:***

Dynamic time warping [14] measures dissimilarity and provides an alignment between the signals by means of non-linear warping of the time axis. This metric is based on evaluating a local cost of similarity between all possible pairs of dimensions between two signals and creating a lattice. Based on this lattice, the signals are aligned so as to have the maximum overall overlap (or minimum cost in the optimization framework). The steps involved are as follows:

For two signals,  $x$  and  $y$ , let  $\rho_{ij}$  be the Euclidean distance between  $i^{\text{th}}$ -dimension of  $x$  and  $j^{\text{th}}$ -dimension of  $y$ . All pairwise distances  $\rho_{ij}$  are arranged into a lattice  $C_{i,j}(x, y)$  of size  $t \times t$ . Then  $\rho_{dtw}$  searches through the lattice for a path parameterized by two sequences of the same length such that

$$\sum C_{i,j}(x, y) \quad (8)$$

is minimum. The chosen path is such that both signals are aligned, without skipping dimensions and without repetition of signal dimensions. Any non-linear variation in the time-domain are taken into account here. Being a dissimilarity measure, dynamic time warping is bounded below by 0 and unbounded above. It is also scale-variant and is applicable to the general case where signals are of varying lengths in time although in case of BOLD signals, the signals lengths are the same.

#### ***Earth Mover's Distance:***

Earth mover's distance, also known as Wasserstein metric [15], is a dissimilarity measure which assumes each signal to be a probability distribution and represents the minimum cost of converting one distribution into the other. Treating  $x$  and  $y$  as probability distributions with:

$$x = \{(t_{x_1}, x_1), (t_{x_2}, x_2), \dots (t_{x_m}, x_m)\}$$

and

$$y = \{(t_{y_1}, y_1), (t_{y_2}, y_2), \dots (t_{y_n}, y_n)\} \quad (9)$$

where each  $x_i$  is a cluster (=amplitude) of the signal  $x$  at time-point  $t_{x_i}$  and each  $y_j$  is a cluster (=amplitude) of signal  $y$  at time-point  $t_{y_j}$ . While  $m$  and  $n$  do not have to be necessarily equal in general, i.e., Earth mover's distance can be computed for signals of differing lengths, in case of BOLD signals, they can be considered to be the same for a given individual and determined by the scan length. Then the ground distance between clusters at  $p_i$  and  $q_j$  can be encoded in the matrix

$$D = [d_{i,j}] \quad (10)$$

with a flow between clusters at  $p_i$  and  $q_j$  represented by the matrix

$$F = [f_{i,j}] \quad (11)$$

The objective is to minimize the overall cost

$$\min \sum_{i=1}^m \sum_{j=1}^n f_{i,j} d_{i,j} \quad (12)$$

while satisfying the following constraints:

$$f_{i,j} \geq 0 \text{ for } 1 \leq i \leq m, 1 \leq j \leq n \quad (13)$$

$$\sum_{j=1}^n f_{i,j} \leq t_{x_i} \text{ for } 1 \leq i \leq m \quad (14)$$

$$\sum_{i=1}^m f_{i,j} \leq t_{y_j} \text{ for } 1 \leq j \leq n \quad (15)$$

$$\sum_{i=1}^m \sum_{j=1}^n f_{i,j} = \min \left\{ \sum_{i=1}^m t_{x_i}, \sum_{j=1}^n t_{y_j} \right\}. \quad (16)$$

Earth mover's distance can then be defined as the amount of work needed to transform distribution  $x$  to distribution  $y$ , normalized by the total flow

$$\rho_{emd}(x, y) = \frac{\sum_{i=1}^m \sum_{j=1}^n f_{i,j} d_{i,j}}{\sum_{i=1}^m \sum_{j=1}^n f_{i,j}} \quad (17)$$

Similar to  $\rho_{dtw}$ ,  $\rho_{emd}$  considers non-linear interactions between signals, is scale-variant, and applicable to general signals of unequal length. This measure is scale-bounded below by the distance between the centroids of the distributions or signals and values closest to it represent greater similarity.

### 2.3. Experiments

Three experiments were designed to closely assess each of the alternative measures relative to Pearson's correlation as well as to compare them to each other:

**Experiment 1 (E1):** The consistency of each FC measure was evaluated by comparing task and resting-state functional MRI in specific brain networks.

**Experiment 2 (E2):** The contribution of each FC measure was studied in an age-based classification problem in several standard large-scale brain networks.

**Experiment 3 (E3):** The potential dependence of brain organization into large-scale networks was tested for each FC measure.

For all the experiments in this section, imaging data (i.e., task and resting-state functional MRI) were acquired and preprocessed similarly. The commonalities across the experiments are described as follows:

***Data Acquisition:*** Neuroimaging data were acquired from recruited participants on 3T GE 750 scanners (GE Healthcare, Waukesha, WI, USA) with an 8-channel head coil. An axial localizer scan was obtained to verify subject positioning and plan slice acquisition.

***Structural MRI:*** Five min T1-weighted axial structural images were acquired at the beginning of each session using FSPGR BRAVO sequence (TR = 8.132 ms, TE = 3.18 ms, TI = 450 ms,  $256 \times 256$  matrix, 156 slices, flip angle =  $12^\circ$ , FOV = 25.6 cm, slice thickness = 1 mm).

***Task functional MRI:*** Each task functional MRI followed a block design consisting of four 20-s blocks alternating with five 20-s blocks of rest, for a total scan time of 3 min. The first followed a finger tapping task paradigm targeted at capturing motor network activation in which participants alternated between tapping fingers one hand at a time and resting based on visual cues. The second used a verbal fluency task functional MRI paradigm aimed at capturing language network activation in which participants alternated between verbalizing words starting with a given letter ("F", "A", "S", "T") and resting based on visual cues.

Participants used earplugs to attenuate scanner noise, were padded with foam pads around their head and were instructed to hold their heads still during the scan in order to minimize movement.

***Resting-state functional MRI:*** Ten min resting-state functional MRI were obtained using single-shot echo-planar T2\*-weighted imaging with the following acquisition parameters: TR = 2.6 s, 231 time-points, TE = 22 ms, FOV = 22.4 cm, flip angle = 60°, voxel dimensions 3.5 mm × 3.5 mm, 3.5 mm slice thickness, 40 slices with eyes closed. Two types of task functional MRI were collected via echo-planar T2\*-weighted imaging either with the same parameters as the resting-state scan or with parameters: TR = 2.0 s, 90 time-points, TE = 22 ms, FOV = 22.4 cm, flip angle = 60°, voxel dimensions 3.75 mm × 3.75 mm, 4.0 mm slice thickness, 40 slices.

***Data Preprocessing:*** All imaging data were preprocessed on AFNI [16] using standard steps as described below.

***Task functional MRI:*** For each of the task functional MRI (left motor, right motor, language), data were first aligned to the anatomical and normalized to standard Montreal Neurological Institute (MNI) space. The first four volumes were discarded to allow for steady-state imaging. Images were then resampled to 3.0 mm isotropic, de-spiked, volume registered, and spatially smoothed using a 4 mm full-width at half-maximum Gaussian kernel. The standard activation maps were computed using a general linear model (GLM) with a canonical gamma variate hemodynamic response function convolved with a boxcar reference waveform and six rigid-body motion parameters and their derivatives regressed. Motion censoring (per TR motion > 0.25 mm) was included in the general linear model. Standard activation maps were also derived using AFNI's 3dClustSim ( $p < 0.05$ ,  $\geq 20$  voxels).

***Resting functional MRI:*** Data were de-spiked, slice time corrected, motion corrected, aligned with the structural MRI, normalized to MNI space, resampled to 3.5 mm<sup>3</sup>, and spatially smoothed with a 4-mm FWHM Gaussian kernel. Motion censoring (per TR motion > 1 mm or 1°), nuisance regression, and bandpass filtering (0.01–0.1 Hz) were performed simultaneously in one regression model. Nuisance signals



regressed out included six motion estimates and their temporal derivatives, and the voxel-wise locally averaged white matter signal.

**Data Analysis:** All data analyses to follow were carried out with the Statistics and Machine Learning Toolbox in MATLAB R2018a (The MathWorks, Inc., Natick, Massachusetts, United States).

### 2.3.1. E1: Consistency of functional connectivity

**Objective:** In order to understand whether the alternative measures capture FC based on resting-state data, it is important establish the ground truth FC for each. To do this, the FC derived from resting-state data was compared with the FC derived from task-functional MRI data to evaluate the consistency of each measure.

**Participants:** Neuroimaging data were acquired from 22 young healthy right-handed participants (age = 18-28 years). Of the 22 participants, 3 were excluded due to excessive head movement as a result of motion censoring leading to too few degrees of freedom, leaving data from 19 participants for subsequent analyses.

Detailed demographic information for included participants can be found in **Table 7.1**.

**Table 7. 1.** Characteristics of young healthy participants included in E1.

Characteristic	Value
N	19
Age (M $\pm$ SD in years)	21.89 $\pm$ 2.42
Gender	9 females
Education (M $\pm$ SD in years)	16.21 $\pm$ 2.32
Handedness	19 right-handed

Note: M = mean; SD = standard deviation;

**Data Analysis:** BOLD time courses were extracted from preprocessed task functional MRI and resting-state functional MRI data in the motor and language networks based on standard functional (Power) atlas [17]. For the left and right finger-tapping task functional MRI, the motor network, comprised of 35 regions, was used. For the verbal fluency task functional MRI, the working memory network including 30 regions

was used. All these networks were also evaluated for resting-state functional MRI. Within each network, pairwise FC was evaluated, generating a  $35 \times 35$  and  $30 \times 30$  matrix for motor and language (fronto-parietal and working memory areas) functions respectively for each individual.

FC matrices for all individuals were averaged to generate a group-level mean FC matrix for each network. Then the mean group-level FC matrix was thresholded at one standard deviation higher than the mean overall FC value to reveal a binarized FC pattern within a given network. Binarized FC patterns were compared between task functional MRI and resting-state functional MRI by computing a Sørensen-Dice similarity coefficient [18; 19] which measures the consistency of each of the alternative FC measures.

### **2.2.2. E2: Population-based classification using functional connectivity**

*Objective:* After examining the consistency of the various measures of FC, a data-driven comparative analysis was performed to further evaluate the alternative measures. This consisted of population-based, specifically age-based, classification in the healthy population. The goal was to compare and contrast the different FC measures at the brain network-level in differentiating between younger brains from older ones.

*Participants:* Neuroimaging data were acquired from 64 healthy right-handed participants, subdivided into 32 older (age = 46-74 years) and 32 younger (age = 18-45 years) participants. The two groups differed significantly by age but were matched in terms of gender distribution, education, verbal fluency and head motion to avoid all possible confounds. These criteria led to the exclusion of 8 older and 3 younger adults, leaving 24 older and 29 younger participants for further analysis. Greater head movement in older adults may be a potential reason for exclusion of a greater number [20]. Group-wise characteristics are provided in **Table 7.2**.

**Table 7. 2.** Characteristics of younger and older healthy participants included for E2.

Characteristic	Younger Healthy	Older Healthy	Group difference ( <i>p</i> -value)
N	29	24	-
Age (M ± SD in years)	25.8 ± 7.880	58 ± 7.587	< <b>0.001*</b>
Gender	16 females, 13 males	16 females, 8 males	0.416
Education (M ± SD in years)	16.4 ± 2.244	16.9 ± 2.857	0.476
Handedness	29 right	24 right	1
Translation in x (M ± SD in mm)	0.038 ± 0.120	-0.022 ± 0.122	0.073
Translation in y (M ± SD in mm)	0.001 ± 0.330	-0.075 ± 0.290	0.373
Translation in z (M ± SD in mm)	0.003 ± 0.123	-0.009 ± 0.255	0.821
Rotation in x (M ± SD in degrees)	-0.014 ± 0.185	0.090 ± 0.304	0.128
Rotation in y (M ± SD in degrees)	-0.007 ± 0.089	-0.045 ± 0.153	0.270
Rotation in z (M ± SD in degrees)	-0.022 ± 0.067	-0.023 ± 0.071	0.951
Euclidean norm of motion	0.053 ± 0.021	0.067 ± 0.029	0.054
DVARs	26.224 ± 4.294	27.123 ± 5.974	0.527
FWD	3.001 ± 1.473	3.928 ± 1.929	0.052

Note: M = mean; SD = standard deviation; DVARs = spatial root mean square after temporal differencing; FWD = framewise displacement; \*significantly different with *p*-value < 0.05;

**Data Analysis:** BOLD time courses were extracted from preprocessed resting-state functional MRI in 9 major brain networks based on a second standard functional (Willard) atlas [21] as it has a specific language network defined (used in subsequent analysis). The networks included dorsal and ventral default mode networks (D. DMN, V. DMN), left and right executive control networks (L. ECN and R. ECN), anterior and posterior salience networks (A. Salience and P. Salience), auditory, language and motor networks. Within each network, pairwise FC was evaluated, generating a symmetric square matrix for each individual.

Each network-based FC matrix was vectorized to extract only the unique pairwise FC coefficients for each participant (from either the upper or lower triangular matrix). Then these vectors were compiled and fed into a binary support vector machine classifier. A nested cross-validation approach with leave-one-out strategy was adopted, whose inner loop determined useful discriminatory FC features with neighborhood component analysis (NCA) and outer loop was used for model selection. Performance of classifier was assessed using accuracy and area under the curve. These steps were repeated for each of the FC measures and results were compared. In addition to examining the discriminatory power of each FC measure separately, the above steps were also repeated by combining (concatenation) FC measures from all identified metrics, forming a multi-metric FC measure, i.e.,

$$\rho_{multi-metric} = (\rho_{corr} | \rho_{xcorr} | \rho_{coh} | \rho_{wcoh} | \rho_{mutual\_info} | \rho_{euclidean} | \rho_{cityblock} | \rho_{dtw} | \rho_{emd}) \quad (18)$$

### 2.2.3. E3: Large-scale brain configurations based on functional connectivity

**Objective:** The large-scale brain networks, such as the DMN, ECN, language, etc., are typically derived from activation patterns from task functional MRI [22; 23; 17; 21]. In experiments so far, these networks were assumed to be pre-defined and used to compare all FC measures. The goal of this experiment was to further characterize each FC measure by testing whether this assumption holds true across the alternative FC measures. In other words, the aim was to understand if FC patterns are dependent on the metric used to define it.

**Participants:** Data from only the young healthy group of 29 participants included in **E2** were considered here since these effects would first need to be tested and validated in a typical brain.

**Behavioral Data:** In addition to neuroimaging, behavioral data were collected from these participants. Specifically, behavioral verbal fluency was measured by completing the following examination outside the scanner. Forms of the Controlled Oral Word Association Test (COWAT) [24], were administered which requires participants to produce words beginning with the letters, “F,” “A,” “S” in three respective 1-min

trials. Responses to each letter were recorded and verbal fluency scores were based on the total number of correct responses (after excluding preservative and rule-breaking errors) produced by the participants across the three letter conditions. Since verbal fluency can be impacted by age and education, the raw scores were adjusted for each individual. The normalized verbal fluency score served as a behavioral outcome, most likely reflective of the language or working memory network in the brain.

**Data Analysis:** The analysis followed five main steps which are pictured in **Supplementary Figure 7.1**.

For each of the 9 FC measures:

- (i) Ten large-scale brain networks consisting of 68 regions were included to generate a whole-brain symmetric FC matrix of size  $68 \times 68$  for each individual. A mean FC matrix across all participants was used as a representative of group-level FC in subsequent steps. The ideal block structure along the diagonal of the FC matrix with 10 networks was defined as depicted in **Supplementary Figure 7.1 (c)**. These matrices represent the *original brain configuration*.
- (ii) The group mean FC matrix was shuffled by randomly permuting rows (and corresponding columns) so as to maintain the symmetry in FC matrix as an initialization step.
- (iii) An unsupervised  $k$ -means clustering algorithm was applied to this initialized, shuffled FC matrix with  $k=10$  and a sparsity (L1) distance function. Since the clustering by  $k$ -means algorithm is not unique, it was applied for 1000 iterations, each iteration initialized with a randomly shuffled FC matrix. An ideal block structure along the diagonal of the FC matrix with 10 clusters was defined for the clustered FC matrix as depicted in **Supplementary Figure 7.1**. Clustered FC matrix and corresponding ideal FC matrix from each iteration represent an *alternative brain reconfiguration*.
- (iv) Sørensen-Dice similarity coefficient was computed for the *original brain configuration* and each of the alternative *brain reconfigurations* by comparing the ideal FC structure and the thresholded FC matrix in each case. The two overlap coefficients were compared to determine the best possible functional configuration.

- (v) To validate the plausibility of an *alternative brain reconfiguration*, brain-behavior associations were examined. A data-inspired linear regression was applied to study the association between the mean FC within each network (or cluster) of individual participants and their normalized verbal fluency scores. Presumably, the language network in the brain would show the strongest association with this outcome. In the *original brain configuration*, this was performed only for the language network since the ground truth is known. In the best *alternative brain reconfiguration*, however, this was performed for each identified cluster since there does not exist a ground truth. The strengths of this brain-behavior association were compared between the *original brain configuration* and the best observed *alternative brain reconfiguration*. Finally, a multi-metric approach was adopted similar to that in **E2**. The mean FC within the language network was evaluated for all FC measures, concatenated for multi-metric representation and associated with the normalized verbal fluency scores for the *original brain configuration*. In the best *alternative brain reconfiguration*, the mean FC from a single cluster exhibiting greatest association with the normalized verbal fluency score was computed for each FC measure. A stepwise regression model was employed which was initialized by including all linear terms of features (i.e., FC measures) and added/removed features with the criterion of maximizing the coefficient of determination ( $R^2$ ).

### **3. Results**

#### **3.1. Incomplete characterization of functional connectivity**

Cases of the like presented in **Figure 7.1** were found to be not limited to DMN alone in healthy participants. Such cases are evidence in support for the claim that FC cannot always be completely quantified by Pearson's correlation. This can also be mathematically substantiated by considering the extreme case of zero Pearson's correlation between two signals. If two signals are uncorrelated, independence is not necessarily implied. More generally, in cases where a low value of Pearson's correlation is observed, it may be incorrect to assume that there is no dependence between them. It simply means that there is no *linear* dependence between them.

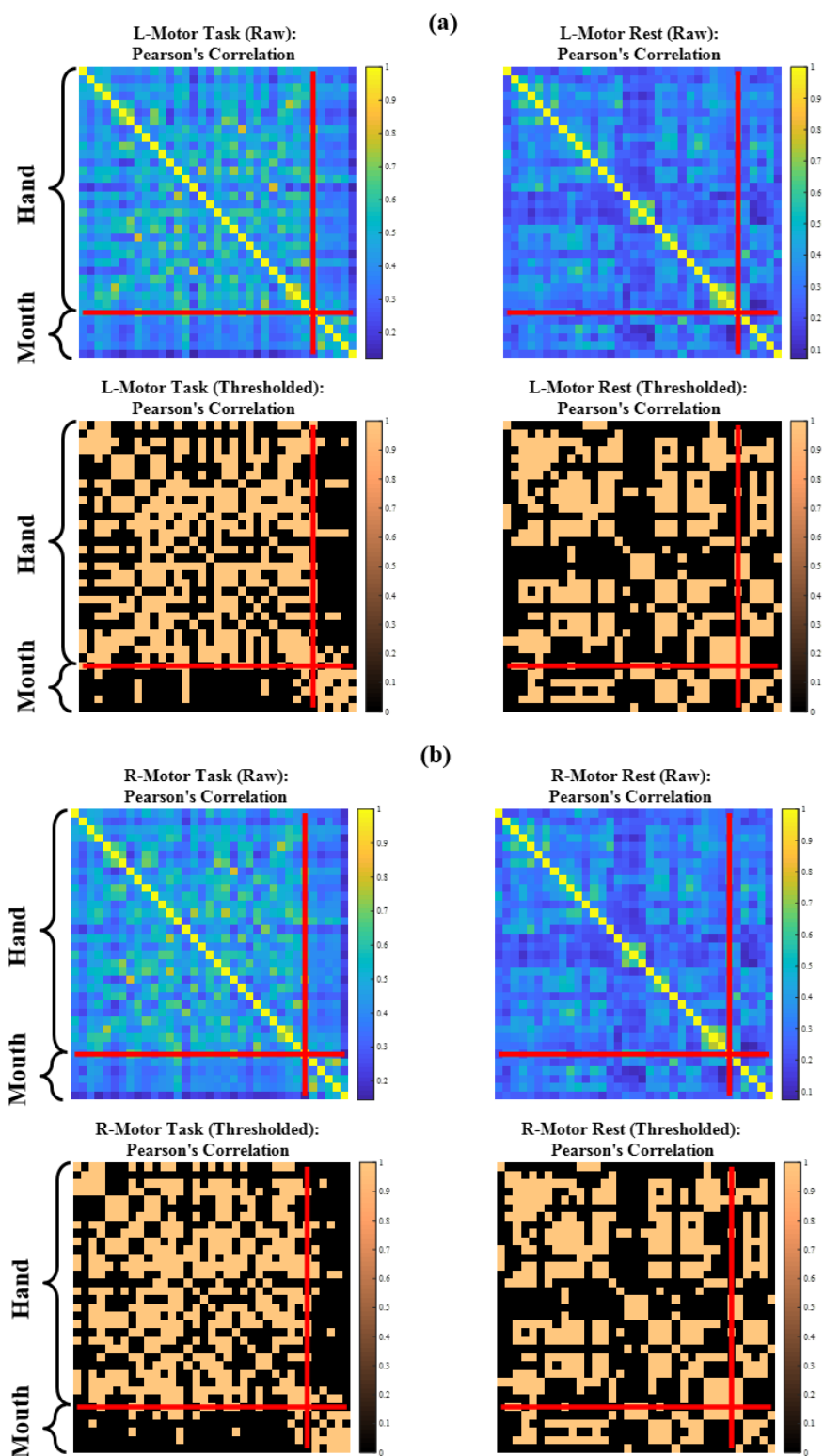
#### **3.2. Experimental Findings**

##### **3.2.1. E1: Consistency of functional connectivity**

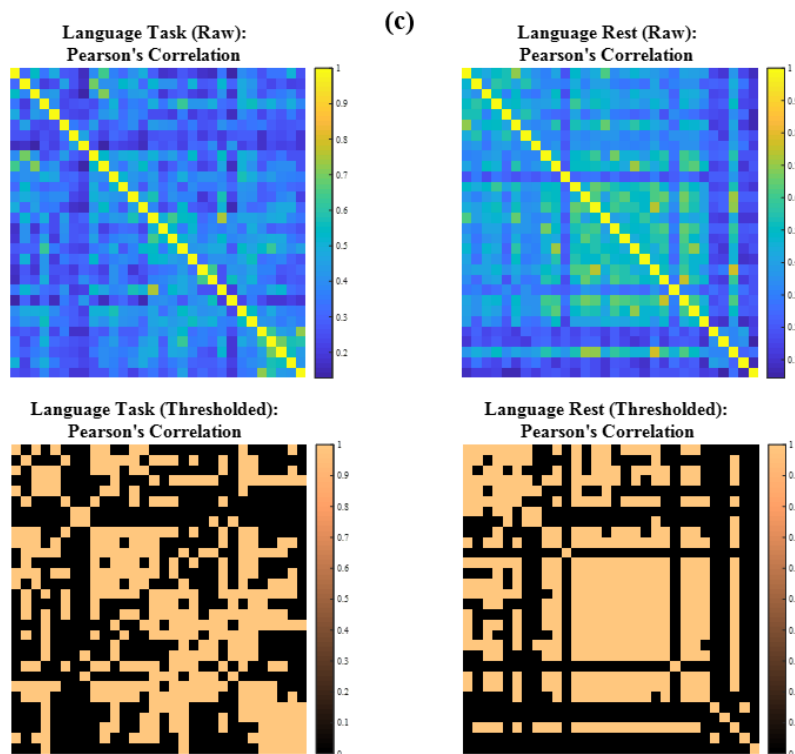
Consistency of all of the identified FC measures was evaluated by comparing task functional MRI and resting-state functional MRI. Since the activation pattern may be different for each FC measure, the task functional MRI data offer a form of ground truth. Thresholded FC maps (threshold = one standard deviation above grand mean) between task and resting-state conditions as illustrated for Pearson's correlation in **Figure 7.2** and remaining FC measures in **Supplementary Figure 7.2**.

*Figure 7. 2. Comparison of FC based on Pearson's correlation in young healthy adults between task and resting-state conditions for EI in:*

*(a) left motor (b) right motor and (c) language networks*







Note: defined based on Power functional atlas. In each sub-image, the top row represents the FC matrix averaged across all participants and the bottom row represents the thresholded FC matrix averaged across all participants. The red lines in (a) and (b) show the separation between hand-motor and mouth-motor brain regions. Similar matrices for the alternative measures of FC can be found in **Supplementary Figure 7.2**.

Consistency of resting-state FC was quantified based on Sørensen-Dice similarity coefficient and tabulated in **Table 7.3 (a)** for the motor and language networks. While mostly comparable across many FC measures, the overlap coefficients for Pearson's correlation are not necessarily the best in any of these tested networks.

**Table 7.3.** Consistency of each measure of FC

(a) Consistency as measured by Sørensen-Dice similarity coefficient between task and resting-state conditions in three networks used in **E1**

<b>Metric</b>	<b>L-Motor vs Rest</b>	<b>R-Motor vs Rest</b>	<b>Language vs Rest</b>
Correlation	0.502	0.466	0.508
Cross-correlation	<b>0.506</b>	0.496	0.492
Coherence	0.450	0.440	0.473
Wavelet coherence	0.500	<b>0.537</b>	0.525
Mutual information	0.3438	0.386	0.460
Euclidean distance	0.455	0.438	0.592
Cityblock distance	0.448	0.432	0.604
Dynamic time warping	0.444	0.446	0.584
Earth mover's distance	0.497	0.514	<b>0.618</b>

Note: Functional networks defined based on Power atlas in **E1**. The highest overlap in each network is represented in **bold**.

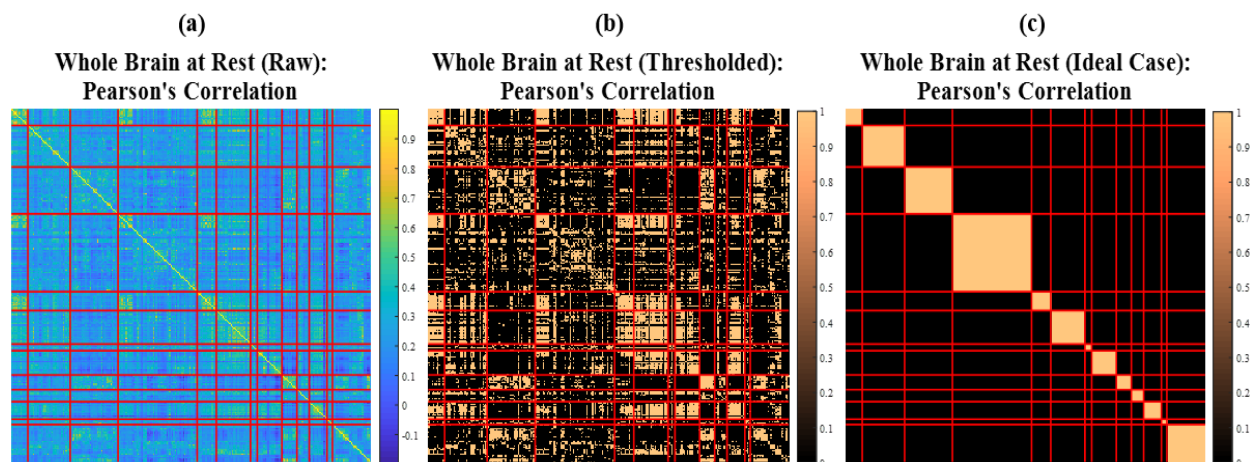
(b) Consistency as measured by Sørensen-Dice similarity coefficient between the observed thresholded FC matrix (**Figure 7.3 (b)**) and ideal thresholded FC matrix (**Figure 7.3 (c)**) based on Power atlas in **EI**

<b>Metric</b>	<b>Observed vs Ideal FC</b>
Correlation	<b>0.256</b>
Cross-correlation	0.252
Coherence	0.224
Wavelet coherence	0.239
Mutual information	0.180
Euclidean distance	0.225
Cityblock distance	0.225
Dynamic time warping	0.213
Earth mover's distance	0.188

Note: The highest overlap is represented in **bold**.

It was possible to validate the consistency for motor and language networks based on task functional MRI whereas the same could not be performed for other networks due to lack of corresponding task functional MRI in this cohort. An alternate procedure to evaluate the consistency of the resting-state FC at a whole-brain level was conducted by, first, simulating an ideal FC structure with a block structure along the diagonal as shown in **Figure 7.3 (c)** and second, comparing the observed resting-state FC to it by means of Sørensen-Dice similarity coefficient between them. This is visually represented for Pearson's correlation in **Figure 7.3** (and for all other measures in **Supplementary Figure 7.3**) and quantified for all FC measures in **Table 7.3 (b)**. Most of the FC measures showed comparable overlap with Pearson's correlation showing the highest overlap. This would then lead to the question: is it possible to do better than the current observed overlap?

**Figure 7.3.** Whole brain resting-state FC in young healthy adults defined based on Pearson's correlation in 13 distinct brain networks given by Power functional atlas in E1



**Note:** (a) FC matrix averaged across all participants; (b) thresholded FC matrix averaged across all participants; (c) simulated ideal FC matrix. The red lines represent the separation between brain regions belonging to a specific network. The regions are grouped in the following order: audio, visual, motor, default mode, cingulo-opercular task, fronto-parietal task, memory, salience, dorsal attention, ventral attention, subcortical, cerebellar, uncertain networks. Similar matrices for the alternative measures of FC can be found in **Supplementary Figure 7.3**.

### 3.2.2. E2: Population-based classification using functional connectivity

The younger and older groups had significant age-based differences as reported in **Table 7.2**. The goal, here, was to determine if these age-differences could be detected on the basis of resting-state FC of various brain networks. The support vector machine classifier models, implemented using NCA feature selection and leave-one-out testing, were evaluated by the peak accuracy and area under the curve achieved. The accuracy levels are tabulated in **Table 7.4** and area under the curve along with number of features used by each classifier are listed in the **Supplementary Table 7.2 (a)** and **(b)** respectively. As seen in **Table 7.4**, Pearson's correlation does not always stand out while differentiating the young from the old. Comparing performances of alternative FC, no one single FC measure particularly performed consistently better than the rest. Importantly, when we concatenate all these measures of FC, the combined metric almost always performs better or comparable to Pearson's correlation. This could be due to contribution of alternative FC measures which potentially augment the discriminatory power of Pearson's correlation.

**Table 7. 4.** Age-based classification between younger and older healthy adults in nine major brain networks

Metric	D. DMN	V. DMN	L. ECN	R. ECN	A. Salience	P. Salience	Auditory	Language	Motor
Pearson's Correlation	45.28%	56.60%	52.83%	<b>66.03%</b>	75.47%	62.26%	58.49%	58.49%	56.60%
Cross-correlation	54.72%	52.83%	54.72%	60.37%	79.24%	58.49%	58.49%	54.72%	54.71%
Coherence	54.71%	50.94%	50.94%	54.71%	60.37%	50.94%	58.49%	56.60%	<b>69.81%</b>
Wavelet coherence	49.06%	52.83%	52.83%	54.71%	67.92%	50.94%	62.26%	54.71%	52.83%
Mutual Information	62.26%	<b>75.47%</b>	62.26%	52.83%	77.35%	58.49%	52.83%	54.71%	54.71%
Euclidean distance	64.15%	69.81%	62.26%	<b>66.03%</b>	71.69%	50.94%	54.72%	54.71%	52.83%
Cityblock distance	<b>71.69%</b>	71.69%	64.15%	64.15%	83.01%	50.94%	52.83%	<b>64.15%</b>	54.72%
DTW	69.81%	73.58%	<b>69.81%</b>	62.26%	79.24%	56.60%	52.83%	60.37%	50.94%
EMD	52.83%	62.26%	64.15%	52.83%	66.03%	52.83%	52.83%	50.94%	66.03%
Combined	66.04%	69.82%	<b>69.81%</b>	54.72%	<b>84.91%</b>	<b>73.58%</b>	<b>69.81%</b>	58.49%	62.26%

Note: Brain networks are defined by the Willard functional atlas with a support vector machine classifier. Performance represents accuracy levels (%) with a leave-one out testing. The highest performing metric is represented in **bold** for each network. Additional performance measures are included in **Supplementary Table 7.2**; D.DMN = dorsal default mode network; V.DMN = ventral default mode network; L.ECN = left executive control network; R.ECN = right executive control network; A.Salience = anterior salience; P.Salience = posterior salience; DTW = dynamic time warping; EMD = earth mover's distance;

### 3.2.3. E3: Large-scale brain configurations based on functional connectivity

The goal of this experiment was to inspect the assumption that resting-state FC may be organized in the form of a fixed number of networks, each involving a specific number of brain regions. While this may be the case for Pearson's correlation, it may not necessarily be true for the alternative measures. Based on **E3**, the findings are:

- (i) For every FC measure, the group mean whole-brain FC matrix representing the *original brain configuration* could be clustered into 10 major large-scale brain networks more efficiently resulting in *alternative brain reconfigurations* for each FC measure.
- (ii) A number of *alternative brain reconfigurations* demonstrated an improved Sørensen-Dice similarity coefficient (between each observed configuration and the corresponding expected ideal configuration) relative to the *original brain configuration* for each FC measure as reported in **Table 7.5**. The best possible *alternative brain reconfiguration* based on each FC measure demonstrated a greater dice overlap than the *original brain configuration*. Dynamic time warping distance had the greatest improvement (155.77%) while cross-correlation had the smallest improvement (13.15%) suggesting that the current predefined configuration may be optimal for correlation-based FC measure, however, the overall functional configuration of the brain may vary if the nature of the information captured by the FC measure deviates further from correlation-based ones. Overall, reconfigurations based on mutual information, dynamic time warping distance and Earth mover's distance did consistently better than the *original brain configuration* as seen in **Supplementary Figure 7.4**.

**Table 7. 5.** Comparison of Sørensen-Dice similarity coefficient between the original brain configuration and the best possible reconfiguration obtained via clustering into 10 clusters or networks.

Metric	Original Brain Configuration	Alternative Brain Reconfiguration
Pearson's Correlation	0.460	0.528
Cross-correlation	<b>0.464</b>	0.525
Coherence	0.405	0.467
Wavelet Coherence	0.416	0.472
Mutual Information	0.212	0.337
Euclidean	0.316	0.361
Cityblock	0.311	0.441
Dynamic Time Warping	0.235	<b>0.601</b>
Earth Mover's Distance	0.259	0.433

Note: Cross-correlation and dynamic time warping exhibited the best overlap in the *original brain configuration* and best *alternative brain reconfiguration* respectively. A distribution of 1000 reconfigurations is visualized in **Supplementary Figure 7.4** by comparing the overlap with the original one.

- (iii) The plausibility of the best *alternative brain reconfiguration* was validated with the help of a data-inspired regression model in which the mean FC within each cluster/network for all participants was associated with the normalized verbal fluency as a behavioral outcome and can be found in **Table 7.6 (b)**. The goodness-of-fit ( $R^2$ ) was compared with that of the *original brain configuration* and can be found in **Table 7.6 (a)**. The best *alternative brain reconfiguration* associated with the normalized verbal fluency scores was significant in some measures including Pearson's correlation, wavelet coherence, and cross-correlation and marginally significant in some others such as Earth mover's distance. This could imply, that subject to a larger sample size, there may exist an alternative functional rearrangement of the brain regions which may be indicative of behavioral outcomes.

- (iv) Parallel to the multi-metric approach described in **E2** for the purpose of population-based classification, the same approach was extended for the prediction of behavioral outcomes. The results are tabulated in **Table 7.6 (c)**. Similar to classification results, the combined FC measure was more consistent than individual measures in correlating with the behavioral outcome. The multi-metric representation of FC from the *alternative brain reconfiguration* performed better than that from the *original brain configuration* which may suggest that there is room for a better design of the functional configuration of the brain on the basis of measures adopted to quantify FC relative to the conventional correlation-based large-scale brain configuration.



**Table 7. 6. Brain-behavior relationship in original and reconfigured brain**

(a). Association ( $R^2$ ) between the mean FC within each of the 10 networks and the normalized verbal fluency scores in 29 young healthy adults is shown below using the predefined **original brain configuration** as found with a stepwise regression model.

<b>Original Brain Configuration</b>	<b>D.DMN</b>	<b>V.DMN</b>	<b>L.ECN</b>	<b>R.ECN</b>	<b>A.Sal.</b>	<b>P.Sal.</b>	<b>Aud.</b>	<b>Lang.</b>	<b>Motor</b>	<b>Visual</b>
<b>Metric Showing Highest Association</b>	Pearson's correlation	Cross-correlation	Mutual information	EMD	Mutual information	Wavelet coherence	Cross-correlation	Cross-correlation	Pearson's correlation	Cross-correlation
<b>R<sup>2</sup></b>	<b>0.188</b>	<b>0.208</b>	0.027	0.047	0.015	0.107	0.098	0.022	<b>0.310</b>	0.106
<b>p-value</b>	<b>0.019*</b>	<b>0.013*</b>	0.393	0.258	0.533	0.084 <sup>†</sup>	0.099 <sup>†</sup>	0.446	<b>0.002*</b>	0.085 <sup>†</sup>

Note: Only the FC measure showing greatest associations with the outcome have been reported. Significant associations are represented in **bold**; D.DMN = dorsal default mode network; V.DMN = ventral default mode network; L.ECN = left executive control network; R.ECN = right executive control network; A.Sal. = anterior salience; P.Sal. = posterior salience; Aud. = auditory; Lang. = language; DTW = dynamic time warping; EMD = earth mover's distance; R<sup>2</sup>: coefficient of determination; \*association is significant with  $p$ -value < 0.05; <sup>†</sup>association is marginally significant with  $p$ -value < 0.1;

(b). For each FC measure, this table shows the association ( $R^2$ ) between each cluster (C1 through C9) of the best **alternative brain reconfiguration** found by clustering and the normalized verbal fluency score with a stepwise regression model.

Metric	C 1	C 2	C 3	C 4	C 5	C 6	C 7	C 8	C 9	C 10
Pearson's Correlation	0.013	0.031	<b>0.197*</b>	0.042	0.051	0.001	0.036	<b>0.233*</b>	0.091	<b>0.109†</b>
Cross-correlation	0.024	0.027	0.072	0.073	<b>0.103†</b>	0.081	0.043	0.011	<b>0.106†</b>	<b>0.208*</b>
Coherence	0.001	0.002	0.002	0.001	0.000	0.000	0.025	0.001	0.074	0.002
Wavelet coherence	0.069	0.000	0.021	0.009	0.060	0.026	<b>0.145*</b>	0.017	0.006	0.022
Mutual information	0.023	0.020	0.001	0.016	0.019	0.014	0.015	0.051	0.018	0.006
Euclidean	0.023	0.068	0.009	0.059	0.019	0.023	0.072	0.011	0.012	0.055
Cityblock	0.031	0.014	0.013	0.027	0.007	0.022	0.031	0.001	0.024	0.055
DTW	0.012	0.009	0.005	0.005	0.007	0.031	0.023	0.014	0.032	0.012
EMD	0.002	0.006	0.022	0.004	0.015	0.000	0.004	0.001	<b>0.110†</b>	0.045

Note: C1 through C9 represent clusters obtained by k-means; DTW = dynamic time warping; EMD = Earth mover's distance; \*association is significant with  $p$ -value  $< 0.05$ ; †association is marginally significant with  $p$ -value  $< 0.1$ ;

(c). Comparison between brain-behavior relationship of the **original brain configuration** and the best **alternative brain reconfiguration** using the multi-metric definition of FC as found with a stepwise regression model.

	<b>Combined FC Metric from <i>Original Brain Configuration</i> ~ Normalized Verbal Fluency</b>	<b>Combined FC Metric from <i>Alternative Brain Reconfiguration</i> ~ Normalized Verbal Fluency</b>
R <sup>2</sup>	0.495	0.606
<i>p</i> -value	0.026*	0.0014*
Measures Selected	Coherence : Wavelet Coherence*	Dynamic Time Warping*
	Mutual Information*	Euclidean*
	Dynamic Time Warping*	Pearson's Correlation : Earth mover's distance
	Euclidean*	Cityblock
	Cross-correlation	Pearson's Correlation
	Wavelet Coherence	Earth mover's distance
	Coherence	

Note: R<sup>2</sup> = coefficient of determination; †interaction term; \*associated *p*-value < 0.05;

## **4. Discussion**

### **4.1. Hypotheses derived from Experimental Findings**

In light of preliminary evidence based on the resting-state functional MRI data used in this study, two major hypotheses were formulated:

#### **4.1.1. Hypothesis 1: Functional connectivity could be better characterized with a multi-metric representation**

Using FC derived from resting-state functional MRI, it was possible to not only perform population-based classification in **E2** but also regression to study the relationship between FC and behavioral outcome in **E3**. A comparison of contribution of all FC measures in these experiments showed that there was not necessarily one single FC measure that consistently outperformed others. However, combination of multiple measures by concatenation followed by a feature selection procedure was relatively more consistent and, in most cases, performed better than Pearson's correlation. Thus, the first hypothesis suggests that a more complete measure of FC could be developed by combining information from multiple measures. This would be advantageous as it would augment the correlation-based FC with complementary measures which capture linear, non-linear, similarity, dissimilarity, time-, frequency- and wavelet-domain properties and interactions between the signals.

#### **4.1.2. Hypothesis 2: Canonical brain network configurations are metric-dependent**

Decomposition of the whole brain into component networks is a way to understand interacting regions functioning in synchronization which may be responsible for specific traits and/or behavior. However, these networks/clusters are most conventionally based on a correlation-based measure. **E3** suggested that the same set of regions in the brain may be rearranged and clustered into alternative brain configurations with networks/clusters distinct from those defined for Pearson's correlation. The variation in alternative brain reconfigurations by FC measure may signal that the large-scale brain networks are a function of the measure

that quantifies synchronization among the regions. Since the alternative measures explored in this study elicit information complementary to that by Pearson's correlation, it is likely that the functional connectomic view of the brain would be variable.

## **4.2. The Big Picture**

A growing number of prior studies have indicated the need for characterizing FC using alternative measures. The advantages of harnessing both temporal and spectral information has been illustrated with the use of wavelet coherence to capture non-stationarity in BOLD signals in resting-state functional MRI [25] and for population-based classification [26]. Mutual information, which could be interpreted as the amount of information flowing between the given regions, has been shown to perform better in the context of task functional MRI [27] as well as resting-state functional MRI [28]. Dynamic time warping has been demonstrated to capture the non-stationarity in simulated functional MRI data [29]. The importance of non-linear and directional dependencies among BOLD signals is highlighted by means of mutual connectivity [30].

The present study adds to these works by comparing and contrasting multiple alternative FC measures and investigating not only the neural interactions differing between subgroups in a given population but also brain-behavior relationships arising from these measures. The goal of this work is to encourage development of a more holistic view of functional connectivity rather than reliance on a single measure.

## **4.3. Methodological Considerations**

While this study outlines a number of ways of quantifying FC, it is important to recognize the assumptions and choices made in the experiments which may have bearing on the current findings. First, the number of samples used to investigate effects varied from 19 in **E1**, to 53 in **E2**, to 29 in **E3**. Evaluation of research

questions in these relatively different but overlapping datasets offers confidence in the findings to some degree. However, it is important to acknowledge that these are modest sample sizes. This study should be considered as a proof-of-concept and the generalizability of the effects found here would need to be substantiated in much larger samples in healthy as well as pathological population groups.

Second, in weighing out the contribution of the various FC measures in **E2** and **E3**, 10 major large-scale networks were considered. These tests assume that the FC in the whole brain can largely be divided into 10 groupings. While this may be the optimal number for Pearson's correlation, it may not be appropriate for the alternative FC measures. Considering the possibility that the brain connectome can vary by FC measure, it is also possible that the number of decomposable brain networks is a function of the FC measures. This requires further examination.

Thirdly, included within this investigation were FC measures which capture undirected interactions between BOLD signals under the supposition that the dependency between BOLD signals arising from two brain regions is symmetric. However, BOLD signals need not necessarily adhere to this and directional information could further supplement and inform the multi-metric approach by incorporating potential causal changes in the brain.

Next, the premise behind organized networks in the brain was based upon achieving an ideal brain configuration with a tight block-like structure along the diagonal of a symmetric FC matrix (such as the one in **Supplementary Figure 7.1 (c)**) which represents a structure that is strongly connected within a given network (shown in beige color; value=1) and weakly connected between networks (shown in black color; value=0). Whether this is a desirable ideal brain configuration needs further investigation. In other words, a question to explore would be: should distinct brain networks be treated as independent groupings of brain areas operating in synchrony or should there be a certain level of dependence between networks?

Finally, to enable a fair comparison across FC measures, only the absolute magnitude of each was utilized. Some measures, however, have additional properties that may be useful in understanding BOLD interactions better. For instance, coherence offers the specific frequency and wavelet coherence offers both temporal and spectral instances at which maximum similarity is observed. These additional details could enhance the characterization of FC and should be considered in subsequent studies.

#### **4.4. Future Directions**

As a pilot study pointing towards a comprehensive multi-metric notion of FC, this study holds promise for further exploration in several directions, some of which are outlined as follows:

- (i) Only a small number of alternative FC measures were studied here. Although these covered a wide range of properties by encompassing measures of similarity, dissimilarity, from time-, frequency- and wavelet-domains, captured linear and non-linear relationships among BOLD signals, there may be other measures to better capture FC.
- (ii) The idea of multi-metric definition was realized and executed by a straightforward concatenation of the distinct metrics. Forming a multi-metric representation could be approached by alternate means such as identification of a linear, quadratic or higher order, log transformation, weighting, or convolutional method, of combining the FC measures.
- (iii) A majority of the studies in the neuroimaging literature have relied upon an elementary design of FC by considering pairwise BOLD interactions of nodes. Future studies should move from pairwise FC towards generalized FC to gain a clearer picture of the brain connectome by considering multi-nodal models and analyzing BOLD interactions among a group of nodes (more than a pair) simultaneously.
- (iv) The introduction of multiple measures requires a deeper understanding of their properties, especially if they are likely to capture complementary information of the same signal. This

could be entail studying of statistical properties, dependence on noise in the signal, and the sensitivity to outliers of each FC measure.

## **5. Conclusion**

While the effects observed here need further experimentation and validation in independent samples and populations, empirical findings from this exploratory study point towards the need for a better and more comprehensive characterization of FC. One approach to attain this is presented here by introducing a multi-metric technique. The promise of this approach was demonstrated in age-based classification and brain-behavior regression applications. Further, investigation of alternative measures indicated that organization of large-scale brain networks may be a function of the specific measure(s) used to characterize the FC.



## References

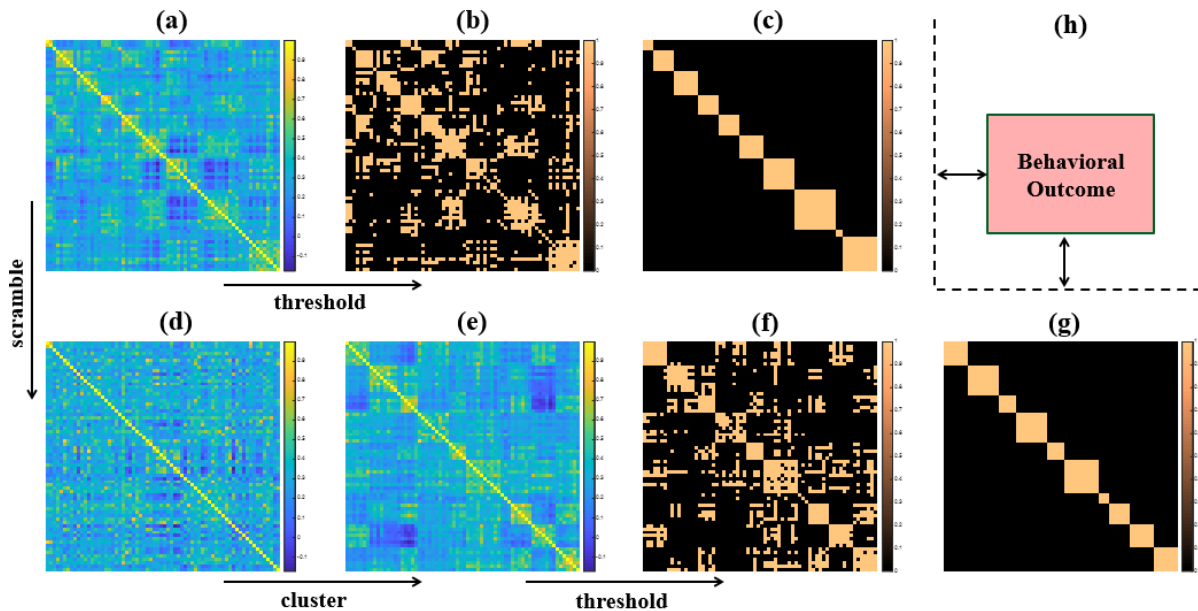
- [1] E. Bullmore, O. Sporns, Complex brain networks: graph theoretical analysis of structural and functional systems. *Nature reviews neuroscience* 10 (2009) 186.
- [2] O. Sporns, G. Tononi, R. Kötter, The human connectome: a structural description of the human brain. *PLoS computational biology* 1 (2005) e42.
- [3] M.P. Van Den Heuvel, R.C. Mandl, R.S. Kahn, H.E. Hulshoff Pol, Functionally linked resting-state networks reflect the underlying structural connectivity architecture of the human brain. *Human brain mapping* 30 (2009) 3127-3141.
- [4] G. Tononi, O. Sporns, G.M. Edelman, A measure for brain complexity: relating functional segregation and integration in the nervous system. *Proceedings of the National Academy of Sciences* 91 (1994) 5033-5037.
- [5] D.S. Bassett, N.F. Wymbs, M.A. Porter, P.J. Mucha, J.M. Carlson, S.T. Grafton, Dynamic reconfiguration of human brain networks during learning. *Proceedings of the National Academy of Sciences* 108 (2011) 7641-7646.
- [6] B. Horwitz, The elusive concept of brain connectivity. *Neuroimage* 19 (2003) 466-470.
- [7] K.J. Friston, Functional and effective connectivity in neuroimaging: a synthesis. *Human brain mapping* 2 (1994) 56-78.
- [8] B. Biswal, F. Zerrin Yetkin, V.M. Haughton, J.S. Hyde, Functional connectivity in the motor cortex of resting human brain using echo-planar mri. *Magnetic resonance in medicine* 34 (1995) 537-541.
- [9] J.D. Gibbons, S. Chakraborti, *Nonparametric statistical inference*, Springer, 2011.
- [10] J.R. Buck, M.M. Daniel, A. Singer, *Computer explorations in signals and systems using MATLAB*, Prentice Hall Upper Saddle River, NJ, USA:, 2002.
- [11] A.G. González, J. Rodríguez, X. Sagartzazu, A. Schumacher, I. Isasa, Multiple coherence method in time domain for the analysis of the transmission paths of noise and vibrations with non stationary signals. *Proceedings of ISMA 2010* (2010).
- [12] A. Grinsted, J.C. Moore, S. Jevrejeva, Application of the cross wavelet transform and wavelet coherence to geophysical time series. *Nonlinear processes in geophysics* 11 (2004) 561-566.
- [13] C.E. Shannon, A mathematical theory of communication. *Bell system technical journal* 27 (1948) 379-423.
- [14] K.K. Paliwal, A. Agarwal, S.S. Sinha, A modification over Sakoe and Chiba's dynamic time warping algorithm for isolated word recognition. *Signal Processing* 4 (1982) 329-333.
- [15] Y. Rubner, C. Tomasi, L.J. Guibas, The earth mover's distance as a metric for image retrieval. *International journal of computer vision* 40 (2000) 99-121.
- [16] R.W. Cox, AFNI: software for analysis and visualization of functional magnetic resonance neuroimages. *Computers and Biomedical research* 29 (1996) 162-173.
- [17] J.D. Power, A.L. Cohen, S.M. Nelson, G.S. Wig, K.A. Barnes, J.A. Church, A.C. Vogel, T.O. Laumann, F.M. Miezin, B.L. Schlaggar, Functional network organization of the human brain. *Neuron* 72 (2011) 665-678.
- [18] L.R. Dice, Measures of the amount of ecologic association between species. *Ecology* 26 (1945) 297-302.
- [19] T. Sørensen, A method of establishing groups of equal amplitude in plant sociology based on similarity of species and its application to analyses of the vegetation on Danish commons. *Biol. Skr.* 5 (1948) 1-34.
- [20] J.R. Andrews-Hanna, A.Z. Snyder, J.L. Vincent, C. Lustig, D. Head, M.E. Raichle, R.L. Buckner, Disruption of large-scale brain systems in advanced aging. *Neuron* 56 (2007) 924-935.
- [21] W. Shirer, S. Ryali, E. Rykhlevskaia, V. Menon, M. Greicius, Decoding subject-driven cognitive states with whole-brain connectivity patterns. *Cerebral cortex* 22 (2012) 158-165.

- [22] J. Damoiseaux, S. Rombouts, F. Barkhof, P. Scheltens, C. Stam, S.M. Smith, C. Beckmann, Consistent resting-state networks across healthy subjects. *Proceedings of the national academy of sciences* 103 (2006) 13848-13853.
- [23] N.U. Dosenbach, B. Nardos, A.L. Cohen, D.A. Fair, J.D. Power, J.A. Church, S.M. Nelson, G.S. Wig, A.C. Vogel, C.N. Lessov-Schlaggar, Prediction of individual brain maturity using functional MRI. *Science* 329 (2010) 1358-1361.
- [24] T.N. Tombaugh, J. Kozak, L. Rees, Normative data stratified by age and education for two measures of verbal fluency: FAS and animal naming. *Archives of clinical neuropsychology* 14 (1999) 167-177.
- [25] K. Müller, G. Lohmann, J. Neumann, M. Grigutsch, T. Mildner, D.Y. von Cramon, Investigating the wavelet coherence phase of the BOLD signal. *Journal of Magnetic Resonance Imaging: An Official Journal of the International Society for Magnetic Resonance in Medicine* 20 (2004) 145-152.
- [26] A. Bernas, A.P. Aldenkamp, S. Zinger, Wavelet coherence-based classifier: A resting-state functional MRI study on neurodynamics in adolescents with high-functioning autism. *Computer methods and programs in biomedicine* 154 (2018) 143-151.
- [27] B. Chai, D. Walther, D. Beck, L. Fei-Fei, Exploring functional connectivities of the human brain using multivariate information analysis, *Advances in neural information processing systems*, 2009, pp. 270-278.
- [28] Z. Wang, A. Alahmadi, D. Zhu, T. Li, Brain functional connectivity analysis using mutual information, 2015 IEEE Global Conference on Signal and Information Processing (GlobalSIP), IEEE, 2015, pp. 542-546.
- [29] R.J. Meszlényi, P. Hermann, K. Buza, V. Gál, Z. Vidnyánszky, Resting state functional MRI functional connectivity analysis using dynamic time warping. *Frontiers in neuroscience* 11 (2017) 75.
- [30] A.M. DSouza, A.Z. Abidin, U. Chockanathan, G. Schifitto, A. Wismüller, Mutual connectivity analysis of resting-state functional MRI data with local models. *NeuroImage* 178 (2018) 210-223.

## APPENDIX I

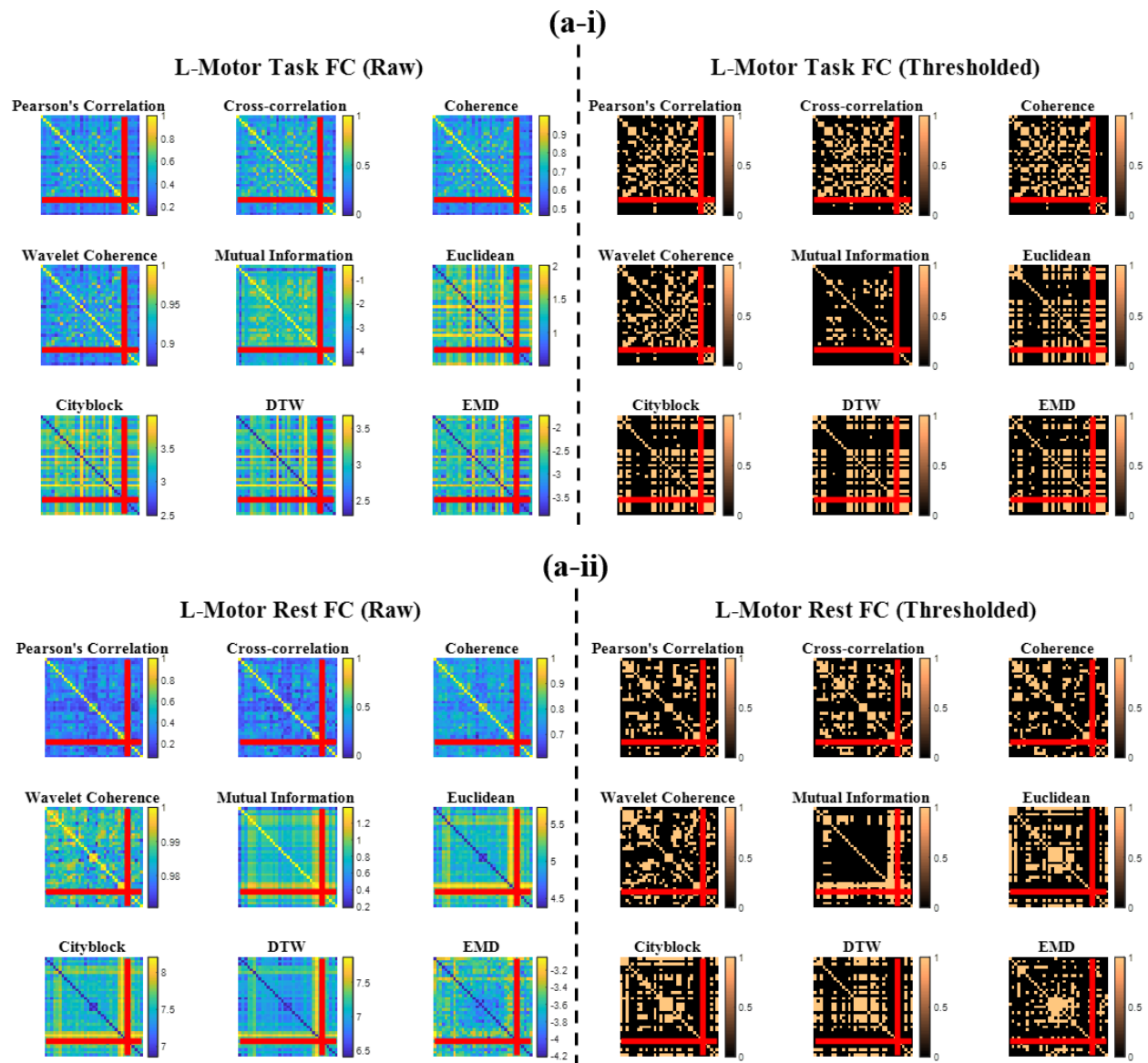
## Rethinking Measures of Brain Connectivity via Feature Extraction

Supplementary Figure 7. 1. The pipeline designed for E3 (shown for Pearson's correlation)

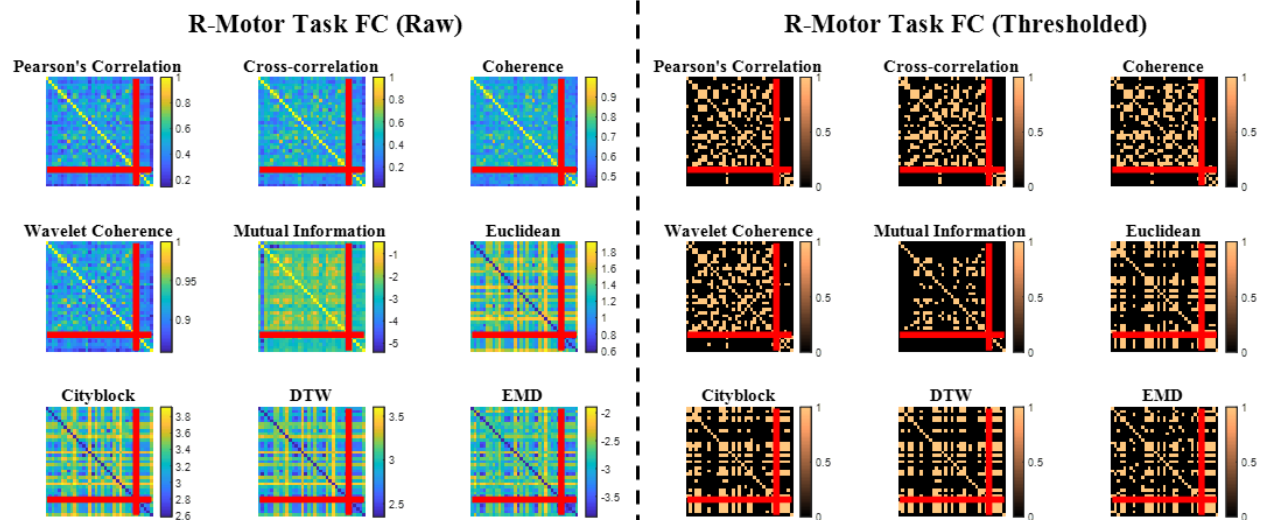


**Note:** (a) *original brain configuration* consisting of 68 regions and 10 large-scale brain networks averaged over FC matrices of 29 young healthy adults; (b) thresholded version of *original brain configuration*; (c) an ideal block structure corresponding to the *original brain configuration*; (d) a random scrambling of the *original brain configuration* as an initialization step for clustering; (e) clustered FC matrix based on  $k$ -means with  $k=10$  and a sparsity-based distance function resulting in an *alternative brain reconfiguration*; (f) thresholded version of *alternative brain reconfiguration*; (g) the ideal block structure corresponding to the *alternative brain reconfiguration*; Sørensen-Dice similarity coefficient for the *original brain configuration* and the *alternative brain reconfiguration* are compared to find whether the latter is a better arrangement; (h) plausibility of reconfigured arrangement is validated by associating FC from (g) with behavioral outcome, i.e. normalized verbal fluency score and compared to association between (c) with behavioral outcome.

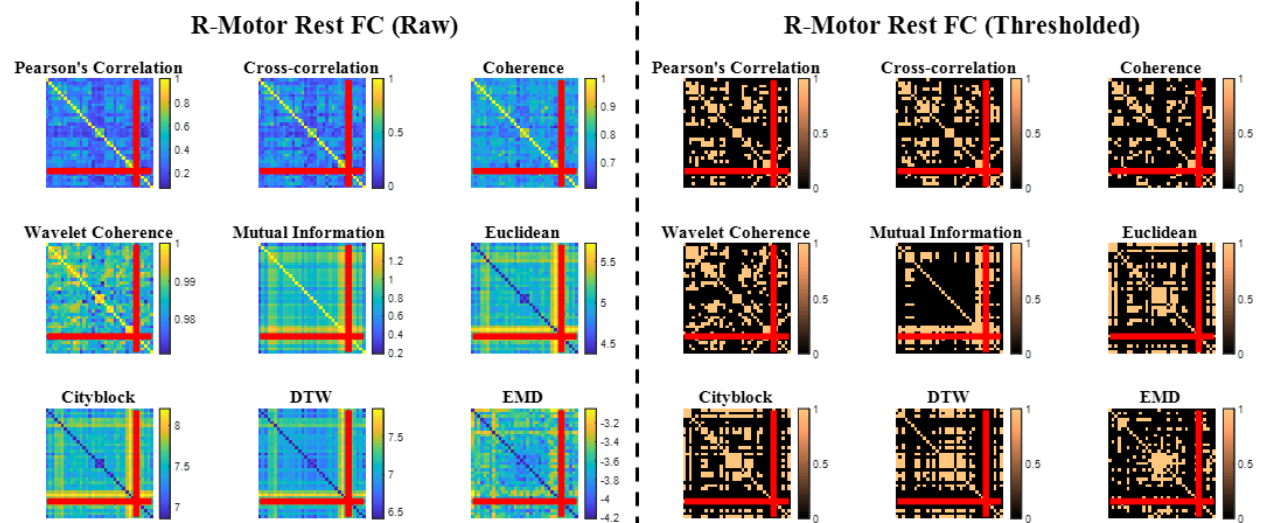
**Supplementary Figure 7. 2.** Comparison of FC based on all measures in young healthy adults for *E1* in: (a) left motor (b) right motor and (c) language networks between task (sub-images *i*) and resting-state conditions (sub-images *ii*)

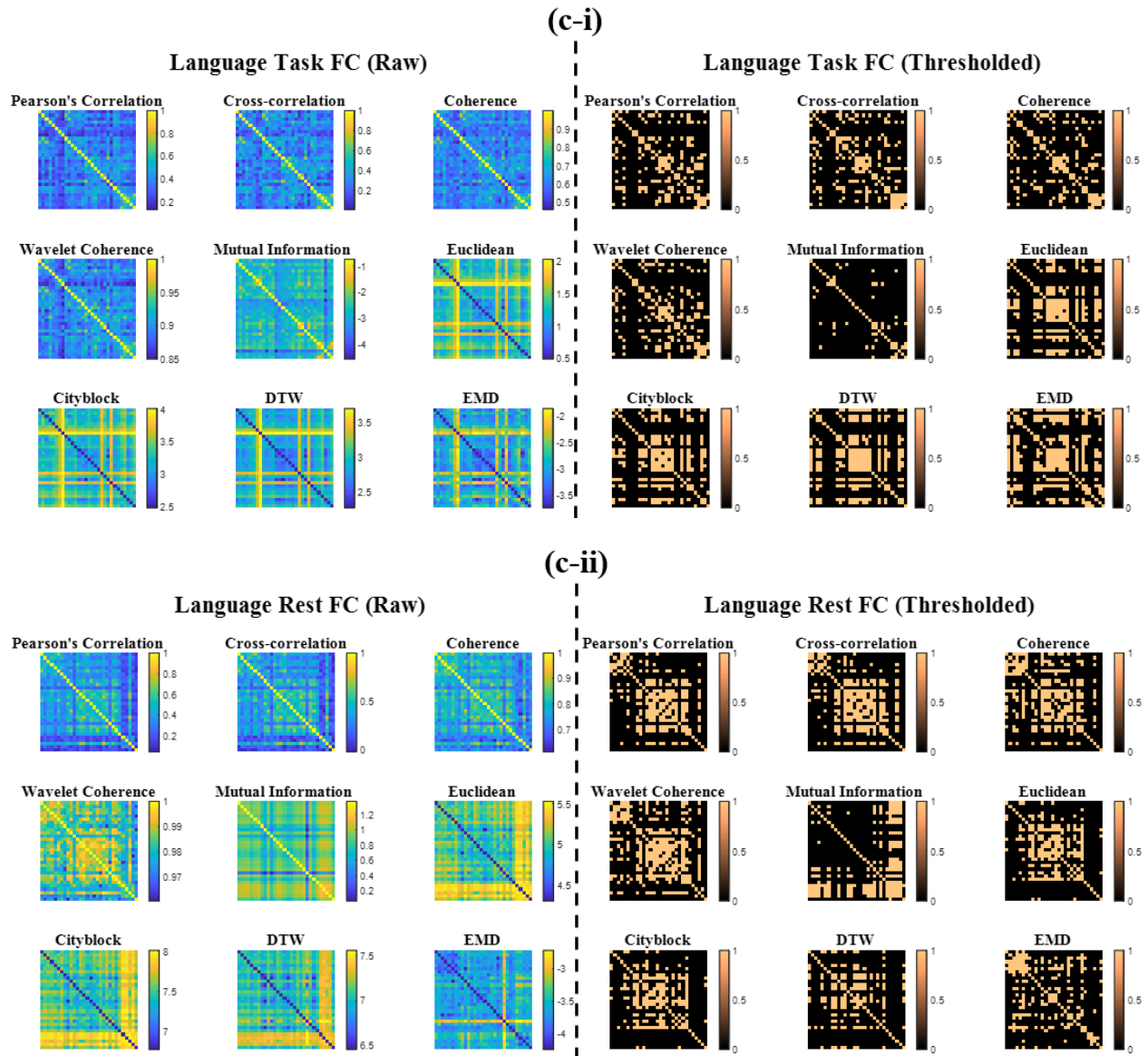


(b-i)



(b-ii)

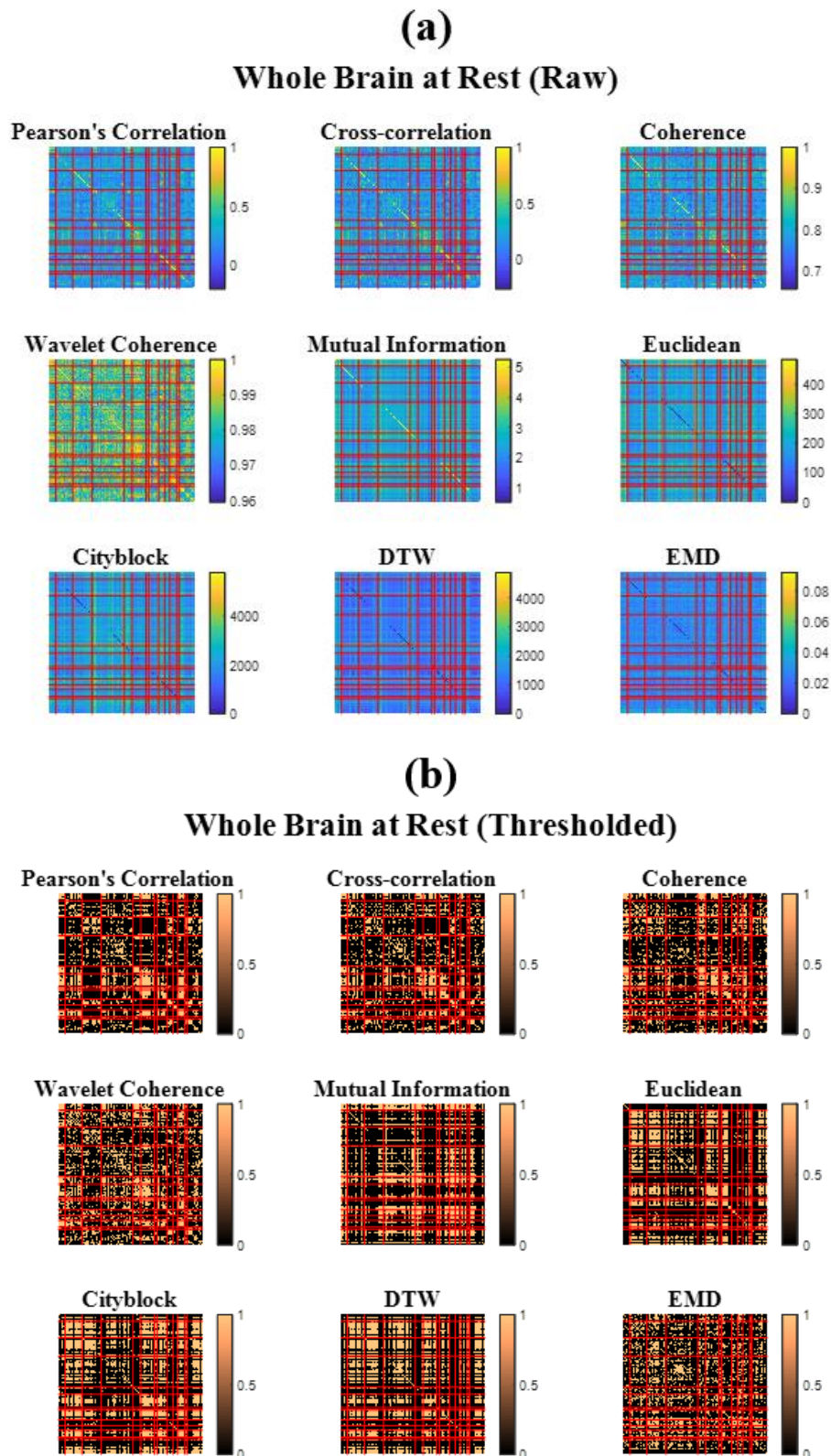




Note: Brain networks are defined based on Power functional atlas; In each image, matrices on the left represent FC averaged across all participants and those on right represent thresholded FC matrix averaged across all participants. The red lines in (a) and (b) show the separation between hand-motor and mouth-motor brain regions.

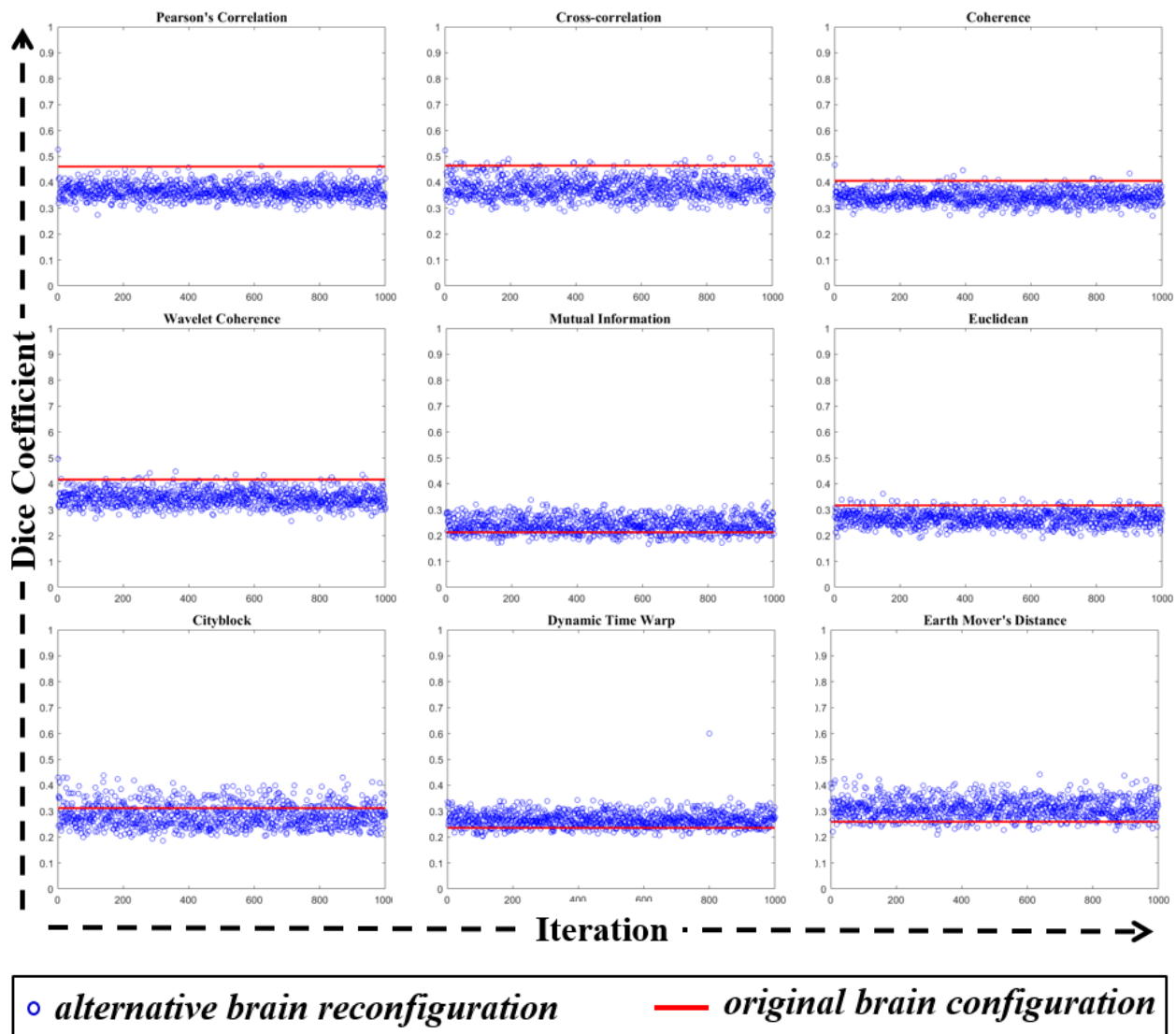


**Supplementary Figure 7. 3.** Whole brain resting-state FC in young healthy adults defined based on various measures in 13 distinct brain networks in **E1**: **(a)** FC matrix averaged across all participants; **(b)** thresholded FC matrix averaged across all participants.



Note: Brain networks are defined on the basis of Power atlas. The red lines represent the separation between brain regions belonging to a specific network. The regions are grouped in the following order: audio, visual, motor, default mode, cingulo-opercular task, fronto-parietal task, memory, salience, dorsal attention, ventral attention, subcortical, cerebellar, uncertain networks.

**Supplementary Figure 7. 4.** The distribution of Sørensen-Dice similarity coefficients obtained for 1000 iterations of k-means clustering.



Note: The red line represents the Sørensen-Dice similarity coefficient achieved in the *original brain configuration* whereas the Sørensen-Dice similarity coefficient obtained for each of the *alternative brain reconfigurations* is represented by a blue circle.



*Supplementary Table 7. 1. Multiple measures used to characterize FC and their properties*

<b>Measure</b>	<b>Properties</b>
Pearson's Correlation	<ul style="list-style-type: none"> <li>• Time-domain</li> <li>• Similarity</li> <li>• Linear</li> <li>• Scale-invariant</li> </ul>
Cross-correlation	<ul style="list-style-type: none"> <li>• Time-domain</li> <li>• Similarity</li> <li>• Linear</li> <li>• Scale-invariant</li> </ul>
Coherence	<ul style="list-style-type: none"> <li>• Frequency-domain</li> <li>• Similarity</li> <li>• Linear</li> <li>• Scale-invariant</li> </ul>
Wavelet coherence	<ul style="list-style-type: none"> <li>• Time-frequency-domain</li> <li>• Similarity</li> <li>• Linear</li> <li>• Scale-invariant</li> </ul>
Mutual information	<ul style="list-style-type: none"> <li>• Time-domain</li> <li>• Similarity</li> <li>• Non-linear</li> <li>• Scale-variant</li> </ul>
Euclidean distance	<ul style="list-style-type: none"> <li>• Time-domain</li> <li>• Dissimilarity</li> <li>• Linear</li> <li>• Scale-variant</li> </ul>
Cityblock distance	<ul style="list-style-type: none"> <li>• Time-domain</li> <li>• Dissimilarity</li> <li>• Linear</li> <li>• Scale-variant</li> </ul>
Dynamic time warping	<ul style="list-style-type: none"> <li>• Time-domain</li> <li>• Dissimilarity</li> <li>• Non-linear</li> <li>• Scale-variant</li> </ul>
Earth mover's distance	<ul style="list-style-type: none"> <li>• Time-domain</li> <li>• Dissimilarity</li> <li>• Non-linear</li> <li>• Scale-variant</li> </ul>

*Supplementary Table 7. 2. Age-based classification between younger and older healthy adults in nine major brain networks in E2.*

*(a) Area under the curve for each classifier is listed below*

<b>Metric</b>	<b>D. DMN</b>	<b>V. DMN</b>	<b>L. ECN</b>	<b>R. ECN</b>	<b>A. Sal.</b>	<b>P. Sal.</b>	<b>Auditory</b>	<b>Language</b>	<b>Motor</b>
Pearson's Correlation	0.42	0.50	0.38	0.61	0.83	0.63	0.65	0.55	0.51
Cross-correlation	0.50	0.50	0.46	0.65	0.82	0.60	0.56	0.47	0.56
Coherence	0.59	0.50	0.52	0.51	0.61	0.60	0.53	0.52	0.65
Wavelet coherence	0.36	0.47	0.55	0.57	0.70	0.45	<b>0.69</b>	0.58	0.26
Mutual Information	0.73	0.71	0.66	0.55	0.77	0.55	0.52	0.57	0.61
Euclidean	0.67	<b>0.73</b>	0.71	<b>0.68</b>	0.82	0.53	0.47	0.55	0.49
Cityblock	0.70	0.74	0.70	<b>0.69</b>	0.83	0.49	0.51	0.63	0.52
DTW	<b>0.79</b>	0.72	<b>0.77</b>	0.66	0.83	0.59	0.50	<b>0.66</b>	0.36
EMD	0.47	0.65	0.66	0.55	0.68	0.58	0.56	0.45	<b>0.67</b>
Combined	0.74	0.64	0.75	0.53	<b>0.91</b>	<b>0.69</b>	0.68	0.53	0.54

Note: Brain networks are defined by Willard functional atlas; classification is performed with a support vector machine classifier; performance represents area under the curve with a leave-one out testing; the highest performing metric is represented in **bold** for each network; D.DMN = dorsal default mode network; V.DMN = ventral default mode network; L.ECN = left executive control network; R.ECN = right executive control network; A.Sal. = anterior salience; P.Sal. = posterior salience; DTW = dynamic time warping; EMD = Earth mover's distance;

*(b) The minimum and maximum number of features selected in each classification model in the format [minimum, maximum]*

<b>Metric</b>	<b>D. DMN</b>	<b>V. DMN</b>	<b>L. ECN</b>	<b>R. ECN</b>	<b>A. Salience</b>	<b>P. Salience</b>	<b>Auditory</b>	<b>Language</b>	<b>Motor</b>
Pearson's Correlation	[3, 7]	[4, 9]	[3, 8]	[2, 6]	[1, 3]	[4, 8]	[1, 1]	[3, 21]	[3, 5]
Cross-correlation	[1, 7]	[3, 9]	[2, 6]	[1, 4]	[1, 3]	[3, 8]	[3, 3]	[1, 21]	[1, 4]
Coherence	[3, 10]	[3, 8]	[2, 4]	[1, 15]	[3, 5]	[3, 11]	[1, 1]	[1, 7]	[1, 1]
Wavelet coherence	[1, 4]	[1, 5]	[2, 4]	[1, 2]	[1, 2]	[1, 5]	[1, 2]	[1, 2]	[1, 15]
Mutual Information	[1, 3]	[1, 3]	[2, 3]	[2, 3]	[1, 2]	[1, 4]	[3, 3]	[1, 1]	[1, 2]
Euclidean distance	[3, 5]	[1, 3]	[1, 3]	[1, 1]	[2, 3]	[2, 4]	[3, 3]	[1, 3]	[1, 4]
Cityblock distance	[3, 4]	[1, 3]	[1, 4]	[1, 2]	[2, 3]	[3, 7]	[3, 3]	[2, 4]	[1, 4]
DTW	[3, 6]	[1, 4]	[1, 2]	[1, 2]	[1, 2]	[2, 5]	[1, 3]	[1, 2]	[1, 2]
EMD	[1, 36]	[5, 8]	[2, 5]	[1, 15]	[2, 2]	[3, 11]	[3, 3]	[2, 5]	[1, 3]
Combined	[7, 15]	[5, 17]	[5, 13]	[5, 14]	[5, 8]	[9, 20]	[3, 5]	[5, 17]	[3, 9]

Note: Brain networks are defined by Willard functional atlas; classification is performed with a support vector machine classifier; D.DMN = dorsal default mode network; V.DMN = ventral default mode network; L.ECN = left executive control network; R.ECN = right executive control network; A.Sal. = anterior salience; P.Sal. = posterior salience; DTW = dynamic time warping; EMD = Earth mover's distance;

## CHAPTER 8: Automated Classification of Ink Strokes in van Gogh's Drawings using Dictionary Learning

---

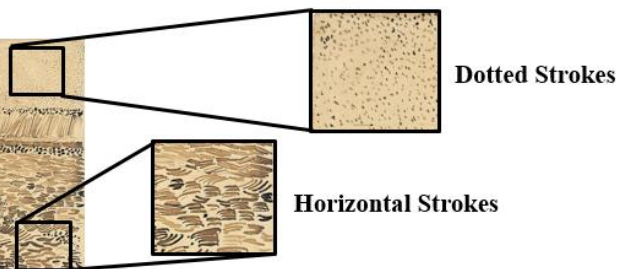
### Graphical Summary



van Gogh's Painting



van Gogh's Drawing



### Research Question

Can we automatically identify the different types of ink strokes found in van Gogh's drawings?

### Publication

Mohanty, R., Sethares, W. A., Meedendorp, T., van Tilborgh, Louis, "Dictionary Learning-based Classification of Ink Strokes in Vincent van Gogh's Drawings", 2019, *International Journal of Arts and Technology*, 11 (1), 80-98.

### Abstract

Discriminative dictionary learning techniques are applied in an art historical context with the goal of automatic classification of an ink drawing based on the type of stroke. Two kinds of K-SVD-based multi-class classification are tested on van Gogh's drawings. First is a classical dictionary method where atoms are learned from pixels directly. A second feature-based dictionary method is introduced where atoms are learned based on features characterizing collections of individual ink strokes. Results indicate that feature-based method provides better classification while incurring significantly less computational expense than the classical method. A multi-level feature-based method extends K-SVD for larger images. Such an automated classification would provide a new resource for scholars of van Gogh and students learning the art of drawing, be useful in automated photograph to computer drawing translation and point towards the more difficult problem of identifying painted brush strokes. Algorithms and data are provided to encourage modifications and extensions.

## 1. Introduction

Vincent van Gogh's letter of 1883 states that 'drawings are the root of everything' [27]. A variety of ink and pencil strokes can be observed clearly and distinctly in Vincent's work: cross hatchings, dots, vertical, horizontal, blunt, curved, etc. strokes that are both long and short, light and dark. These are illustrated in **Figure 8.1**, which shows the drawing *Sower with Setting Sun*. A variety of different strokes are evident, including bold slashes in the foreground that represent the field, thin vertical lines depicting the grain, dots capping the grain, smaller dots speckled throughout the sky, and the relatively complex cross-hatching that forms the clothes of the sower. While any single drawing can be segmented by eye, carrying this out on a large collection of an artist's drawings would be challenging without an automated system or algorithm; this paper provides a step in the direction of such a method.

*Figure 8. 1. A portion of Sower with Setting Sun by Vincent van Gogh*

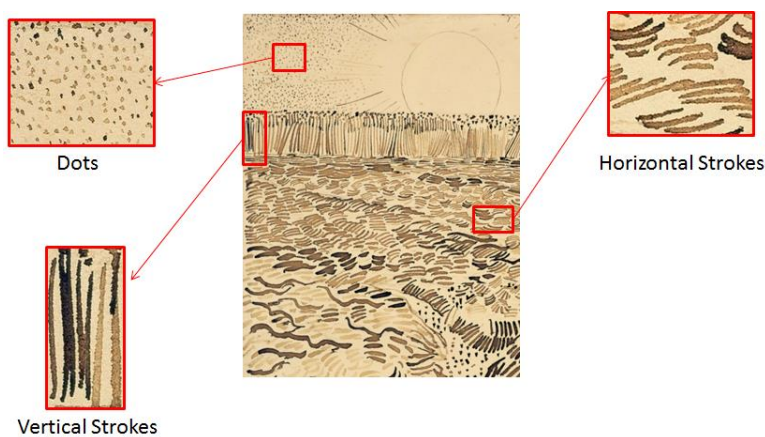


Note: Date: August 1888; medium: pencil, pen and reed pen and ink on paper; image dimensions: 3269×2048.  
 Source: Kröller-Müller Museum, Otterlo, Netherlands

The problem of automatically segmenting a drawing into regions, as illustrated in **Figure 8.2**, can be modeled as a multi-class classification problem where each class corresponds to a different kind of ink stroke. This may be approached in an unsupervised manner, as described in the precedent study [1], or in a supervised manner. This paper extends the previous methods by focusing on supervised dictionary learning algorithms and by introducing a feature-based dictionary method.

The repetitive nature of strokes found in ink drawings allows for sparse representation of the images. Dictionary learning approaches are built upon the sparsity constraint by learning an overcomplete representation of an image [2; 3; 4]. While reconstructive dictionary learning is well studied and illustrated in applications such as denoising, inpainting, demosaicing, texture synthesis, etc. [5; 6; 7], the investigation of the discriminative power of dictionary learning is relatively more recent [8; 9; 10]. Such previous studies have applied discriminative dictionary learning to facial recognition, identification of digits, or object recognition. This paper expands to consider art historical questions. Moreover, common dictionary learning methods operate on pixel-based patches of the images. In contrast, this paper considers an alternative feature-based dictionary learning approach which provides a significant reduction in the dimensionality of the data and scales well as the size of image grows. Many methods have been proposed in order to take advantage of the manifestation of information of images on multiple scales [11; 12; 13; 14], and other methods exploit a direct multi-scale approach that is compatible with K-SVD and can also be applied in feature-based dictionary learning.

**Figure 8. 2.** A patch from the *Sower with Setting Sun*, 1888 by Vincent van Gogh illustrates the selection of regions in which three basic types of strokes appear: dots, vertical strokes and horizontal strokes



Most previous computational approaches to artistic style analyze information derived from paintings [15; 16; 17]. Analyzing drawings instead can have several advantages. First and most obvious, drawings are simpler in form and typically uncolored. Drawings are often precursors to paintings, and so can be considered as basic building blocks which may capture relevant information about the structure of strokes that ultimately lead to a more thorough understanding of brush strokes.

The goal of this work is to automatically classify the various kinds of ink strokes found across Vincent's 1100 works on paper, to segment each drawing into regions, each of which is dominated by a single style of stroke. This is achieved by implementing multi-class classification hinging on a K-SVD-based [18] discriminative dictionary learning algorithm with a multi-scale implementation [13] to account for size variations among the different classes. Each stroke-type is treated as a class. Classical dictionary learning, as described and implemented in Section 2, involves learning an overcomplete dictionary directly from the pixel-level information of the given image. This provides a baseline for performance and is followed by classification of test images based on the learned dictionary.

A second approach, introduced in Section 3, uses a multi-scale feature-based dictionary learning classification where the dictionary is learned over a set of useful features (instead of pixel-level information). This facilitates not only a reduction in the dimensionality of the dictionary elements (also called atoms), but also allows adding information from a larger number of scales without a significant increase in learning time. Third, since K-SVD is limited to handling modestly sized image patches, a multi-level feature-based variation is presented that can handle larger image patches without suffering a large computational burden. Additionally, unlike the quadtree model for multi-scale K-SVD proposed in [13], which learns multiple dictionary atoms corresponding to different scales, the multi-scale approach presented here learns one dictionary per class over all scales. This allows the use of more scales and easier extension to more classes.

*Figure 8. 3. Arums by Vincent van Gogh, drawing*



Note: Date: May–June 1889; medium: reed pen and pen and ink on paper; image dimensions: 3840 × 2902.  
Source: van Gogh Museum, Amsterdam

The algorithms are tested on several ink drawings by Vincent and a series of experiments in Section 4 compares the three approaches. In terms of applications, successful classification of Vincent's ink drawings may be useful in several ways: conversion from photograph to computer-based drawing [19], better understanding of Vincent's drawings for advanced scholars, as well as novices interested in learning the art of drawing, and those interested in identification of brush strokes appearing in paintings [20].



**Figure 8. 4. Street in Saintes-Maries-de-la-Mer by Vincent van Gogh**



Note: Date: July 1888, medium: reed pen, quill, and ink over chalk on wove paper, image dimensions: 1916 × 1500.  
Source: Metropolitan Museum of Art, New York (and privately owned)

## 2. Classical dictionary learning paradigm

The classical dictionary learning method [21] aims to find an optimal set of basis elements by learning representative atoms of the dictionary and a sparse representation of the data as a linear combination of the learned atoms. For images, data consists of patches of pixels. For the supervised learning step, a collection of patches is selected (manually) from each class, which is chosen so as to represent a single type of stroke in the drawing. A square patch of size  $n \times n$  can be vectorized into elements  $x_{train} \in \mathbb{R}^{n^2}$ . Classification is implemented by learning dictionaries with a discriminative cost function [8] by adapting one dictionary  $D_i \in \mathbb{R}^{n^2 \times p}$  that is overcomplete consisting of  $p$  atoms, by solving

$$J(x_{train}, D_i) = \min_{\alpha \in \mathbb{R}^p} \|x_{train} - D_i \alpha\|_2 \text{ subject to } \|\alpha\|_0 < L \quad (1)$$

where the vectors  $x_{train}$  are drawn from the patches of the  $i^{\text{th}}$  class selected for training,  $D_i$  is the learned dictionary for the  $i^{\text{th}}$  class, and  $L$  is the sparsity parameter. The learning phase involves alternating between the sparse coding and the dictionary update steps using an iterative method such as orthogonal matching

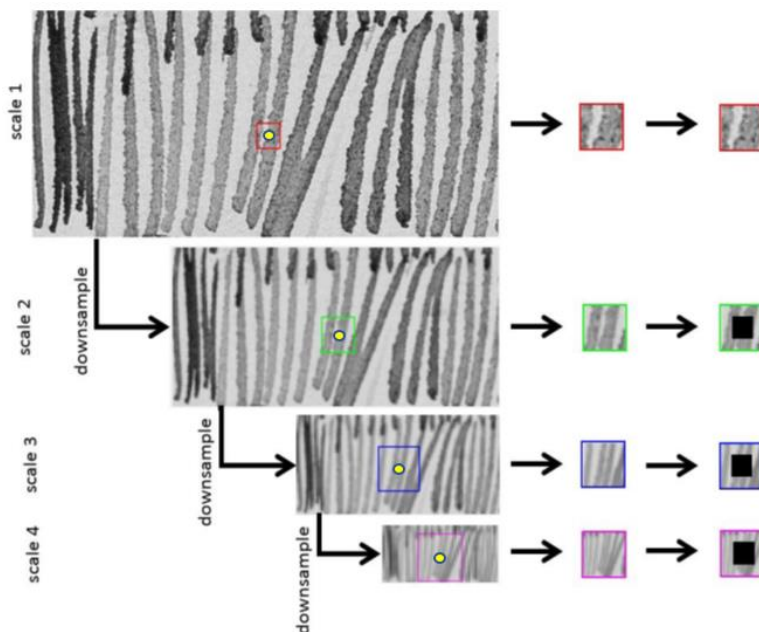
pursuit (OMP) [22]. After learning the dictionaries, they can be used in the classification stage by assigning a patch  $x_{test}$  of unknown class to the class with the best-fit sparse  $\alpha$ , i.e., to class that optimizes

$$\min_i J(x_{test}, D_i) \quad (2)$$

## 2.1 Multi-scale approach

Ink drawings contain strokes of varying shapes and sizes, i.e., the strokes appear over multiple scales, and this suggests the use of a multi-scale representation to better capture the large-scale structure within the images. Rather than learning dictionary atoms corresponding to each scale, a single dictionary encompassing information across all scales was learned. Next, redundant information supplied by addition of a new scale was eliminated, retaining only new and relevant information in subsequent scales. This approach to multi-scaling is elaborated in a detailed manner in [23] and is shown diagrammatically in **Figure 8.5**.

*Figure 8. 5. Breakdown of the multi-scale approach*



Note: An example of a training patch from the ‘vertical’ class of the *Sower* image is shown. Four scales are exhibited. The three columns are described. *Left*: The point of interest is marked by the yellow circle in each image. The topmost image is successively downsampled by a factor of two up to four levels. A constant window size of dimensions  $20 \times 20$  is maintained across all scales. The  $20 \times 20$  window successively captures larger areas of the image as the level of downsampling progresses. *Middle*: The  $20 \times 20$  extracted patch at each scale around the point of interest is shown. Colored squares denote the area from the original image that is extracted. The combined feature vector derived from these patches would be of length  $1600 \times 1$  at each point of interest. *Right*: Patches from the image are extracted at four scales followed by removal of redundant parts of the image. Repeated portions are subtracted, and only new information is added at each scale. No data were removed at scale 1. The reduced combined feature vector derived in this case would be of length  $1300 \times 1$  at each point of interest.

For the case of **Figure 8.1**, four classes, namely, regions dominated by dots, horizontal, vertical strokes, and blank spaces were examined. A patch of size  $400 \times 180$  was utilized as a training patch for each class. One thousand random points were used as training samples for each class. The dictionary was initialized with 100 atoms randomly chosen from among the 1000 samples. These are iteratively updated as each of the 1000 samples are reconstructed during the training phase. The final dictionary consisted of 400 atoms composed of 100 atoms from each representative class. In the course of the testing phase, a feature vector of size  $1300 \times 1$  was computed per test patch. The details of feature vectors and respective dimensions are shown in **Table 8.1**. The feature extraction was followed by finding a sparse code for each test patch in the final dictionary so as to best minimize the reconstruction error.

**Table 8. 1.** *Feature dimensions of the pixel-based features of classical dictionary learning*

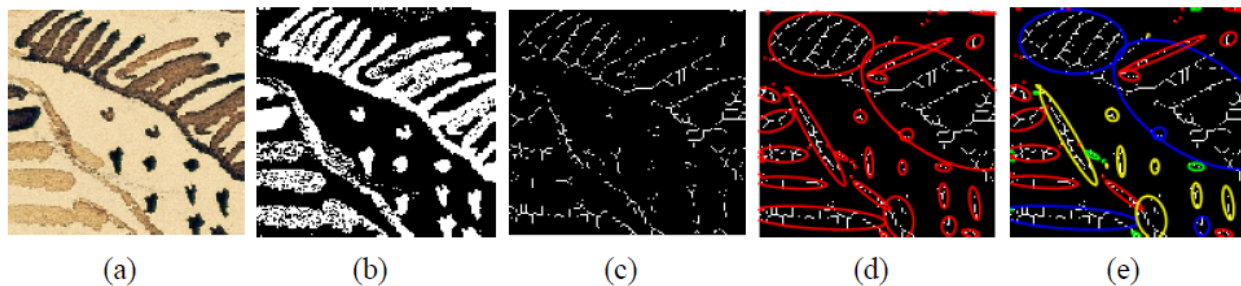
<b>Feature Scale</b>	<b>Patch Size</b>	<b>Complete Vector</b>	<b>Reduced Vector</b>
Scale 1	20 × 20	400 × 1	400 × 1
Scale2	20 × 20	400 × 1	300 × 1
Scale 3	20 × 20	400 × 1	300 × 1
Scale 4	20 × 20	400 × 1	300 × 1
Combined Features	-	1600 × 1	1300 × 1

### **3. Feature-Based Dictionary Learning Paradigm**

The classical method learns an optimal dictionary directly from the pixels of the given image. For large images, this suffers from the drawback of having high dimensional data which increases the computational complexity and time to learn the dictionary. This section addresses this by considering a ‘feature-based’ method in which the representative vector consists of low-dimensional features derived from image patches. Clearly, the quality of the learned dictionary is dependent upon the features over which it is learned. The features of a given patch are chosen by extracting relevant characteristics that encapsulate both high-level and low-level information about the patch. These include:

- a. regional sub-features characterizing the global properties of the given patch
- b. individual stroke sub-features characterizing the local properties of individual strokes found in the given patch.

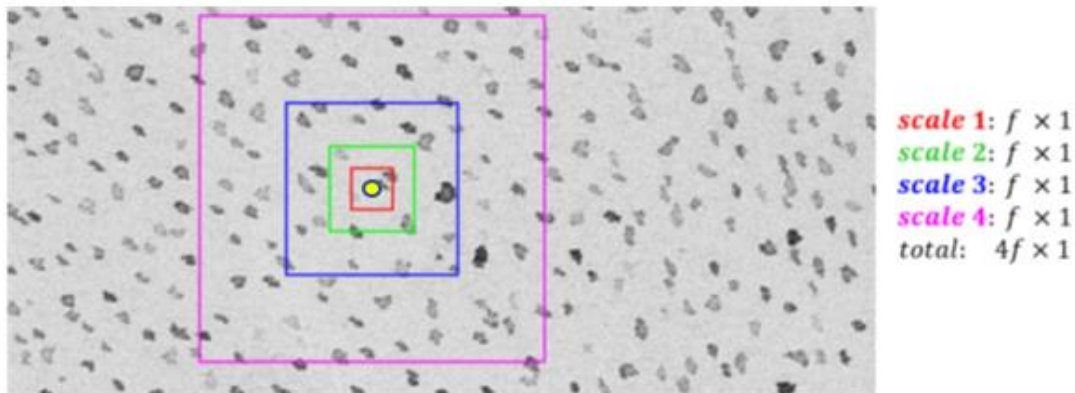
*Figure 8. 6. The experimental process of individual sub-feature extraction*



Note: (a) a patch from the *Sower* drawing (b) the result after binarization using adaptive thresholding (c) the skeletonized structures (d) the best-fit ellipses in red to each of the connected skeletons; specific features are derived from each of these ellipses (e) the desired classification result where ellipses of the same color belong to the same class, i.e., similar stroke type

In order to compute regional sub-features, gray-scale images were manipulated directly, and gross statistics of a given patch were calculated. In the case of individual stroke sub-features, each image patch was binarized using local adaptive thresholding [24; 25], skeletonized such that the structure of the strokes were one pixel wide, and connected components were identified in order to characterize individual strokes. Several individual stroke sub-features were built by finding a best-fitting ellipse to each of the connected components in a given patch and then computing properties of these ellipses. The flow of the process of extraction of individual sub-features is presented in **Figure 8.6**. A square patch of size  $n \times n$  is vectorized into elements  $x'_{train} \in \mathbb{R}^m$  where  $x'_{train} < x_{train}$  and  $m \ll n$ . This reduction in dimension becomes appreciable as  $n$ , the size of the patch, increases. The training and testing pipelines are the same as in the previous section, replacing  $x_{train}$  and  $x_{test}$  from Section 2 with  $x'_{train}$  and  $x'_{test}$  respectively.

**Figure 8. 7.** An example of a training patch from ‘dots’ class is utilized to illustrate that feature-based dictionary learning can extend the application of *K-SVD* to large sized patches



Note: The (single-scale) multi-level idea is presented with colored squares for each level. In each case, the selected patch is centered at the yellow circle. The regions inside the red, green, blue and magenta squares contain  $20 \times 20$ ,  $40 \times 40$ ,  $80 \times 80$ , and  $160 \times 160$  sized patches respectively. The number of levels can be varied by choice. The dimensions of features extracted from each scale are identified by colored text on the right. The value of  $f$  is 99 at each level. By combining regional and individual stroke sub-features, a feature vector was extracted from each level and concatenated to form the final feature vector of size  $396 \times 1$ , i.e.,  $4f \times 1$ . This is considerably lower than the atom size in the classical learning.

As in Section 2, consider the specific case in **Figure 8.1**. There are four classes, regions dominated by dots, horizontal, vertical strokes, and blank spaces. A patch of size  $400 \times 180$  was utilized as a training patch for each class. One thousand random points were used as training samples for each class. For each of the 1000 samples, the following features were extracted:

- a. Regional sub-features computed over each patch:
  - normalized central moments up to third order [25]
  - local binary patterns (LBP) [26]
  - eigenfeatures derived from eigenvalue decomposition of the covariance matrix
  - entropy [25] directional gradients in the horizontal and vertical directions.
- b. Individual stroke sub-features computed over each stroke in each patch:
  - density of strokes per unit pixel
  - mean and standard deviation of intensity in the color image
  - mean lengths of major axis, minor axis and eccentricity of the ellipses fitting individual strokes
  - mode of quantized orientations of the ellipses fitting individual strokes

- mean of perimeters of the ellipses fitting individual strokes.

In addition to being intuitive, these features provide several advantages. For example, the central moments are translational invariant, LBPs are rotational invariant, the eigenvectors corresponding to the largest eigenvalues can approximate the global structure of a given patch, entropy reflects information about the overall contrast in an image, and directional gradients can provide information about orientation of structures in an image. In addition, individual stroke sub-features present finer details about the structure, spacing and design of strokes that constitute the image. The capacity of the feature-based dictionary learning to handle larger patches with the K-SVD and to incorporate information from multiple scales is realized with the help of a multi-level approach and a multi-scale approach.

### 3.1 Multi-level approach

In the multi-level approach, the patch size over which an optimal dictionary is learned is successively increased. Consider a training image from a given class (such as that representing the dots in the sky of **Figure 8.1**). If the patch centered at  $(x; y)$  is one of the 1000 training samples, four levels can be constructed at the original scale of the training images, namely,  $20 \times 20$ ,  $40 \times 40$ ,  $80 \times 80$  and  $160 \times 160$  patches around the point of interest. This is demonstrated in **Figure 8.7**. The merit of combining this kind of feature extraction with multi-level approach is that the dimensionality of feature vector is the same at each scale. In contrast, in the pixel-based dictionary learning, the vector size grows rapidly with increase in patch size. Thus, the multi-level provides one way to bypass the limitation of K-SVD of being restricted to small-sized image patches.

### 3.2 Multi-scale approach

On one hand, the multi-level approach described above allows the use of large image patches. On the other hand, it works only on a single scale. The multi-scale approach to feature-based dictionary rescales and the procedure remains consistent with that described in Section 2, with one modification. Regardless of whether

the multi-scaling is realized by taking into account the complete patch or the reduced patch, as portrayed in **Figure 8.5**, the size of the feature vector remains constant at any given point of interest. Hence, all of the processing steps for multi-scale realization in this section use complete patches, as pictured in the second column of **Figure 8.5**.

In both cases, multi-level and multi-scale techniques, training uses 1000 samples from each class: dots, horizontal, vertical, and blank regions of **Figure 8.1** for four levels and four scales respectively. All vectorized features were normalized by computing a z-score so as to have a zero-mean and unit standard deviation to ensure that the features with greater magnitude do not dominate. The feature dimensions are given in **Table 8.2**. One dictionary consisting of 100 atoms per class was learned. Information from all the scales were combined in this single dictionary. The initial dictionary was assigned with 100 random vectors chosen from among the 1000 sample vectors. By iterative updating, an optimal dictionary was learned. Dictionary for each class was concatenated to create a single dictionary with 400 atoms. During the testing phase, features are extracted from each test patch to generate a vector of size  $396 \times 1$ . Then, an OMP sparse coding algorithm finds a sparse combination of dictionary atoms that best minimizes the reconstruction error. Three values for the sparsity parameter  $L$ , i.e., 3, 5 and 7, were tested.



**Table 8. 2.** Feature dimensions of the regional and individual stroke features in feature-based dictionary learning

Feature Name	Feature Vector (single-scale single-level)	Feature Vector (SSML or MSSL)
Central Moments	$7 \times 1$	$28 \times 1$
LBP	$36 \times 1$	$144 \times 1$
Eigenvalues	$9 \times 1$	$36 \times 1$
Entropy	$1 \times 1$	$4 \times 1$
Gradient nodes in x-direction	$9 \times 1$	$36 \times 1$
Gradient edges in x-direction	$10 \times 1$	$40 \times 1$
Gradient nodes in y-direction	$9 \times 1$	$36 \times 1$
Gradient edges in y-direction	$10 \times 1$	$50 \times 1$
Individual stroke sub-features	$8 \times 1$	$32 \times 1$
Combined Features	$99 \times 1$	$396 \times 1$

Note: Same feature dimensions are applicable to single-scale multi-level (SSML) as well as multi-scale single-level (MSSL) methodologies.

## 4. Experiments and comparisons

### 4.1. Data

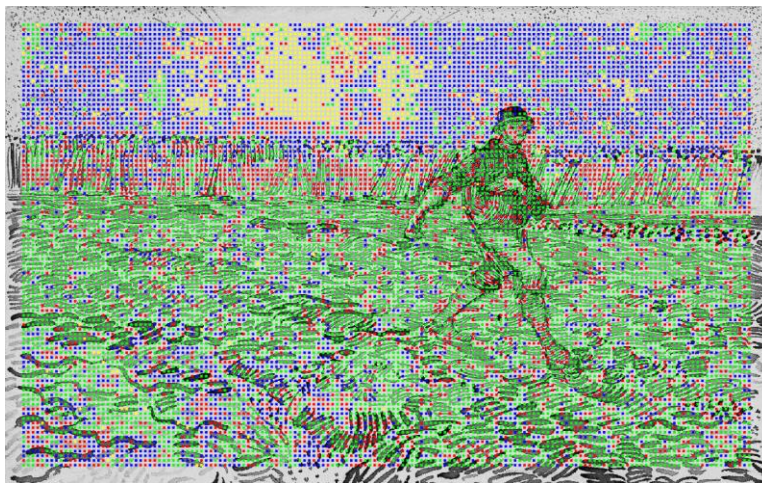
High resolution images of van Gogh's ink drawings (<http://www.vangoghmuseum.nl/>), the Metropolitan Museum of Art (<http://www.metmuseum.org/>) and The Kröller-Müller Museum (<https://krollermuller.nl/>)] were used for the experiments in this work. In particular, we have used the *Sower*, *Arums* and *Street in Saintes-Maries-de-la-Mer* as shown in **Figures 8.1, 8.3, 8.4** respectively. These images are chosen as they were all drawn with a reed pen on paper and showcase a variety of simple as well as complex stroke types that can serve as classes for the classification problem. Specific classes were chosen from each image by visual inspection. Portions of each image were employed in the training phase and independent portions of

each image were deployed for testing and performance evaluation. The experiments consider a four-class classification applied to the three ink drawings of **Figures 8.1, 8.3, 8.4**. The results are presented by comparing various aspects of the performances of classical dictionary learning to the feature-based dictionary learning. The data and code are available at <https://uwmadison.box.com/s/f7yckfd3596nd89iyuo9h09hgoc55a41>.

#### **4.2. Qualitative assessment of feature-based dictionary learning paradigm**

The learned dictionary is used to classify the full ink drawings into regions dominated by specific types of strokes. Results from the classical dictionary learning paradigm can be found in [23] while the results of the feature-based dictionary learning schemes are presented here. **Figures 8-10** present the complete classification for the multi-level method of Subsection 3.1. **Figures 8.11-8.13** present the complete classification for the multi-scale method of Section 3.2. Each colored spot was chosen as a test point and a sparse code with  $L = 3$  was chosen to pick top three dictionary elements of feature vectors, which when linearly combined, best represent the features at that location. The mean of weights on the chosen dictionary atoms was computed to find the contribution of atoms of each class. The location was assigned to the class with the largest mean weight and designated with the corresponding color. Misclassifications were generally due to the presence of multiple types of stroke within the same neighborhood. In addition, the sparsity parameter was varied, i.e.,  $L = 3, 5, 7$ .  $L = 3$  provided the best classification results across all the three drawings. Overall, the multi-scale method significantly outperformed the multi-level classification.

*Figure 8. 8. The Sower with the setting Sun of Figure 8.1 is superimposed on the multi-level classification scheme of Subsection 3.1*

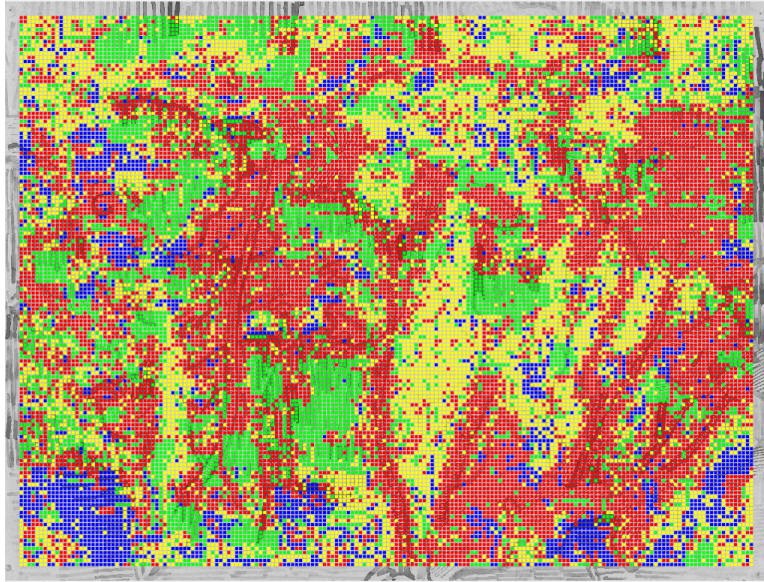


Note: The stroke types are color coded as follows: blue, red, green, yellow denote regions dominated by dots, vertical strokes, horizontal strokes and blank regions respectively.

#### **4.3. Qualitative comparison between classical and feature-based paradigms**

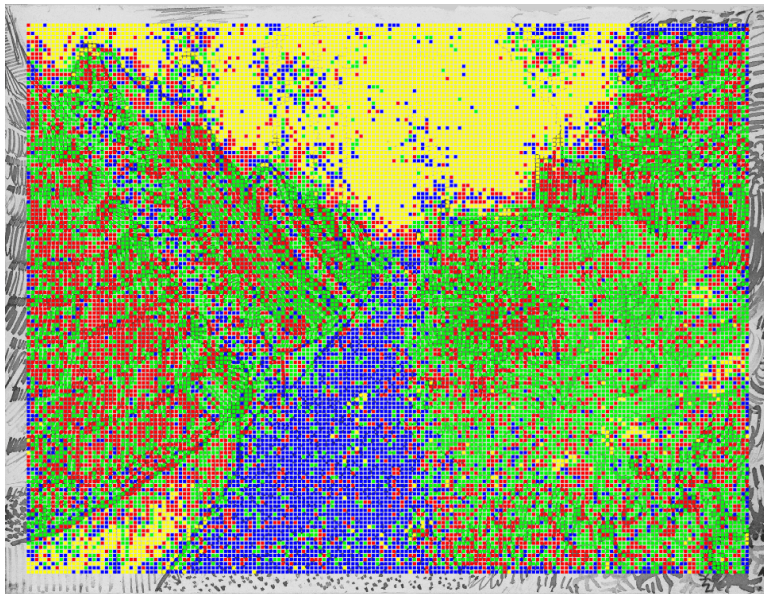
**Figure 8.15** provides a visual comparison of the segmentation when using the classical method, the multi-level method of Subsection 3.1 and the multi-scale method of Subsection 3.2. Each colored point represents a single test point that is the center of a neighborhood from which image patches or low-level features are extracted.

**Figure 8. 9.** The drawing Arums of **Figure 8.3** is superimposed on the multi-level classification of Subsection 3.1



Note: The color code is as follows: blue, red, green, yellow are markers of the regions consisting mainly of thicker horizontal strokes, finer horizontal strokes, vertical strokes and blank spaces.

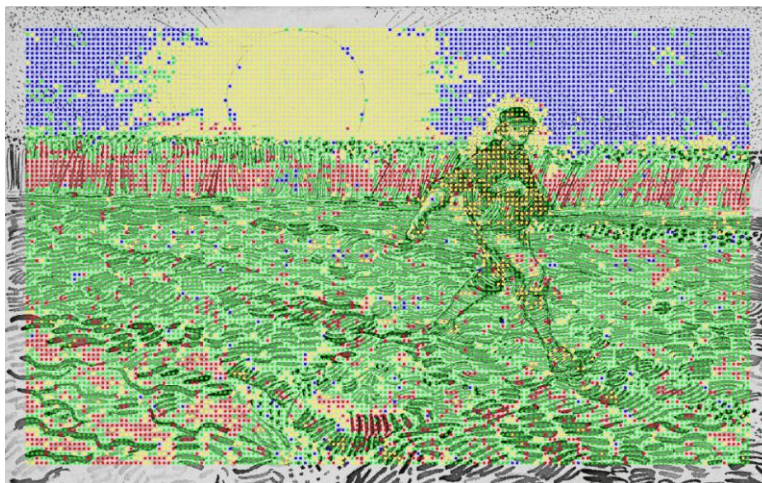
**Figure 8. 10.** The *Street in Saintes-Maries-de-la-Mer* of **Figure 8.4** is superimposed on the multi-level classification of Subsection 3.1



Note: The color code is as follows: blue, red, green and yellow represent dots, vertical strokes, curved strokes and blank spaces respectively.

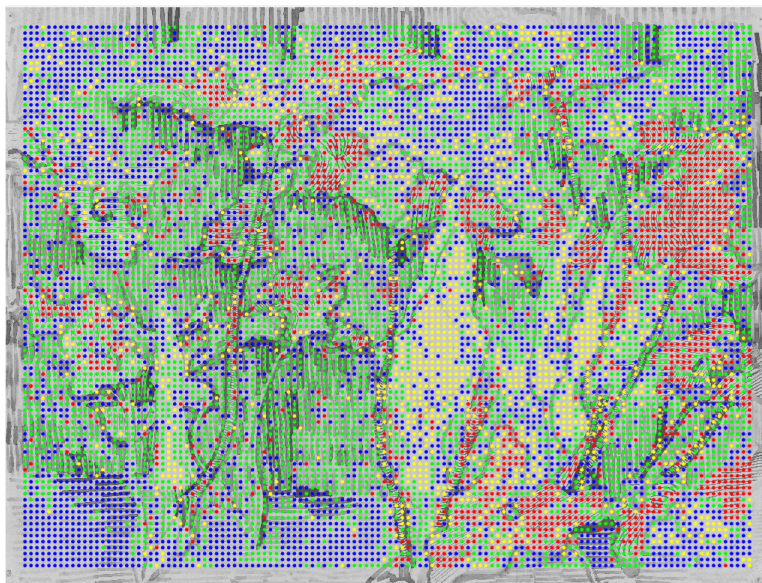


**Figure 8. 11.** *The Sower with the setting Sun* of **Figure 8.1** is superimposed on the multi-scale classification of **Subsection 3.2**



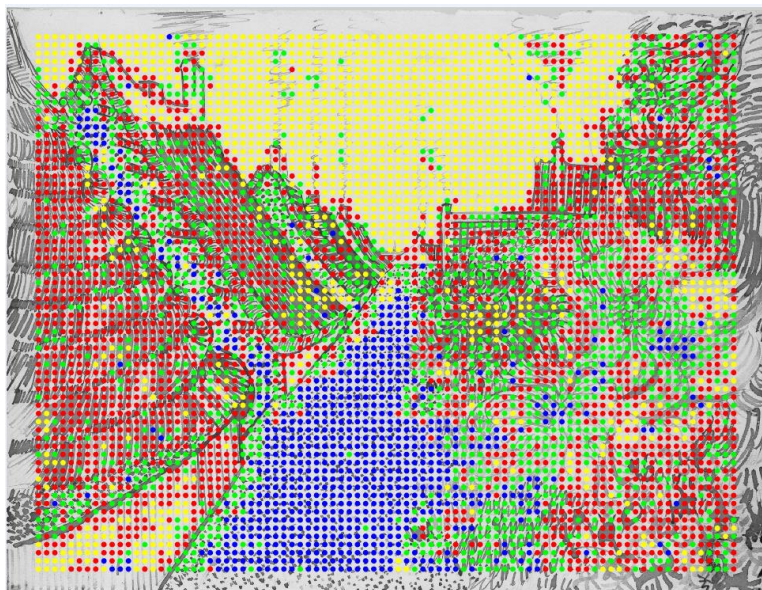
Note: The stroke types are color coded as follows: blue, red, green, yellow denote regions dominated by dots, vertical strokes, horizontal strokes and blank regions respectively.

**Figure 8. 12.** *The drawing Arums* of **Figure 8.3** is superimposed on the multi-scale classification of **Subsection 3.2**



Note: The color code is as follows: blue, red, green, yellow are markers of the regions consisting mainly of thicker horizontal strokes, finer horizontal strokes, vertical strokes and blank spaces.

*Figure 8. 13. The Street in Saintes-Maries-de-la-Mer of Figure 8.4 is superimposed on the multi-scale classification of Subsection 3.1*



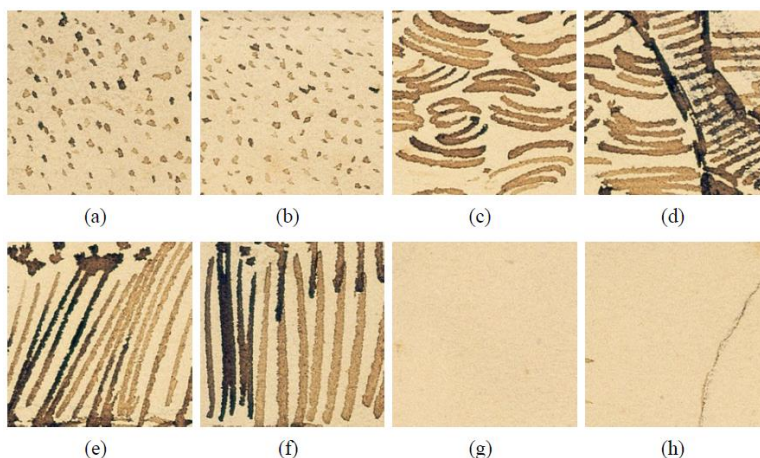
Note: The color code is as follows: blue, red, green and yellow represent dots, vertical strokes, curved strokes and blank spaces respectively.

#### 4.4. Quantitative comparison between classical and feature-based paradigms

The performances of the various dictionary learning techniques were evaluated by testing the classification accuracy on the same set of test patches. A set of image patches was extracted that consisted of patches different from the ones utilized in the training phase. These test patches for the *Sower* drawing are pictured in **Figure 8.14**. For a four-class classification, two patches were selected from each class. A total of 50 random points encompassing each image were chosen for feature extraction. In each case, the result of the classification is shown using a confusion matrix as presented in **Tables 3-5**. As observed from the confusion matrices, in many cases, the multi-scale feature-based dictionary learning classification provides better performance than the others. In particular, the ‘blank’ class was poorly classified by the classical method. A four-class random classifier would provide an accuracy of 25%. In comparison, the performance of dictionary learning-based classification is well above this baseline in almost all cases. While the result from the classical method is comparable in some cases, the feature-based methodology is always computationally less expensive.



**Figure 8. 14.** Depict eight independent test patches from the *Sower*



Note: (a)–(b) are from the ‘dots’ class (c)–(d) are from ‘horizontal’ strokes class (e)–(f) are from the ‘vertical’ strokes class (g)–(h) are from the ‘blank/background’ class; Each image is of size  $200 \times 200$ .

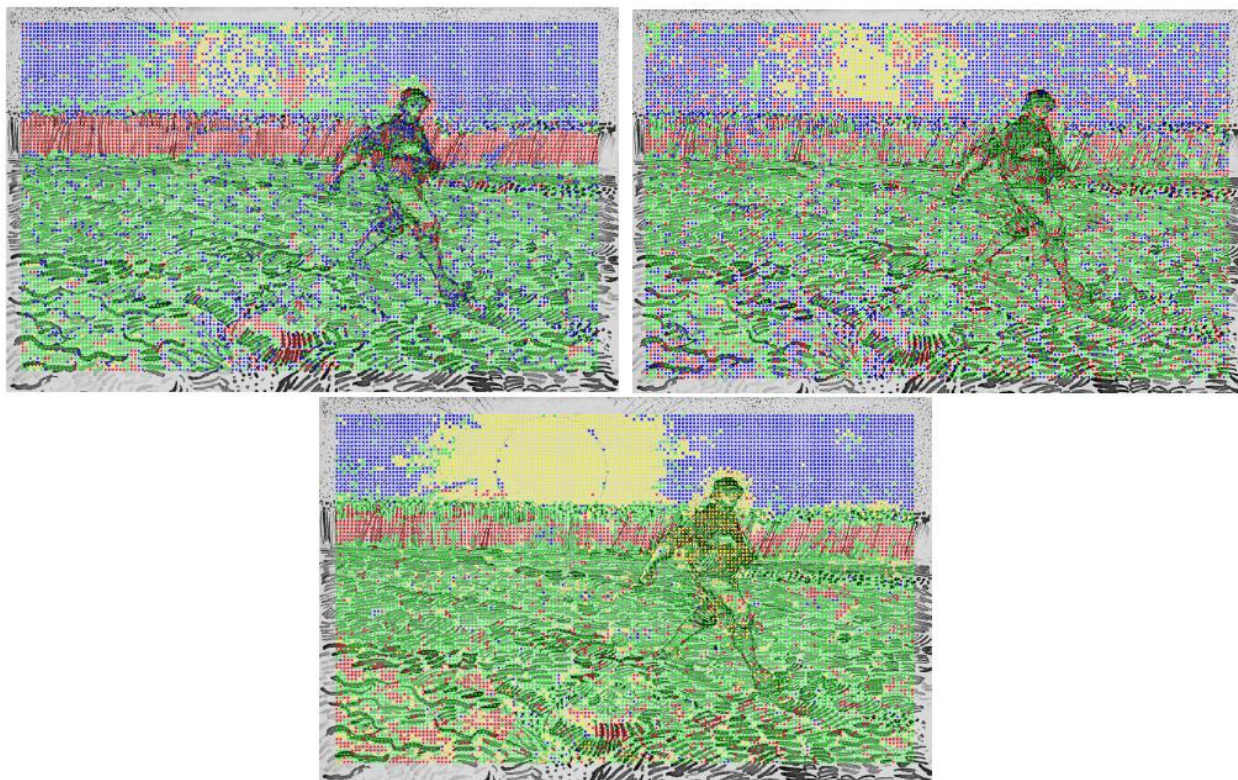
Finally, **Table 8.6** displays the time (in seconds) required to learn the optimal dictionary. The time to learn the dictionary is the time needed to complete 100 iterations and reach convergence for each of the four classes of the given ink drawing. Since the feature-based methods operate on derived features, the vectors are smaller than those in pixel-based dictionary learning, and the time is significantly smaller than for the pixel-based methods.

## 5. Conclusions

This work examined the classification problem of different types of strokes in Vincent van Gogh’s ink drawings under the dictionary learning paradigm. Several approaches were implemented and compared: a pixel-based classical dictionary learning, a multi-scale feature-based dictionary learning, and a multi-level feature-based learning. Results are reported for region-based segmentation in all cases, i.e., regions of the image are classified based on the predominant stroke type. The classical approach consumes a longer time for training and learning in comparison to the feature-based approaches, which enjoy a major reduction in the dimensions of the atoms of the dictionary. Though the K-SVD is limited to smaller dimensions, the feature-based approaches allow it to be applied to larger patch sizes. Overall, the multi-scale feature-based method appears to provide better classification performance.

The work here is limited to patch-based classification; it would be helpful to be able to apply similar techniques to attempt to discern individual strokes in the image with the hope of achieving reliable results like those of **Figure 8.6**. To this end, it is important to separate the components into individual strokes first. The feature-based methods presented here are either SSML or MSSL. It may be profitable to combine both into a multi-scale multi-level feature-based technique. Generalizing such methods to apply to the brush strokes of a painting remains a long-term goal.

*Figure 8. 15. The Sower of Figure 8.1 is used to compare several classification schemes*



Note: The first figure shows the classification using classical dictionary learning method while the second and third show classification results of the multi-level and multi-scale feature-based methods respectively. The color code is as follows: blue, red, green and yellow represent dots, vertical strokes, horizontal strokes and blank spaces respectively.



**Table 8. 3.** Classification test for classical dictionary learning: confusion matrix from testing the image patches of *Sower*

	<b>Dots</b>	<b>Horizontal</b>	<b>Vertical</b>	<b>Blank</b>
(a) Dots-1	62	38	0	0
(b) Dots-2	66	32	2	0
(c) Horizontal-1	24	66	10	0
(d) Horizontal-2	18	62	20	0
(e) Verical-1	22	6	72	0
(f) Vertical-2	2	0	98	0
(g) Blank-1	48	24	2	26
(h) Blank-2	48	28	8	16

Note: The labeling (a) through (h) correspond to images in **Figure 8.14**. Elements of confusion matrix are presented as percentage of points classified into a specific class.

**Table 8. 4.** Classification test for multi-level feature-based dictionary learning: confusion matrix from testing the image patches of *Sower*

	<b>Dots</b>	<b>Horizontal</b>	<b>Vertical</b>	<b>Blank</b>
(a) Dots-1	64	28	8	0
(b) Dots-2	8	44	0	48
(c) Horizontal-1	4	76	20	0
(d) Horizontal-2	0	68	32	0
(e) Verical-1	12	52	36	0
(f) Vertical-2	2	20	78	0
(g) Blank-1	4	42	0	54
(h) Blank-2	36	6	16	42

Note: The labeling (a) through (h) correspond to images in **Figure 8.14**. Elements of confusion matrix are presented as percentage of points classified into a specific class.

**Table 8. 5.** Classification test for multi-scale feature-based dictionary learning: confusion matrix from testing the image patches of *Sower*

	<b>Dots</b>	<b>Horizontal</b>	<b>Vertical</b>	<b>Blank</b>
(a) Dots-1	80	20	0	0
(b) Dots-2	98	2	0	0
(c) Horizontal-1	0	100	0	0
(d) Horizontal-2	0	88	8	4
(e) Vertical-1	0	8	92	0
(f) Vertical-2	0	8	92	0
(g) Blank-1	0	0	0	100
(h) Blank-2	0	0	0	100

Note: The labeling (a) through (h) correspond to images in **Figure 8.14**. Elements of confusion matrix are presented as percentage of points classified into a specific class.

**Table 8. 6.** Time required to learn the optimal dictionary with  $L = 3$

<b>Class of Sower</b>	<b>Dictionary Learning Time (Classical)</b>	<b>Dictionary Learning Time (Multi-level Feature-based)</b>	<b>Dictionary Learning Time (Multi-scale Feature-based)</b>
Dots	153.42 s	64.13 s	96.18 s
Horizontal	186.48 s	53.37 s	77.83 s
Vertical	143.63 s	57.39 s	81.73 s
Blank	164.84 s	67.35 s	89.08 s

## References

- [1] R. Mohanty, W.A. Sethares, T. Meedendorp, L. van Tilborgh, Automated classification of pen strokes in van Gogh's drawings, *Signals, Systems and Computers*, 2016 50th Asilomar Conference on, IEEE, 2016, pp. 125-129.
- [2] K. Kreutz-Delgado, J.F. Murray, B.D. Rao, K. Engan, T.-W. Lee, T.J. Sejnowski, Dictionary learning algorithms for sparse representation. *Neural computation* 15 (2003) 349-396.
- [3] M.S. Lewicki, T.J. Sejnowski, Learning overcomplete representations. *Neural computation* 12 (2000) 337-365.
- [4] B.A. Olshausen, D.J. Field, Sparse coding with an overcomplete basis set: A strategy employed by V1? *Vision research* 37 (1997) 3311-3325.
- [5] M. Elad, M. Aharon, Image denoising via sparse and redundant representations over learned dictionaries. *IEEE Transactions on Image processing* 15 (2006) 3736-3745.
- [6] J. Mairal, M. Elad, G. Sapiro, Sparse representation for color image restoration. *IEEE Transactions on image processing* 17 (2008) 53-69.
- [7] G. Peyré, Sparse modeling of textures. *Journal of Mathematical Imaging and Vision* 34 (2009) 17-31.
- [8] J. Mairal, F. Bach, J. Ponce, G. Sapiro, A. Zisserman, Discriminative learned dictionaries for local image analysis, MINNESOTA UNIV MINNEAPOLIS INST FOR MATHEMATICS AND ITS APPLICATIONS, 2008.
- [9] M. Yang, L. Zhang, X. Feng, D. Zhang, Fisher discrimination dictionary learning for sparse representation, 2011 International Conference on Computer Vision, IEEE, 2011, pp. 543-550.
- [10] Q. Zhang, B. Li, Discriminative K-SVD for dictionary learning in face recognition, 2010 IEEE Computer Society Conference on Computer Vision and Pattern Recognition, IEEE, 2010, pp. 2691-2698.
- [11] M.N. Do, M. Vetterli, Framing pyramids. *IEEE Transactions on Signal Processing* 51 (2003) 2329-2342.
- [12] E. Le Pennec, S. Mallat, Bandelet image approximation and compression. *Multiscale Modeling & Simulation* 4 (2005) 992-1039.
- [13] J. Mairal, G. Sapiro, M. Elad, Learning multiscale sparse representations for image and video restoration. *Multiscale Modeling & Simulation* 7 (2008) 214-241.
- [14] B. Ophir, M. Lustig, M. Elad, Multi-scale dictionary learning using wavelets. *IEEE Journal of Selected Topics in Signal Processing* 5 (2011) 1014-1024.
- [15] P. Abry, H. Wendt, S. Jaffard, When Van Gogh meets Mandelbrot: Multifractal classification of painting's texture. *Signal Processing* 93 (2013) 554-572.
- [16] I. Berezhnoy, E. Postma, J. van den Herik, Computer analysis of van Gogh's complementary colours. *Pattern Recognition Letters* 28 (2007) 703-709.
- [17] L. Shamir, What makes a Pollock Pollock: a machine vision approach. *International Journal of Arts and Technology* 8 (2015) 1-10.
- [18] M. Aharon, M. Elad, A. Bruckstein, K-SVD: An algorithm for designing overcomplete dictionaries for sparse representation. *IEEE Transactions on signal processing* 54 (2006) 4311.
- [19] L. Coconu, O. Deussen, H.-C. Hege, Real-time pen-and-ink illustration of landscapes, *Proceedings of the 4th international symposium on Non-photorealistic animation and rendering*, ACM, 2006, pp. 27-35.
- [20] C.R. Johnson, E. Hendriks, I.J. Berezhnoy, E. Brevdo, S.M. Hughes, I. Daubechies, J. Li, E. Postma, J.Z. Wang, Image processing for artist identification. *IEEE Signal Processing Magazine* 25 (2008) 37-48.
- [21] R. Rubinstein, A.M. Bruckstein, M. Elad, Dictionaries for sparse representation modeling. *Proceedings of the IEEE* 98 (2010) 1045-1057.

- [22] J.A. Tropp, A.C. Gilbert, Signal recovery from random measurements via orthogonal matching pursuit. *IEEE Transactions on information theory* 53 (2007) 4655-4666.
- [23] R. Mohanty, W.A. Sethares, T. Meedendorp, L. van Tilborgh, Automated classification of pen strokes in van Gogh's drawings, 2016 50th Asilomar Conference on Signals, Systems and Computers, IEEE, 2016, pp. 125-129.
- [24] E.R. Davies, *Machine vision: theory, algorithms, practicalities*, Elsevier, 2004.
- [25] R.C. Gonzalez, *Digital Image Processing*/Richard E. Woods. Interscience, NY (2001).
- [26] T. Ojala, M. Pietikäinen, T. Mäenpää, Multiresolution gray-scale and rotation invariant texture classification with local binary patterns. *IEEE Transactions on Pattern Analysis & Machine Intelligence* (2002) 971-987.
- [27] van Gogh, V. (2000) *The Complete Letters*, Bulfinch, Boston, Massachusetts, USA.

## CHAPTER 9: Conclusion

---



The final chapter of this thesis includes an overview of the aims described previously, their implications and relevance in the grander scheme, as well as addresses the open questions worth exploring in the future. The work presented here illustrates the utility of signal processing techniques in multiple applications including neuroimaging and art history dealing with distinct kinds of data via feature extraction. Under the neuroimaging application, a number of research questions were investigated based on functional MRI data, which are of relevance to the stroke, aging as well as healthy populations. Within the stroke population, chapters 2 and 3 (aims 1 and 2) examined the impact of BCI interventional training on non-targeted brain areas [1] and neural correlates of targeted behavioral outcomes in chronic stroke survivors [2] with motor impairments by means of machine learning models respectively. In chapter 4 (aim 3), the focus was on identifying subclinical language deficit in acute (early-stage) stroke survivors in an automated manner [3]. These three objectives broadly address not only the long-term but also short-term brain changes and patient outcomes occurring after an event of stroke. Within the aging population, chapters 5 and 6 (aims 4 and 5) analyzed the association between neural changes and cognitive performance [11] as well as inflammatory

response [12] respectively. These two chapters draw attention toward the neural alterations linked with outcomes of undergoing major surgery in old age. Under the application demonstrating image-based art conservation, an automated classification of different kinds of ink strokes appearing in van Gogh's work was presented in chapter 8 (aim 7) on the basis of imaging data of several ink drawings [4]. This provided an initial step toward better characterization of brushstrokes found in his paintings.

The most important focal point of this thesis, however, lies in chapter 7 (aim 6) [13], which was motivated by and connects all of the neuroimaging studies reported in the preceding chapters. Whereas the previous chapters were targeted at specific applications, this chapter was geared toward developing a more rigorous methodology that could improve each of those applications. The remainder of this final chapter is dedicated to the discussion of relevance, implications and open areas of research of chapter 7.

## **1. Relevance within the Big Picture**

The fundamental conceptualization of functional MRI-based brain connectivity was investigated in the light of feature extraction. In the neuroimaging literature, majority of the studies rely upon a linear time-domain definition using Pearson's correlation of functional (brain) connectivity which, while simple and useful, may not be sufficient to comprehensively describe the very notion of connectivity. Identified, within the present thesis, are several alternative measures of functional connectivity and compared against the conventional Pearson's correlation with the goal of (i) achieving a better classification between brain states of distinct population groups, and (ii) better describing the underlying relationship between brain and behavior.

Experiments testing the aforementioned goals suggested that Pearson's correlation does not necessarily outperform other measures of functional connectivity. In fact, no particular measure of functional connectivity consistently stands out. On the basis of empirical findings, a key implication of this could be

utilized to form the following hypothesis: given that the alternative measures of functional connectivity harness complementary information (time-, frequency-, wavelet-domains, linear, non-linear, similarity and dissimilarity), it is plausible that the canonical configurations of standard brain networks (such as default mode, language, salience, executive control, etc. networks) are a function of the measure used to define functional connectivity. More importantly, rather than relying on a single measure of functional connectivity, a multi-metric definition realized by combining multiple complementary measures may offer a more meaningful characterization. Such an augmented representation would refine the idea of brain connectivity further and could especially hold promise for differentiation of subtypes of a disease or disorder, given the heterogenous nature and variants of these data observed in most pathological conditions.

These findings could additionally contribute to the ongoing debate on reliability of resting-state functional MRI data, based on which functional connectivity is derived. Being task-free and time-efficient, resting-state data are easier to acquire, especially in challenging clinical population groups such as children [5] or patients in vegetative or minimally conscious states [6]. However, it is now well established that in these data, head movement is a major issue and can drive the indirect neural response leading to artifactual effects, raising concerns on reliability of functional connectivity [7]. In lieu of the resting-state MRI acquisition paradigm, recent works have propositioned shifting towards an acquisition paradigm utilizing a low distraction stimulus (such as movies) to minimize head movements while minimally engaging the brain via naturalistic paradigms [8; 9]. It could be speculated that while such newer paradigms could be useful, and the field would benefit by adapting to newer and more efficient acquisition models, they would likely take effect gradually over an extended period of time, after a rigorous understanding of the most appropriate paradigm has been attained. Meanwhile, at least in the short-term, it would be crucial to be able to salvage as much existing resting-state data as possible, given the time, effort and cost incurred in acquiring them over the past two decades. A multi-metric approach, such as presented here, to compute brain connectivity would be one potential way to reliably extract useful information and avoid artifactual effects to some degree. It could be argued that if multiple complementary measures of brain connectivity derived from the



same data point towards an emerging pattern in classification or prediction problems, we are likely to have greater confidence that the effects being observed are real by the principle of consilience [10].

## **2. Opposing Views**

As part of reasonable critique, it would be important to acknowledge and present differing propositions to those presented here. Opposing the multi-metric thesis to better explain functional brain connectivity, one could reason that it is in violation of the basic principle of Occam's razor or the law of parsimony in science. In other words, it could be argued that a simpler conceptualization of functional connectivity (such as that described on the basis of Pearson's correlation) would be the most plausible explanation. In such a scenario, introduction of alternative metrics, especially in combination by concatenation for a multi-metric representation, would serve as a more complicated or unnecessary construction of the idea of connectivity.

This logic could be rebutted by considering the evidence emerging from the data in this work. Among the alternative measures explored, connectivity in the brain appears to vary depending on the measure used to describe it, leading to alternate plausible configurations of neural networks. If the use of multiple measures were to guide us toward similar brain configurations, it could be argued that they do not necessarily add value to the knowledge of how the brain is wired (functionally). However, this does not seem to be the case. Aside from this, the goal of applying a feature selection procedure in the statistical models enables the search for a subset of multiple measures, directed toward identifying a relatively simpler model, rather than forcing the model to utilize all possible measures.

### 3. Future Directions

While investigations in chapter 7 highlight the need for a more comprehensive notion of functional brain connectivity, it would be essential to recognize the limitations which, in turn, also offer fertile grounds for a number of experiments for future research and are outlined as follows.

First, the alternative and multi-metric definitions of connectivity were tested within a limited sample of the true population. In the context of data-driven approaches using machine learning techniques, a much larger dataset would be necessary to validate whether these trends hold up and thus, provide better generalizations. Future studies should, thus, evaluate the reproducibility and test-retest reliability of the presented proposition in larger datasets from a variety of population groups and subgroups.

Second, the bulk of the studies in neuroimaging, including this thesis, examining connectivity within the brain simplify the idea under the assumption that connectivity occurs in a pair-wise fashion, i.e., measures are computed by considering interactions between two nodes or regions of the brain at a time. In order to form a more complete picture of neural mechanisms in any population, further investigations should strive to generalize the concept of connectivity beyond interdependence between simply two regions. Connectivity in the brain must be formulated as a multi-node problem rather than a two-node problem.

Third, this thesis examined a total of nine measures of functional brain connectivity based on a thorough literature review in the disciplines of neuroimaging as well as signal processing. While several of these measures possess properties complementary to each other, there is no reason to believe that this set of measures is exhaustive by any means. Moreover, the proposed multi-metric functional connectivity was realized by a simple concatenation of all the distinct alternative measures. Subsequent experimentation should explore useful measures, outside of the ones tested here, and evaluate more efficient and sophisticated methods of combining multiple measures.

In a nutshell, the central idea postulated in this thesis provides preliminary evidence for expanding the notion of functional brain connectivity by augmentation of the current conventional definition which, when utilized by data-inspired and data-driven statistical approaches, can facilitate better differentiation among population groups and improved quantification of brain-behavior relationships in a more meaningful way.

## References

- [1] R. Mohanty, A.M. Sinha, A.B. Remsik, K.C. Dodd, B.M. Young, T. Jacobson, M. Mcmillan, J. Thoma, H. Advani, V.A. Nair, Machine Learning Classification to Identify the Stage of Brain-Computer Interface Therapy for Stroke Rehabilitation Using Functional Connectivity. *Frontiers in neuroscience* 12 (2018).
- [2] R. Mohanty, A.M. Sinha, A.B. Remsik, K.C. Dodd, B.M. Young, T. Jacobson, M. McMillan, J. Thoma, H. Advani, V.A. Nair, Early Findings on Functional Connectivity Correlates of Behavioral Outcomes of Brain-Computer Interface Stroke Rehabilitation Using Machine Learning. *Frontiers in neuroscience* 12 (2018).
- [3] R. Mohanty, V.A. Nair, N. Tellapragada, L.M. Williams Jr, T.J. Kang, V. Prabhakaran, Identification of Subclinical Language Deficit Using Machine Learning Classification Based on Poststroke Functional Connectivity Derived from Low Frequency Oscillations. *Brain connectivity* (2018).
- [4] R. Mohanty, W.A. Sethares, T. Meedendorp, L. Van Tilborgh, Dictionary learning-based classification of ink strokes in Vincent van Gogh's drawings. *International Journal of Arts and Technology* 11 (2019) 80-98.
- [5] M.E. Thomason, E.L. Dennis, A.A. Joshi, S.H. Joshi, I.D. Dinov, C. Chang, M.L. Henry, R.F. Johnson, P.M. Thompson, A.W. Toga, Resting-state functional MRI can reliably map neural networks in children. *Neuroimage* 55 (2011) 165-175.
- [6] H. Di, M. Boly, X. Weng, D. Ledoux, S. Laureys, Neuroimaging activation studies in the vegetative state: predictors of recovery? *Clinical Medicine* 8 (2008) 502-507.
- [7] K.R. Van Dijk, M.R. Sabuncu, R.L. Buckner, The influence of head motion on intrinsic functional connectivity MRI. *Neuroimage* 59 (2012) 431-438.
- [8] K.L. Bottenhorn, J.S. Flannery, E.R. Boevig, M.C. Riedel, S.B. Eickhoff, M.T. Sutherland, A.R. Laird, Cooperating yet distinct brain networks engaged during naturalistic paradigms: A meta-analysis of functional MRI results. *Network Neuroscience* 3 (2018) 27-48.
- [9] T. Vanderwal, J. Eilbott, E.S. Finn, R.C. Craddock, A. Turnbull, F.X. Castellanos, Individual differences in functional connectivity during naturalistic viewing conditions. *Neuroimage* 157 (2017) 521-530.
- [10] E.O. Wilson, *Consilience: The unity of knowledge*, Vintage, 1999.
- [11] R. Mohanty, H. Lindroth, S. Twadell, V.A. Nair, V. Prabhakaran, R. D. Sanders, "Neural Correlates of Perioperative Executive Function associated with Noncardiac Surgery in the Elderly", currently under peer review for publication in the *British Journal of Anaesthesia*.
- [12] R. Mohanty, H. Lindroth, C. Casey, V.A. Nair, V. Prabhakaran, R. D. Sanders, "Changes in Functional Connectivity Associated with the Inflammatory Response to Noncardiac Surgery in Older Adults", currently in preparation for publication in the *Journal of Neuroinflammation*.
- [13] R. Mohanty, W. A. Sethares, V.A. Nair, V. Prabhakaran, "Meaning of functional MRI-based brain connectivity: empirical evidence and hypotheses", currently in preparation for publication in the *Nature Neuroscience*.